LOW FLOW HYDRAULICS IN RIVERS FOR ENVIRONMENTAL APPLICATIONS IN SOUTH AFRICA

Angelina Alekseevna Jordanova

A thesis submitted to the Faculty of Engineering and the Built Environment, University of the Witwatersrand, Johannesburg, in fulfillment of the requirements for the degree of Doctor of Philosophy.

Johannesburg, 2008

DECLARATION

I declare that this thesis is my own unaided work. It is being submitted to the Degree of Doctor of Philosophy to the University of the Witwatersrand, Johannesburg. It has not been submitted before for any degree or examination to any other University.

……

…….day of…….year…..……

ABSTRACT

Implementation of the National Water Act in South Africa requires that an ecological Reserve be determined for all significant resources. The ecological Reserve determination is the estimation of the amount of water required to maintain the system in a particular ecological condition. Because aquatic habitats are defined in terms of local hydraulic variables rather than amounts of water, hydraulic analysis provides a crucial link in relating hydrological conditions and river ecosystem integrity. Over the last decade, considerable effort has been devoted to developing hydraulics for the Reserve determination. The hydraulics needs for Reserve determination are primarily for low flow analysis, and appropriate methods still need to be developed.

This thesis deals with hydraulics under low flow conditions. Its emphasis is on developing appropriate methods for describing the hydraulic characteristics of South African rivers under conditions of low discharge, and the influence of vegetation and large bed roughness. The following methods have been developed:

- A new equation for prediction of overall flow resistance under large-scale roughness, and a new approach for estimation of intermediate-scale roughness resistance that distinguishes the influences of large and intermediate scale roughness components.
- Prediction methods for velocity distributions with large roughness elements. Under low flows, rocks and boulders may control the local velocity and depth distributions. Distributions of velocities and depth are related to rapidly spatially varied flow caused by the boundary geometry rather than flow resistance phenomena. With increasing discharge, the multiple local controls become submerged and the flow tends towards a resistance controlled condition. Available information addressing the distinction between resistance controlled and multiple local controls conditions is limited. This thesis contributes to understanding the transformation between multiple local controls and the resistance controlled conditions.
- Practical conveyance prediction methods for three situations pertaining to the occurrence of vegetation in rivers and wetlands. In-channel and riparian vegetation makes an important contribution to the creation of physical habitats for aquatic animals, but also has significant effects on flow resistances that need to be predicted.

ACKNOWLEDGEMENTS

It was long road that led me to this point. A road filled with laughter but also full of sadness. I could not have reached this point without the help of a number of great people to whom I grateful for various forms of assistance and aid.

First and foremost I offer my sincerest gratitude to my supervisor, **Chris James**, who has supported me throughout my thesis with his patience, knowledge and guidance. I attribute the level of my doctoral degree to his encouragement and effort and without him this thesis, too, would not have been completed or written. One simply could not wish for a better or friendlier supervisor who managed to make time for the many consultations and discussions I needed. He is an outstanding supervisor, and I am grateful to have been a student of his.

I would like to thank the **Water Research Commissions** for making this research possible through a three-year funding. I would particularly like to thank **Dr Mitchell**, **Dr Liphadzi**, and the **Reference Group** of the research for their comments and suggestions; their contribution was greatly appreciated.

My thanks goes to the **School of Civil & Environmental Engineering** at the **University of the Witwatersrand** which provided the laboratory facilities, office space, computer facilities and technical assistance as well as bursary support for the additional nine months I required beyond the contract period.

I am grateful to **Prof. Thoms** from the University of Canberra (Australia) who provided the Cotter River Field data.

I would like to thank my family and my friends for their love and support and their patience as they had to put up with my endless ravings for the duration of this thesis.

The useful guidance on the use of River 2D was graciously provided by **Peter Hirschowitz**, who was always available for discussion regarding the research; this was greatly appreciated.

As well as keeping the administration and financial control of the research, **Wendy Midgley** provided me with something much greater: a friendly smile and encouragement whenever we met.

Last but not least, I would like to express my gratitude to **Bruce Randall**, **Ralph Heath** and **Trevor Coleman** for their encouragement and support, but mostly for their belief in me.

CONTENTS page

LIST OF FIGURES

LIST OF TABLES

LIST OF SYMBOLS

Acceleration due to gravity	g
applied force per unit plan area	F_A
approach velocity	$\overline{V}$
approach velocity	V_x
area of the i^{th} subsection	A_i
asymptotic approach velocity	u_{a^∞}
average velocity	V
averaged dominant roughness	D
averaged rod diameter	D
base area of the roughness elements	A_b
basic value of n for a straight, uniform, smooth channel	n_b
bed shear stress	τ_B
bed shear velocity	U^*
bottom friction coefficient	c_f
boundary between logarithmic and linear flow regions	d
channel width	b
Chézy resistance coefficient	C
cobble diameter	d
coefficient varies with the cross-sectional geometry of flow	a
constant	b_0
constants	c_0, c_1, c_2
correction factor for meandering of the channel	m
correction factor for the effect of surface irregularities	n_1
cross-sectional area of roughness elements exposed to flow	A_d
cross-stream diameter	D
Darcy-Weisbach friction factor	f
dimensionless coefficient	a
discharge	Q
discharge per unit width	q
distance between reed stems in the lateral direction	a_y
drag coefficient as a function of the cylinder Reynolds number	C_D
drag coefficient	C_d
drag force	F_d
effective drag coefficient	C_{De}
effective hydraulic radius	R'
empirical coefficient	a
empirical coefficient	b
empirical coefficient	c
energy gradient	S
exponent	b
factor accounts for the change in frontal area with inundation	A
fitted parameters	A, B and a
flow depth	H
flow depth	d

flow depth	y
flow velocity defect	u_d
flow width	W
fluid density	r
flume width	B
fraction of surface covered by roughness elements	P
Froude number	Fr
general coefficient	B
hemisphere radius	k
hydraulic radius of the i^{th} subsection	R_i
hydraulic radius	R
kinematic viscosity of water	υ
large roughness element concentration	λ
local flow velocity	v
longitudinal bed slope	S
longitudinal cylinder spacing	a_x
longitudinal dimension of a roughness element	d_x
Manning resistance coefficient	n
mean flow velocity	U
Nikuradse roughness	k_s
number of roughness elements per unit area	n
number of roughness elements per unit area	N
numbers of stems in the lateral direction	n_y
numbers of stems in the longitudinal direction	n_x
numerical coefficients	b_0, b_1 and b_2
parameter depending on roughness geometry	m
projected area of elements	A_p
ratio of basal area of a roughness element to the area of bed considered	p
relative depth, equal to h/H	x
relative point velocity, equal to v/V.	x
representative roughness length characterizing the bed material	d
resistance coefficient for large-scale roughness	F
resistance coefficient	λ_d
resistance coefficient	C_x
resistance force per unit plan area contributed by the bed	F_B
resistance force per unit plan area contributed by the vegetation	F_V
Reynolds number	Re
roughness coefficient	G
roughness element diameter	D
roughness element height	h
roughness size	k_s
sediment size characteristic	D_g
shape parameter equal to $1/b$	c
shape parameter of the point velocity distribution	s
shape parameter	t
shape related factor	s_1
shape related factor	s_2
shear stress	τ_s

shear stress	τ_0
slope of a plot of *v* versus V*(v)*on log-log scale	b
slope	α
spread of a wake	s_w
standard deviation of the bed elevation	s
stem area projected in the flow direction	A_{pr}
stem diameter	D
submerged height of a roughness element	d_z
submerged volume of an individual roughness element	$V_{r.el}$
the equivalent value	n_e
the lateral distance relative to the obstruction	z
total area	A
transverse dimension of a roughness element	d_y
unit weight of water	g
value for obstructions	n_3
value for vegetation and flow conditions	n_4
value of variations in shape and size of the channel cross section	n_2
vegetation density	n
velocity profile parameter	P
von Karman's constant in turbulent velocity profile	K
wake length	x_N
wake width	z_N
water depth	h
water surface slope	S_w
wetted perimeter	P
width of the roughness element	w
x percentile particule grain size	D_x

1 INTRODUCTION

1.1 River Management and Hydraulics

Effective management and utilization of water-linked ecosystems requires the ability to predict biological responses to management actions. The growing need to predict the biological impacts related to water management activities demands further understanding of the relationships between hydrological variability and river ecosystem integrity (Richter et al, 1997). The linkage between hydrology and biological response must be made through hydraulics. It is, however, local variables such as flow velocity and depth, rather than discharge that define aquatic habitat. The movement, dispersion and dilution of pollutants are also determined by hydraulic conditions, as is the movement and distribution of sediment which, to a large degree, determine channel form.

In South Africa, management actions are usually manifest in rivers as changes to the hydrological regime, which is also the fundamental driver of biological processes. Hydrology and aquatic ecology are both mature disciplines, and techniques developed for ecosystem management (e.g. Hughes and Munster, 2000; Davies et al, 1993) are founded on well-established precedent. River hydraulics, on the other hand, is poorly developed, and relies heavily on overseas experience. This overseas experience has limited applicability to South Africa's unique rivers. Further, most hydraulics methodology emanates from the engineering fraternity and is intended for flood, or at least relatively high flow applications.

In the South African water law (National Water Act, NWA, Act 36 of 1998), the quantity of water required to maintain riverine functions is included in the Reserve (Uys, 2001). Implementation of the NWA requires that a Reserve (basic human needs requirements and ecological) be determined for all the country's rivers, with those for which development is planned receiving priority attention. Statutory provisions are made for environmental flow requirement in the NWA to determine the ecological component of the Reserve for all significant water resources.

Hydraulic analysis is therefore a crucial component in the determination of the ecological Reserve in terms of both quantity and quality, as well as in any river rehabilitation measures.

Vegetation and large substrate material are common features of South African rivers. Under low flow conditions vegetation patches and rocks become relatively large, and sometimes effectively discrete roughness features. These kinds of roughness features usually act as obstacles to the flow. The drag force from such obstacles modifies the average velocity and velocity distributions. The controls on flow depth and velocity therefore become more localized than for high flows, requiring different analysis approaches.

This thesis is related to development of methods for hydraulics under low flow conditions required for environmental applications in South Africa.

1.2 Specific Research Objectives

The aim of the project is development of appropriate methods for describing the hydraulic characteristics of South African rivers under conditions of low discharge, and the influence of vegetation and large bed roughness. The specific objectives for achieving this aim are methods for predictions:

- Flow velocity and depth distributions,
- Large roughness element resistance, and
- Vegetation resistance.

The objectives have been addressed by undertaking literature survey, experimental investigation, data analyses, theoretical development and computer modelling.

1.3 Layout of the Thesis

The thesis is organized around the following nine chapters:

1. **Introduction**. This chapter provides an overview of the problem dealt with in this thesis.

2. **Background**. This chapter provides information regarding South African policies; approaches and procedures for protection of water resources; review of methodologies developed for determination of flow requirements; the relation between fish and microinvertebrate physical habitats and hydraulic variables; and a review of published information related to approaches and equations developed internationally for predicting flow resistance under large and intermediate scale roughness.
3. **Experimental Investigation of Resistance Controlled Flow Conditions**. This chapter includes experimental investigations, related to overall flow resistance under large and intermediate scale roughness, under different hydraulic conditions. The experimental work shows that the density of large roughness elements of the channel bed has a significant influence on the overall flow resistance of the channel. It has been found that resistance is caused primarily by the largest clasts and that the maximum resistance occurs with the areal coverage of 30% - 40%.
4. **Prediction Methods for Resistance Controlled Conditions**. Conventionally, flow resistance in rivers is described using equations (such as those of Chézy, Darcy-Weisbach and Manning) that implicitly assume the dominant resistance phenomenon to be boundary shear stress. Such equations are inherently unsatisfactory for low flow conditions, where the size of roughness elements is comparable to the flow depth and resistance is dominated by form drag. New methods are proposed for the conditions of large- and intermediate-scale roughness, i.e. when the flow depth is less than the height of the roughness elements and between one and four times the height of the roughness elements. This chapter presents the development and verification of these methods.
5. **Experimental Investigation of Velocity Distribution with Large Roughness Elements**. This chapter describes experimental investigations of velocity distributions with large roughness. It is shown that velocity and depth distributions are significantly different under multiple local control and resistance control conditions, both of which are common and can occur at the same site for different discharges.

6. **Prediction Methods for Velocity Distributions with Large-scale Roughness**. In this chapter prediction methods for velocity distributions with large roughness are presented. It is concluded that the situation is too complex for conventional flow analysis, and computational modelling is considered to be the appropriate approach. A public domain 2-dimensional model, River2D, is identified as a suitable tool. It is shown to be able to predict velocity distributions reliably under large-scale roughness conditions, and especially for the trans-critical flows associated with multiple local controls.
7. **Vegetation Flow Resistance**. Practical conveyance prediction methods are presented for three situations pertaining to the occurrence of vegetation in rivers and wetlands, viz. flow through emergent vegetation, flow in channels with emergent vegetation boundaries, and flow in channels with discrete vegetation patches. The three approaches presented show the appropriateness of different treatments of different levels of system complexity: uniform vegetation resistance can be described by a single, simple equation; resistance estimation for channels with vegetated banks requires composite resistance coefficient determination as well; flow description in channels with fragmented vegetation patches requires computational modelling.
8. **River2D Application to Field Data**. This chapter addresses the modelling of river hydraulics using two-dimensional River2D software. The freely available River2D model has been shown to be an effective tool for predicting velocity and flow depth distributions in rivers under low flow conditions,
9. **Conclusions and Recommendations**. This chapter presents conclusions of the project and recommendations regarding further research. The project has produced methods for predicting low flow conditions in rivers that are complete and usable but, as with all methods that rely wholly or partly on empiricism, further strengthening of the data base and further field confirmation would be valuable.

2 BACKGROUND

2.1 Introduction

The primary purpose of this thesis is the development of appropriate methods for describing the hydraulic characteristics of South African rivers under conditions of low discharge, and the influence of vegetation and large bed roughness. The main reason why new methods need to be developed is for implementation of the National Water Act (No.36 of 1998) (NWA). The implementation of the NWA requires that an ecological Reserve be determined for all significant resources. Hydraulic analysis is therefore a crucial component in the determination of the ecological Reserve in terms of both quantity and quality, as well as in any river rehabilitation measures.

The ecological Reserve determination is an estimation of the amount of water required for maintaining the system in a particular ecological condition. Researchers in environmental flow tend to quantify the water needs of the various biotic components in terms of hydraulic parameters such as water depth, flow velocity, wetted perimeter and water surface width (Rowlston et al, 2000). The results of hydraulic analyses and modelling therefore form the essential link between the way in which the hydrologists, engineers and water managers express the flow of water in the river in terms of flow rate, and the way in which river ecologists express the water requirements of the river ecosystem itself in terms of variables like the flow depth and velocity (Birkhead, 2002).

The work that has been done internationally on river hydraulics has limited applicability to South Africa's unique rivers. The hydraulics needs for environmental applications in South Africa are primarily for low flow analyses, and adequate and appropriate techniques still need to be developed.

For development of the appropriate techniques it is essential to understand why we need a new development. Methodologies related to determination of instream flow requirements have already been developed, and therefore it is necessary to review available methods and methodologies and check their applicability to

South African conditions.

The aims of this chapter are to identify South African policies, approaches and procedures for the protection of water resources, to review methodologies developed for the determination of flow requirements, to recognize fish and microinvertebrate physical habitats and how these can be described by hydraulic variables, and to verify available methods related to hydraulics under low flow conditions that can be applied in South Africa.

2.2 National Policy on the Protection of Rivers in South Africa

Water resources in South Africa are limited and their management and protection is, apart from any biodiversity considerations, critically important for the sustainable economic and social development of the country. Over the last decade, much effort has been devoted to developing policies, structures and methodologies for the management and protection of South African water resources. New ways of applying information and making decisions on resource protection and management have been under development at the Department of Water Affairs and Forestry (DWAF, Resource Quality Services), and by other agencies responsible for natural resource management (DWAF, 1999).

The Department of Water Affairs and Forestry and other agencies (including the Department of Environmental Affairs and Tourism (DEAT) and the Department of Agriculture) responsible for natural resource management have been developing approaches for making decisions on resource protection and management (DWAF, 1999). A number of institutions and organizations, such as the Water Research Commission (WRC), Institute for Water Research (IWR, Rhodes University), Southern Waters, Centre for Water in the Environment (CWE, University of the Witwatersrand), Freshwater Research Unit (University of Cape Town), South African National Parks, Council for Scientific Industrial Research (CSIR), have contributed to research and development of methods and approaches related to the protection of South African rivers.

As a result, a variety of new policies, tools, approaches and procedures have been developed including:

- The National Water Act (DWAF, 1998),
- The National Environmental Management Act (Government Gazette, 1998),
- The Water Law Principles (DWAF, 1996c),
- The National Water Policy (DWAF, 1997),
- The Environmental Conservation Act (DEAT, 1989),
- The Conservation of Agricultural Resources Act (Department of Agriculture, 1983),
- The Integrated Environmental Management Process (DEAT, 1994),
- The South African Water Quality Guidelines for Aquatic Ecosystems (DWAF, 1996b),
- Various environmental flow requirement methods (Tharme, RE and King, JM, 1998; O'Keeffe JH and Hughes, DA, 2004; Brown et al, 2005),
- The Index of Habitat Integrity (Kleynhans, 1996),
- The Fish Assemblage Integrity Index (Kleynhans, 1999),
- The South African Scoring System (Dickens and Graham, 2002),
- The National Aquatic Ecosystem Biomonitoring Programme (Murray, 1999),
- The South African Water Quality Guidelines for Domestic Use (DWAF, 1996a), and
- Resource Directed Measures for determining the ecological Reserve (DWAF, 1999).

In the NWA the main provisos affecting the way water resources are managed are:

- The development of a national water resource strategy,
- The development of catchment management strategies,
- Protection of the water resources by developing a classification system and setting resource quality objectives,
- Determination of the Reserve, and

- Monitoring of the water resource.

Protection of water resources ensures their availability for human use as well as maintaining their ecological functioning. To achieve the aim, two approaches are proposed (DWAF, 1999):

- Resource-Directed Measures (RDM), and
- Source-Directed Controls.

The RDM's focus is on resource quality, in terms of the health or integrity of water resources. This includes water quantity and water quality, in-stream and riparian habitats, and the condition and distribution of the aquatic biota.

The RDM include the following components:

- Development of a National Classification System,
- Determination of the class of specific water resources, and
- Establishment of resource quality objectives, and determination of the Reserve, with reference to the relevant class.

Source-Directed Controls deal with implementation of appropriate management of water uses including:

- Best management practice measures that apply nationally,
- Special measures, derived from catchment management strategies and/or plans, and
- Site specific measures, stemming from the authorisation process, taking account of considerations specific to the water use being considered.

The NWA has been developed to provide a fundamental reform of the law relating to water resources. The NWA views the river as a "resource" rather than a "user" of water. The term resource "*is used to include the health of all parts of the water resources, which together make up an ecosystem, including plant and animal*

communities and their habitats" (DWAF, 1997; DWAF, 1998). The Act is revolutionary because it recognises the central role of ecosystems in water supply. Sustainability and equity are identified as central guiding principles of the Act in the protection, use, development, conservation, management and control of water resources. The NWA provides for a river's ecological requirements founded on environmental flows, which will maintain ecological structure and function, channel, bed and floodplain form, function and connectivity, and a measure of its natural flow characteristics. Implementation of the NWA requires that an ecological Reserve be determined for all significant resources, with those for which development is planned receiving priority attention.

Ecological Reserve determination is an estimation of the flow requirements of different components of a river. It focuses on the amount of water required to maintain the system in a particular ecological condition. The estimation of flow required for different aquatic components is a complex procedure, and development of methodologies suitable for this estimation, was therefore required.

As a result of work of many specialists, a generic seven-step RDM methodology was developed, as described in Water Resources Protection Policy Implementation: Resource Directed Measures for Protection of Water Resources (DWAF, 1999):

Step 1: Initiate the RDM study
Step 2a: Determine the ecological type of each resource
Step 2b: Delineate resource units within the study area
Step 2c: Select survey sites within the study area
Step 3: Determine the reference conditions for each resource unit
Step 4a: Assess the present status of the resource units
Step 4b: Assess the ecological importance and sensitivity of the resource units
Step 5: Set the management class for each resource unit
Step 6a: Quantify the Reserve for each resource unit
Step 6b: Set resource quality objectives for each resource unit

Step 7: Design an appropriate resource monitoring programme.

The level of detail or intensity of RDM determination is closely related to the ecological importance and sensitivity of the water resource, the scale and degree of the impact of proposed water use, and the urgency of the Reserve determination.

There are four levels of Reserve determination:

- Desktop,
- Rapid,
- Intermediate, and
- Comprehensive.

The desktop determination is a quick, often very low confidence assessment proposed for use in the National Water Balance Model. For the desktop estimation a local desktop reserve model for an initial low confidence estimate of the quantity component of the Reserve for rivers was therefore developed (Hughes and Hannart, 2003). The rapid determination is a low confidence estimation using the desktop model with quick field assessment of present ecological status, proposed for use in unstressed catchments of low ecological importance and sensitivity. The intermediate determination is a medium confidence assessment. It is a team field study proposed for use in relatively unstressed catchments. A higher level of confidence is provided by the comprehensive assessment, where extensive field data should be collected and used by specialists for the quantification of the Reserve. The approach is proposed to be applied for very ecologically important and/or sensitive catchments (the size of the river/reach as well as the type and extent of water resource development are important considerations.)

The principles required to provide hydraulic information for different Reserve estimations are the same, regardless of the level. The differences between rapid, intermediate and comprehensive assessment lie in the amount of measured

hydraulic data, and therefore in the accuracy of and confidence in the results produced. It is clear that greater confidence is expected for higher levels of determination (Birkhead, 2002).

Determination of the ecological Reserve is a complex procedure requiring involvement of a wide range of experts such as aquatic scientists, social scientists, hydrologists, geomorphologists, hydraulicians, engineers and resource economists. Understanding of instream flow requirements of river ecosystems, and development and application of appropriate methods are inalienable parts of the whole process. There are a number of international and South African methodologies and methods that can be applied in instream flow requirement studies. Some of them are discussed in the next section.

2.3 Instream Flow Requirement Methodology

Initially, the impetus of instream flow requirements studies came from western North America, where salmon fisheries of significant commercial value were threatened (Tharme, 1996; Nestler et al, 1989). As early as the late 1940s, the first study relating to the influence of the Granby Dam on the Colorado River on downstream conditions was performed by the U.S. Fish and Wildlife Service (Tharme, 1996). The main aim of instream flow studies is to identify a quantity of water and its distribution in time and space required for maintenance of the river ecosystem. The development and application of methods and techniques for prescribing the instream flow requirements (IFRs) started in the 1950s, and since then many different types of methodologies and approaches have been proposed (King and Tharme, 1994).

2.3.1 International methodologies

Several reviews and evaluations of these methodologies and approaches have been published (Mosley, 1983; Wesche and Rechard 1980; Stalnaker and Arnette, 1976). A comprehensive review of international methodologies for the quantification of the instream flow requirements of rivers has been conducted and

published in South Africa (Tharme, 1996). In general, methodologies can be divided into four basic categories (Tharme, 2002):

1 Methodologies based on historical flow records,
2 Methodologies based on the relationship between physical habitat and discharge,
3 Methodologies based on the instream habitat simulation methods (with habitat defined in terms of the requirements of a particular target species), and
4 Holistic methodologies and alternative approaches to instream flow assessment.

Methodologies based on historical flow records: these methods are based on hydrological data. Historical flow records are used for instream flow recommendations. The most common of these methodologies is the Montana Method, (Tennant, 1976) which was developed in the 1970s in North America. Recommended minimum flows are based on percentages of the average annual flow, with different percentages for winter and summer months.

Other historical flow record approaches such as Hoppe, 1975 (cited in Gordon et al, 1992) and a Decision Support System (Hughes and Münster, 2000) are based on flow duration curves, and develop the relationships between recommended instream flow and the percentage of the time that it is exceeded. The main benefit of these approaches is that a rough estimation can be made if gauged records are available, alleviating the effort and necessity for field data collection for analysis.

The best application of these methodologies is to provide quick, simple, and low-confidence assessment for planning purposes. However, they are limited by the lack of any ecological interpretation of the hydrology.

Methodologies based on the relationship between physical habitat and discharge: These methods are designed to assess various conditions of physical variables in

relation to fluctuations in discharge, and are primarily focused on maintenance flows for target riverine biota.

Hydraulic rating methodologies are single cross-section methods, which involve the development of relationships between discharge and other hydraulic variables, such as, wetted perimeter, water depth and velocity. One of the most often used is the Wetted Perimeter Method (Collings, 1972). The wetted perimeter method assumes that the slope breakpoint on a plot of wetted perimeter against discharge represents the quantity of water preferred by fish. The first break in slope on the curve is an indication of the optimum rearing discharge (Gordon et al, 1992). Although these methods take biota into consideration, the scale and extent of the hydraulic interpretation is very limited.

Methodologies based on the instream habitat rating or simulation: these methods combine physical habitat and habitat preferences of a given species to estimate the amount of habitat available for this species over a range of discharges.

Habitat rating methods integrate an approach referred to as Multiple Transect Analysis (Tharme, 1996). This technique involves the collection of field data at transects in a stream reach where the maintenance of flows is most critical for a target species or biological activity. Hydraulic variables are used to develop a relationship between physical habitat represented by hydraulic parameters, such as flow velocity, flow area and flow depth, and discharge.

Of all currently availably habitat simulation methodologies, the Instream Flow Incremental Methodology (IFIM) and its Physical Habitat Simulation Model, PHABSIM II (Milhous et al, 1989) are the most widely used methods worldwide. IFIM was developed by the United States Fish and Wildlife Service for assisting in the assessment of instream flow requirements of rivers (Bovee, 1982). The IFIM is a problem-solving tool made up of a collection of analytical procedures and computer models. An application of IFIM consists of the following steps (Tharme, 1996; King and Tharme; 1994, Gordon et al, 1992):

- Identification of the study objectives, river study reaches, and target species,
- The assessment of catchment equilibrium and macrohabitat suitability,
- Development of functions integrating macrohabitat and microhabitat availability of the present system,
- Collection of physical data, and defining physical microhabitat,
- Collection of biological data for the habitat suitability curves,
- Connection between physical and biological data using PHABSIM II, and
- Hydraulic, and microhabitat simulation using PHABSIM II.

PHABSIM II is a collection of some 240-computer programs that form a major component of IFIM. It comprises two basic components: hydraulic simulation and habitat simulation. Comprehensive information of concepts and practicalities of PHABSIM II can be found in King and Tharme (1994), Tharme (1996), and PHABSIM for Windows: User's Manual and Exercises (www.fort.usgs.gov.)

Holistic methodologies and alternative approaches to instream flow assessment: Holistic methods for the determination of ecological flow requirements quantify the flows for the various biotic components of rivers in terms of parameters such as flow depth, flow velocity and wetted perimeter, adding time as a parameter by referring to the frequency of exceedance of a particular flow rate, or the duration of inundation resulting from a particular flooding event (Tharme, 1996). In the holistic approach, important and critical flow events are identified in terms of most of the criteria defining flow variability (Tharme, 2002). The Building Block Methodology (BBM), Holistic Approach and Expert Panel Assessment Method are holistic methodologies that have been developed in the last decade (Tharme, 2002).

IFIM is widely used in the USA, and has been applied in Australia, New Zealand and Britain. It has been applied in South Africa for the Sabie River (Gore et al, 1992) and the Olifants River (Western Cape) (King and Tharme, 1994). Some details of the application to the Olifants River follow.

2.3.2 Methodologies developed in South Africa

In South Africa, activities addressing the influence of modified flow regimes on riverine ecosystems were initiated in 1987, and the needs for the methodologies for assessing the instream flow requirements of rivers were recognised. New research in the field of instream flow requirements therefore began in 1989 (King and Tharme, 1994).

Firstly, the IFIM approach was applied in South Africa. The Olifants River (Western Cape) was chosen for learning and applying the methodology. During the study, it was found that:

- IFIM is difficult and time-consuming to learn to use because it incorporates concepts and skills from a wide range of disciplines,
- IFIM is difficult to apply because in places it is vague, non-pragmatic or still largely conceptual,
- PHABSIM II is complex and difficult to master, and
- At that time, the state of development of IFIM did not allow compilation of a comprehensive modified flow regime for a regulated river in the way required by the South African Department of Water Affairs and Forestry.

It was concluded that IFIM is not applicable for South African river conditions, because of the exceptionally long time required to achieve a satisfactory result, its extensive requirement for quantified biological data, and difficulty in describing the low-flow hydraulics of complex river channel morphology. Consequently, development of local instream methodologies to provide guidance on the sustainable use of rivers' water-resources started in 1989 (King and Tharme, 1994).

Building Block Methodology (BBM): the BBM was the first method developed for assessing the environmental flow requirements (EFR) of rivers in South Africa. The conceptual basis of the BBM is that some flows within the total flow regime are more important than others for maintenance of that river ecosystem. These flows can be described in terms of their magnitude, frequency, duration and

timing (King and Tharme, 1994; King, 1996; Tharme & King 1998; King and Louw, 1998). The methodology assumes the following:

- Biota associated with a river can cope with base flow conditions that naturally occur in it "often", and may be reliant on higher flow conditions that naturally occur in it at certain times,
- Identifying what are derived to be the most important components of the natural flow regime, and ensuring that they are incorporated as part of the modified flow regime, will facilitate maintenance of the natural biota and natural functioning of the river, and
- Certain kinds of flow influence channel geomorphology more than others, and incorporating such flows into the modified flow regime will aid maintenance of the natural channel structure and diversity of physical biotopes.

Downstream Response to Imposed Flow Transformations (DRIFT): DRIFT is a second generation methodology for instream flow assessments that was developed by Southern Waters Ecological Research and Consulting (South Africa) and SMEC International (Australia) specifically for the assessment of environmental flows for the Lesotho Highlands Water Project (Brown et al, 2005).

DRIFT is an interactive, scenario-based process, which address the biophysical consequences of progressive reductions in flows and socio-economic links. The process involves a number of post data collection activities as described below:

- Preparation of the hydrological data,
- Linkage of the hydrological data to cross-sectional river features,
- Reduction of different flow components, and description of the biophysical consequences,
- Entry of the consequences into a custom-built database,
- Querying the database to describe the changes in river condition caused by one or more potential flow regimes (scenarios),
- Identification of the social impacts of each scenario,
- Calculation of the economic cost of compensation and mitigation for each

scenario, and

- Calculation of the impact on system yield for each scenario.

The BBM and DRIFT are both holistic type methodologies, with three primary differences:

- DRIFT is a scenario-based interactive approach, in which a database is created that can be queried to describe the biophysical consequences of any number of potential future flow regimes. However, it does not specifically address the present ecological state in relation to the minimally modified system. BBM is a prescriptive approach that requires identification of a single predetermined condition in relation to the expected minimally modified condition, after which a single flow regime is described to facilitate maintenance of that condition,
- BBM "builds up" a recommended flow regime from scratch, whereas DRIFT takes the present-day flow regime as a starting point, and describes the consequences for all aspects of the river of further reducing the flow regime in different ways, and
- DRIFT is designed to describe and quantify the links between changing river condition and the social and economic impacts for the riparian people who rely on the river for subsistence.

Flow-Stressor Response (FSR): FSR is a newer method designed to be used on its own or as part of holistic methods such as the BBM and DRIFT. The FSR is based on the application of a generic index describing the progressive consequences to the flow-dependent biota of flow reduction. The indices of stress range from 0 (corresponding to a condition of no stress) to 10 (very high stress stage). Flow hydraulics and associated habitat changes are related to biotic responses in terms of abundance, life stages, and persistence (O'Keeffe and Hughes, 2004).

The application of the method consists of the following steps:

- Site selection, site survey, and description of sites in terms of hydraulic

parameters (depth, flow velocity and wetted perimeter) at a range of discharges,

- Development of curves that describe the relationship between changing discharge and stress for critical flow-dependent species or groups,
- Converting the natural and any other flow time series to a stress time series,
- Developing stress profiles which describe the magnitude, duration and frequency of stress levels experienced by target species for different flow scenarios,
- Assessing the relative changes in biotic stress for various flow scenarios, and
- Identifying the scenario for which the stress profile will impose the least additional stress to the biota.

Application of any of the South African methodologies (BBM, DRIFT or FSR) to set the ecological flows requires an interface between hydrology and water requirements of different components of a river. This interface is found in the hydraulic analysis of flow in natural open channels. The results of hydraulic analyses and modelling therefore form the essential link between the way in which the hydrologists, engineers and water managers express the flow of water in the river in terms of flow rate, and the way in which river ecologists express the water requirements of the river ecosystem itself in terms of hydraulic variables such as depth and velocity (Birkhead, 2002).

The success and confidence with which flow requirements are assessed therefore depends to a large extent on the quality and reliability of the hydraulic information used. The role of hydraulics for estimation of Ecological Flow Requirements (EFRs) is discussed below.

2.4 Ecological Flows and Hydraulics

EFRs specify the flows for the various biotic components of a river in terms of parameters such as flow depth, flow velocity and wetted perimeter, adding time as

a parameter by referring to the frequency of exceedance of a particular flow rate, or the duration of inundation resulting from a particular flooding event (Tharme, 1996).

Approaches have been developed for the application of river hydraulics in EFR assessment based on collaboration with specialists, including hydrologists, fluvial geomorphologists, fish and invertebrate biologists (Rowlston et al, 2000). These approaches are discussed with reference to the location of appropriate sites for ecological flow assessment, topographical river channel surveys, requirements for the collection of hydraulic data, appropriate hydraulic analysis and modelling, and the presentation of hydraulic information for use by specialists assessing the ecological flow requirements during an EFR's specialist meeting.

The Terms of Reference for the hydraulic specialist in the descriptions of the tasks necessary to carry out the study as sat out in the Manual for the Building Block Methodology (King et al, 2000) are:

- Site selection,
- Site cross-sectional and longitudinal profile surveys,
- Collection of hydraulic data,
- Reduction of survey and hydraulic data,
- Hydraulic analysis and modelling,
- Reporting, and
- EFR specialist meeting.

The responsibility of the hydraulic specialist is to carry out hydraulic analysis and modelling, to provide hydraulic information to assist aquatic scientists in determining ecological flow requirements. Researchers in environmental flow tend to quantify the water needs of the various biotic components in terms of parameters such as water depth and flow velocity (Rowlston et al, 2000). The primary product of hydraulic work comprises a series of relationships between flow rates and flow depth, flow velocity, wetted perimeter and water surface

width. Fluvial geomorphologists and ecologists use this information to make flow recommendations.

A number of studies have been conducted on the ecological effects of flow regulations on river biota (e.g., Armitage et al, 1987, Gore et al 1989, Morgan et al, 1991, Petts et al, 1993, Finlayson et al, 1994, Englund and Malmqvist, 1996, Ward and Stanford, 1979, Cortes et al, 2002). The influence of flow in regulated rivers on river biota and fauna can be interpreted through the physical response of the rivers to modified flow, which affects the aquatic habitats. Throughout the world, aquatic animals have been used to assess the biological integrity of stream ecosystems (Rosenberg and Resh, 1993, Barbour et al, 1996) as they offer a good reflection of the prevailing flow regime and water quality in a river.

For effective and ecologically responsible river management, an understanding of aquatic animals' habitats and links with the physical hydraulic parameters in rivers is therefore essential.

2.4.1 Defining hydraulic habitat for aquatic animals

Surface flow types or aquatic biotopes are distinct patches of hydraulic character and they have been used widely in the U.K and elsewhere for broad scale habitat assessment (Kemp, et al, 1999). Biotope identification is based on a visual assessment of the surface flow character at a site. The surface flow patches have been classified as follows:

- BSW - Broken standing waves,
- USW – Unbroken standing waves,
- CF – Chute flow,
- UF – Upwelling flow,
- RF – Ripple flow,
- NPF – No perceptible flow, and
- SBT – Smooth boundary turbulent.

The approach that uses the aquatic biotopes is predicated on the notion that a surface flow type represents a distinct suite of hydraulic conditions that have biological relevance. It has been used for differentiation of benthic habitat in river assessment and sampling programs (Newson and Newson, 2000, Palmer, et al., 2000). Many streams exhibit a diversity of surface flow types and their spatial arrangement changes significantly in association with even small flow changes (Dyer and Thoms, 2006). Thoms and Reid (2007) demonstrated that the surface flow types do not always provide a clear measure of benthic hydraulic conditions. While the surface flow types associated with higher energy conditions – BSW, USW and CF clearly differentiate from the lower energy surface flow types of UF, RF and NPF there is limited distinctiveness in terms of near bed flow character between these groups. Thus the use of surface flow types should be used with caution.

Application of hydraulic biotopes (suggested by Wadeson (1996) and Rowntree and Wadeson (1998)) for description of biota habitats in South Africa has been discussed by Jordanova and James (2004). Hydraulic biotopes are recognised primarily by the appearance of the water surface and reflect the governing hydraulic control, although this is rarely recognized explicitly. The main types recognised are backwaters, pools, glides, runs, riffles and cascades. Although identification of hydraulic biotopes is essentially descriptive and subjective, Rowntree and Wadeson (1998) maintain that they can be objectively characterized by quantitative hydraulic indices. The indices selected are the Froude number, the velocity/depth ratio, the Reynolds number, the shear velocity and the roughness Reynolds number. It should be noted that with the exception of the shear velocity (which is most relevant for describing near-bed conditions), these indices are dimensionless and give no indication of absolute values of depth or velocity which are what aquatic animals actually respond to. Although identification of a hydraulic biotope is useful in broadly categorizing the flow, which enables the appropriate control and hydraulic analysis method to be identified, it cannot provide values of flow depth and velocity for comparison with species preference.

The velocity-depth distributions and associated substrate and cover features provide a wide range of habitats for aquatic animals. Predictions of these hydraulic parameters are crucial for determining ecological flow requirements for fish and macroinvertebrates because aquatic animal occurrences are strongly correlated with the most important physicochemical factors in an ecosystem, which in turn influence species richness, population dynamics, resilience and abundance (Poff and Ward, 1990).

As fish and macroinvertebrates have been used in South Africa to assess EFRs, a discussion related to their physical habitats in term of hydraulics is presented in the following sections 2.4.2 and 2.4.3 respectively.

2.4.2 Hydraulic habitat for fish

The quality and quantity of available fish habitat is an indicator of occurrence of individual fish species. For the assessments and evaluation of the fish response to habitat conditions, it is essential that fish habitat and its components be properly defined (Bain and Stevenson, 1999):

- Habitat: "specific type of places where individuals, populations, or assemblages can find the physical and chemical features needed for life. Habitat features include water quality, spawning sites, feeding areas, and migration routes,"
- Habitat components: "single elements (such as velocity, depth or cover) of the habitat where an organism lives or occurs. Component is synonymous with attribute," and
- Habitat diversity: The number of different habitat types within a given area.

Fish experience upstream-downstream gradients in natural environmental variability. Such patterns of upstream-downstream environmental variation and the consequent adaptations of life history characteristics are reflected in the temporal variation in the community structure of fish (Schlosser, 1995). Environmental conditions of the upstream and downstream areas are associated

with changes in flow regime, channel morphology, and physical-chemical attributes such as temperature and oxygen. Structural characteristics of stream reaches consist of sequences of habitat channel units such as pools and riffles.

Hydraulic morphological units relevant to fish habitats as identified by Bisson, et al (1982) are:

1. Pools:
    - Bluff,
    - Lateral,
    - Obstruction,
    - Mid-channel,
    - Forewater,
    - Backwater, and
    - Edgewater.
2. Runs
3. Riffles:
    - High-gradient,
    - Medium-gradient, and
    - Low-gradient.

The links between physical and biological fish habitats have been studied (Probst et al, 1984, Todd and Rabeni, 1989, and Livingston and Rabeni, 1991), and it has been found that fish have affinities for particular habitat units, which differ between species, and by time of day and season.

However, the channel unit scale of resolution is not sufficient to describe habitat preferences for fish. For this reason, in each channel habitat unit, habitat at a smaller scale can be classified in different ways, which reflect the importance of variables such as flow depth, current velocity, current variability, substrate coarseness, and substrate heterogeneity.

One classification of channel habitat at a smaller scale is in term of subunits. Five subunits were proposed as midstream of riffles (MR), pool tail (PT), pool head (PH), fast-current edge (FE), and slow-current edge (SE). It has been shown that longitudinal variations in the abundance of fish are related to the abundance of subunit habitat rather than channel-unit habitat (Inoue and Nunokawa, 2002).

In South Africa fish habitat classification is determined by flow-depth classes. Kleynhans (1999) suggested that the hydraulic information necessary to characterize habitat for fish is depth-averaged velocity (*V*) and flow depth (*D*). Together with substrate and vegetation cover information, these are sufficient to broadly describe fish habitat. Further, he suggests that velocity and depth need only be specified coarsely, and has proposed the following four velocity-depth classes (hydraulic habitat types), as adapted from Oswood and Barber (1982):

- *Slow (<0.3 m/s) and shallow (<0.5 m)*: This includes shallow pools and backwaters,
- *Slow (<0.3 m/s) and deep (>0.5m)*: This includes deep pools and backwaters,
- *Fast (>0.3 m/s) and shallow (<0.3 m)*: Shallow runs, rapids and riffles fall in this class, and
- *Fast (>0.3 m/s) and deep (>0.3 m)*: Deep runs, rapids and riffles fall under this class.

For each velocity-depth class, the presence of features that provide cover for fish (i.e. refuges from high velocity, predators and high temperatures) are also taken into consideration (Kleynhans, 1999). These features include:

- *Overhanging vegetation*: thick vegetation overhanging water by approximately 0.3 m and not more than 0.1 m above the water surface. This includes marginal vegetation,
- *Undercut banks and root wads*: banks overhanging water by approximately 0.3 m and not more than 0.1 m above the water surface,

- *Stream substrate*: various substrate components (rocks, boulders, cobbles, gravel, sand, fine sediment and woody debris "snags") that provide cover for fish,
- *Aquatic macrophytes*: submerged and emergent water plants, and
- *Water column*: used to assess depth in relation to the size of fish.

The velocity-depth descriptions and associated substrate and cover features provide a broad categorisation of hydraulic habitats for fish that can be used through hydraulic modelling for EFRs.

2.4.3 Hydraulic habitat for macroinvertebrates

Riverbed substrate elements are important in the creation of suitable habitat for macroinvertebrates. Near-bed flows can be described by combining flow velocity, flow depth and substrate roughness to provide a means of quantifying the flow regime occurring within the microhabitats of stream benthos (Davis and Barmuta, 1989, Young, 1992, and Young, 1993).

The physical factors of flow depth and roughness height, longitudinal spacing, and density, can be used to explain the distribution and abundance of stream benthos. Five categories of near-bed flows related to habitat for macroinvertebrates were recognized (Davies and Barmuta, 1989):

- hydraulically smooth,
- hydraulically rough - chaotic flow,
- hydraulically rough - isolated roughness flow,
- hydraulically rough - wake interference flow, and
- hydraulically rough - skimming flow.

The longitudinal spacing between substrate elements was identified as the dimension of greatest importance in determining the nature of the flow microenvironment. If the roughness elements are far apart and the wake zone and vortex zone at each element are completely developed then isolated roughness flow will occur. When the roughness elements are placed close together and the

wake and vortex zones at each element are not completely developed a flow named wake interference will occur. Skimming flow occurs when the roughness elements are so close together that the flow skims the tops of the elements (Morris, 1954). The threshold between wake interference flow and skimming flow is physically not as well defined as the threshold between wake interference and isolated roughness flows.

Each of the near-bed flow regimes has a number of different flow zones where velocities are different. Flow velocity is an important hydraulic parameter that relates to the physical habitat of benthic invertebrates. From an analysis of near-bed flow velocities measured in a reconstruction of a cobble river bed in a flume, four hydraulically different habitats have been identified (Young, 1996):

- the exposed tops of roughness elements (TOPS),
- the sheltered lees of roughness elements (LEES),
- the exposed faces of roughness elements (FACE), and
- the partly sheltered areas mid-way between roughness elements (MIDS).

The flow zones have been suggested as more relevant to the prediction of benthos distribution than habitat classification in terms of pools, runs and riffles.

The differences in flow velocities between the four hydraulic habitat types were determined by Young (1996). Analysis of these measurements showed that both sheltered and exposed hydraulic elements exist in the near-bed regime and that there are significant differences between the four hydraulic habitat elements. The average velocities were 1.7 % and 14 % of the mean mainstream velocity in the sheltered habitat and in the partly sheltered habitat types respectively. This study shows that mean stream velocity does not characterize the habitat diversity of different roughness elements in cobble bed streams sufficiently for effective ecological interpretation and prediction. Benthic flow conditions are very complex, and the mean flow velocity and the mean flow depth are not considered useful in ecological studies (Statzner et al, 1988).

Velocities around boulders under natural field conditions can now be measured with the aid of highly developed instruments such as the acoustic Doppler velocitimeter (ADV). The ADV can be used to measure velocity at fine-scale for a given point of interest as well to estimate turbulence intensity and shear stress. Field velocities measurements around boulders showed complex flow patterns, especially when a large roughness element predominated in determining the flow configuration (Bouckaert and Davis, 1998). Near-bed velocities measured at the front and wake regions didn't show significant difference while the benthos differed significantly between these regions. This suggested that benthic macroinvertebrate communities may be influenced by turbulent regimes rather than directly by velocities and associated drag forces.

In South Africa hydraulic requirements of different invertebrate groups were tabulated, and it has been shown that some species or taxa are less sensitive to depth changes (O'Keeffe and Dickens, 2000). Therefore the main hydraulic parameter used in the classification of macroinvertebrate hydraulic habitat is depth-averaged velocity. This, together with substrate type and vegetation, may be used to broadly describe macroinvertebrate habitat. Two of the proposed habitat type definitions are modifications of the well-known macroinvertebrate-based biotope classifications: "Stones in Current" (SIC) and "Stones out of Current" (SOC). These definitions originate from the SASS (South African Scoring System) index for broadly assessing river condition on the basis of the sensitivity of macroinvertebrate families present at a site. These biotope definitions are not particularly meaningful from hydraulics (i.e. use of the term "current") or geomorphological (i.e. use of the word "stones") perspectives, and have therefore been modified. The proposed five habitat type classifications are (Jordanova et al, 2004):

- *SCS: Slow (< 0.3 m/s) flow over/around Coarse Sediments (size > 16mm) and bedrock*, and
- *FCS: Fast (> 0.3 m/s) flow over/around Coarse Sediments (size > 16 mm) and bedrock.*

The SIC and SOC substrate classifications have been modified to include substrates other than gravels (equivalent of "stones" in the original biotope classification), although it is recognised that large gravel and loose cobbles generally provide better substrate habitat than boulders and bedrock for rheophilic taxa. Un-embedded sediments with interstitial spaces also provide superior quality habitat than embedded sediments. The quality of substrate provided by submerged and emergent (partially submerged) coarse sediments also differs, and relative flow depth therefore needs to be taken into account when evaluating the suitability of these two habitat types.

- *SV: Slow (< 0.3 m/s) flow through Vegetation*, and
- *FV: Fast (> 0.3 m/s) flow through Vegetation*.

These two habitat types include both fringing and aquatic vegetation. Leafy vegetation is recognised as providing more suitable habitat for vegetation-dwelling taxa than, for example, sedges or reed stems.

- *SFS: Slow (< 0.3 m/s) flow over Fine Sediments (size < 16mm)*

This habitat type includes sediments ranging from clays and silt to gravels. The abrasive action of mobile sediments (particularly sand) reduces the quality of this habitat type for target macroinvertebrate taxa.

The proposed habitat types have been classified hydraulically using only velocity, with depth incorporated through relative submergence of coarse substrates and bedrock (FCS and SCS categories). A threshold velocity of 0.3 m/s is used to distinguish between slow and fast flow, and additional divisions of these categories may be required, e.g. very slow (< 0.1 m/s) and very fast (> 0.6 m/s). These velocity classes will require refinement based on future development and testing. Velocity is defined by cross-sectional average values, recognising that the spatial distribution of velocity is complex and highly variable in rivers characterised by large relative roughness under low flow conditions.

2.5 Low Flow Hydraulics

From the discussion above (section 2.4.2 and 2.4.3) it can be seen that physical habitats of aquatic animals are linked to the velocity and depth distributions. The bed of a river under low flow conditions affects the velocity and depth distributions. The hydraulics under low flow conditions, where the flow depth is the same order of magnitude as the bed material size, is very complex, and knowledge is limited. Under such conditions, flow within the channel is characterised by increasing resistance as well as causing flow separation and turbulent velocity fluctuations making estimation of the depth and velocity and their distributions very difficult. On the other hand under low flow there is a wide diversity of the physical habitats. Understanding of flow regimes with relatively large bed elements as well as vegetation influencing overall flow resistance is essential for environmental studies such as Reserve determination, river restoration and rehabilitation in which hydraulic parameters are used for characterizing aquatic animals' habitats.

Hydraulics under low flow is known as a condition of large-scale roughness. Successful prediction of flow resistance of the large-scale roughness depends on general understanding of the nature of the flow resistance, and application of the appropriate approaches for its prediction. Open channel flow resistance and approaches that have been developed internationally for predicting flow resistance under different conditions governed by roughness scales are discussed below.

2.5.1 Open channel flow resistance

Flow resistance describes a process in river streams by which the physical shape and bed roughness of the channel control the depth, width and mean velocity of flow in the stream. Theoretical aspects of open channel flow resistance are documented in some publications such as Leopold et al (1960), Rouse (1965), Bathurst (1982), and Yen (2002). In natural open channels the resistance to flow arises from various energy loss mechanisms associated with form resistance, channel irregularity, channel curvature and drag induced by objects in the flow,

including vegetation. The flow resistance in an open channel could be combined into four contributing components (Yen, 2002):

- Skin friction,
- Form resistance,
- Wave resistance, and
- Flow unsteadiness.

Prediction of flow resistance in natural open channels is therefore a complex task.

Successful prediction of flow resistance depends on an understanding of flow resistance phenomena as well as application of an appropriate approach for this prediction. Channel roughness and the presence of vegetation are the main flow resistance sources in most situations.

The relative depth, y/h, (where y is a flow depth, and h is the bed roughness height) describes the average degree of submergence of the surface roughness and it used to distinguish three flow regimes related to scale of bed roughness: large, intermediate and small (Bayazit, 1976; Bathurst et al, 1981; Bray, 1987). Bathurst et al (1981) proposed roughness scales classifications using D_{50} or D_{84} as follow:

- $y/D_{50} < 2$ or $y/D_{84} < 1.2$ – large-scale roughness,
- $< y/D_{50} < 7.5$ or $1.2 < y/D_{84} < 4$ – intermediate-scale roughness, and
- $y/D_{50} > 7.5$ or $y/D_{84} > 4$ – small-scale roughness.

Lawrence (1997) strongly stated: "a fundamental dimensionless parameter for evaluating overland flow hydraulics is a measure of the extent of the inundation of the surface roughness, as this parameter determines the dominant physical mechanism controlling the frictional resistance to flow." She distinguished three flow regimes by relative depth Λ defined as the ratio of flow depth y and the characteristic roughness scale for the surface h: $y/h > 4$, $1 < y/h < 4$ and $y/h < 1$. Three equations describing the dependence of the frictional resistance (f) on the relative submergence for each of the flow regimes were proposed. Available published field and laboratory data were used for evaluation of the proposed

equations. The frictional resistance (f) is plotted as a function of an inundation ratio, ($\Lambda = y/h$) in Figure 2-1.

Figure 2-1 demonstrates significant changes of flow resistance f with the roughness scales. It can be seen that highest flow resistance was recorded for the relative submergence of 1. It also can be seen that for relative submergences higher than 10, for the condition of small-scale roughness, the friction resistance f is not constant yet. It is apparent (Figure2-1) that the intermediate scale roughness condition extends for a range of inundation ratio greater than 7.5.

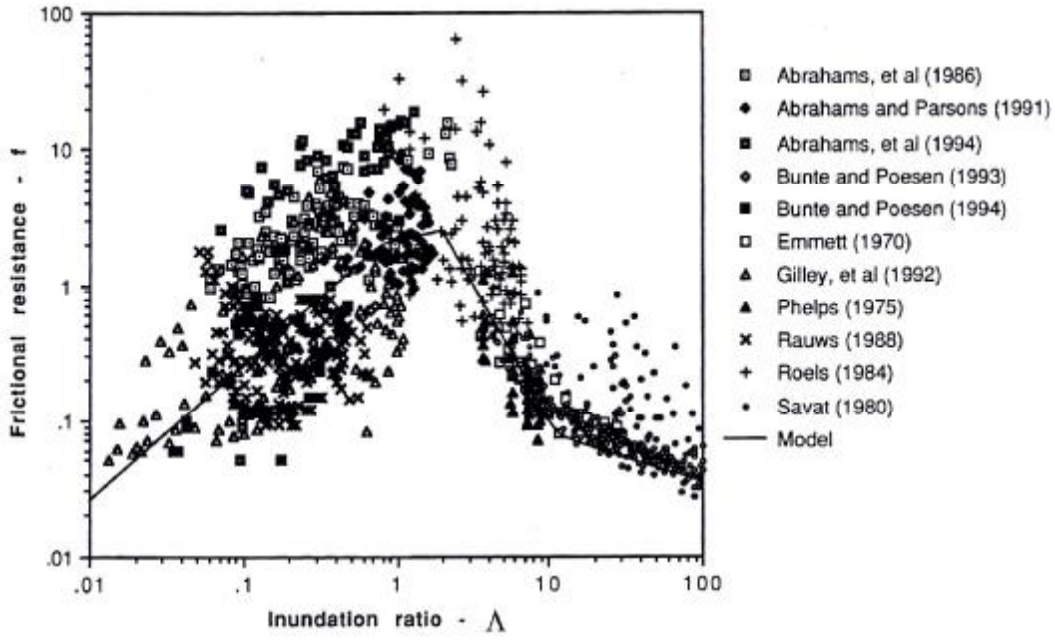

Figure 2-1 Frictional resistance as a function of flow inundation (Lawrence, 1997)

The flow regimes with small, intermediate and large-scale roughness are characterized by very different functional dependencies of resistance origin. Well-inundated flows can be described by rough turbulent flow hydraulics. In this regime, the roughness elements are very small relative to the flow depth, and they do not significantly alter a one-dimensional flow field. When the roughness is at intermediate scale, the size of the roughness elements relative to the flow depth controls the degree of vertical mixing in the flow so that frictional

resistance tends to decrease very rapidly with increasing depth of flow. For large-scale roughness, when the flow depth is less than or equal to the height of the substrate, the drag force derived from individual roughness elements cause most of the flow resistance. Lawrence also presents models for the prediction of large- and intermediate-scale flow resistance for very shallow overland flows rather than flow over boulders in rivers. Also, the resistance is represented by the Darcy-Weisbach friction factor *f*, and Darcy-Weisbach is a surface resistance equation, which is not really appropriate for large-scale roughness conditions.

Vegetation plays a vital role in protecting the bed and banks from erosion, and preventing scour as well as providing environmental habitats for aquatic animals. On the other hand, vegetation increases flow resistance by increasing roughness and reducing channel capacity due to its bulk and the increased turbulence around trees, vines and brush. Its effects therefore need to be fully understood in order to describe and predict river processes.

Flow resistance of small-scale, intermediate-scale and large-scale roughness as well as the influence of vegetation on flow resistance is discussed in the following sections.

2.5.2 Flow resistance of small-scale roughness

When we consider the flow resistance of small-scale roughness, the boundary resistance is the result of shear and pressure forces acting on the grains comprising the boundary, and the applied force per unit plan area is balanced by a resisting boundary stress

$$t_0 = gRS \qquad 2.1$$

where τ_0 : shear stress at the boundary,

γ : specific weight of fluid,

R : hydraulic radius, and

S : longitudinal bed slope.

The proportionality between boundary shear and average flow velocity can be described by (e.g. Henderson, 1966)

$$t_0 = arV^2 \qquad 2.2$$

where a : dimensionless coefficient,

r : fluid density, and

V :average flow velocity.

Combining equations (2.2) and (2.3) gives

$$V = \sqrt{\frac{g}{a} RS} \qquad 2.3$$

where g is the gravitational acceleration.

Various equations, based on the assumed proportionality between boundary shear and average flow velocity have been proposed. All of these account for the resistance processes with a single coefficient of resistance (Bathurst, 1982). The most commonly used equations are the following:

Darcy-Weisbach:

$$V = \sqrt{\frac{8g}{f}} \sqrt{RS} \qquad 2.4$$

where f is Darcy-Weisbach friction factor.

Chézy:

$$V = C\sqrt{RS} \qquad 2.5$$

where C is Chézy resistance coefficient.

Manning:

$$V = \frac{1}{n} R^{2/3} S^{1/2} \qquad 2.6$$

The Manning equation has become the most popular resistance equation for natural rivers. Some publications such as "Guide for Selecting Manning's Roughness Coefficients for Natural Channels and Flood Plains" (US Geological Survey, 1989) describe procedures for determining the flow resistance in natural open channels using the Manning equation (2.7) where the value of n indicates not only the roughness of the wetted perimeter but also the effect of all types of irregularity. The procedure involves, first, the selection of a basic value of n_b for a straight, uniform, smooth channel in natural materials that represents the skin friction, and then estimation of five factors regarding irregularity of the surface of the channel sides and bottom, variations in shape and size of cross sections, obstructions, vegetation and meandering of channel.

According to US Geological Survey (1989) the value of n for natural channels and flood plains can be calculated as

$$n = (n_b + n_1 + n_2 + n_3 + n_4)m \qquad 2.7$$

where n : Manning resistance coefficient,

n_b : basic value of n for a straight, uniform, smooth channel in natural materials,

n_1 : correction factor for the effect of surface irregularities,

n_2 : value of variations in shape and size of the channel cross section,

n_3 : value for obstructions,

n_4 : value for vegetation and flow conditions, and

m : correction factor for meandering of the channel.

The Manning's equation has come to be the most widely used resistance equation in practical river hydraulics. Tables of values of Manning's n for different surface roughnesses are presented in most open channel flow textbooks.

Various refinements have been made to the friction factor estimation. The ASCE Task Force on Friction Factors in Open Channels (1963) reviewed the information available at the time and recommended using f rather than n because it correlates

better with experimental data over a wide range of conditions. The following equations are recommended for estimating *f*.

For hydraulically rough flow:

$$\frac{1}{\sqrt{f}} = c\log\left(\frac{aR}{k_s}\right) \qquad 2.8$$

For hydraulically smooth flow:

$$\frac{1}{\sqrt{f}} = c\log\left(\mathrm{Re}\frac{\sqrt{f}}{b}\right) \qquad 2.9$$

For transitional flow:

$$\frac{1}{\sqrt{f}} = -c\log\left(\frac{k_s}{aR} + \frac{b}{\mathrm{Re}\sqrt{f}}\right) \qquad 2.10$$

where *Re* : Reynolds number and

k_s : Nikuradse roughness.

The Task Force presented values of the coefficients *a*, *b* and *c* derived from various data sets. Representative values are $a = 12$, $b = 2.51$ and $c = 2$.

Values of k_s for concrete and masonry surfaces are presented in most open channel textbooks. Values range from 0.15 mm for very smooth concrete to 1.5mm for gunite or shot concrete to greater than 5 mm for rubble masonry.

2.5.3 Flow resistance of intermediate-scale roughness

From laboratory experiments (Bayazit, 1976) it was found that once relative submergence, y/h is less than a value of 3.3, the resistance of the flow is higher than that predicted by the logarithmic resistance equation (2.8) for small-scale

roughness, therefore the resistance equations for small-scale roughness are not appropriate for these cases. When the relative submergence, *y*/*k* lies between 1 and 3.3, both, form drag and skin friction contribute significantly to flow resistance, and the roughness is intermediate-scale.

The total shear stress, τ_0 for the condition of the intermediate-scale roughness can be expressed in dimensionless form as the sum of two components (Roberson and Wright, 1973)

$$\frac{t_s}{t_0} + \frac{t_r}{t_0} = 1.0 \qquad 2.11$$

where τ_s : shear stress on the background surface, and

τ_r : effective shear stress due to drag of the discrete roughness elements.

The effective shear stress due to drag of the discrete roughness elements, τ_r is obtained as follows

$$t_r = \frac{l F_d}{A_b} \qquad 2.12$$

where λ : large roughness element concentration,

F_d : drag force of the roughness elements, and

A_b : base area of the roughness elements.

The roughness concentration is proposed to be defined by

$$l = n\frac{A_b}{A_t} \qquad 2.13$$

where n is number of roughness elements with base area A_b in a total boundary area A_t.

The drag of the roughness element can be related to an approach velocity by

$$F_d = C_d \int_{A_p} \frac{1}{2} r \overline{V}^2 dA_p \qquad 2.14$$

where C_d : drag coefficient,

$\overline{V}$: approach velocity, and

A_p : projected area of the roughness element.

The drag coefficient, C_d was determined to be 1.70 from an experimental study by Mirajgaoker and Charlu, (1963) who studied flow in flumes with sand and gravel.

Hey (1979) modified the Colebrook-White equation (2.8) making explicit allowance for the effect of cross-sectional shape, differences in bed and bank roughness and nonuniform sediment on the resistance to flow

$$\frac{1}{\sqrt{f}} = 2.03 \log\left(\frac{a R'}{3.5 D_{84}} \right) \qquad 2.15$$

where a :coefficient varies with the cross-sectional geometry of flow, and

R' : effective hydraulic radius.

Field data were used to evaluate the proposed flow resistance equation (2.15). Equation (2.15) is recommended for use when R/D_{84} is higher than 1 (Thorne and Zevenbergen, 1985).

The friction factor equation for fully developed turbulent flow can also be expressed in power form, i.e.

$$\frac{1}{\sqrt{f}} = a \left(\frac{y}{D_g} \right)^b \qquad 2.16$$

where a : coefficient,

b : exponent, and

D_g : sediment size characteristic.

Field data from natural gravel-bed rivers have been used for development of the friction factor equations for different sediment characteristics (Bray, 1979) given by

$$\frac{1}{\sqrt{f}} = 1.78\left(\frac{y}{D_{90}}\right)^{0.268} \qquad 2.17$$

A friction factor equation for the variation of $1/f^{1/2}$ with R/D_{50} for the relative submergence of $1<R/D_{50}<200$ is (Griffiths, 1981)

$$\frac{1}{\sqrt{f}} = 1.33\left(\frac{R}{D_{50}}\right)^{0.287} \qquad 2.18$$

It can be seen that the relative submergence for which the equation (2.18) was developed covers two roughness categories, intermediate and small-scale roughness.

A similar equation describing the dependence of the friction resistance on the relative submergence for the intermediate scale was proposed by Lawrence (1997):

$$f = 50\left(\frac{h}{y}\right)^2 k^2 \qquad 2.19$$

where k is the von Karman's constant in turbulent velocity profile

Nikora et al (2001) suggested that double averaged momentum equations could be used as a natural basis for the hydraulics of rough-bed open channel flows. Relationships for the vertical distribution of the total stress for two-dimensional, steady, uniform, spatially averaged flow over a rough bed with flat free surface were derived. The following relationships for the condition of the intermediate-scale roughness (Eqs 2.20 and 2.21) were suggested

$$\sqrt{\frac{8}{f}} = \frac{a}{g}\frac{m}{H}\frac{d}{H} \qquad 2.20$$

or

$$f = \frac{8g^2}{a^2 m^2}\left[\frac{H}{d}\right]^2 \qquad 2.21$$

where α : slope,

m : parameter depending on roughness geometry,

d : boundary between logarithmic and linear flow regions, and

H : maximum flow depth.

2.5.4 Large-scale roughness

Under low flow conditions the main source of energy loss in water flowing over a rough surface is the generation, spreading, and dissipation of vortices from the wake and separation zones behind each roughness element. Three basic flow types have been denoted as isolated-roughness flow, wake-interference flow, and quasi-smooth (or skimming) flow (Morris, 1954). Isolated-roughness flow occurs when roughness elements are far apart, and the individual elements act as isolated bodies, developing drag forces on the flowing water. Under this condition, the wake zone and vortex-generating zone at each element are completed and dissipated before the next element is reached. Wake-interface flow appears with roughness elements placed sufficiently close together that the zones of separation and vortex generation and dissipation associated with each element are not completed before the next element is encountered. Quasi-smooth or skimming flow results when the roughness elements are so close together that the flow skims the tops of the elements. Under this condition, there will be regions of dead water containing stable vortices between the elements.

A number of studies have been carried out to investigate flow resistance over rough surfaces with different relative submergences, and methods and equations for its prediction have been proposed (Dittrich and Koll, 1997; Lawrence, 1997; Lawrence, 2000; Nikora et al, 2001; Smart et al, 2002).

Various attempts at prediction of flow resistance under large-scale roughness conditions have resulted in a number of different approaches that can be classified into the following groups:

- Non-dimensional semilogarithmic,
- Dimensional power,
- Non-dimensional power,
- Deterministic, and
- Numerical.

Nondimensional semilogarithmic approaches

Semi-logarithmical approaches have been based on boundary layer theory, and these are of the form:

$$\frac{1}{\sqrt{f}} = c_0 \log\left(\frac{R}{c_2 D_x}\right) + c_1 \qquad 2.22$$

where f : Darcy-Weisbach friction factor,

R : hydraulic radius,

D_x : x percentile particle grain size,

c_0, c_1, c_2 : constants.

A number of equations have been developed for gravel-bed channels that take into account the effect of cross-sectional shape, differences between bed and bank roughness, and the effect of nonuniform sediment on flow resistance.

Bathurst (1985) validated application of the semilogarithmic resistance equation (equation (2.15)) that has been developed for intermediate scale roughness, for application to large-scale roughness conditions. He concluded that equation (2.15) under-predicts flow resistance, and proposed the following equation (2.23)

$$\left(\frac{8}{f}\right)^{1/2} = 5.62 \log\left(\frac{y}{D_{84}}\right) + 4 \qquad 2.23$$

where y is flow depth.

When bed roughness elements are large relative to flow depth, determination of the hydraulic radius as the ratio of flow area to wetted perimeter becomes ambiguous. The volumetric hydraulic radius (R_v) is therefore proposed by some researchers to be used instead of the conventional hydraulic radius (e.g., Bathurst et al, 1981; Smart et al, 2002). The volumetric hydraulic radius is defined as the volume of overlying water per unit plan area of bed.

Smart et al (2002) proposed a flow resistance equation in terms of the volumetric hydraulic radius given by

$$\frac{U}{U^*} = 2.5\ln\left(\frac{R_v}{d}\right) + B \qquad 2.24$$

where d : representative roughness length characterizing the bed material,

B : general coefficient,

U : mean flow velocity, and

U^* : bed shear velocity.

Nondimensional power approaches

Several investigators (Bray, 1979; Griffiths, 1981; Bathurst, 2002) have developed nondimensional power equations based on field data for gravel rivers. A general form of the nondimensional power equation is:

$$\frac{1}{\sqrt{f}} = b_0\left(\frac{R}{b_2 D_x}\right)^{b_1} \qquad 2.25$$

where b_0, b_1, b_2 are constants.

Bathurst (2002) analysed 27 field data sets to derive separate at-a-site relationships and investigated how they could be collapsed into a single formula. It was suggested that flow resistance can be more accurately described by a power law than by a semi-logarithmic law. Relative submergence based on D_{84} was found to be the primary predictor of the flow resistance. Two power law relations

related to channel slope were identified, and two equations were therefore proposed.

Channel slope, $S < 0.8\%$:

$$(8/f)^{1/2} = 3.84\ (y/D_{84})^{0.547} \qquad 2.26$$

Channel slope, $S > 0.8\%$:

$$(8/f)^{1/2} = 3.10\ (y/D_{84})^{0.93} \qquad 2.27$$

Field data for investigating the flow resistance and development of the equations (2.26 and 2.27) have not been distinguished for the different scale roughnesses. The range of the relative submergence of field datasets used for development varied from 0.37 to 11.4.

Dimensional power approaches

Another empirical approach to derive a relationship for flow resistance is by means of power laws. The relationship between the mean velocity and the discharge can be formulated as:

$$V = c\ Q^m \qquad 2.28$$

where c and m are regression coefficients.

Some of the existing power approaches for resistance prediction under low flow conditions introduce additional variables such as the channel slope and the roughness parameter (D_x). Rickenmann (1994, 1996) proposed the following equations for different slopes:

Channel slope, $S>0.6\%$:

$$V = 0.37\ g^{0.33} Q^{0.34}\ S^{0.20}\ D_{90}^{-0.35} \qquad 2.29$$

Channel slope, $S<1\%$:

$$V = 0.96\ g^{0.36} Q^{0.29}\ S^{0.35}\ D_{90}^{-0.23} \qquad 2.30$$

Based on field data from 21 streams in the Rocky Mountains of Colorado, multiple-regression analyses yielded an equation for predicting Manning's resistance coefficient (n) as a power function of the hydraulic radius and the friction slope (Jarrett, 1984):

$$n = 0.39 R^{0.38} S^{-0.16} \qquad 2.31$$

As flow resistance under low flow conditions depends on the roughness geometry, its determination requires definition of a roughness parameter. It can be seen that a characteristic index of grain roughness (D_{90}) is incorporated into Eqs 2.29 and 2.30, while the hydraulic radius is used in Equation 2.31. A single grain size gives a coarse description of the roughness geometry, while calculation of the hydraulic radius based on the wetted perimeter is problematic when flow depth and height of substrate are of the same order of magnitude (Aberle and Smart, 2003). The standard deviation of the bed elevation as characteristic of roughness structure of rough beds was therefore introduced and based on laboratory experiments the following equation was proposed by Aberle and Smart (2003):

$$V = 0.96 g^{0.20} S^{0.20} q^{0.60} s^{-0.40} \qquad 2.32$$

where g : acceleration due to gravity,

q : specific discharge per unit width,

s : standard deviation of the bed elevations.

Flow resistance depends strongly on the bed roughness geometry, however, determination and application of a roughness parameter to be incorporated into resistance prediction is still problematic. On the one hand, it should be measurable in the field but at the same time it should give a realistic description of the bed geometry. Bed roughness characterization is therefore discussed below.
Aberle and Smart (2003) investigated the statistical properties of a series of bed profiles in order to quantify the effect of bed roughness on flow resistance. Analysis of longitudinal bed profiles from laboratory experiments identified the standard deviation (s) of the bed elevations as an appropriate roughness

parameter. The following equation for prediction of flow velocity over a rough bed was proposed:

$$\bar{u} = 0.96 g^{0.20} S^{0.20} q^{0.60} s^{-0.40} \qquad 2.33$$

where g : acceleration due to gravity,

S : slope,

q : discharge per unit width,

s : standard deviation of the bed elevation.

It was concluded that the use of the standard deviation as a characteristic roughness leads to an improvement in estimation of flow resistance compared to the results obtained by using only the characteristic of sediment size (D_n) as a roughness parameter.

Deterministic approaches

In a natural stream with bed roughness elements that are comparable in size to flow depth, large elements act as obstacles to the flow. When flow is forced around the large elements, drag forces are exerted on those elements and the momentum of flow is locally reduced, thus modifying the velocity distribution. The bed roughness configuration affects the overall velocity distribution. Prediction of the cross-sectional averaged velocity as well as the velocity distribution over a rough river bed requires partitioning of the total bed shear component into a fluid component and a form-drag component associated with flow around bed roughness elements (Wiberg and Smith, 1991).

For an isolated roughness element skin friction is not significant, and the drag force (F_d) causing the flow resistance can be described by

$$F_d = \frac{1}{2} C_d \, r \, V_x^2 \, A_d \qquad 2.34$$

where C_d : drag coefficient,

ρ : density of water,

V_x : approach velocity, and

A_d : cross-sectional area of roughness elements exposed to flow.

The cross-sectional area of the roughness elements exposed to flow (A_d) is a function of the roughness element shape and size,

$$A_d = s_1 d_y d_z \qquad 2.35$$

where s_1 : shape related factor,

d_y : transverse dimension of a roughness element, and

d_z : submerged height of a roughness element.

If a roughness element has semi-elliptical shape then the shape related factor (s_1) is $s_1=\pi/4$.

The drag force is assumed to be transferred to the bed as a shear stress (τ_s) acting on area of bed (A_s) i.e.

$$F_d = t_s A_s = t_s s_2 d_y d_x \qquad 2.36$$

where s_2 : another shape related factor, and

d_x : longitudinal dimension of a roughness element.

For a semi-elliptical shape of roughness element, the shape related factor is $s_2=s_1=\pi/4$.

If the shear force is transferred only by the roughness elements, then the average shear stress over a particular area of the bed is

$$t_0 = t_s p \qquad 2.37$$

where p is a ratio of basal area of a roughness element to the area of bed considered.

Combining equations (2.34 – 2.37) an approach velocity can be calculated as (Smart et al, 2002)

$$V_x = \sqrt{\frac{2t_0 s_2 d_x}{C_d r s_1 d_z p}} \qquad 2.38$$

Jonker et al (2001) proposed an equation for mean flow velocity in rivers under conditions of large-scale roughness:

$$V = \sqrt{2g}\sqrt{\frac{dS_o}{C_x}} \qquad 2.39$$

where d : cobble diameter,

S_o : channel gradient, and

C_x : resistance coefficient.

Extensive published data were used for evaluation of the applicability of equation (2.39). From these data, corresponding values of resistance coefficients (C_x) were calculated and plotted (Figure 2.2). Correlation between resistance coefficient (C_x) and relative submergence (R/d_{50}) was derived as:

$$C_x = 0.5285\left(\frac{R}{d_{50}}\right)^{-2.166} \qquad 2.40$$

where R is the hydraulic radius.

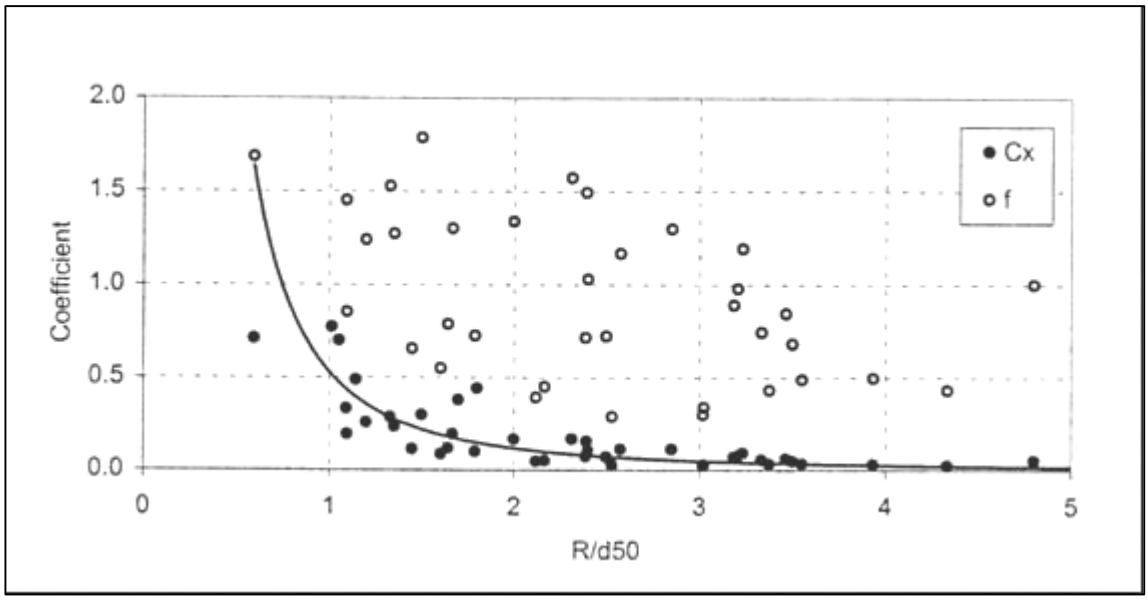

Figure 2-2 Relationship between C_x and R/d_{50} (Jonker et al, 2001)

It can be seen (Figure2-2) that good correlation exists between C_x and R/d_{50}, but values of the Darcy-Weisbach resistance coefficient f as calculated from the Darcy-Weisbach equation do not explain the data well. It also is evident that only one data point for relative submergence less than one was used. It is apparent that good correlation exists between theoretical and experimental values under conditions of intermediate scale roughness, but further investigation for the condition under large-scale roughness is still required.

Wohl and Ikeda (1998) used seven different configurations of bed roughness as well as a plane bed to study the effect of bed roughness configuration on velocity distribution. Sixteen conditions of varying discharge and slope were performed for each configuration. The flow resistance for each configuration was calculated in terms of the resistance coefficient:

$$l_d = 22gdS_w / V^2 \qquad 2.41$$

where λ_d : resistance coefficient,

d : flow depth,

S_w : water surface slope, and

V : mean velocity.

Vertical velocity profiles were measured at 1 cm increments over the crest of the roughness elements. The laboratory results indicate the following:

- The velocity profile shape remains fairly constant for a given roughness bed configuration and slope as discharge increases.
- Velocity profiles become less linear at the measurement point immediately downstream from the roughness element as slope increases.
- The maximum value of flow resistance in term of the resistance coefficient (equation (2.41)) was observed for all values of discharge and slope for roughness length/height ratio of about 9.
- Longitudinal patterns of roughness elements create much less flow resistance than transverse patterns.

Using double averaged momentum equations, Nikora et al (2001) proposed the following equations for the condition of the large-scale roughness:

$$\sqrt{\frac{8}{f}} = Cm\frac{H}{d} \qquad 2.42$$

or

$$f = \frac{8}{C^2 m^2}\left[\frac{d}{H}\right]^2 \qquad 2.43$$

where C is parameter of velocity distribution.

Lawrence (1997) investigated flow resistance under large-scale roughness condition and proposed the following equation:

$$f = 8nh^2 C_d MIN\left[\frac{p}{4}, \frac{y}{h}\right] \qquad 2.44$$

where n : number of roughness elements per unit area,

C_d : drag coefficient of a roughness element,

MIN [a,b] : the minimum possible value taken on by either variable a or b.

Further investigation and laboratory experiments were performed (Lawrence, 2000), and a drag model was developed that accounts for the contributions of individual roughness elements to total flow resistance under the large-scale roughness condition was proposed. A proposed equation for calculation of flow resistance in terms of friction factor f is:

$$f = \frac{2P\mathrm{A}(y/h)C_d}{[1-PV(y/h)]^3} \qquad 2.45$$

where P : fraction of surface covered by roughness elements,

C_d : drag coefficient,

$A(y/h)$: factor accounts for the change in frontal area with inundation,

$V(y/h)$: factor to account for volume of roughness elements.

The drag coefficient (C_d) drops off rapidly once the roughness elements become submerged. Based on experimental data with 18 % areal coverage, the following relationship was proposed:

$$C_d = A + B\tanh[a(y/h-1)] \qquad 2.46$$

where A, B and a are fitted parameters.

Flow resistance for the large-scale roughness condition is associated with high values of effective frictional factor. These high resistance values may result from increased resistance due to the effects of hydrostatic wave drag around elements associated with deformation of the free surface on protruding or marginally inundated roughness elements, and the drag force derived from individual roughness elements. This regime is very complex and therefore cannot be explained using simple drag models only (Lawrence, 2000). The mixing length model (following) that was developed for intermediate scale roughness was extended into the range of large-scale roughness for moderate Reynolds numbers (Lawrence, 2000).

Lawrence (2000) proposed the following mixing length model for the large-scale, which combines the turbulent mixing length scale with the height of the roughness elements as

$$f=10C_sP \qquad 2.47$$

in which C_s is a roughness height scaling coefficient and P is the fractional cover.

Ferro (2003) presented an attempt to modify the mixing length and drag models proposed by Lawrence (1997, 2000) and a quasi-theoretical model that was calibrated by available experimental gravel bed data. Using experimental data (Ferro and Giordano, 1991; Baiamonte and Ferro, 1997; Ferro, 1999) the drag coefficient (C_d) values were calculated by the following equation deduced by equation 2.45:

$$C_d = \frac{1}{2\Gamma}\left[1-\frac{2\Gamma}{3(y/d_{50})}\right] \qquad 2.48$$

where Γ is the concentration of coarse elements, defined as $\Gamma=100$ (N/N_{max}) on with N is number of randomly arranged coarser elements and N_{max} is maximum number of coarser elements it is possible to arrange in the reference area.

By the statistical analysis of the available experimental data, a power equation for f was proposed (Ferro, 2003):

$$f = 10^{b_0}\left(\frac{y}{D_{84}}\right)^{b_1} Fr^{\,b_2} \qquad 2.49$$

where b_0, b_1 and b_2 are numerical coefficients.

Relationships between the numerical coefficients (b_0, b_1 and b_2) and the concentration (Γ) for a given ratio of median size of a coarse to a median size of fine components were proposed.

Numerical approaches

The flow structure over a rough bed is very complex, and numerical modelling is an option for simulation of such a complex phenomenon. Recent advances in numerical modelling mean that now it is possible to use two and three dimensional models to simulate flow patterns under complex flow conditions. Nicholas (2003) used Hydro2de to simulate flow within a braided reach of the Avoca River, New Zealand. Field measurements obtained at low flow conditions were used to validate performance of the model. Comparison of modelled and measured variables showed that field data exhibit greater spatial variability than modelled results, but generally the modelled results reproduced the systematic trends in measured data.

Two- and three-dimensional models are powerful tools that are now in common use for generating hydraulic information. Today, using such powerful tools simulation of flow patterns within channels, overbank flows, and flows in estuaries can be performed and show good correlation with field data (Hervouet and Van Haren, 1996; Connell et al, 1998; Stewart et al, 1999). This kind of modelling requires not only two-dimensional or three-dimensional software and an understanding of how to use it, but also requires comprehensive survey and field data. This kind of modelling is appropriate if the project requires a very detailed level of results.

2.5.5 Bed roughness characterization

Riverbed substrates influence properties of average flow, flow resistance, turbulence, and sediment motion. Characterization of a riverbed substrate for many different purposes such as channel roughness, bed load transport, and habitat description is therefore required as an essential part of river hydraulics and fluvial geomorphology (Wohl et al, 1996; Nikora et al, 1998). Flow resistance is controlled by substrate composition, and flow resistance prediction under small, intermediate or large-scale depends on quantitative description of the bed roughness. Methods for quantifying riverbed roughness are discussed below.

Nikora et al (1998) reviewed current methods for quantifying river bed roughness and combined them into two groups:

- Particle size approach, and
- Random field approach.

The first approach characterizes the surface of a riverbed by the characteristic diameter (D_n) that represents bed roughness, such as D_{50}, D_{84} or D_{90}. The second considers the bed surface as a random field of bed elevation.

Particle size approach

The purpose of the particle size approach is to evaluate the size distribution of bed particles and to produce one measure of sediment size, such as D_{50}, D_{84} or $D_{90.}$ This approach is widely used in river engineering, fluvial geomorphology, and stream ecology. The approach originated from Wolman (1954). Wolman (1954) proposed measuring the intermediate axes of 100 clasts sampled from a grid system, with the grid size determined by the size of the sampling area. This sample would represent the areal distribution of material of the bed. According to Wolman (1954), 100 clasts are sufficient to ensure that there are no significant differences between operators or between samples for a given operator (Wohl et al, 1996).

The techniques most often used for sampling bed surfaces can be divided into the following categories: areal, grid and transect. Grid and transect techniques are widely used for sampling coarse bed surfaces (D > 8 mm) but are not appropriate for small particles (Diplas and Sutherland, 1988).

Areal sampling:

An areal sample consists of the grains of the bed that are exposed to the flow within a predetermined area of the channel bed. The areal sample collected by using adhesives, clay or wax, is most often analysed as a frequency distribution by weight. The primary advantage of areal sampling is that adhesives remove the

smaller particle size range while the disadvantage is that it requires the sample area to be dry (Diplas and Sutherland, 1988; Flipp and Diplas, 1993).

Grid sampling:

This technique is widely used for sampling coarse bed surfaces in the field. Grid sampling involves the removal by hand of stones found at specific points. These points can be established on the bed surface by using predetermined distances on a survey tape. The simplest variant of grid sampling is known as the Wolman walk method where an operator would stop at each pace and remove the stone found under his toe, the eyes being averted or closed (Wolman, 1954). The grid sample is usually analysed as a frequency distribution of number. The use of the intermediate average diameter of each sampled stone is recommended (Hey and Thorne, 1983).

Transect sampling:

This approach is similar to the previous one, involving the collection of the grains that are located along a predetermined line. The volume of the sample depends on the axes of the removed particles that are normal to the line (Diplas and Sutherland, 1988). The transect samples are interpreted in terms of a frequency by weight or by number for a line sample.

Accuracy of surface sampling for coarse sediments is associated with operator and sampling errors, as well as with the choice of sampling procedure (Hey and Thorne, 1983; Wohl et al, 1996).

Random field approach

Another way to describe the bed roughness is a random field of bed elevations $Z(x, y, t,$ where x and y are the longitudinal and transverse coordinates, and t is time). In this approach, a quantitative description of riverbed roughness is reproduced by means of dimensional probability functions (m). From limited published information an important advantage of the random field approach that makes it preferable to the approach based on the use of the single particle size has

been recognised. Further investigation in using the random field approach for gravel-bed roughness characterization resulted in the development of a model based on the structure function parameterization (Nikora et al, 1998).

Standard deviation approach

Determination of flow resistance requires the definition of bed roughness geometry. As mentioned above, a single characteristic grain size (D_x) derived from the grain size distribution of the surface material is incorporated into large number of flow resistance equations (e.g., Bray, 1979; Bathurst, 1985, 2002; Hey, 1979; Jonker, 2001). Disadvantages of this approach have been reported and alternative parameters to be used as roughness definitions proposed (Nikora et al 1998; Smart et al, 2002; Aberle and Smart, 2003). The standard deviation of bed elevation s is one of the parameters that has been introduced as a new characterization of the riverbed geometry (Aberle and Smart, 2003). Through analysis of published experimental data sets of longitudinal bed profiles (Koll, 2002) it was shown that the use of the standard deviation s as a roughness parameter instead of the single grain size (D_x) leads to an improvement in prediction of flow resistance.

Volumetric hydraulic radius approach

As already mentioned, the hydraulic radius is a parameter that becomes ambiguous when the bed roughness is large relative to flow depth. The conventional hydraulic radius is the ratio of cross-sectional flow area to wetted perimeter, but estimation of the wetted perimeter for conditions where the roughness elements intersect the water surface is practically impossible. The volumetric hydraulic radius (R_v) and standard deviation of bed surface elevation (d_z) have therefore been proposed to be used to describe bed roughness for large-scale conditions (Smart et al, 2002). The volumetric hydraulic radius is defined as the volume of overlying water per unit plan area of bed, a definition used before by other researchers (Kellerhals, 1967; Bathurst et al, 1981). A practical procedure for determination of the volumetric hydraulic radius (R_v) and the standard deviation of bed surface elevation (d_z) in the field is given in Smart

(2001). A graphical representation of the volumetric hydraulic radius is shown in Figure2-3.

It is suggested that the standard deviation of bed surface elevations is a rational measure suitable for large relative roughness conditions. The results of the investigation showed that head-losses for large-scale relative roughness could be related to R_v/d_z. The exponent of R_v/d_z in power law resistance equations increases from 1/6 to more than 1/2 as relative roughness increases.

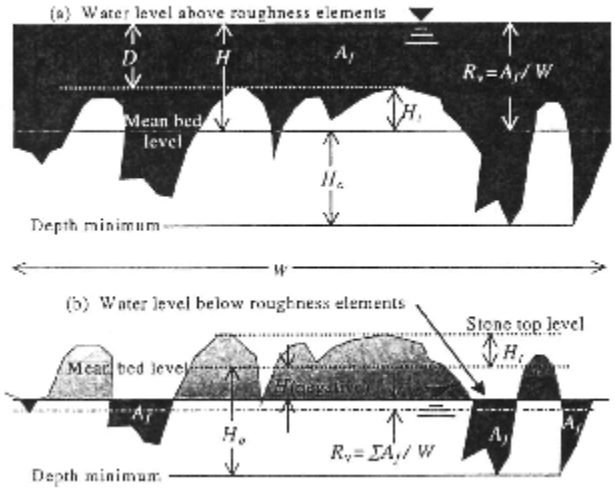

Figure 2-3 Graphical representation of the volumetric hydraulic radius (Smart et al, 2002)

From the above it is clear that the resistance of flow over rough beds with large and intermediate scales is a complex subject. Prediction of flow resistance requires understanding of the resistance phenomenon. When roughness elements are situated far apart, each acts as an individual body, creating different hydraulic habitats for aquatic animals. Investigations related to flow around a single bed roughness element is therefore discussed in the next section.

2.5.6 Vegetation and flow resistance

In-channel and riparian vegetation have significant effects on flow resistance. Presence of vegetation reduces the flow area, increases roughness and generates additional turbulence by oscillatory moment (Starosolszky, 1983). The influence

of vegetation on flow resistance has been widely investigated (Dawson and Charlton, 1988), and many recommendations have been proposed for prediction of the effect of vegetation on flow resistance.

There are three situations pertaining to the occurrence of vegetation in rivers and wetlands: flow through emergent vegetation, flow in channels with emergent vegetation boundaries, and flow in channels with discrete vegetation patches.

Several methods have been proposed for estimation of the resistance within a fully vegetated channel. By analysing the forces on vegetation under steady, uniform flow conditions, Petryk and Bosmajian (1975) derived an expression for the total Manning's n as:

$$n = n_b \sqrt{1 + \frac{C_D \sum A_i}{2gAL} \left(\frac{1}{n_b} \right)^2 R^{4/3}} \qquad 2.50$$

in which n_b is the Manning n value excluding the influence of vegetation, A is the cross-sectional area of the flow, A_i is the projected vegetation area and L is the length of channel under consideration.

In most cases where formulations of Manning's n include the drag coefficient (C_D), a value of C_D of about 1.0 is recommended. Based on experimental measurements, Li and Shen (1973) confirm a value of 1.2 for the cylinder Reynolds number greater than about 8×10^3 within the regime before laminar separation of the boundary layer occurs. Li and Shen (1973) used Petryk's (1969) linear superposition of velocity defect model to determine the variation of local drag coefficient in two basic, parallel and staggered, cylinder distribution patterns.

Lindner (1982) extended Li and Shen's (1973) work and proposed that the effective drag coefficient for a large group of cylindrical rods can be estimated as

$$C_{De} = \left(1 + 19\frac{d_p}{a_z} C_D\right) V_r^2 + \Delta C_D \qquad 2.51$$

The first term in equation (2.51) accounts for the narrowing effect of neighbouring cylinders and the second term accounts for the resistance due to gravitational force. In this equation d_p is the cylinder diameter, a_z is the transverse cylinder spacing, C_D is the value for a single cylinder in two-dimensional flow, and V_r is a velocity ratio given by

$$V_r^2 = 0.923\left(\frac{x_N}{a_x}\right)^{-0.374} + 0.61\left(\frac{z_N}{a_z}\right)^{1.33} \qquad 2.52$$

where a_x is the longitudinal cylinder spacing, x_N and z_N are the wake length and width respectively.

James et al (2001) proposed a simulation model to predict basic vegetation resistance by accounting for the fundamental processes involved. The model is based on force balance principles, and accounts for both bed roughness and vegetation resistance. The force applied to the vegetation is described using the well known drag force function with an effective drag coefficient.

Emergent vegetation is a common feature along river sides. Under such conditions, the additional resistance afforded by the vegetation is through momentum transfer across the interface between the vegetated zones, where basic resistance is high and the velocity low, and the clear channel zone where the basic resistance is relatively low and the velocity relatively high. Overall channel conveyance may be therefore considered by dividing the channel laterally into separate zones, and estimating the discharge for each individually.

Seven different longitudinal strip patterns of emergent vegetation were studied by James et al, 2001. All of these patterns contained the same total number of stems, with the same local density and the same overall areal coverage of 50% of the

channel area - only the arrangement pattern was different. The relationships between Manning's *n* and flow depth for all the strip patterns showed that the distribution of the strips has a significant effect on overall channel resistance. It was found that for basic vegetation resistance, Manning's *n* varies strongly with flow depth, suggesting that it is inadvisable to use a single value of *n* for channels with bank vegetation or instream strips of vegetation.

Some methods (Nuding, 1991 and 1994) for predicting the conveyance of channels with strips have been proposed, suggesting that vegetated zone discharge may be estimated by simply assuming the unaffected velocity throughout this region, and neglecting the zonal interaction.

Naot et al (1996) carried out an investigation on the hydrodynamics of turbulent flow in partly vegetated open channels. Three channel configurations were studied, consisting of a rectangular open channel with a vegetated bank, a vegetated corner and a vegetated floodplain. A phenomenological model was proposed to predict complex hydrodynamic behaviour. Two sets of experiments of three-dimensional turbulent flow in partly vegetated rectangular channels were conducted for comparison. It was found that an increase in vegetation density affects the streamwise velocity and the energy of turbulence until the nondimensional vegetation density (*N*) equals 32, after which the vegetated domain becomes practically impenetrable. The nondimensional vegetation density (*N*) was specified as:

$$N = 100nHD \qquad 2.53$$

where n : vegetation density (rods per unit area),

H : flow depth, and

D : averaged rod diameter.

For discrete vegetation patches there is also a significant form resistance contribution to overall resistance which is probably best addressed using a distributed drag force approach, similar to the treatment of individual stems in the

basic reed resistance models, but with the applied force balanced by the bed resisting force and vegetation drag components at a larger scale.

James et al (2001) reported experimental work on overall flow resistance of discrete patches. Fifteen different patterns were tested. For these patterns the areal coverage wasn't constant as for the strip experiments, and ranged from 12.5% to 50% of the channel area. Flow resistance in term of the Manning's *n* showed a general increase of *n* with areal coverage, but the wide spread in the values of *n* suggested that other influences are important. It was concluded that resistance is strongly influenced by the distribution pattern as well as the overall areal coverage. A simple method for predicting conveyance for channels with this kind of reedbed distribution has not yet been developed, and the issue is addressed in Chapter 7 of this thesis.

2.5.7 Flow patterns

Flow around a single bed roughness element

Flow around a single roughness element produces different flow patterns, thus presenting a wide range of hydraulic habitats for aquatic animals. As was discussed in sections 2.4.2 and 2.4.3, aquatic animals' habitats can be associated with physical hydraulic parameters. A review of investigations of flow patterns around a single element is presented here.

The patterns around a single bed element can be recognized as vortex systems, wakes, and separation points on the bed in front of the roughness element, and on the roughness element itself. Shamloo et al (2001) used a single hemisphere as a roughness element, and dye plumes which were introduced upstream of the hemisphere to study the formation of flow patterns. Four flow regimes around the hemisphere based on the relative depth were classified:

Regime 1: When the relative depth is greater then 4, a bed element does not affect the water surface, and the top layer of flow does not mix with the wake. The vortex system around the bed element consists of a horseshoe and arch-vortices.

Regime 2: If the relative depth is in the range of 1.3 to 4, the regime is similar to regime 1, except that surface wakes are apparent.
Regime 3: For relative depths in the range of 1 to 1.3, the free shear layer from the roughness of the body causes mixing through the whole depth of flow as well as some backward flow at the water surface.
Regime 4: When the relative depth is less then 1, the top of the roughness element is above the water surface and a Karman vortex street is present with a strong backward flow behind the element.

The wake geometry, the velocity field and bed shear are different for these four regimes. These show that a wide range of hydraulic flow regimes can exist around a single bed element.

Flow around a single cylinder positioned in an open channel (Regime 4) has been investigated and three-dimensional flow patterns have been identified (Graf and Yulistiyanto, 1998). Due to the presence of the cylinder, the flow separation is composed of a complex flow system, known as the horseshoe-vortex system (Figure 2-4).

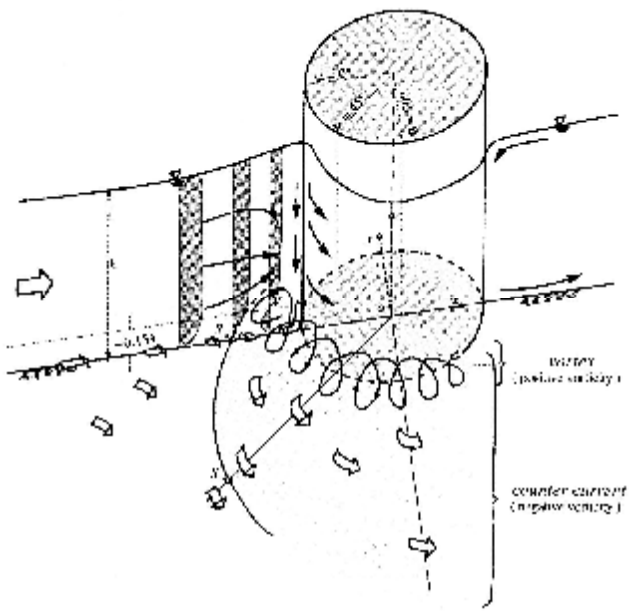

Figure 2-4 Scheme of the horseshoe-vortex system (Graf and Yulistiyanto, 1998)

An Acoustic Doppler Velocity Profiler was used to measure the complex vertical velocity distributions around the cylinder. The flow patterns around the cylinder can be described as follows:

- In the plane of symmetry, the horseshoe-vortex system consists of a vortex, driving a counter-current of negative vorticity,
- The system becomes stronger and closer to the base of the cylinder with increasing flow velocity,
- The horseshoe-vortex system stretches while moving around the cylinder in the streamwise direction. Downstream of the cylinder separation with flow reversal is evident, and
- The horseshoe-vortex system produces a high bed-shear stress beneath it.

Lloyd and Stansby (1997) investigated recirculating flow around a conical obstacle with a gently sloping side. Four shapes of conical obstacles called islands were tested for relative depths less than 1.0 (Regime 4). A "wake stability parameter" (S) proposed by Ingram and Chu (1987) was used to classify the island wakes into "vortex shedding" or "unsteady bubble" types. The stability parameter (S) is a measure of the stabilizing effect of bed friction relative to the destabilizing influence of transverse shear given by

$$S = \frac{c_f D}{h} \qquad 2.54$$

where c_f : bottom friction coefficient,
D : cross-stream diameter for the body, and
h : water depth.

The experiments were designed in such way that different stability parameters were examined. As the depth of the flow decreases, both the magnitude of the bed-friction coefficient (c_f) and the effective diameter of the island (D) increase. Experiments were performed for a range of the stability parameter (S) from 0.06 to 0.40, and blue dye was released upstream of the island to produce images of the recirculating wake zone. The results of the experiments showed that for small

values of the wake stability parameter (S <0.20) the island wakes were characterized by a well-organized vortex shedding system. When the stability parameter (S) increased, regular vortex shedding occurred, but moved further downstream. With S=0.4, any form of well-organized vortex shedding ceased to exist, and the wake appeared as an "unsteady bubble" flow, confirming that bed friction can act to suppress the development of vortex shedding in the wake of conical islands. During the experiments, the time taken for the dye-saturated wake to clear was recorded as well. The results showed that with S = 0.40 the time was approximately nine times longer than for S = 0.06.

Laboratory investigations of the transition from localized supercritical to sub-critical flow around a single roughness element were carried out by Zgheib (1994). In order to simulate the supercritical-to-subcritical flow transition around a single roughness element, smooth and angular rocks of different sizes and shapes were placed in a laboratory flume. During the investigation the following hydraulic conditions were identified:

- A deflect jet occurs at the upstream face of the roughness element, resulting from the impact of the flow on the roughness element,
- A spillway effect results from flow of water around the roughness element,
- Intermixing of flow happens along the sides of the roughness element where largest mean velocities appear,
- Hydraulic jumps transform flow from supercritical to sub-critical, and
- Tumbling flow is a condition of flow dominated by scattered regions of alternate acceleration and deceleration through critical flow over large bed elements.

Transitional tumbling flow of water around the single roughness element follows one of three possible surface profiles as shown in Figures 2-5 to 2-7.

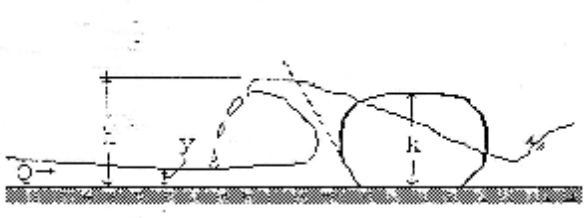

Figure 2-5 Backward breaking jet (Zgheib, 1994)

Figure 2-6 Stationary non-breaking jet (Zgheib, 1994)

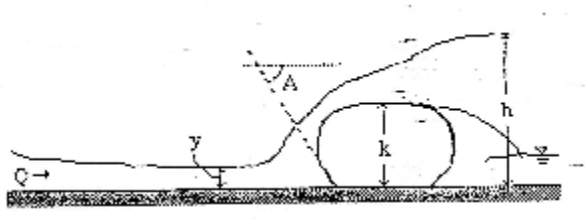

Figure 2-7 Forward shooting jet (Zgheib, 1994)

The conditions of occurrence of each profile depend on the roughness element size and shape, and flow condition. A dimensionless parameter in the form of the Froude number (*Fr*) is used to distinguish between the three surface profiles, i.e.

$$Fr = Q/(B-w)y^{3/2}g^{1/2} \qquad 2.55$$

where B : flume width,

w : width of the roughness element,

Q : discharge,

y : upstream flow depth, and

g : acceleration of gravity.

For $Fr > 18$, the forward shooting jet occurs (Figure 2-7), for $12 < Fr < 18$, all three surface profiles (Figures 2-5, 2-6 and 2-7) are possible, and for $Fr < 12$ the backward breaking and the stationary non-breaking jets occur (Figure 2-5 and Figure 2-6).

From the above it is clear that the flow pattern around a single roughness element depends on roughness element size and shape, and the flow pattern changes with flow condition. It is obvious that even a single bed roughness element can provide a wide range of hydraulic habitats for aquatic animals. Used of various flow patterns for an identification of the aquatic animals' habitat is essentially descriptive and subjective.

The expression of flow patterns (Zgheib, 1994) in terms of a dimensionless parameter in the form of the Froude number gives no indication of absolute values of depth or velocity. As fish habitat can be defined by flow depth and flow velocity, it is presumed that velocity-depth classification is more meaningful and useful.

Flow around multiple elements

During low flow conditions in a riffle area different flow patterns, similar to those discussed in the above section, could be created around each rock and boulder, resulting in a wide range of flow depths and velocities. Under such conditions, statistical descriptions of the velocity and depth frequency distributions are a potentially useful approach for environmental flow assessment.

Multiple local controlled conditions. During low flow in a riffle area a wide range of flow depths and velocities occur that are controlled by rocks and boulders, creating local hydraulic features such as hydraulic jumps, local backups, contractions and critical controls. Furthermore, these features occur over the whole riffle area and change with discharge. Multiple local controlled conditions are very complex, and are expressions of rapidly varied flow, as discussed below.

Rapidly varied flow occurs as a sudden or local change of hydraulic conditions (particularly flow depth and velocity) due to variations in channel geometry (particularly bed elevation, channel width, and obstruction to flow) or a change in the regime of the flow. Sudden changes in the channel topography cause flow separations, create eddies and swirls of many forms, and the water surface profile changes over a short distance (Chadwick et al, 2004). Flow over a region of rapidly varied topography therefore includes local backups, transitions, critical controls and hydraulic jumps (Figure 2-8).

Figure 2-8 Hydraulic controls resulting from multiple local controls of varying scale

Furthermore, the flow surface may become discontinuous if the flow depth changes rapidly, creating hydraulic jumps. The following characteristics related to rapidly varied flow should be noted (Chow, 1959):

- The pressure distribution cannot be assumed to be hydrostatic,
- The variation in flow regime takes place over a relatively short distance,
- When rapidly varied flow occurs in a sudden-transition structure, the physical characteristics of the flow are determined by the boundary geometry of the structure as well as by the state of the flow,

- The energy (or Coriolis) velocity distribution coefficient α and the momentum (or Boussinesq) velocity distribution coefficient β are usually far greater than unity and cannot be accurately determined, and
- The separation zones, eddies, and rollers tend to complicate the flow pattern and to distort the velocity distribution in the stream.

Theory that assumes a parallel flow with hydrostatic pressure distribution, as used for uniform flow and gradually varied flows, does not apply for rapidly spatially varied flow, even with a continuous flow profile.

Some distinct cases of rapidly varied flow phenomena are

- Channel Transitions,
- Critical Controls, and
- Hydraulic Jumps.

Under multiple local controlled conditions a combination of several isolated cases of rapidly varied flow exists, which makes estimation of the velocity and depth distributions more difficult. Lately, statistical numerical approaches have therefore become an alternative solution to generalize the velocity and depth distributions of a stream area under low flow conditions.

Statistical approach. Statistical descriptions of the velocity and depth frequency distributions as functions of hydraulic parameters such as discharge, mean roughness, mean width, and mean depth, are a potentially useful approach for providing the necessary information for environmental flow assessment.

Based on a theoretical and statistical analysis, Dingman (1989) proposed a power law for the cumulative distribution of point velocity in a regular and highly irregular natural stream cross-section, given by:

$$F(v) = (v/V)^c \qquad 2.56$$

where v : local flow velocity,

V : maximum cross-sectional velocity, and

c : shape parameter equal to 1/b, and

b : slope of a plot of v versus V(v)on log-log scale.

Values of the shape parameter, c, were calculated from field data, and they range from 0.356 to 0.942 for an extensive sample, and from 0.164 to 0.6118 and from 0.497 to 0.912 for intensive samples for pool and riffle cross sections respectively. There is no clear procedure for estimation of the maximum cross-sectional velocity (V) and the shape parameter (c).

Lamouroux et al (1995) developed a velocity prediction model with distribution parameters that are related to descriptors of hydraulic variables in reaches. They analyzed velocity data of 37 French stream reaches including pools and riffle sites. Relative depth-averaged velocities were estimated from three vertical measured points at 0.2, 0.4 and 0.8 of the depth above the bed. The measured frequency-velocity distributions varied from centred to decentred distributions.

A probability density function was proposed as a combination of a Gaussian distribution (centred), and Gaussian and exponential distributions, given by:

$$f\left(x=\frac{v}{V},s\right)=s\left\{3.33e^{-\frac{x}{0.193}}+0.117e^{-\left(\frac{x-2.44}{1.73}\right)^2}\right\}+(1-s)\left(0.653e^{-\left(\frac{x-1}{0.864}\right)^2}\right) \qquad 2.57$$

where s : shape parameter of the point velocity distribution,

v : point velocity,

V : averaged reach velocity, and

x : relative point velocity, equal to v/V.

The shape parameter of the velocity distribution, s, was suggested to be a function of Froude number (Fr) and relative roughness (D/H), as:

$$s=-0.275-0.237\ln(Fr)+0.27(D/H) \qquad 2.58$$

where D : averaged dominant roughness, and

H : averaged reach depth,

A similar approach was applied by Jonker et al (2001) to predict the distributions of local flow velocities in cobble and boulder rivers of the Western Cape under low flow conditions. The rivers are characterized by different types of morphological units, and three dominant morphological units were recognized. These units are pool, plane bed, and rapid/riffle. Based on observed frequency distributions of relative velocity it was concluded that:

- The Weibull distribution provides the best estimate of the frequency distribution of the relative point velocities within pool morphological units,
- The Weibull and Extreme distributions both provide the best fit to the observed data within the plane bed morphological units, and
- Within rapid and riffle morphological units the Extreme distribution displays the best fit to the observed data, followed by the Weibull distribution.

For predicting the frequency distribution of relative velocity in cobble and boulder reaches, the following hydraulic parameters were selected as possible explanatory variables:

- Froude number,
- Velocity/depth ratio,
- Reynolds number,
- Relative submergence (y/d_{50} or y/d_{84}), and
- Width/depth ratio.

Through analyses of the velocity data it was found that within pool and rapid/riffle morphological units the distribution of local sets of point velocities could be related to the average velocity, flow depth, flow width and relative roughness within a cross-section, and used to predict the frequency distribution of point velocity in these morphological units. For plane bed morphological units, no statistically significant relationships were found. The accuracy of the proposed

predictions has not been checked, since the models have not been verified against independent field data.

Lamouroux (1998) proposed depth probability models based on analyses of data from different stream reaches in France and Germany. The reaches contained several pool-riffle sequences. The depth probability distributions tended from exponential to normal with increasing stage. The depth probability distribution was expressed as:

$$f\left(x=\frac{h}{H},t\right)=t\,e^{-x}+0.951(1-t)\,e^{-\left(\frac{x-1}{0.593}\right)^2} \qquad 2.59$$

where t : shape parameter varying from 0 (normal distribution) to 1 (exponential distribution),

x : relative depth, equal to h/H (h is flow depth, and H is mean reach depth).

Prediction of depth distribution by this model as a function of discharge requires an estimation of the shape parameter at a given stage and the depth-discharge relationship for the reach.

Stewardson and McMahon (2002) proposed a stochastic model of the joint depth and velocity probability distribution in streams. The model is based on theoretical considerations and samples of velocity and depth from a wide range of stream types, and was proposed to quantify the joint probability distribution of depth and velocity for general application in river studies. The model is based on the assumption that if velocity increases with depth across a channel, and velocity decreases with depth along a channel, then velocity and depth are not independent variables. Then, depth and velocity are transformed to provide two independent variables, one (ψ_a) that varies across the channel but is invariant along the channel, the other (ψ_b) that is invariant across the channel, but varies longitudinally. It has been found that the probability distributions of ψ_a and ψ_b can be represented by a normal and a truncated normal density functions,

respectively. Four parameters related to channel geometry were proposed for these density functions.

From the above it can be seen that:

- The model of Lamouroux et al (1995) has been developed for pool-riffle sequences and not homogeneous geomorphologic features, but appears to be the most tested one, and
- In general, all statistical models of the available velocity distribution in the literature do not distinguish between the two possible flow conditions: multiple local controlled and resistance controlled conditions.

2.6 Conclusion

The implementation of the NWA requires that an ecological Reserve be determined for all significant resources. Hydraulic analysis is a crucial component in the determination of the ecological Reserve in terms of both quantity and quality, as well as in any river rehabilitation measures. It focuses on the amount of water required to maintain the system in a particular ecological condition. Habitats for different life history stages of aquatic animals are related to hydraulic parameters such as flow velocity and flow depth, and therefore it is required that the amount of water should be determined so as to provide such parameters. This thesis contributes to the development of hydraulics under low flow conditions and forms a critical link in the ecological Reserve determination process.

In ecological Reserve studies considerable attention is focussed on the low flow component of the hydrological regime, and sites often characterized by large-scale roughness. Hydraulics under low flow conditions has attracted much research attention. A number of equations (logarithmic, power and semi-logarithmic) for prediction of flow resistance have been developed for flow with large and intermediate relative roughness conditions. Some of the equations have been developed based on experimental or field data, while others have been proposed as modifications of Manning's, Darcy-Weisbach or Chézy equations. Data that have been used for the development of equations are not clearly restricted to either

the large or intermediate relative roughness conditions. This thesis presents the development of a new equation for the prediction of overall flow resistance under large-scale roughness, and a new approach for the estimation of intermediate-scale roughness resistance that distinguishes between the influences of large and intermediate scale roughness components.

Under low flows, rocks and boulders may control the local velocity and depth distributions. Flow for such conditions is rapidly varied, and the occurrence of particular local velocities and depths is caused by the boundary geometry rather than by flow resistance phenomena. With increasing discharge, the multiple local controls become submerged and the flow tends towards a resistance controlled condition. Available information addressing the distinction between resistance controlled and multiple local controlled conditions is limited. This thesis contributes to understanding the transformation between multiple local controls and the resistance controlled conditions by presenting prediction methods for velocity distributions with large roughness elements.

Vegetation provides important river features that create physical habitats for aquatic animals. On the other hand, in-channel and riparian vegetation has significant effect on flow resistance and the influence of vegetation on overall flow resistance has to be predicted. This thesis presents practical conveyance prediction methods for three situations pertaining to the occurrence of vegetation in rivers and wetlands.

3 EXPERIMENTAL INVESTIGATION OF RESISTANCE CONTROLLED CONDITIONS

3.1 Introduction

Large substrate material is a common feature of South African rivers. Under low flow conditions rocks are relatively large and control the flow depth and velocity. Individual roughness elements within a natural channel vary in number, size, shape and distribution, and therefore create a wide range of physical habitats for aquatic animals. The prediction of flow depth and velocity for a given discharge is therefore an important part of environmental studies.

As has been discussed in Chapter 2, a number of logarithmic, power and semi-logarithmic equations have been developed for the prediction of overall flow resistance for large and intermediate relative roughnesses. These equations do not distinguished between large-scale and intermediate-scale roughnesses. This chapter presents the results of laboratory investigations undertaken to provide data for the development of new resistance equations to distinguish between large-scale and intermediate-scale roughnesses.

Laboratory experiments were conducted in the hydraulics laboratory of the School of Civil and Environmental Engineering, University of the Witwatersrand.

An experimental programme was carried out in laboratory flumes under controlled and idealized situations in order to establish the effects of roughness elements on flow resistance under different hydraulic conditions determined by bed slope and discharge, and to develop resistance prediction methods. Experiments were carried out using different sizes and areal densities of roughness elements. Roughness elements were simulated by hemispherical shells constructed of concrete. Laboratory experiments were conducted in Flume B (Series 1) and Flume C (Series 2). The results of the experimental work are presented in this chapter.

3.2 Flow Resistance

3.2.1 Flume B experiments

Under low flow conditions, resistance is determined by the largest or most exposed rocks in the channel bed. Their effect is thought to be related to their degree of submergence and preponderance in the substrate. The first set of experiments was carried out to assess these effects, using single-sized roughness elements at different areal densities and under intermediate and small-scale conditions. The experiments were conducted in a 0.38m wide, 15.0m long, glass-sided tilting laboratory flume under controlled and idealized conditions. A tailgate fixed downstream of the flume was used to control the flow depth in the channel to ensure uniform flow. Water was supplied to the flume through a closed circulation system, and two valves situated in the supply pipe at the head of the experimental flume were used to control the discharge. The discharge was varied by opening/closing these control valves and measured using a V-notch, which was installed at the downstream end of the flume, as well as an electronic flow meter with sensors situated in the water pipe that discharges into the flume.

All experiments were carried out under uniform flow conditions. Experiments were carried out for two size of hemispherical roughness elements, with diameters D = 47mm (Series 1.1) and D = 72mm (Series 1.2); the corresponding roughness heights, h, were therefore 23.5mm and 36mm. The roughness elements were arranged in a staggered pattern with equal longitudinal and transverse spacings (Figure 3-1).

Series 1.1 experiments were performed with one size of roughness elements (D = 47mm), two bed slopes and four densities, for a range of discharges (Q) and corresponding flow depths (y) for each set-up (Table 3-1). The density, Λ, was defined as the ratio of the plan area of the elements to the channel area. The Darcy-Weisbach f values were calculated for each experiment using the side-wall correction procedure of Vanoni and Brooks (1957), and the results are plotted in Figure 3-2. The experimental conditions of Series 1.1 experiments are summarized in Table 3-1.

Figure 3-1 Arrangement of roughness elements in Flume B (Test 1.1.5 shown)

Table 3-1 Experimental conditions of Series 1.1 experiments

Test	Density, Λ (%)	Slope	y/h	Discharge, Q (l/s)
1.1.1	82	0.0011	1.45 – 6.14	0.6 – 15.2
1.1.2	82	0.0021	1.29 – 4.72	0.4 – 15.2
1.1.3	47	0.0011	2.28 – 6.43	1.4 – 14.8
1.1.4	30	0.0011	1.85 – 6.85	0.9 – 15.9
1.1.5	22	0.0011	1.26 – 6.19	0.4 – 13.9

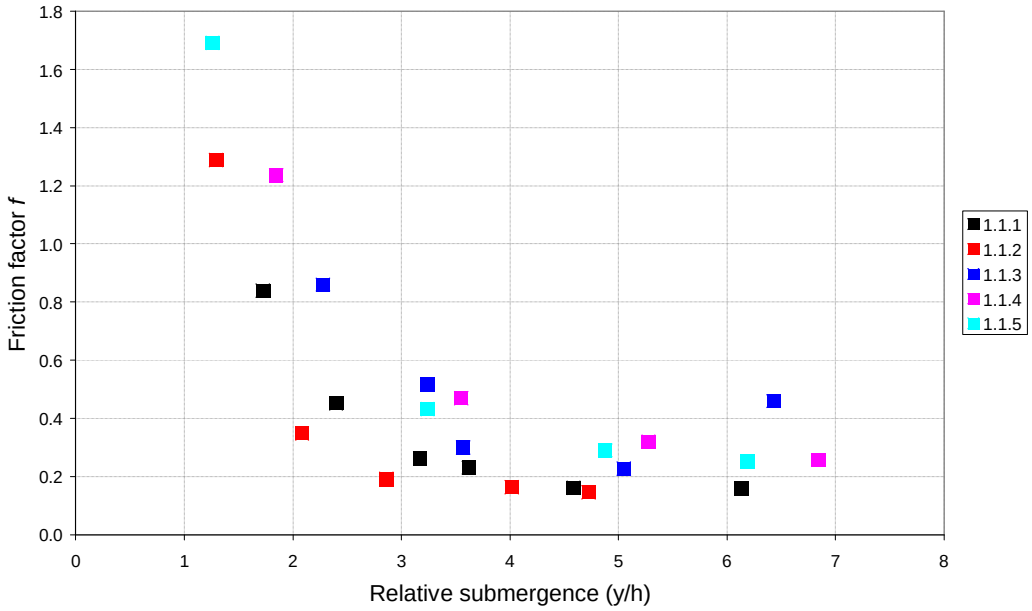

Figure 3-2 Variation of friction factor *f* with flow depth for Series 1.1 experiments

Tests 1.1.1 and 1.1.2 were carried out with the same roughness element density but different bed slopes, showing that the slope has influence, with resistance being slightly lower for the steeper slope (Figure 3-2).

Tests 1.1.1, 1.1.3, 1.1.4 and 1.1.5 were conducted with the same bed slope but different densities. The influence of density on flow resistance for five different relative submergences is shown in Figure 3-3.

From the graph (Figure 3-3) it is clear that the density of the roughness elements had a significant effect on overall flow resistance. It also can be seen by comparing curve "y/h = 1" (for the relative submergence equal to 1) with curve "y/h = 6" (for the relative submergence equal to 6) that the effect of density on overall resistance decreases with increasing relative submergence. Furthermore, the flow resistance increases with density, reaching its highest value at an areal coverage of 30%, and then decreasing for higher densities. This effect is consistent for all flow conditions, from large to small relative submergences.

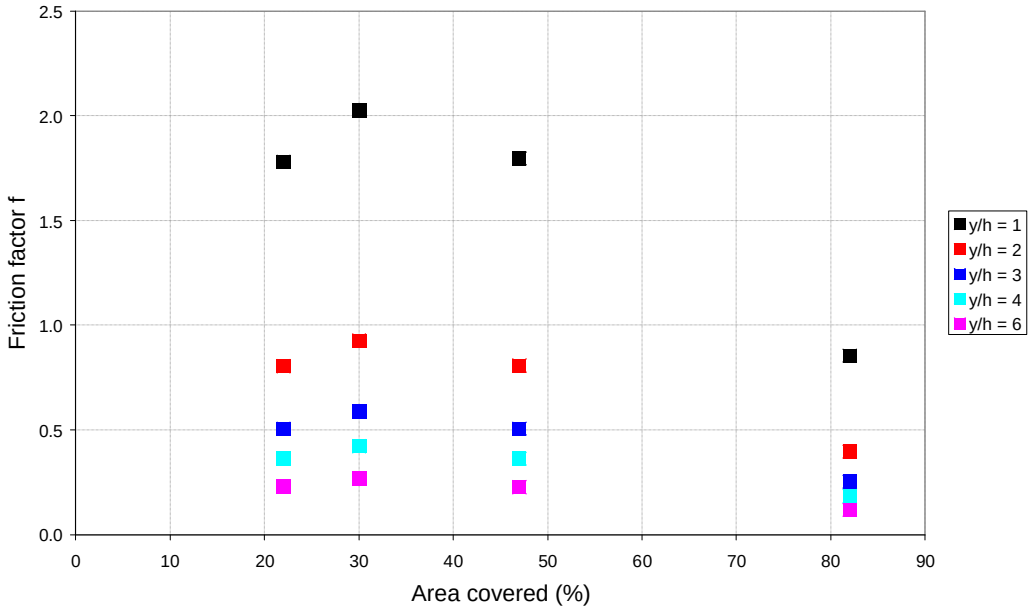

Figure 3-3 Influence of areal coverage on flow resistance in term of Darcy-Weisbach *f* for different relative submergences

The field data of Bathurst (2002) suggest that the effective friction factor under low-flow conditions depends on channel slope. From the Series 1.1 experiments it was found that bed slope has influence on flow resistance. The Series 1.2 experiments were therefore performed to investigate the influence of bed slope on flow resistance under controlled conditions.

The Series 1.2 experiments were carried out with one size of roughness element (D = 72mm), 5 bed slopes and one density (27%). Two (low and high) discharges for each slope were tested. The experimental conditions are listed in Table 3-2. As before, the flow resistance in terms of Darcy-Weisbach *f* was calculated using the side-wall correction procedure of Vanoni and Brooks (1957), and the results are plotted in Figure 3-4.

Table 3-2 Experimental conditions for Series 1.2 experiments

Test	Slope	y/h	Discharge, Q (l/s)
1.2.1	0.00443	1.01 and 3.95	0.88 and 22.00
1.2.2	0.00329	0.95 and 3.96	0.63 and 18.00
1.2.3	0.00215	1.03 and 4.53	0.57 and 17.00
1.2.4	0.00101	1.01 and 5.42	0.29 and 13.00
1.2.5	0.00089	1.07 and 7.93	0.30 and 22.00

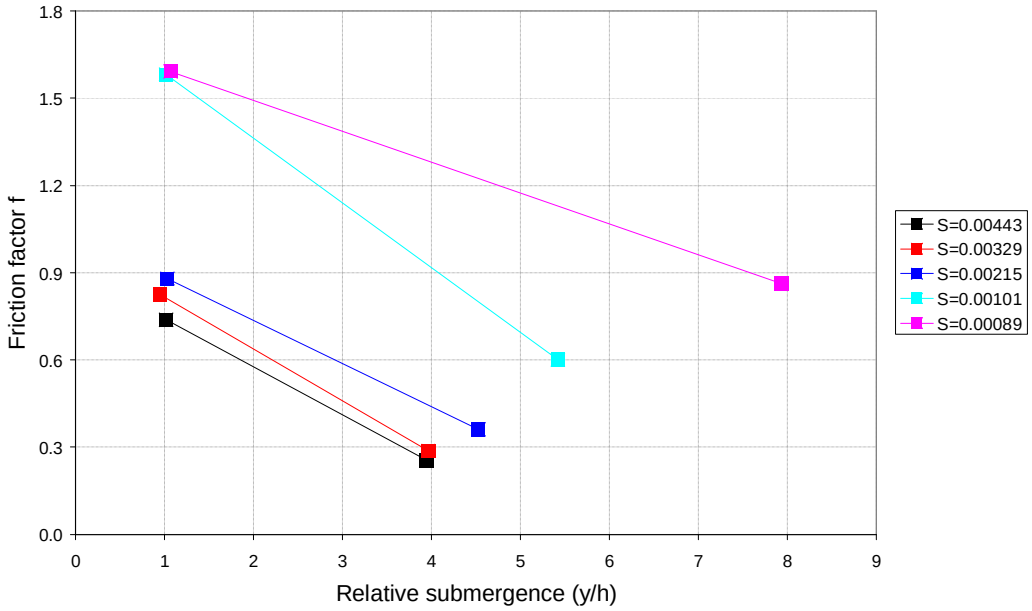

Figure 3-4 Influence of bed slopes on overall flow resistance

The results suggest that channel slope does have an influence on resistance; the f values are higher for milder than for steeper slopes.

The Series 1 experimental data are listed in Appendix A, Table A-1.

3.2.2 Flume C experiments

The largest rocks in a river bed are distributed randomly in space. Therefore this series of experiments was designed to examine the effects on overall resistance of the size of rocks and their distribution pattern, in particular the effect of longitudinal disruption of the flow and the effect of smaller rocks interspersed amongst the largest ones. Experiments were carried out in a 2.00m wide, 12.0m long laboratory flume (Figure 3-5). Two Series (2.1 and 2.2) of experiments were

conducted to investigate these effects on flow resistance under controlled and idealized large and intermediate scale roughness conditions. Roughness elements were again simulated by hemispheres with constant shape.

Figure 3-5 Flume C with a staggered pattern of hemispheres

Series 2.1 experiments

The first series of experiments was carried out to investigate the influence of roughness element size and pattern on overall flow resistance. Eight different arrangements of roughness elements were tested, shown diagrammatically in Figure 3-6 and described below; photographs of all patterns are included in Appendix B.

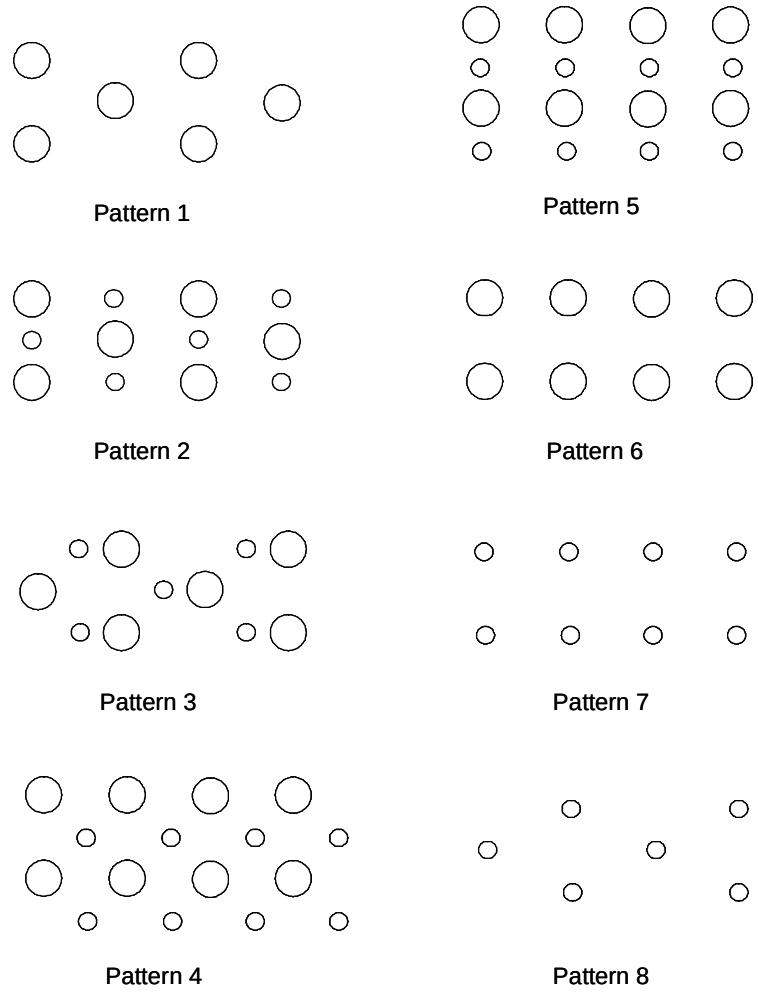

Figure 3-6 Roughness element arrangements for Series 2.1 experiments (flow is left to right)

Pattern 1: (Large hemispheres, LH, only) The hemispheres, D = 116mm, were arranged in a staggered grid pattern with equal longitudinal and transverse spacing of 285mm (Appendix B, Figure B-1).

Pattern 2: (Large, LH, and small, SH, hemispheres) The large hemispheres had the same arrangement as in Pattern 1, and small hemispheres (D = 54mm) were placed between and in line with large hemispheres (Appendix B, Figure B-2). The small hemispheres were arranged in a staggered pattern as well with the same spacing of 285mm as the large ones.

Pattern 3: (Large, LH, and small, SH, hemispheres) The large hemispheres were placed as in Pattern 1 while the small ones were positioned longitudinally in line with, but transversely staggered with respect to the large hemispheres (Appendix

B, Figure B-3). Each size individually was arranged in a staggered pattern with spacing of 285mm.

Pattern 4: (Large, LH, and small, SH, hemispheres) The large hemispheres were arranged in a parallel grid pattern with equal longitudinal and transverse spacing of 285mm. The small hemispheres were arranged in the same pattern as the large ones, but longitudinally and transversely between them (Appendix B, Figure B-4).

Pattern 5: (Large, LH, and small, SH, hemispheres) The hemispheres were arranged in a parallel grid pattern. The large hemispheres were arranged in a parallel pattern of 285mm spacing. A longitudinal row of small hemispheres was placed between each longitudinal row of large hemispheres (Appendix B, Figure B-5).

Pattern 6: (Large hemispheres, LH, only) The hemispheres were arranged in a parallel grid pattern with equal longitudinal and transverse spacing of 285mm (Appendix B, Figure B-6).

Pattern 7: (Small hemispheres, SH, only) The hemispheres were arranged in a parallel grid pattern with equal longitudinal and transverse spacing of 285mm (Appendix B, Figure B-7).

Pattern 8: (Small hemispheres, SH, only) The hemispheres were arranged in staggered grid pattern with equal longitudinal and transverse spacing of 285mm (Appendix B, Figure B-8).

Experiments were performed for both emergent and submerged conditions. Only one slope of 0.001 and two sizes of hemispheres, D = 116mm (LH) and D = 54mm (SH) were tested. A summary of experiments is listed in Table 3-3, and measured data are presented in Appendix B, Table B-1.

Stage-discharge relationships for all 8 patterns, together with that corresponding to the basic resistance of the empty flume, are plotted in Figure 3-7. The effects of roughness element arrangements in terms of the Darcy-Weisbach friction factor f and the relative submergence for all 8 patterns are shown in Figure 3-8. It should be noted that the relative submergences for Patterns 2, 3, 4 and 5, where

two sizes of hemisphere comprised the bed arrangements, was calculated using the height of the large hemispheres.

Table 3-3 Experimental conditions of Series 2.1 experiments

Pattern	Roughness shape	Discharge, Q (l/s)	Measured flow depth, y (mm)	Covered area (%)
1	LH	2.7 - 17.4	25 - 74	15
2	LH and SH	1.2 - 12.5	20 – 69	18
3	LH and SH	2.9 – 21.4	28 – 80	17
4	LH and SH	2.0 – 25.7	20 – 85	17
5	LH and SH	1.8 – 24.7	20 – 82	18
6	LH	3.2 – 27.3	25 – 85	15
7	SH	7.0 – 28.3	29 – 55	3
8	SH	5.3 – 28.3	25 - 56	3

LH – Large Hemispheres

SH – Small Hemispheres

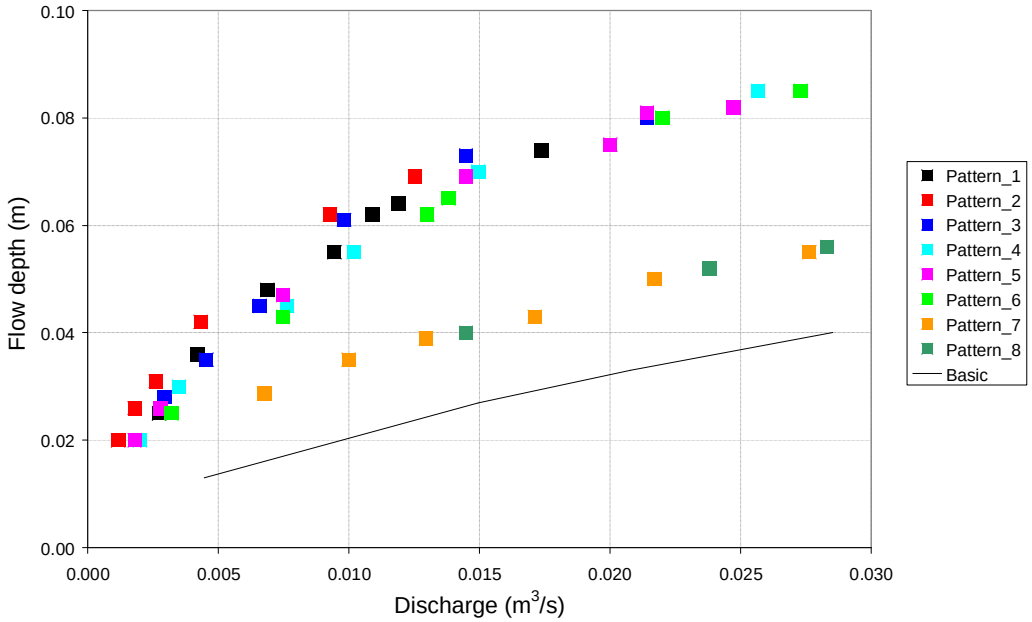

Figure 3-7 Stage-discharge relationship for Series 2.1 experiments

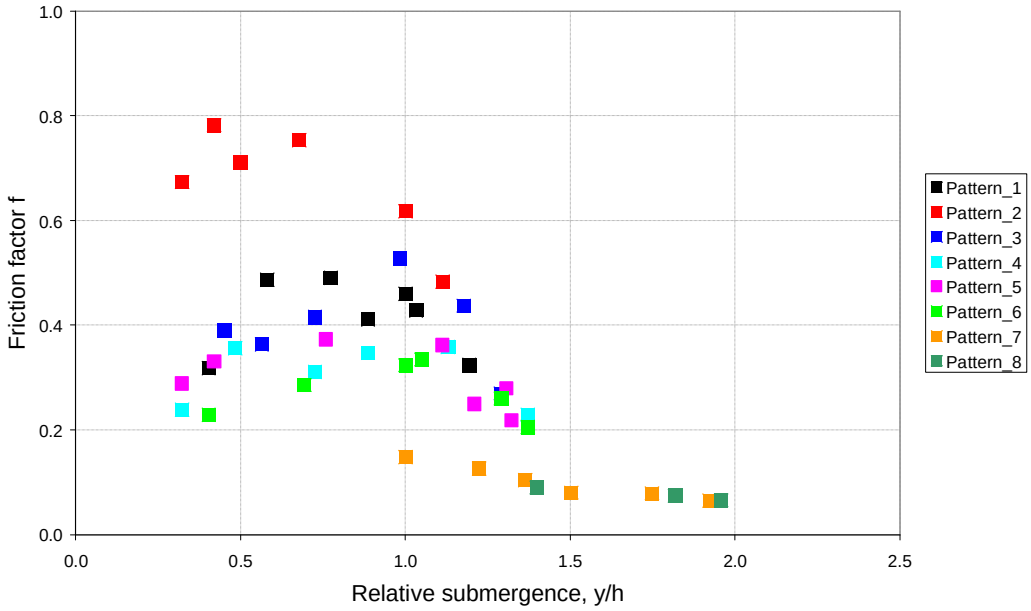

Figure 3-8 Flow resistance in term of Darcy-Weisbach *f* for Series 2.1 experiments

The influence of covered area on flow resistance in terms of the stage-discharge relationship can be seen in Figure 3-7. It is obvious that covered area has an overall effect on flow resistance. Flow resistance for Patterns 1, 2, 3, 4, 5 and 6 for covered areas of 15 to 18% resistance is much higher than for the covered areas of 3% for Patterns 7 and 8.

Patterns 1 and 8 were arranged in a staggered grid. The large hemispheres were used in Pattern 1 and the small in Pattern 8. Patterns 6 and 7 were arranged in a parallel grid with the large and small hemispheres respectively. The effect of the roughness element pattern on overall flow resistance in terms of the Darcy-Weisbach *f* against the relative submergences is shown in Figure 3-9. By comparing the graphs of Patterns 1 and 6 it can be seen that the arrangement of the roughness elements has a significant influence on overall resistance for relative submergences less then 1.0 (i.e. under large-scale roughness condition) but with increasing relative submergence (Pattern 7 and 8) the effect of pattern is insignificant.

In Patterns 2, 3, 4 and 5 the small hemispheres were arranged within staggered and parallel grids of the large hemispheres; their influence on overall resistance is shown in Figure 3-10.

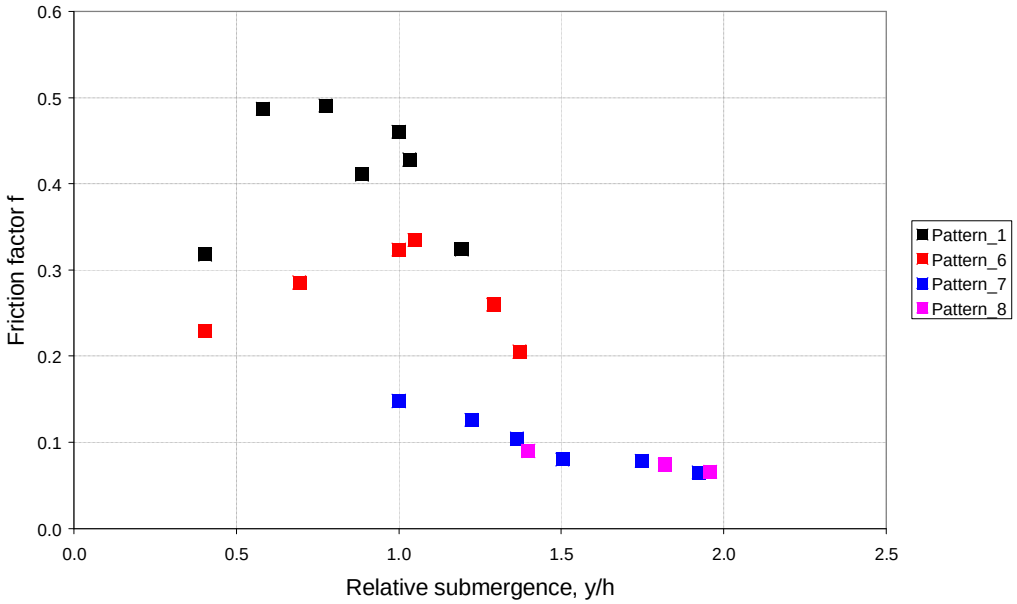

Figure 3-9 Effects of roughness element pattern and size on overall flow resistance, Series 2.1 experiments

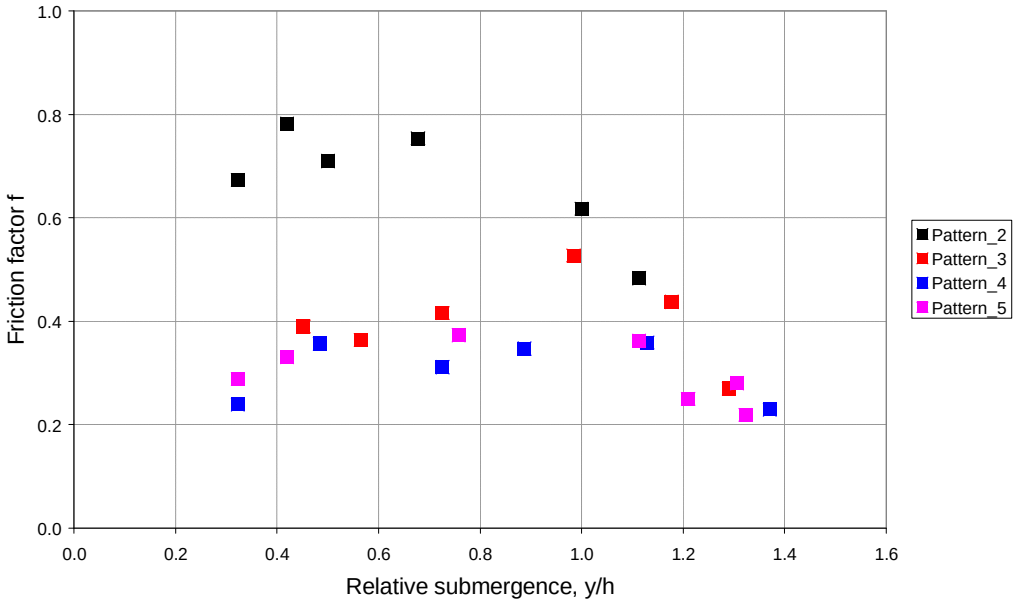

Figure 3-10 Influence of small elements interspersed between large ones on overall flow resistance, Series 2.1 experiments

From the graph (Figure 3-10) it is clear that the roughness element arrangement in Pattern 2 has the highest influence on flow resistance under the large-scale roughness condition, for relative submergence less then 1.0, while for the same flow condition, results of Patterns 3, 4 and 5 arrangements are similar. For the intermediate-scale roughness flow condition with the relative submergence higher than 1.0, the effects of all the small hemisphere patterns within the large hemispheres are similar.

Series 2.2 experiments

Experiments were conducted with one slope of 0.0005 and three sizes of hemispheres named H1, H2 and H3 with diameters of D1 = 108mm, D2 = 72mm and D3 = 46mm respectively. A summary of the experimental conditions for the Series 2.2 experiments is listed in Table 3-4. Measured data from each experiment are included in Appendix C, Table C-1. Photographs of Patterns 1 to 17 are provided in Appendix C in Figures C-1 to C-17. The geometrical arrangements are similar to those used in Series 2.1 and shown in Figure 3-6: Patterns 1 to 7 are as for Series 2.1 Pattern 1, Patterns 8 to 14 as for Series 2.1 Pattern 3, and Patterns 15 to 17 as for series 2.1 Pattern 6.

Stage-discharge relationships for the 17 patterns, together with the basic resistance of the empty flume are plotted in Figure 3-11. Measured flow resistances for the 17 patterns in terms of the Darcy-Weisbach f values as a function of the relative submergence are plotted in Figure 3-12. Plotted results (Figure 3-12) show that the maximum flow resistance occurs when the relative submergence is around 1.0, and the friction factors have similar distributions to those obtained by others who used available published field and laboratory data, and plotted the results of frictional resistance as a function of the relative submergence (Figure 2-1). It also was found that the maximum flow resistance occurs with the relative submergence of 1.0. Regarding the variation in the calculated frictional resistance f, it can be seen that the results of Lawrence (1997) (Figure 2-1) show greater variation than the results of the Series 2.2 experiments (Figure 3-12).

Table 3-4 Experimental conditions for Series 2.2 experiments

Pattern No	Spacing H1	Spacing H2	Spacing H3	Pattern grid	Discharge, Q	Measured flow depth, y	Total areal coverage
	(mm)	(mm)	(mm)		(l/s)	(mm)	(%)
1	125/125			Staggered	0.6-55.7	32-189	54.64
2	200/200			Staggered	1.1-54.7	24-164	21.97
3	300/300			Staggered	2.0-55.2	23-129	12.02
4	400/400			Staggered	2.7-55.2	23-121	6.24
5		400/400		Staggered	3.2-55.2	23-107	2.89
6		200/200		Staggered	2.8-60.0	34-130	9.82
7		125/125		Staggered	4.1-55.2	50-149	23.98
8	200/200	200/200		Staggered	0.7-54.7	20-164	31.79
9	200/200		200/200	Staggered	0.8-43.4	20-145	26.13
10	300/300	300/300		Staggered	1.4-55.2	24-137	16.06
11	300/300		300/300	Staggered	2.0-55.2	26-131	13.73
12	400/400	400/400		Staggered	3.7-55.2	31-129	8.10
13	400/400	400/400		Staggered	2.5-52.2	27-131	8.10
14			200/200	Staggered	3.6-55.7	36-136	4.16
15	110/110			Parallel	0.4-25.0	43-123	74.91
16	110/125			Parallel	0.6-21.4	40-117	62.89
17	125/167			Parallel	0.6-7.8	31-82	41.62

Spacing of hemispheres indicated in the table is given as longitudinal/lateral centre to centre distances

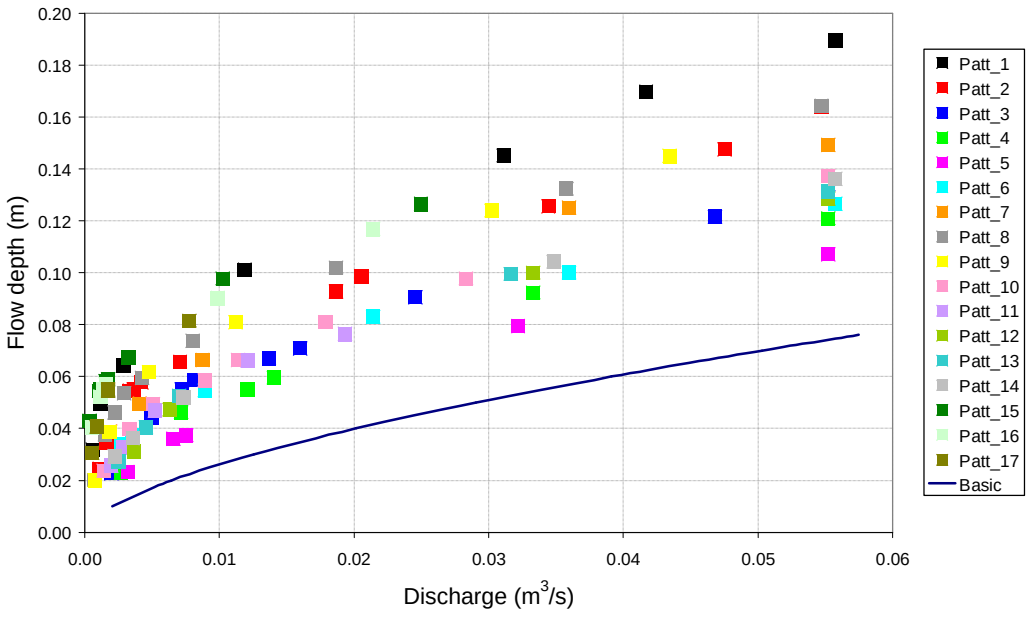

Figure 3-11 Stage-discharge relationship for Series 2.2 experiments

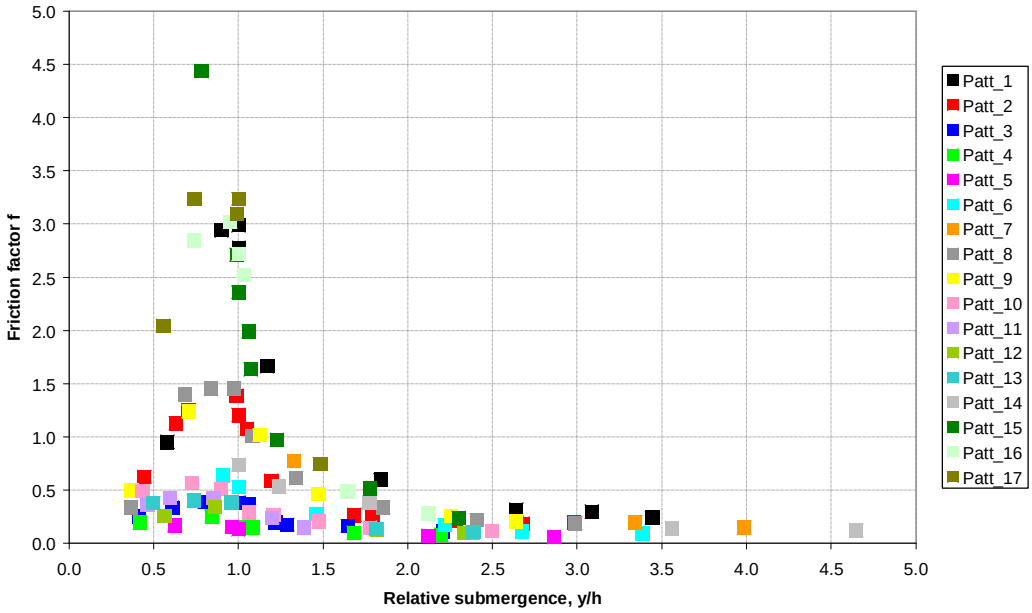

Figure 3-12 Flow resistance in term of Darcy-Weisbach *f* as a fucttion of relative submergence for the all patterns of Series 2.2 experiments

Experiments with Patterns 1, 2, 3, 4, 15, 16 and 17 were carried out with hemispheres H1 only. The results of the experiments can be used to analyse the influence of roughness element density on overall flow resistance. Measured flow resistance, in terms of the Darcy-Weisbach *f* values, is plotted in Figure 3-13. It is clear that roughness element density affects flow resistance significantly. The effect is much greater under large-scale roughness conditions (relative submergence less than 1.0) than under intermediate-scale roughness conditions (relative submergence greater than 1.0). It can also be seen that flow resistance increases with flow depth under large-scale roughness, reaching the highest resistance when the roughness elements are just submerged, before decreasing through the intermediate-scale roughness zone.

The influence of the roughness element density decreases with increasing flow depth in the intermediate-scale roughness zone. The dependence of flow resistance on the areal coverage of roughness elements at the condition of maximum resistance is shown in Figure 3-14, where *f* is plotted against areal coverage for relative submergences equal to 1.0. This shows that resistance

increases with areal coverage, reaching a maximum value at an areal coverage of about 40%, and then reduces. The variation in Figure 3-14 is consistent with the results of the Flume B experiments presented in Figure 3-3 shows that density is much more important than pattern.

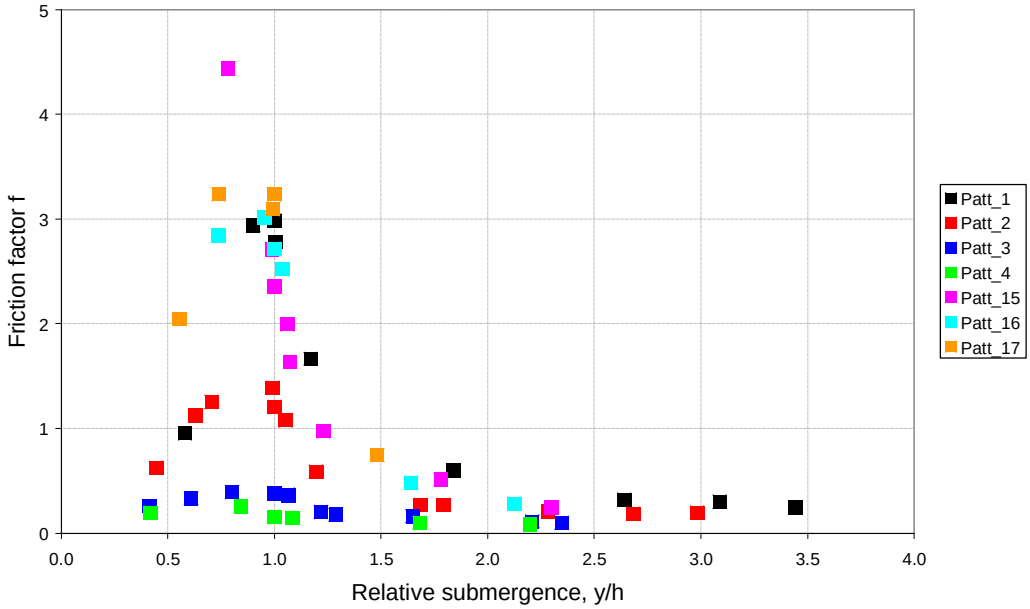

Figure 3-13 Flow resistance in term of Darcy-Weisbach *f* against relative submergence for patterns with hemispheres H1 only

Experiments with Patterns 8, 9, 10, 11, 12 and 13 were performed to investigate the influence of smaller roughness elements (H2 and H3) within the patterns of the large (H1) hemispheres on overall resistance. Patterns 8, 10, 12 and 13 were carried out with hemispheres H1 and H 2 placed in equal longitudinal and lateral spacings of 200mm, 300mm and 400mm (Table 3-4), while Patterns 9 and 11 consisted of hemispheres H1 and H3, arranged with spacings of 200 and 300mm respectively. Patterns 12 and 13 were performed with the same hemispheres and spacing but with a different pattern for the H2 hemispheres. The results of these experiments are presented in Figure 3-15. It is evident that Patterns 8 and 9, with spacing of 200mm, produced the highest resistance, consistent with the previous observation of increasing resistance with density in the large-scale roughness zone. It can also be seen that the difference in resistance between Patterns 8 and 9

is not significant, suggesting that the size of interspersed smaller hemispheres has little influence on overall flow resistance.

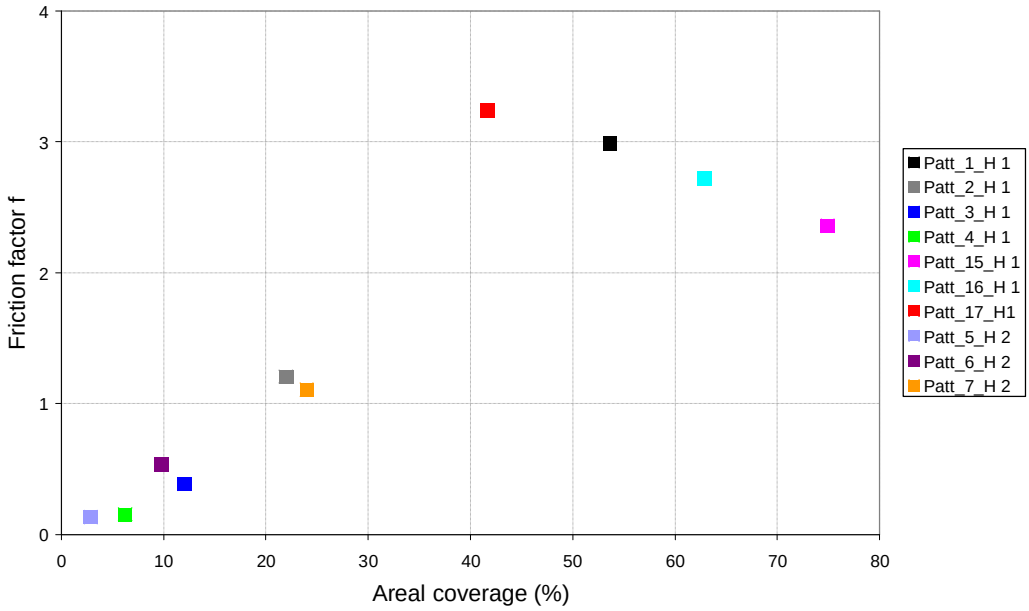

Figure 3-14 Influence of areal coverage on flow resistance in term of Darcy-Weisbach *f*

Patterns 8 and 9 were arranged with hemispheres H1 and H2, and H1 and H3, respectively. The hemispheres H1 were positioned with spacing of 200mm; the smaller hemispheres were placed within the larger ones with the same spacing. Patterns 2, 6 and 14 were arranged with one size of hemispheres only with spacing's of 200mm. The results of the experiments carried out for these patterns (Figure 3-16) show the influence of different hemisphere arrangements on overall flow resistance. The similarity of the results for Pattern 2 (hemispheres H1 only) with those for patterns 8 and 9 (with interspersed H2 and H3) suggests that resistance is caused primarily by the largest clasts in a cobble or boulder river bed. The relationship between the results for Patterns 2, 6 and 14 confirms the influence of areal coverage in the large-scale roughness zone.

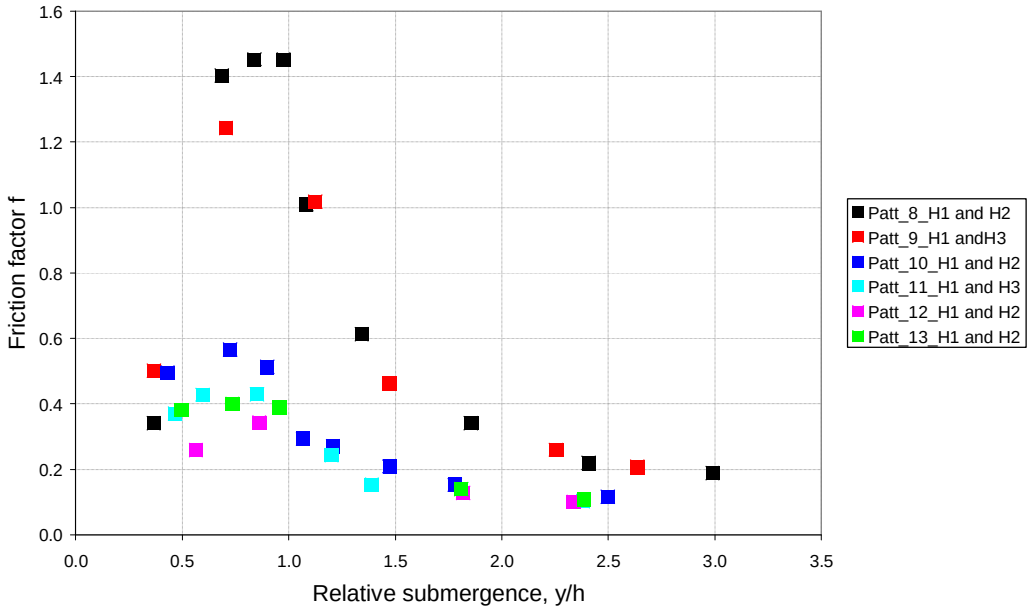

Figure 3-15 Variation of flow resistance in term of Darcy-Weisbach *f* for different combinations of hemisphere sizes

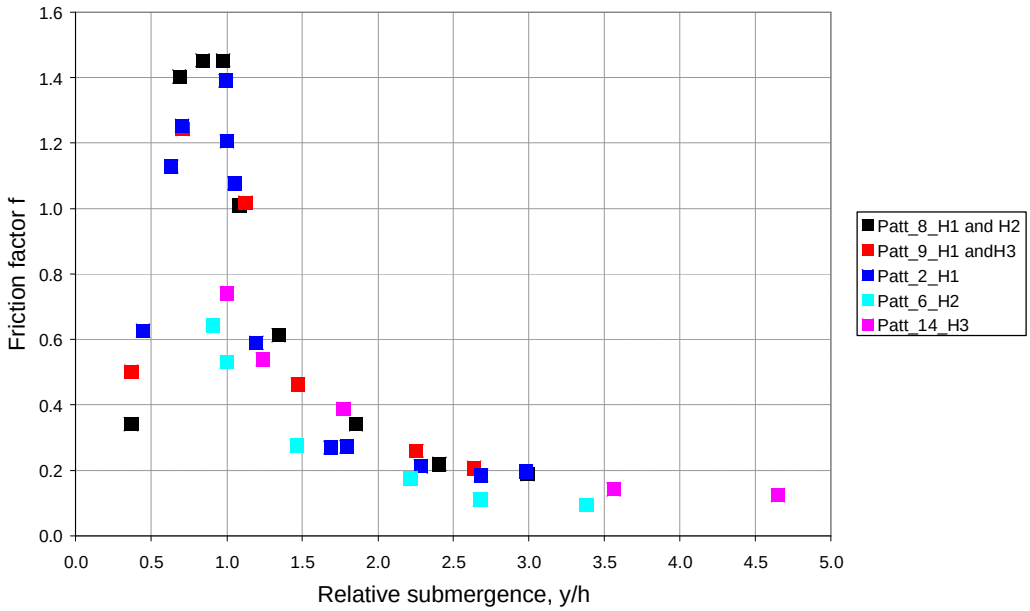

Figure 3-16 Flow resistance in term of Darcy-Weisbach for patterns with spacing of 200mm

3.2.3 Conclusions

This experimental investigation has shown that the density of large roughness elements on the bed of a channel has a significant influence on the overall flow resistance of the channel. The resistance due to the roughness elements increases with increasing density, reaching a maximum for an areal coverage in the range of 30% - 40%. Thereafter, overall resistance decreases with increasing density. This general variation occurs for all scales of relative roughness.

Experiments with different bed slopes indicate higher overall flow resistance for milder slopes than for steeper ones.

Experiments with different sizes of hemispheres suggest that resistance is caused primarily by the largest clasts in a cobble or boulder river bed.

Experiments with staggered and parallel arrangement patterns of large roughness elements indicate that the existence of continuous longitudinal flow paths decreases flow resistance significantly for $y/h < 1$. When the relative submergence is higher than 1, the arrangement of large roughness elements does not have an influence on flow.

Experiments performed for large- and intermediate-scale roughness conditions confirmed that the resistance phenomena under these conditions are different, and different methods are therefore required for this prediction. Flow resistance is a maximum for a relative roughness around 1.0; it decreases rapidly for deeper flows and gradually for shallower flows. The effects of roughness element size, density, pattern, and interspersed smaller elements are all much more pronounced for large-scale roughness conditions than for small-scale and intermediate scale conditions.

3.3 Velocity Distribution

Flow velocity is a physical parameter that is useful for the description of aquatic animals' habitats. The average velocity (ratio of discharge to cross-sectional flow

area) is not a sufficient habitat descriptor for use in environmental studies, and prediction of local velocity distribution is usually required. The velocity distribution changes with flow conditions, making its prediction difficult. Laboratory tests were conducted to investigate how velocity distributions change with discharge, and to provide a data base for testing the recommended prediction method (Chapter 6).

Point velocity measurements were taken around one hemisphere within Pattern 6 of the Series 2.2 described above (Appendix C, Figure C-6) for discharges of Q = 21l/s and Q = 3l/s. A two-dimensional *Nortek Doppler Velocimeter* (NDV) was used to determine the velocity profile around a hemisphere. It was assumed that the velocity profile is symmetrical about the longitudinal axis of the hemisphere, and therefore velocities were measured only on one side. A grid of 20cm by 20cm around the hemisphere was defined (Figure 3-17) and velocities were measured in each block, numbered as indicated.

3.3.1 Velocity measurement for Q = 3.0 l/s

A uniform flow depth of 36mm was measured for a discharge of 3.0l/s. A plan of the velocity measurement grid is shown in Figure 3-17. The hemispheres were just submerged, and only one point velocity was measured along the vertical at each grid block at 0.5 of the flow depth. Measured velocities are listed in Table D-1, Appendix D. An average velocity of 0.044m/s for a discharge of 3l/s was calculated as the ratio of flow to cross-sectional flow area. The measured velocities were grouped into 2cm/s velocity classes. The velocity distribution in histogram format to display the frequency of occurrence of each value in the data set is plotted in Figure 3-18.

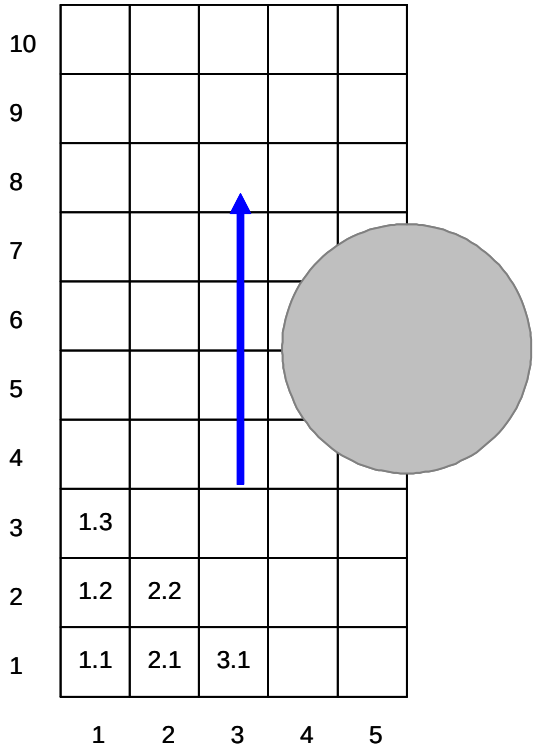

Figure 3-17 Velocity measurement grid

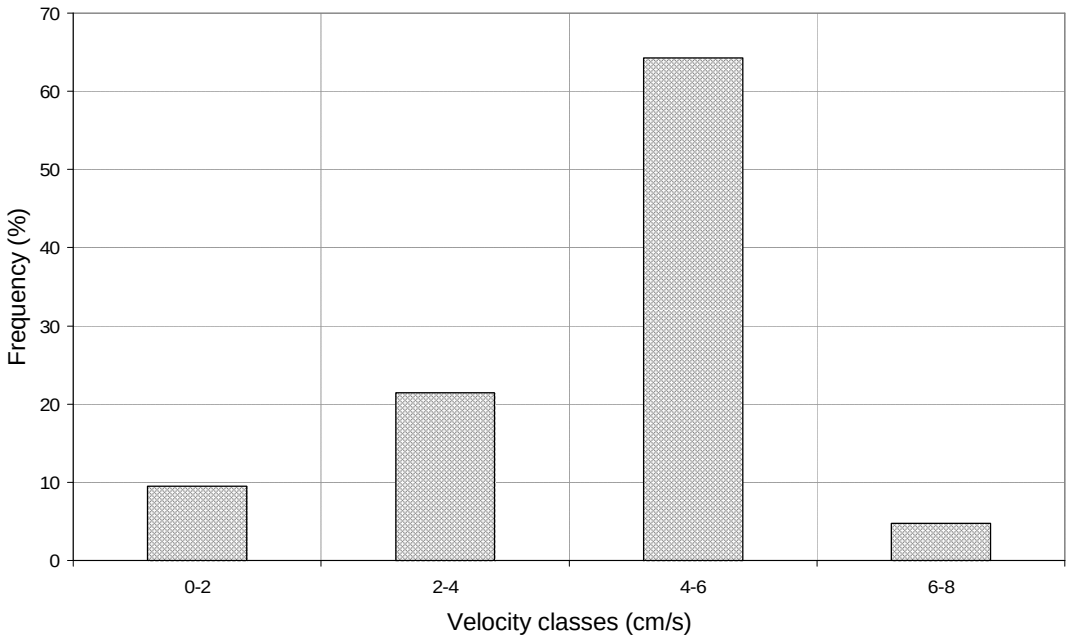

Figure 3-18 Velocity distribution histogram with 0.02 m/s velocity classes for Q=3.0l/s

The histogram is unimodal (has one mode) and skewed to the left. The mode is in the class of 4 to 6cm/s. The lowest and the highest measured velocities for the given discharge are in the 0 to 2cm/s and 6 to 8cm/s velocity ranges respectively.

The average velocity of 4.4cm/s fell into the class of velocity that represents the highest (64.3) percent of measured values. The other measurements are distributed across three other classes, but with less frequent occurrences.

3.3.2 Velocity measurement for Q = 21 l/s

The uniform flow depths and the relative submergences for the test with a discharge of 21l/s were 83mm and 2.31 respectively. Velocities were measured at the plan centre of each of the grid block. Seven vertical velocities were measured in each block at 1 cm intervals. The measured point and depth-averaged velocities at the 5 longitudinal sections (Figure 3-17) are listed in Tables D-2 to D-6 (Appendix D). Vertical velocity distributions are plotted in Figures 3-19 to 3-23.

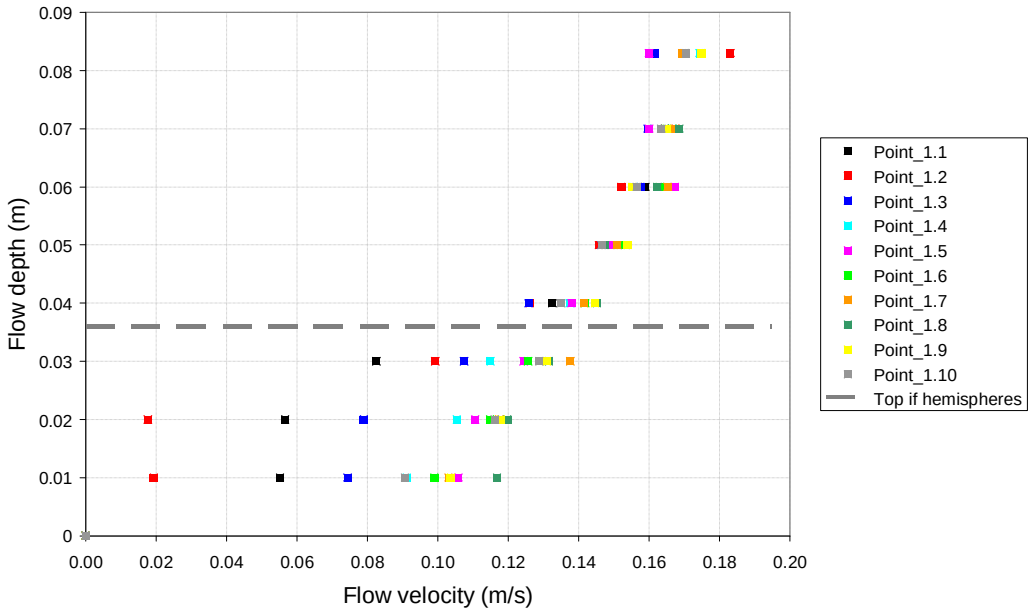

Figure 3-19 Vertical velocity distributions at longitudinal section 1

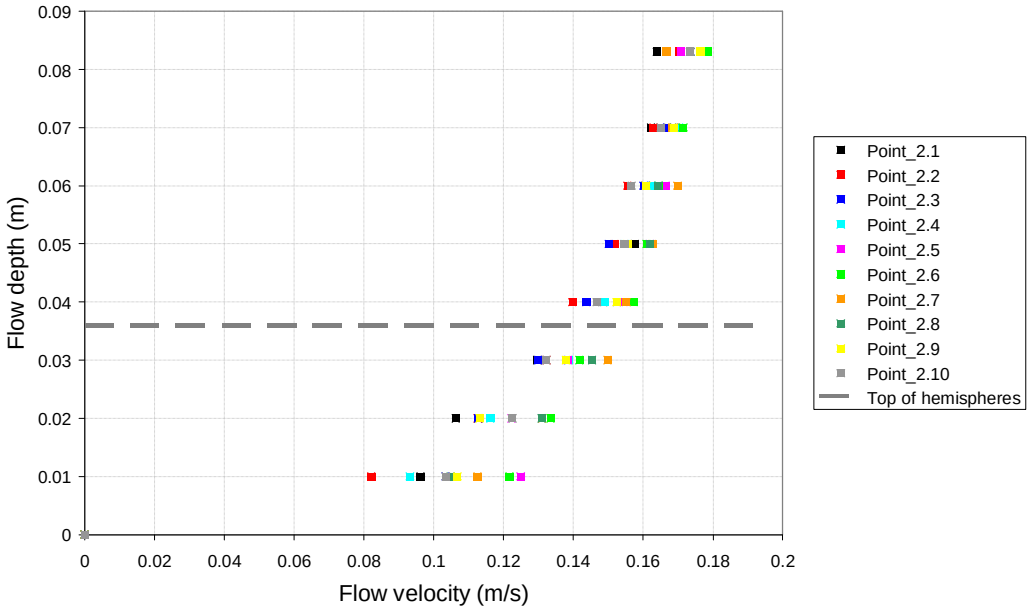

Figure 3-20 Vertical velocity distributions at longitudinal section 2

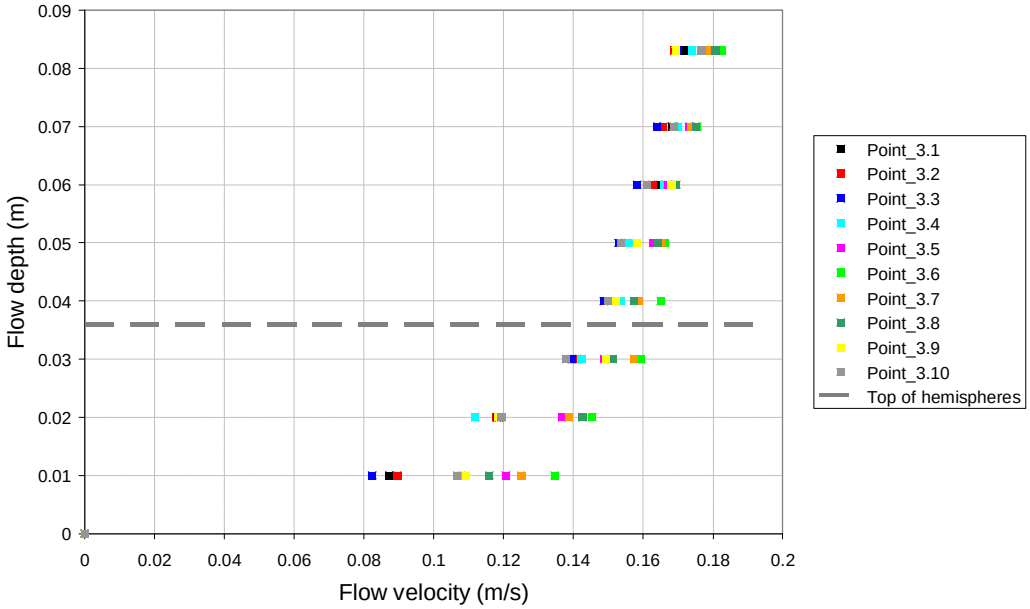

Figure 3-21 Vertical velocity distributions at longitudinal section 3

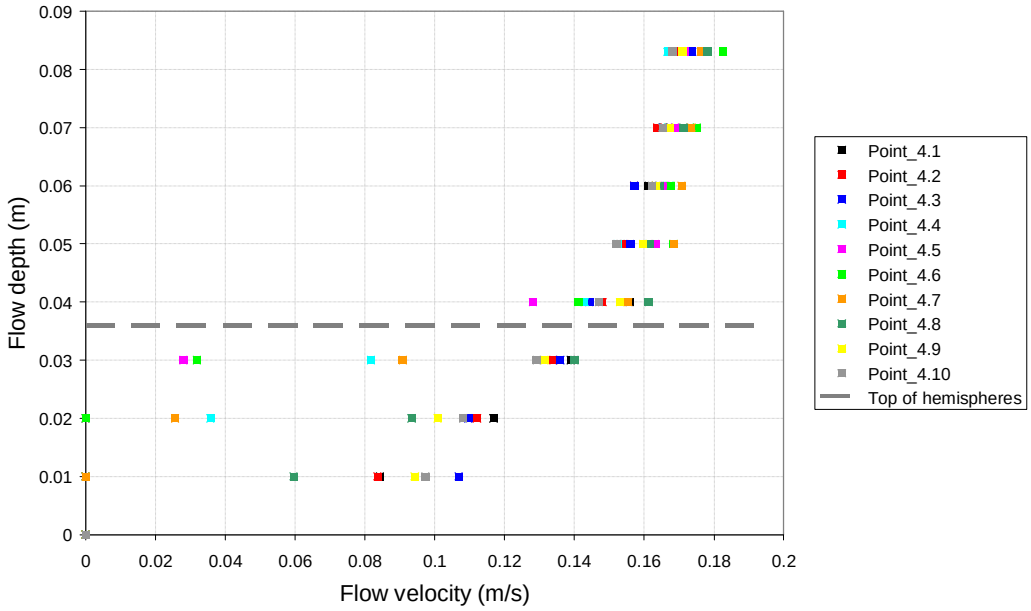

Figure 3-22 Vertical velocity distributions at longitudinal section 4

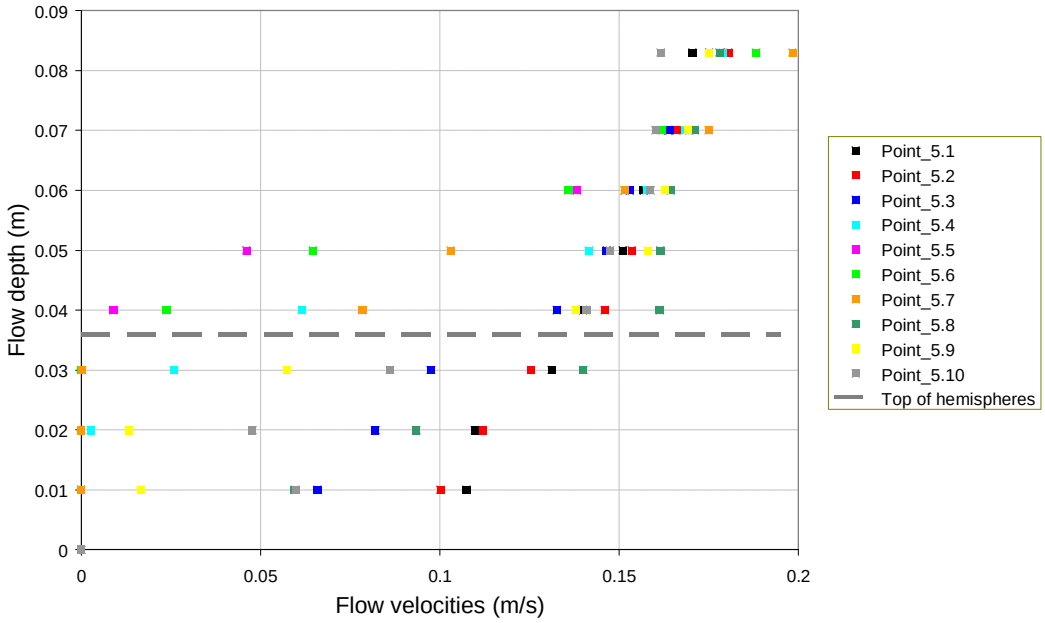

Figure 3-23 Vertical velocity distributions at longitudinal section 5

A depth-averaged velocity for each grid position considered was calculated, and the velocity distribution histogram with the same (as for discharge of 3l/s)

velocity classes of 2cm/s is plotted in Figure 3-24. The histogram is unimodal and skewed to the left. The mode is in the 12 to 14cm/s class. The lowest and the highest measured velocities are in the 4 to 6cm/s and 14 to16cm/s velocity class respectively. Depth-averaged velocities lower than 4 cm/s were not calculated for this discharge.

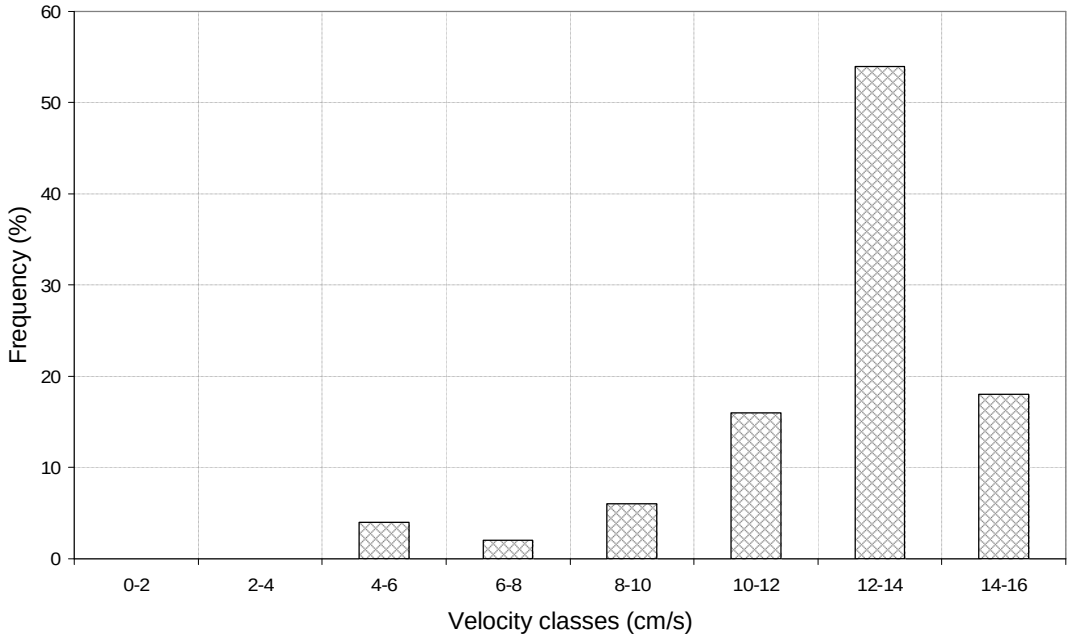

Figure 3-24 Depth-averaged velocity distribution histogram for velocity classes of 2cm/s for Q=21l/s

An average velocity of 0.13m/s for Pattern 6, Series 2.2 experiments was calculated as the ratio of flow to cross-sectional area. From the velocity distribution histogram (Figure 3-24) it can be seen that the average velocity falls within the same velocity class (12-14cm/s) as the mode.

The effect of resolution of hydraulic measurements was assessed by comparing velocity frequency distributions of measured point velocities with frequency distributions of depth-averaged velocity (that were calculated from the same measurements). Graphs of histograms for depth-averaged and point velocity are presented in Figure 3-25. The histograms are different in terms of shape and the

velocity range. As expected, the average velocity (0.13m/s) falls within the same velocity class as the mode for the depth-averaged velocity. However, most point velocities (58% measurements) are greater than 14cm/s. Thus different estimates of the predominant velocity occurring are produced. Point velocity is also spread over a wider range of velocity classes than depth-averaged velocity, including low velocities that were measured on the top of the hemisphere, and also including higher velocities (16-18cm/s) that the depth-averaged distribution. Use of too coarse a resolution may tend to under-estimate habitat diversity. Each resolution of measurement produces a distribution of velocity applicable only at this resolution.

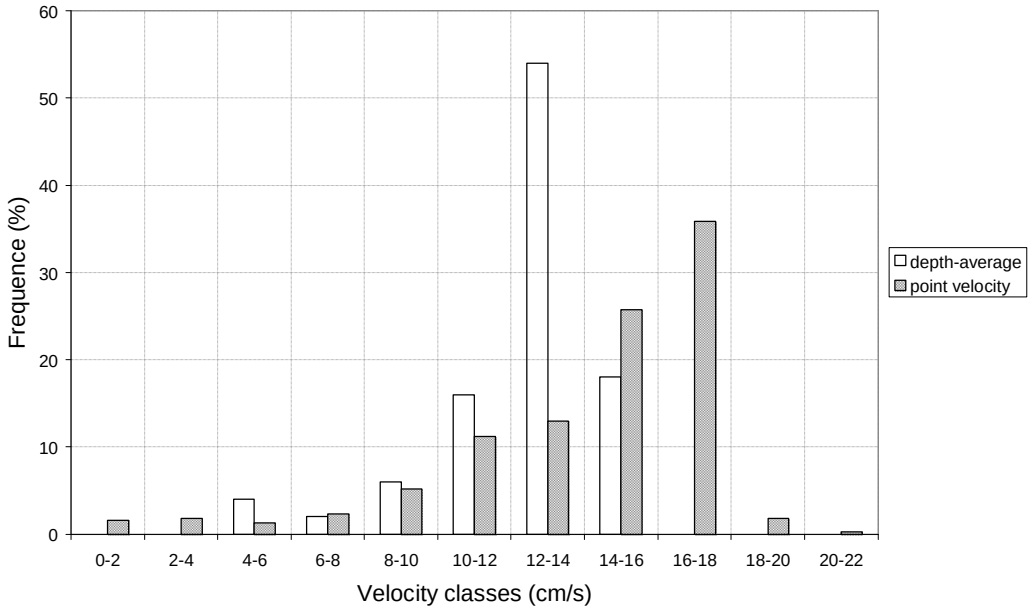

Figure 3-25 Depth-averaged and point velocity frequency distributions for Q=21l/s

3.3.3 Velocity distributions for discharges of 3.0 and 21.0l/s

The effect of discharge was assessed by comparing velocity frequency distributions of measured velocities for Q=3.0l/s with the depth-averaged velocities for 21.0l/s. Graphs of histograms for Q=3.0l/s and 21.0l/s are plotted together in Figure 3-26. Both tests were performed under resistance controlled conditions. The histograms are unimodal and skewed to the left. As expected, the

average velocity is lower for the smaller discharge, and the range of local velocities is wider for the higher discharge.

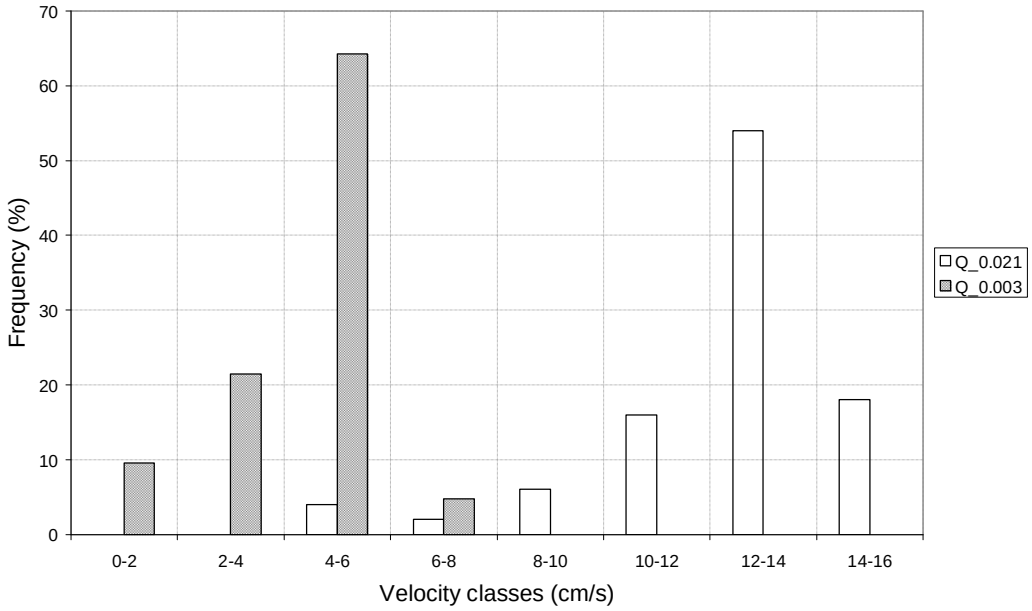

Figure 3-26 Velocity distribution histograms with 0.02 m/s velocity classes for Q=21.0l/s and 3.0l/s

3.3.4 Conclusions

Velocities measured around one hemisphere under resistance controlled condition for two different discharges show:

- The shapes of the histograms are similar for both discharges.
- The average velocity is lower for the smaller discharge.
- The higher discharge provides the wider range of local velocity.
- The coarser resolution tends to underestimate the velocity frequency distribution.

4 PREDICTION METHODS FOR RESISTANCE CONTROLLED CONDITIONS

4.1 Introduction

The resistance to flow in open channels has attracted the attention of researchers for many years. Prediction of open channel flow resistance requires understanding of the influence of the underlying physical effects. Morris (1954) proposed a concept based on an assumption that the loss of energy over rough surfaces is related to the formation of wakes behind each roughness element. The main source of energy loss over a rough surface is the generation, spreading and dissipation of vortices from the wake and separation zones around every roughness element that influences the turbulence structure and energy dissipation phenomena. He presented a concept of flow over rough channel surface that is based on the effect of the longitudinal spacing of surface roughness elements. Three types of flow were recognised:

- If the roughness elements are far apart, each acts as an isolated body, and the wake zone and vortex-generating zone are completely developed and dissipated before the next element is reached. The resulting resistance arises from the form drag of the individual roughness elements, together with the frictional resistance of the surface between the elements. This type of flow is designated as isolated-roughness flow. Under such a condition the friction factor results from the form drag of the roughness elements that depends on the height of the projection of each element, and from the friction drag of the wall surface between elements. The ratio of the longitudinal spacing of the roughness elements to their height is therefore recognised as a significant correlating parameter for the isolated roughness flow condition,

- When the roughness elements are in close proximity, the zone of separation and vortex generation of each element is not completely developed before the next element is encountered. This type of flow is called wake-interference flow. For this condition the frictional resistance of the surface between the roughness elements is negligible, and flow structure is characterised by complex vorticity and turbulent mixing. For this flow type the roughness height is less important in determining resistance, while the longitudinal spacing is the parameter that has the major influence, and
- If the spacing between roughness elements is very small, there will be regions of dead water containing stable vortices between the elements. This type of flow is referred to as quasi-smooth or skimming flow.

Regarding open channel flow resistance, Rouse (1965) wrote: "Yet a glance at publications on the subject during the past decade or so will reveal many a significant anomaly. Momentum and energy analyses are at the same time over-simplified and confused with one other. Representation of parameters by symbols is mistaken for empirical formulation of functions. Flow formulas are sometimes said to involve the Froude number when they do not, and yet the Froude number is as frequently ignored when it is actually essential. Boundary texture and cross-sectional non-uniformity are often discussed without distinction". Forty years later, have we improved our basic understanding of flow resistance? Can we predict flow resistance correctly for different roughness scales?

Three roughness scale types (small, large and intermediate) have been recognised, based on the degree of submergence of the roughness elements. The review in Chapter 2 presented a number of resistance prediction equations for large-scale roughness conditions that have been developed. Most of these, however, are based on modifications of well known resistance equations that were developed for deep flow and their applicability to shallow flows is uncertain.

This chapter includes a short discussion related to small-scale roughness resistance prediction, and presents different types of equations for predicting flow resistance under large- and intermediate-scale roughness conditions.

4.2 Small-Scale Roughness

Under small-scale roughness conditions, the roughness elements are very small compared to the flow depth, and do not significantly alter the one dimensional character of the flow field. The Darcy-Weisbach (equation (2.4)), Chézy (equation (2.5)) and Manning's (equation (2.6)) equations are mostly used for this type of flow.

Various refinements have been made to friction factor estimation. The ASCE Task Force on Friction Factors in Open channels (1963) reviewed the information available at the time, and recommended using the Darcy-Weisbach friction factor, *f*, for estimation of flow resistance. The following equations for estimating *f* for hydraulically rough (equation (4.1)), smooth (equation (4.2)) and transitional (equation (4.3)) flows were recommended:

$$\frac{1}{\sqrt{f}} = c\log\left(\frac{aR}{k_s}\right) \tag{4.1}$$

$$\frac{1}{\sqrt{f}} = c\log\left(\mathrm{Re}\frac{\sqrt{f}}{b}\right) \tag{4.2}$$

$$\frac{1}{\sqrt{f}} = -\log\left(\frac{k_s}{aR} + \frac{b}{\mathrm{Re}\sqrt{f}}\right) \tag{4.3}$$

in which R : hydraulic radius

k_s : roughness size

Re : Reynolds number

a, b, c : empirical coefficients

According to the Task Force, the recommended values of the coefficients *a*, *b* and *c* derived from various data sets are 12, 2.51 and 2 respectively.

In line with the Task Force recommendations, the Darcy-Weisbach friction factor, *f*, is used for all analyses in this study. Values of the Chézy *C* and Manning *n* can easily be obtained from *f* through the equivalence implied by equations (2.4), (2.5) and (2.6).

4.3 Large-Scale Roughness

4.3.1 Background

Flow resistance under large-scale roughness conditions has been investigated previously, and a number of important findings have been reported. It has been shown that a flow resistance equation for large-scale roughness must include a parameter representing the proportion of the coarser elements in the bed surface layer (Bathurst, 1978; Hey, 1979; O'Laughlin and MacDonald, 1964). In describing a gravel-bed surface, it has been shown that the bed arrangement should be characterized by the size ratio between the bed layer and the coarse particles, and the concentration of boulders (Baiamonte and Ferro, 1997; Ferro, 1999).

Flow resistance due to large-scale roughness is related to the form drag of the roughness elements and their disposition in a riverbed. In developing an equation for estimation of the resistance coefficient, it is therefore necessary to account for the processes that determine the drag of individual elements, and the roughness geometry. The form drag of an object varies according to whether the boundary layer on the object is laminar, turbulent, or transitional between these states, which are represented by the Reynolds number. The form drag is also influenced by deformation of the water surface by the object, which depends on the Froude number. The Froude number and Reynolds number are therefore variables that can be related to the drag of the roughness elements (Bathurst et al, 1981).

Flammer et al. (1970) performed laboratory experiments to determine the variables that affect the drag on a hemisphere for various flow conditions, from the relatively simple case of a semi-infinite flow to the more general case of a finite-flow with free surface effects. The semi-infinite flow field refers to conditions where both relative depth and relative width have no effect on the flow, while flow is considered to be finite where it is affected by the relative depth and the relative width.

By dimensional analysis the following dimensionless parameters were obtained:

$$C_d = f(\mathrm{Re}; Fr; P; \frac{y}{k}; \frac{b}{2k}) \qquad 4.4$$

where *Re* : Reynolds number in terms of hemisphere diameter,

Fr : Froude number,

P : velocity profile parameter,

k : hemisphere radius,

y : flow depth,

b : channel width,

y/*k* : relative submergence, and

b/2*k* : relative width.

From experiments related to the large-scale roughness within a flow regime characterized by 'pronounced free surface effects', the following findings were reported:

- Viscous forces are insignificant compared with gravity forces,
- The wave drag caused by the free surface increases the drag coefficient, and
- The maximum wave drag occurs at a Froude number of about 0.5.

The geometry and disposition of the roughness elements have a significant influence on flow resistance, and the determination and incorporation of these influences into flow resistance prediction is essential. Different approaches to account for roughness geometry were discussed in Chapter 2.

Flow resistance of large-scale roughness has been investigated previously, and a general form of velocity equation under such conditions was proposed (James et al, 2001; Jordanova et al, 2004):

$$V = \frac{1}{F}\sqrt{S} \qquad 4.5$$

where F : resistance coefficient and

S : energy gradient.

The following equation for flow resistance coefficient F was proposed in terms of dimensionless parameters (Jordanova et al, 2004):

$$F = \left(\frac{W_{re}}{W_t}\right)^{0.225}\left(\frac{A_p}{A_b}\right)^{-0.465}\left(\frac{WS_{re}}{A_t}\right)^{0.374} \qquad 4.6$$

where:

- The first parameter represents the roughness element concentration, and is expressed as the ratio of the volume of roughness elements within the flow element considered, W_{re}, to the volume of the considered element, W_t,
- The second parameter represents the roughness element shape, and is given as the ratio of the projected cross-sectional area of the individual roughness element, A_p, to its base bed area, A_b, and
- The third parameter represents the roughness element spacing, as the ratio of the wetted surface area of the roughness elements, WS_{re} within the flow element considered, to the considered plan area of the bed, A_t.

Estimation of the flow resistance coefficient F in terms of dimensionless parameters (equation (4.6)) requires a lot of input data. It was therefore suggested that further investigation was required to express the flow resistance coefficient in a simpler form (Jordanova et al., 2004).

Laboratory experiments (Chapter 3) related to the large-scale roughness condition only were further analysed, and a prediction method for flow resistance is proposed.

4.3.2 Prediction approach

Flow resistance under large-scale roughness condition is related to the drag force on the roughness elements, given by

$$F_d = \frac{1}{2} C_d \rho \bar{V}^2 A_p \qquad 4.7$$

where F_d : drag force,
C_d : drag coefficient,
ρ : water density,
V : average velocity, and
A_p : projected area of elements.

Under steady uniform flow conditions, this resisting force is balanced by the weight component of the water. For unit plan area, this component of the weight of water in the downstream direction is given by:

$$W = g\, S(1 \times 1 \times y - N\, V_{r.el}) \qquad 4.8$$

in which g : unit weight of water,
y : flow depth,
S : energy gradient,
N : number of roughness elements per unit area, and
$V_{r.el}$: submerged volume of an individual roughness element.

The component in brackets is the volume of overlying water per unit plan area of bed and is known as the volumetric hydraulic radius, R_V. Equating equations (4.7) for unit plan area and (4.8), with (1x1x $y - N\, V_{r.el}$) = R_V gives

$$V = \sqrt{\frac{1}{C_D N A_p}} \sqrt{R_V} \sqrt{2gS} \qquad 4.9$$

It has been recognized that the drag coefficient, C_D, depends on a number of variables such as the Reynolds number and the Froude number (Flammer et al., 1970), and its estimation is therefore not easy or even possible (Lawrence, 2000; Smart et al., 2002) using a drag type prediction model. Furthermore, the projected area of the roughness elements (NA_p) changes with flow depth and its estimation is complicated. A new, more general expression for resistance under large-scale flow is therefore adopted, as given by

$$V = \frac{1}{F} \sqrt{R_v} \sqrt{2gS} \qquad 4.10$$

where F is the resistance coefficient for large-scale roughness.

Equation (4.10) is superficially similar to the Darcy-Weisbach equation. However, in this case the inclusion of the volumetric hydraulic radius R_v arises from the driving force that is opposed by form drag (equation (4.8)) while the hydraulic radius in the Darcy-Weisbach equation arises from the resisting shear force at the boundary.

Experimental data were used to develop an approach for estimating the resistance coefficient F directly. As the flow resistance of large-scale roughness is mainly due to the form drag, it can be accounted for in terms of the Reynolds number and the Froude number (Section 4.3.1, equation (4.4)). Furthermore, from the laboratory investigation the influence of the roughness elements' density on overall flow resistance is apparent in all the different tests. The following important variables were therefore selected as determinants of F:

- Froude number,
- Roughness elements Reynolds number, and
- Areal coverage of resisting elements.

The resistance coefficient F is proposed to be expressed in terms of dimensionless parameters as

$$F = a\, Fr^{b} Re^{c} \Lambda^{d} \qquad 4.11$$

where the symbol Λ represents the areal coverage calculated as proportion of the bed area covered by the roughness elements.

The experimental data presented in Chapter 3 that satisfy the large-scale roughness criterion ($y/h < 1$) were divided into two sets; one set (listed in Table 4.1) is used in a multiple regression analysis to fit coefficients a, b, c and d for the resistance coefficient, F, and the other set (listed in Table 4.2) is reserved for its verification.

The roughness element Reynolds number was calculated for each run as

$$\mathrm{Re} = \frac{V_{eff} D}{u} \qquad 4.12$$

where D : roughness element diameter

υ : kinematic viscosity of water

The effective flow velocity, V_{eff}, is obtained as the ratio of the volumetric flow rate to the area available for flow,

$$V_{eff} = \frac{Q}{A} = \frac{Q}{W y_{eff}} \qquad 4.13$$

where W is the width of the channel, and y_{eff} is an effective depth calculated as

$$y_{eff} = y_m - N\, V_{r.el} \qquad 4.14$$

where y_m is the measured flow depth above the flume bottom. The submerged volume of a hemisphere can be obtained as

$$V_{r.el} = p\, h^2 y_m - \frac{1}{3} p\, y_m^{\,3} \qquad 4.15$$

where h is the roughness element height.

Table 4-1 Experimental data (Appendices B and C) used in multiple regression analysis

Series	Pattern	Discharge (l/s)	Measured depth (m)	Area covered (%)	Slope
Series 2.1	1	2.7 – 9.5	0.025 – 0.055	14.9	0.001
	3	2.9 – 10.5	0.028 – 0.062	17.3	0.001
	5	1.8 – 12.0	0.020 – 0.062	17.7	0.001
Series 2.2	1	0.6 – 1.6	0.032 – 0.055	54.6	0.0005
	3	0.2 – 7.2	0.023 – 0.055	12.0	0.0005
	5	3.2 – 6.6	0.036 – 0.046	2.9	0.0005
	6	2.8 – 3.5	0.034 – 0.040	9.8	0.0005
	8	0.7 – 4.0	0.020 – 0.060	31.8	0.0005
	9	0.8 – 1.9	0.020 – 0.040	26.1	0.0005
	10	1.4 – 8.9	0.024 – 0.060	16.1	0.0005
	11	2.0 – 5.2	0.026 – 0.047	13.7	0.0005
	13	2.5 – 7.0	0.027 – 0.053	8.1	0.0005
	15	0.4 – 1.2	0.043 – 0.055	74.9	0.0005

Table 4-2 Experimental data (Appendices B and C) used for validation of proposed resistance coefficient *F*

Series	Pattern	Discharge (l/s)	Measured depth (m)	Area covered (%)	Slope
Series 2.1	2	1.2 – 9.3	0.020 – 0.062	17.9	0.001
	4	2.0 – 12.5	0.020 – 0 062	17.0	0.001
	6	3.2 – 12.9	0.025 – 0.062	14.9	0.001
Series 2.2	2	1.1 – 3.7	0.024 – 0.055	22.0	0.0005
	4	2.7 – 12.1	0.023 – 0.055	6.2	0.0005
	12	3.7 – 6.3	0.031 – 0.047	8.1	0.0005
	16	0.6 – 1.6	0.040 - 0.057	62.9	0.0005
	17	0.6 – 1.7	0.031 – 0.055	41.6	0.0005

A multiple regression analysis was performed and the following equation for F was obtained with R^2=0.965:

$$F = 0.16\,Fr^{-0.51}\,\mathrm{Re}^{0.004}\,\Lambda^{0.222} \qquad 4.16$$

4.3.3 Verification of proposed equations (4.10) and (4.16) for the large-scale roughness condition

The performance of the proposed equations (4.10) and (4.16) can be assessed by comparison of measured and predicted values of flow velocity with resistance coefficient F. There are two different questions that need to be answered:

(1) What is the flow resistance in terms of the resistance coefficient F for a known hydraulic condition?,

(2) and (2) What is the flow velocity for a given flow depth?

Two procedures for verification of the proposed equations were therefore applied as follows:

- Procedure 1 - Estimation of Resistance Coefficient (F)

The predictive ability of equation (4.16) has been tested by using measured velocities to calculate values of Froude number and the roughness element Reynolds number, and hence resistance coefficient values from equation (4.16), which were then compared with the measured values.

- Procedure 2 – Prediction of Flow Velocity of a Given Depth

This estimation requires an iterative approach that was applied through four steps:

a) For a specified flow depth a flow velocity, V is assumed, and the Froude number, Fr and the Reynolds number, Re in terms of the roughness element diameter are calculated.
b) The resistance coefficient, F is estimated from equation (4.16).
c) The flow velocity, V is calculated from equation (4.10).
d) The calculated velocity (step (c)) is compared with the initially assumed value (step (a)), and if there is a difference, steps (a) to (c) are repeated until the assumed and calculated velocities are equal.

Verification of proposed equation (4.16) using Procedure 1

Values of resistance coefficient (F) for all experimental runs listed in Table 4-2 were predicted by equation (4.16). These values, designated as F_{pr} were then compared with the measured values, F_m; prediction errors were calculated as absolute values of $(F_{pr} - F_m)/F_m * 100\%$.

Values of predicted and measured resistance coefficient, F for the verification data (Table 4-2) are plotted together with the line of perfect fit in Figure 4-1. The average absolute prediction error was calculated as 8.10%, and the maximum and the minimum as 21.60% and 0.10% respectively, and the standard deviation of the prediction error was calculated as 6.80%.

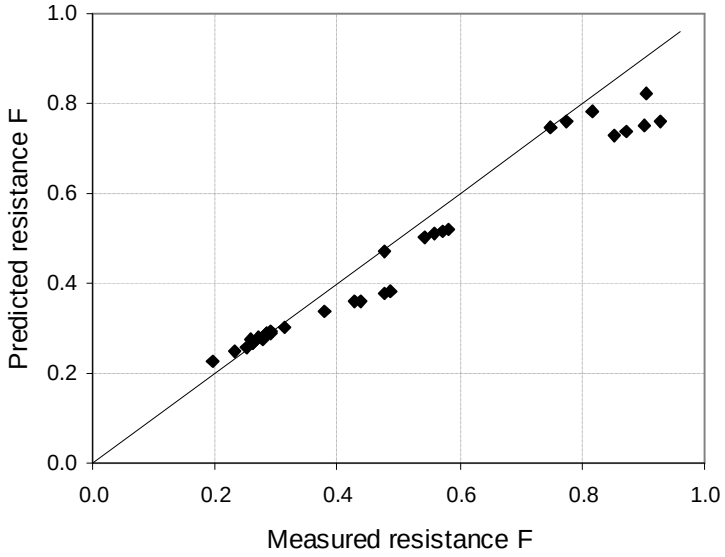

Figure 4-1 Measured and predicted (equation 4.16) values of resistance coefficient *F* together with the perfect fit line for experimental conditions listed in Table 4-2

Figure 4-1 and the corresponding prediction errors show good correlation between predicted and measured values of the resistance coefficients.

Verification of proposed equation (4.10) using Procedure 2

Most flow resistance predictions would be required under conditions where the flow velocity is unknown. True verification of the velocity prediction (equation (4.10)) with the resistance coefficient (equation (4.16)) therefore requires the assumption that flow velocity is unknown. For each experimental run the iterative approach explained above was applied until the value of flow velocity assumed was equal to that calculated (equation (4.10)) with the resistance coefficient estimated by equation (4.16). These velocities and resistance coefficients were then compared with the measured values.

Measured and predicted values of resistance coefficient and flow velocity together with the best fit line and 30% accuracy limits for the verification data (Table 4-2) are plotted in Figures 4-2 and 4-3 respectively.

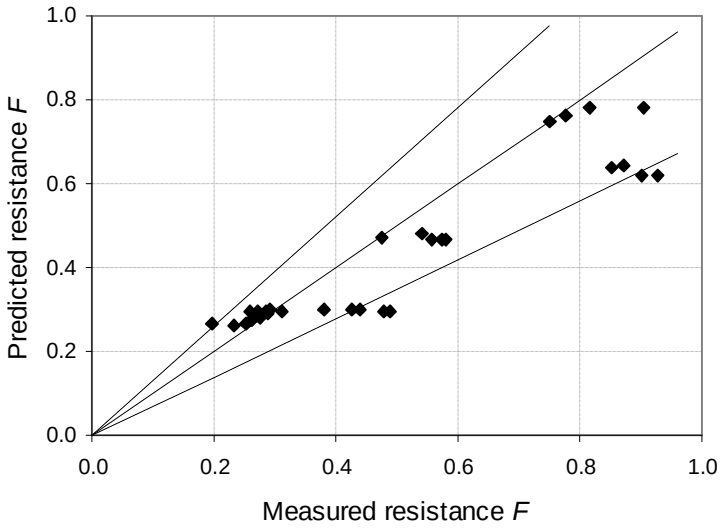

Figure 4-2 Measured and predicted values of resistance coefficient *F* together with the perfect fit line and 30% accuracy limits for experimental conditions listed in Table 4-2

Predicted average, maximum and minimum absolute errors, and the standard deviations of the predicted errors for experiments listed in Tables 4-2 were calculated and presented in Tables 4-3 and 4-4 respectively.

Table 4-3 Resistance coefficient prediction errors in application of Procedure 2

Experimental Data	Average Error (%)	Minimum Error (%)	Maximum Error (%)	Standard deviation (%)
Table 4-2	15.10	0.10	39.30	12.60

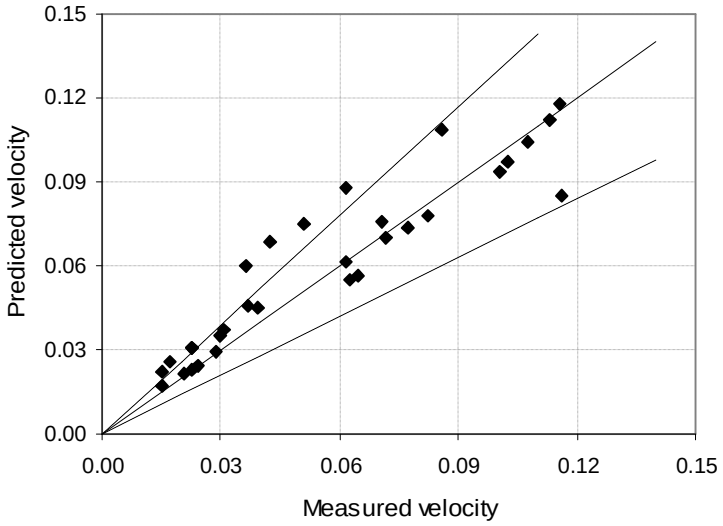

Figure 4-3 Measured and predicted values of flow velocity together with the perfect fit line and 30% accuracy limits for experimental conditions listed in Table 4-2

Table 4-4 Flow velocity prediction errors in application of Procedure 2

Experimental Data	Average Error (%)	Minimum Error (%)	Maximum Error (%)	Standard deviation (%)
Table 4-2	19.20	0.10	64.60	18.90

Verification of the proposed equations (4.10) and (4.16) as assessed by using the iterative procedure (Procedure 2) shows their true predictive ability. It can be seen that prediction errors (Tables 4-3 and 4-4) are higher than were verified by Procedure 1 (Section 4.3.3) but are still within acceptable accuracy limits. Verification of the proposed equations by the two different procedures shows clearly that Procedure 1 indicated better performance because the Froude number and the Reynolds number and hence the resistance coefficient were estimated from the observed flow velocity values. Verification of the proposed equations by Procedure 1 therefore has limited value for assessing velocity prediction. Further verification of the proposed equations (4.10) and (4.16) against field data will therefore be through the iterative approach only.

4.3.4 Equation verification with field data

Depth and velocity distribution data collected in the Cotter River, Australia, are presented in Chapter 8. Two sites, named Vanities Crossing and Spur Hole, were selected for verification of the large-scale resistance prediction method. Photographs of the two sites are presented in Figures 4-4 and 4-5 respectively.

Measurements were carried out at three discharges. The data collected at the lowest discharge satisfy the large-scale roughness criterion, and were therefore used for verification of the proposed equations (4.10) and (4.16). As equation (4.10) was developed for estimation of the average cross-sectional velocity, the measured flow depths were used to calculate the flow area and the average velocity was then calculated as a ratio of the discharge to the flow area.

It should be noted that hydraulic data at these sites were collected for purposes other than estimating flow resistance, and substrate characteristics are given in terms of descriptive substrate classes only (Appendix G). To translate the descriptive substrate classes into particle sizes, the grade scale (adopted from Brakensiek et al (1979) in Gordon et al (1992)) was used for each cross-section considered. The substrate diameters and the areal coverages required for application of the proposed equations ((4.10) and (4.16)) were estimated from the cross-sectional data (Appendix G), and these are listed in Table 4-5. This was done by the following steps:

- Estimation of the biggest substrate clasts present within a cross-section under consideration, and
- Estimation of the area which these clasts covered.

As an example, estimations for Spur Hole Site, cross-section 3 were carried out as follows. The data (Appendix G, cross-section 3) indicate that only two (gravel-cobble and cobble-boulder) substrate classes occur in the cross-section. The areal coverage of the bigger, cobble-boulder substrate size was calculated as the ratio of the number of points where this class was surveyed to the total number of points surveyed within the cross-sectional flow width.

Figure 4-4 The Cotter River, Vanities Crossing Site

Figure 4-5 The Cotter River, Spur Hole Site

Procedure 2 was applied to predict the flow velocity for the given discharges. The volumetric hydraulic radius required for application of the equation (4.10) was calculated as A_f / W (Smart et al, 2002).

Measured and predicted velocities are plotted in Figure 4-6. The average absolute error was calculated as 12.70%.

Table 4-5 The Cotter River field data

Site	Discharge (m^3/s)	Water slope	Roughness diameter (m)	Area covered (%)	V measured (m/s)
Vanities Crossing Cross-section 1	0.3305	0.00250	0.30	53.8	0.273
Vanities Crossing Cross-section 3	0.3305	0.00401	0.40	88.9	0.260
Spur Hole Cross-section 3	0.3427	0.00197	0.30	31.6	0.230
Spur Hole Cross-section 5	0.3427	0.00138	0.08	57.9	0.173

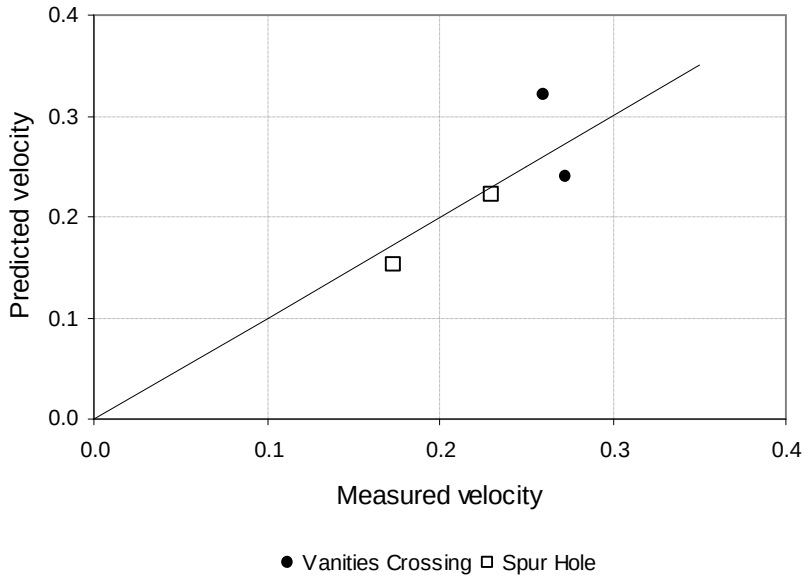

Figure 4-6 Measured and predicted flow velocities for Vanities Crossing and Spur Hole sites of the Cotter River

From field data that satisfied the large-scale roughness condition it can be seen that the proposed equation (4.10) for prediction of the average velocity with the resistance coefficient defined by equation (4.16) reproduced measured flow velocities well. It can also be noted that prediction is better for both cross-sections of the Spur Hole site than for the Vanities Crossing site. The predicted results are quite reasonable considering the limitations of the data - they were collected by a different team, and the only information available includes cross-sections, depth-velocity measurements (Appendix G) and some photographs.

4.3.5 Modification of the prediction approach for field application

Application of the proposed equation (4.16) requires estimation of the areal coverage parameter, representing the plan area covered by larger elements over a total bed area under consideration. This parameter is not practical for use in field applications, as it is not directly measurable. It is, however, related to the bed sediment size distribution, which is more commonly measured.

Statistical parameters such as the geometric standard deviation are therefore more appropriate for representing the resistance-related characteristics of a river bed's substrate. The geometric standard deviation, as defined by Vanoni (1975), is

$$s = \sqrt{\frac{D_{84}}{D_{16}}} \qquad 4.17$$

For lognormally distributed bed material, equation (4.17) can also be expressed in terms of D_{84} and D_{50} as

$$s = \frac{D_{84}}{D_{50}} \qquad 4.18$$

Replacing Λ in equation (4.11) by σ (from equation (4.18)) leads to

$$F = a\,Fr^{b}\,\mathrm{Re}^{c}\,s^{d} \qquad 4.19$$

Application of equation (4.19) requires re-estimation of coefficients *a*, *b*, *c* and *d*. Estimation of these empirical coefficients was carried out using published field data (Bathurst, 1978 and Bathurst, 1985) that satisfied the large-scale roughness criterion ($y/h < 1$). These data were collected from different rivers in Britain. At each site a survey of three cross-sections in sufficient detail was carried out. Mean site values of flow area, width and depth were obtained by averaging the three respective sectional values. The data used in the multiple regression analysis are listed in Table 4-6.

Table 4-6 Published field large-scale roughness data used in multiple regression analysis

Data source	River (site name)	Bed material D_{50} (mm)	Bed material D_{84} (mm)	Number of measurements
Bathurst (1978)	Upper River Tees (Whiddybank)	278	453	3
	Upper River Tees (Cronkley A)	207	380	3
	Upper River Tees(Cronkley B)	185	305	1
Bathurst (1985)	South Tyne	146	240	1
	Alwin	64	143	1
	Glen	60	113	1
	Ettrick	86	193	1
	Tweed	90	183	1
	Almond	118	307	1
	Braan	343	740	2
	Tromie-2	125	387	1
	Dulnain	251	500	2

For each field measurement, the resistance coefficient, F was calculated using equation (4.10). Multiple regression analysis to quantify equation (4.19) resulted in the empirical relationship (equation (4.20)) with R^2=0.747

$$F = 0.05 Fr^{-0.868} \mathrm{Re}^{0.12} s^{-0.228} \qquad 4.20$$

Verification of proposed equation (4.20)

The publication of Hicks and Mason (1998) provided a reference data set for use in visually estimating resistance coefficients for New Zealand rivers. These data were collected from different rivers in New Zealand. The number of cross-sections per reach was generally from thee to five, and the hydraulic parameters provided were calculated by averaging the surveyed cross-section values.

Verification of the proposed equation (4.20) for estimation of flow resistance was carried out by applying the iterative approach to Hicks and Mason (1998) field data that satisfied the large-scale roughness condition (Table 4-7).

Table 4-7 Published Hicks and Mason (1998) field data

Data source	River (site name)	Bed material D_{50} (mm)	Bed material D_{84} (mm)	Number of measurements
Hicks and Mason (1998)	Ruakokapatuna	45	119	5
	Kapoaiaia	78	212	1
	Waiau Water Race	46	80	1
	Stanley Brook	32	106	2

Predicted (equations (4.10 and 4.20)) and measured (Hicks and Mason (1998)) velocities together with the perfect fit line are plotted in Figure 4-7.

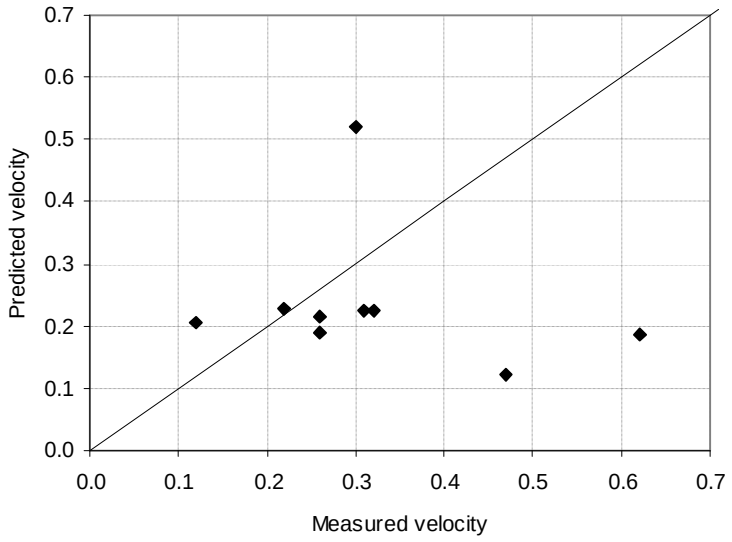

Figure 4-7 Measured and predicted (equations (4.10 and 4.20)) velocities for published Hicks and Mason (1998) field data listed in Table 4-6

Prediction average, minimum and maximum absolute errors and the standard deviation are given in Table 4-8.

Table 4-8 Flow velocity prediction (equations (4.10 and 4.20)) errors in application to field data (Table 4-7)

Field Data	Average Error (%)	Minimum Error (%)	Maximum Error (%)	Standard deviation (%)
Hicks and Mason (1998)	43.47	2.94	73.89	26.42

Taking into account the limitations and uncertainty associated with the field data that have been used in this development, the predictions of equations (4.10 and 4.20) are not unrealistic over a wide range of natural large-scale roughness conditions. While errors are appreciable, performance compares favourably with that of existing methods, as shown in the following section.

Bathurst (2002) equations

Based on twenty-seven published field datasets with $0.37 < y/D_{84} < 11$ and slopes in the range 0.2 – 4%, Bathurst (2002) proposed two equations ((2.18) and (2.19)), for different ranges of channel slope, for predicting flow resistance of rough beds.

Channel slope, $S < 0.8\%$:

$$(8/f)^{1/2} = 3.84\,(y/D_{84})^{0.547} \qquad 2.26$$

Channel slope, $S > 0.8\%$:

$$(8/f)^{1/2} = 3.10\,(y/D_{84})^{0.93} \qquad 2.27$$

These equations are based on data that include both large and intermediate scale roughness conditions. The data were considered together, with no distinction being made between these conditions. Furthermore, the equations have not been verified against independent field data.

For comparison of equations ((2.26) and (2.27)) with the proposed equations ((4.10) and (4.20)), equations ((2.26) and (2.27)) were first applied to the set of data that was used to develop equation (4.20). (This is part of the same data set that was used for the development of equations ((2.26) and (2.27)) that satisfies the large-scale roughness condition.)

Measured flow velocities are compared with those predicted by equations (2.26) and (2.27) (referred to as "Bathurst (2002)") and by equation (4.10) with

resistance coefficient defined by equation (4.20) (referred to as "equation (4.20)") in Figure 4-8.

The average, minimum and maximum absolute errors for flow velocity prediction by equations (2.26) and (2.27) are 15.80%, 1.60% and 44.35% respectively, with a standard deviation of 10.14%. It is clear that equations (2.26) and (2.27) predict velocities better than the proposed equations (4.10 and 4.20), which produced corresponding errors of 38.65%, 1.94% and 98.9% with a standard deviation of 29.5%.

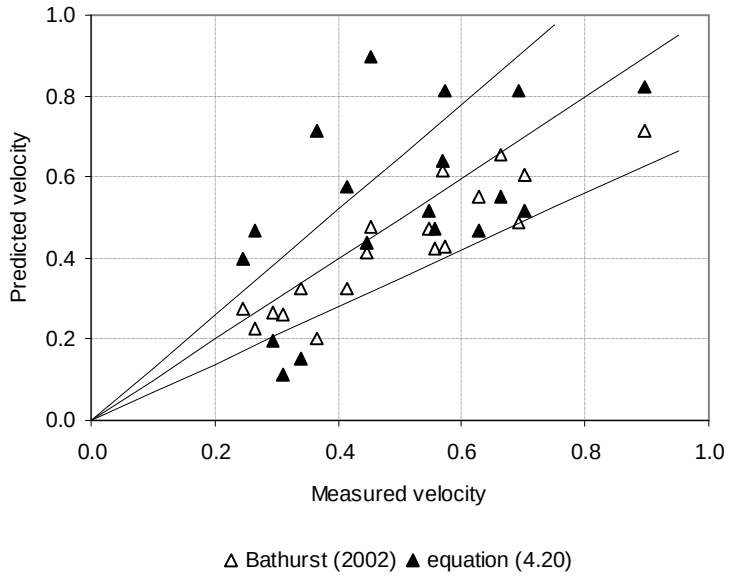

Figure 4-8 Measured and predicted (equations (2.26) and (2.27), and (4.10) and (4.20)) flow velocities with 30% accuracy limits for Bathurst (1978) and (1985) large-scale roughness field data

Equations (2.26) and (2.27) and equations (4.10 and 4.20) were then applied to the Hicks and Mason (1998) field data for large-scale roughness (Table 4-7). The measured and predicted flow velocities are plotted in Figure 4-9.

The prediction errors presented in Table 4-9 show that the proposed equation (4.20) performs better than equations (2.26) and (2.27) for these data. It was shown (Figure 4-8) that equations (2.26) and (2.27) predict flow velocity well for

data (Table 4-6, Bathurst (1978) and (1985)) used for their development. Their performance is considerably poorer, however, for the independent field data of Hicks and Mason (1998).

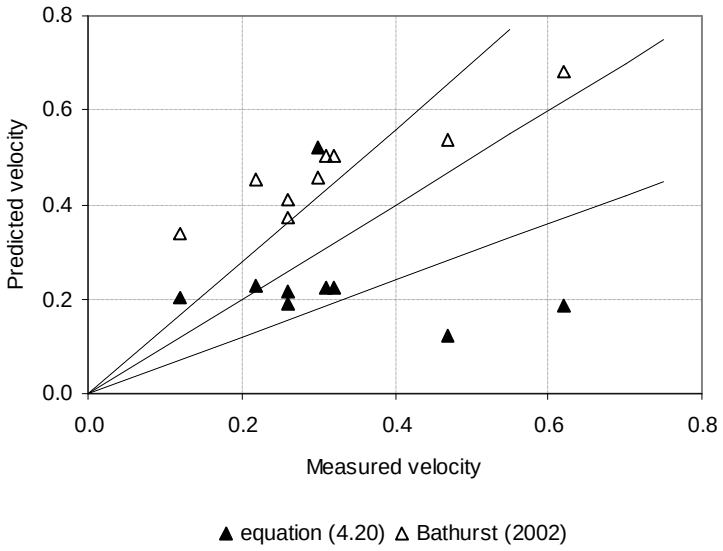

Figure 4-9 Measured and predicted (equations (2.26) and (2.27), and (4.10) and (4.20)) flow velocities with 30% accuracy limits for Hicks and Mason (1998) large-scale roughness field data

Table 4-9 Prediction errors in application of equations ((2.26) and (2.27)) and equations ((4.10) and (4.20)) to Hicks and Mason (1998) field data

Prediction	Average Error (%)	Minimum Error (%)	Maximum Error (%)	Standard deviation (%)
Equations (2.18) and (2.19)	65.29	9.39	183.57	49.66
Equation (4.20)	43.47	2.94	73.89	26.42

4.4 Intermediate-Scale Roughness

When the relative submergence lies between 1.0 and about 4.0, the roughness scale is classified as intermediate. This regime represents a state of flow in which the influence of the roughness elements on flow resistance is manifest as a combination of both element drag and effective boundary shear, or friction. Under such conditions the total discharge can be considered to be the sum of the discharges below and above the tops of the large roughness elements.

Alternatively, the discharge can be calculated using a velocity obtained as a weighted product of velocities reflecting the influences of roughness element drag and boundary friction, with the weighting factor depending on the relative submergence. Both hypotheses were investigated, and two approaches, Approach 1 and Approach 2 are presented below.

4.4.1 Resistance prediction Approach 1

The intermediate-scale roughness condition is shown in Figure 4-10 where $y_{measured}$ is the measured flow depth; y_{eff2} is an effective flow depth (equation (4.14)), and y_{eff1} is an effective flow depth for the discharge below the tops of the large roughness elements.

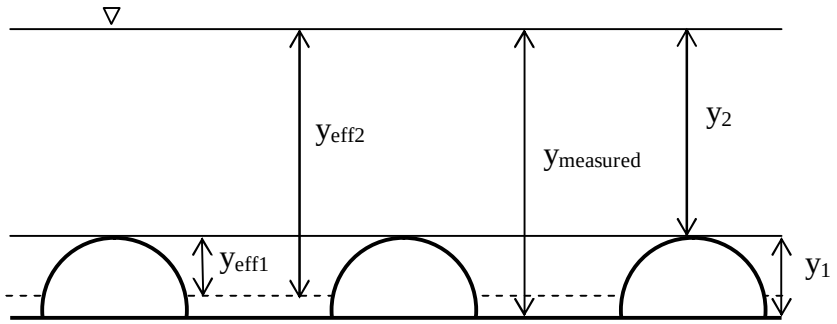

Figure 4-10 Intermediate-scale roughness condition

An equation to estimate the flow resistance under this condition (Figure 4-10) was deduced as follows.

Initially assuming flow to be effectively controlled by shear resistance, the unit width discharge can be estimated through the Darcy-Weisbach equation as

$$q = y_{eff\,2}\sqrt{\frac{8g}{f}}\sqrt{y_{eff\,2}}\sqrt{S} \qquad 4.21$$

The depth of flow y_{eff2} in Figure 4-10is calculated as $y_{measured} - NV_{r.el}$.

Under intermediate-scale roughness the total discharge (q) can be considered to be the sum of the discharges below (q_1) and above (q_2) the tops of the large roughness elements, and can be therefore be expressed as

$$q = q_1 + q_2 \qquad 4.22$$

The lower zone discharge (q_1) is controlled by large-scale type resistance, and therefore, according to equation (4.21),

$$q_1 = y_{eff\,1} V_1 = y_{eff\,1} \frac{1}{F} \sqrt{2 g y_{eff\,1}} \sqrt{S} \qquad 4.23$$

with the value of F corresponding to large-scale roughness conditions.

The flow above the tops of the elements (q_2) is described as shear resisted flow and therefore, with $y_{eff2} - y_{eff1} = y_2$, can be calculated as

$$q_2 = y_2 \sqrt{\frac{8g}{f_2}} \sqrt{y_2} \sqrt{S} \qquad 4.24$$

where f_2 is the friction factor for the flow above the tops of the roughness elements and would have the value corresponding to small-scale roughness conditions.

The total discharge is then

$$q = y_{eff\,1} \frac{1}{F} \sqrt{2 g y_{eff\,1}} \sqrt{S} + y_2 \sqrt{\frac{8g}{f_2}} \sqrt{y_2} \sqrt{S} \qquad 4.25$$

or

$$q = y_2\left(\frac{{y_{eff1}}^{3/2}}{y_2}\frac{1}{F} + \sqrt{\frac{4}{f_2}}\sqrt{y_2}\right)\sqrt{2g}\sqrt{S} = y_2\left(\frac{{y_{eff1}}^{3/2}}{{y_2}^{3/2}}\frac{1}{F} + \sqrt{\frac{4}{f_2}}\right)\sqrt{2g}\sqrt{y_2}\sqrt{S} \qquad 4.26$$

Equating the total discharge from equations (4.21) and (4.26) enables a total effective friction factor to be determined, i.e.

$$\sqrt{\frac{4}{f}}\,{y_{eff\,2}}^{3/2} = {y_2}^{3/2}\left(\left(\frac{y_{eff1}}{y_2}\right)^{3/2}\frac{1}{F} + \sqrt{\frac{4}{f_2}}\right) \qquad 4.27$$

from which

$$\sqrt{\frac{4}{f}} = \left(\frac{y_{eff1}}{y_{eff\,2}}\right)^{3/2}\frac{1}{F} + \left(1 - \frac{y_{eff1}}{y_{eff\,2}}\right)^{3/2}\sqrt{\frac{4}{f_2}} \qquad 4.28$$

Now an average velocity can be calculated by equation (4.29) with $\sqrt{\frac{4}{f}}$ given by equation (4.28),

$$V = \sqrt{\frac{4}{f}}\sqrt{2\,g\,y_{eff\,2}}\sqrt{S} \qquad 4.29$$

The ratio y_{eff1}/y_{eff2} constitutes a weighting factor representing the relative importance of the form and effective shear resistance contributions to total resistance. For deep flows its value will be small, reflecting the minimal contribution of the drag resistance from individual roughness elements; the effective friction factor is then dominated by the second term of equation (4.28), which then closely approximates that for the bed under small-scale roughness conditions. In the intermediate-scale range of flow depths the ratio increases with decreasing flow depth, reflecting the increasing influence of form resistance. When the flow depth is equal to the height of the roughness elements, the ratio becomes equal to 1.0 and the second component of equation (4.28) will equal zero; equation (4.29) then reduces to the form of the equation proposed for large-scale roughness, i.e. equation (4.10).

Prediction Approach 1 verification

The proposed equation (4.29) for estimation of an average velocity, with the effective friction factor given by equation (4.28), was evaluated by comparison of measured and predicted velocities for all laboratory tests performed under the intermediate-scale condition. The values of resistance coefficient F and Darcy-Weisbach friction factor f were determined from experimental data.

Measured and predicted velocities together with the perfect fit line and 25% accuracy limits for Series 2.1, 2.2 and 1.1 experiments are plotted in Figs 4-16, 4-17 and 4-18 respectively.

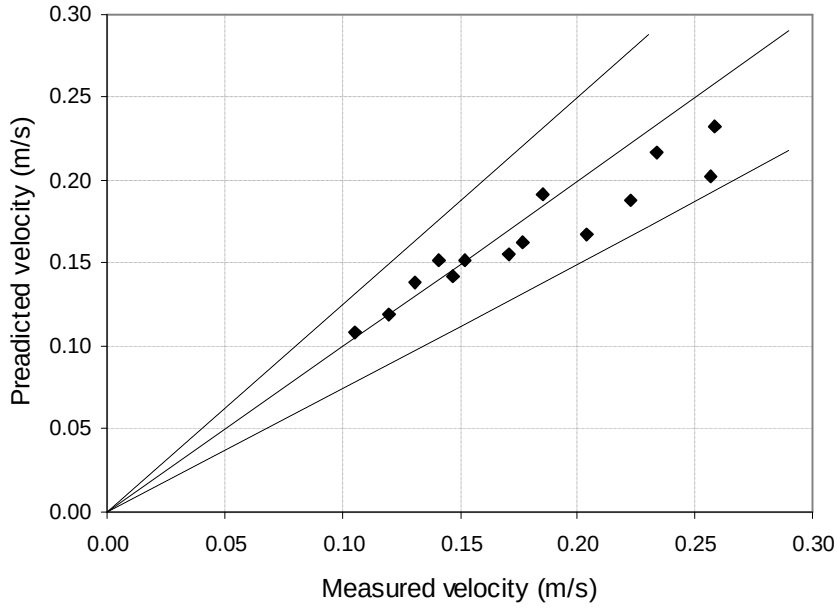

Figure 4-11 Measured and predicted (equations 4.28 and 4.29) velocities with 25% accuracy limits for Series 2.1 experiments.

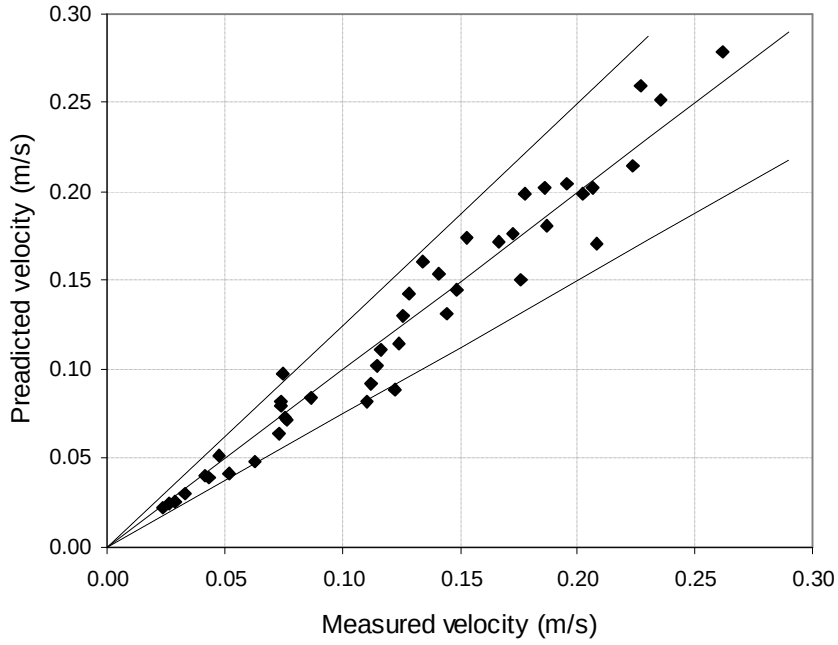

Figure 4-12 Measured and predicted (equations 4.28 and 4.29) velocity with 25% accuracy limits for Series 2.2 experiments

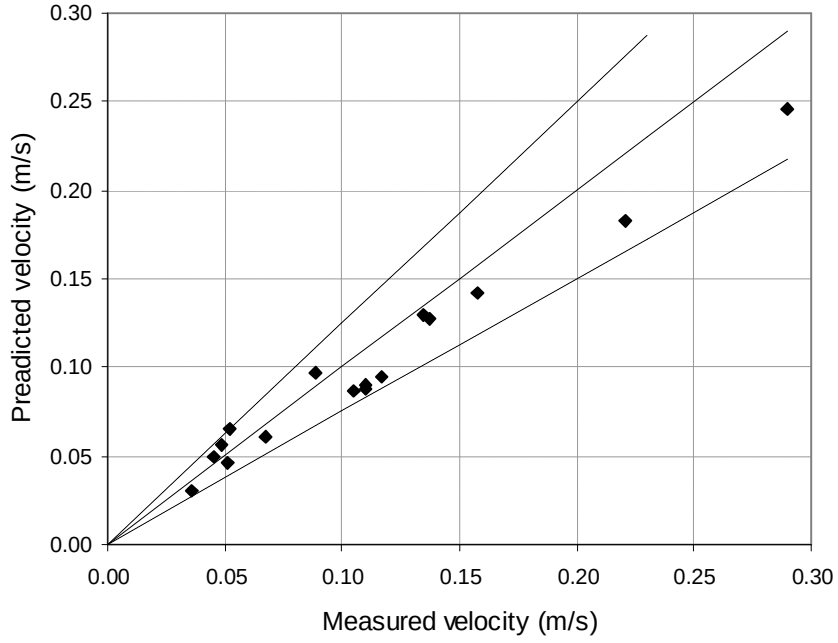

Figure 4-13 Measured and predicted (equations 4.28 and 4.30) velocity with 25% accuracy limits for Series 1.1 experiments

Average, minimum and maximum absolute errors for predicted velocity values for Series 1.1, 2.1 and 2.2 are listed in Table 4-10

Table 4-10 Predicted errors for application equations (4.28) and (4.29)

Experiments	Average absolute error (%)	Maximum absolute error (%)	Minimum absolute error (%)
Series 1.2	12.73	32.12	0.32
Series 2.1	8.08	21.35	0.68
Series 2.2	10.14	31.36	1.60

From the application of the proposed equations (4.28) and (4.29) it can be seen that predicted errors are acceptable. This approach has not been tested against field data.

4.4.2 Resistance prediction Approach 2

Flow resistance under intermediate-scale roughness is imposed by a combination of roughness element drag and boundary friction. A proposed resistance prediction method is based on the following hypothesis:

- If the flow is deep and the relative submergence is greater than four, the boundary friction will dominate, and the velocity can be then calculated by equation (2.4),
- If the relative submergence is less than or equal to one, flow resistance will be dominated by the drag of roughness elements, and the proposed equation (4.10) should then be used,
- With increasing relative submergence from one to four, the dominant resisting effect changes from element drag to friction, and both drag and friction effects therefore contribute to flow resistance. Under such flow conditions, the velocity can be estimated by

$$V = \left(\frac{1}{F}\right)^{a}\left(\sqrt{\frac{4}{f}}\right)^{(1-a)}\sqrt{2\,g\,R_v}\sqrt{S} \qquad 4.30$$

where a is a function of the relative submergence and varies from 1 to 0.

When a is equal to 1, equation (4.30) reduces to the proposed equation (4.10) related to the large-scale roughness condition. With a equal to 0, equation (4.30) will take the form of equation (2.4) for small-scale roughness.

The experimental data related to the intermediate-scale roughness condition were divided into two sets. One set of data (Table 4-11) was used for development of a suitable functional relationship of the coefficient a as a function of the relative submergence.

Table 4-11 Experimental data used for functional development

Flume	Series	Pattern	Relative submergence	Number of runs
B	1.1	1.1.1	1.45 – 3.62	5
		1.1.4	1.02 – 3.55	3
		1.1.5	1.00 – 3.24	3
C	2.1	6	1.00 - 1.37	4
		8	1.00 – 1.96	5
C	2.2	1	1.00 – 3.44	6
		3	1.00 – 2.35	7
		5	1.00 – 2.86	3
		7	1.00 – 3.99	5
		14	1.00 – 4.65	5
		16	1.00 – 2.13	4

Equation (4.30) was applied to each experimental run. Application of equation (4.30) required input of the resistance coefficient F and friction factor f. These values were calculated from the experimental data for the satisfied flow conditions. Average velocities for each experiment were calculated (equation (4.30)) to be equal to the measured velocity by altering input values of the coefficient a only. Values of the coefficient a together with the related relative submergence are plotted in Figure 4-14. A suitable relationship form of the coefficient a as a function of the relative submergence was fitted as

$$a = -0.67\, Ln\left(\frac{y}{h}\right) + 0.992 \qquad 4\text{-}31$$

The other experimental data (Table 4-12) were used for verification of the proposed equations (4.30) and (4.31). Measured and predicted (equations (4.30)

and (4.31)) velocities together with the perfect fit line and 15 % accuracy limits for data measured in flumes B and C experiments are plotted in Figure 4-15.

The average, maximum and minimum absolute prediction errors for Series 1.1, 2.1 and 2.2 experiments were calculated and are listed in Table 4-13.

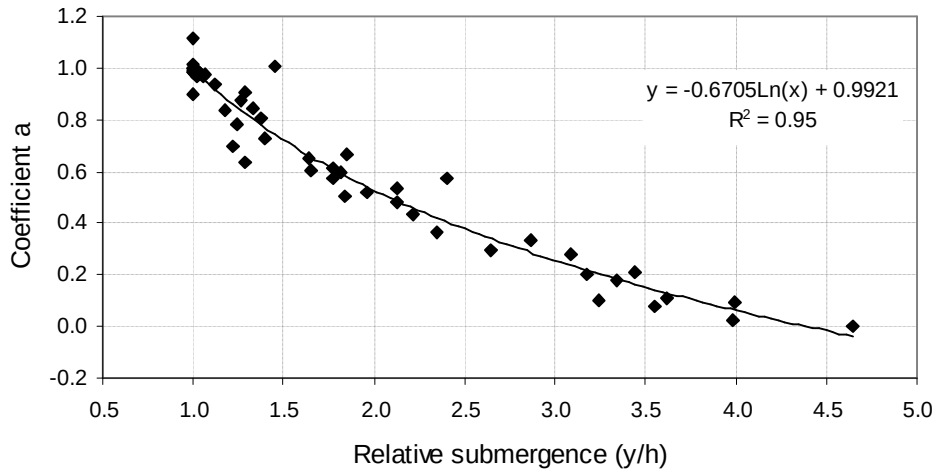

Figure 4-14 Functional relationship of relative submergence and coefficient *a*

Table 4-12 Experimental data used for verification of equation

Flume	Series	Pattern	Relative submergence	Number of runs
B	1.1	1.1.2	1.02 – 4.02	5
		1.1.3	1.02 – 3.57	4
C	2.1	1	1.00 - 1.19	3
		7	1.00 – 1.92	6
C	2.2	2	1.00 – 2.98	8
		4	1.00 – 2.20	4
		6	1.00 – 3.38	5
		15	1.00 – 2.30	6

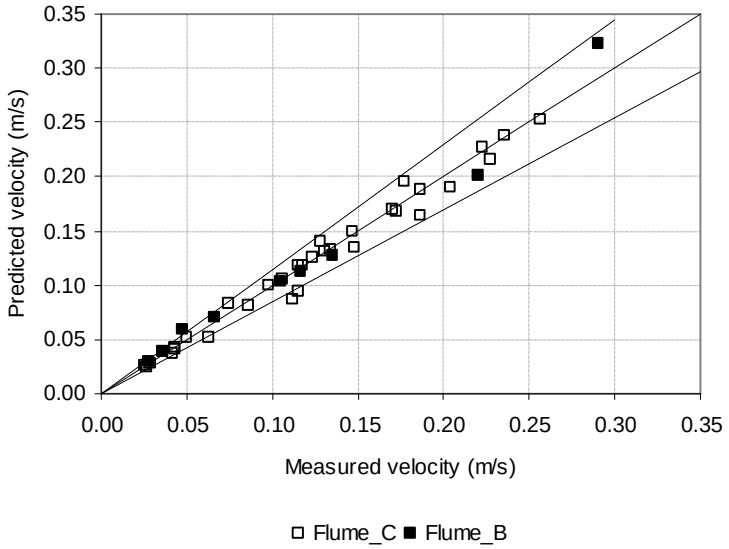

Figure 4-15 Measured and predicted (equations (4.30) and (4.31)) velocities with 15 % accuracy limits for experiments listed in Table 4-11

Table 4-13 Average, maximum and minimum absolute prediction errors for application of equations (4.30) and (4.31)

Flume	Series	Average (%)	Maximum (%)	Minimum (%)	St. Deviation of prediction error (%)
B	1.1	7.55	23.45	1.54	6.30
C	2.1	1.79	7.07	0.10	1.98
C	2.2	7.49	22.94	0.07	6.13

Verification of proposed equations (4.30) and (4.31) with Bathurst et al., (1981) published experimental data

Published experimental data of Bathurst et al (1981) were used for further verification of equations (4.30) and (4.31). Bathurst's experiments were carried out at Colorado State University in a flume with a length of 9.54m and a width of 1.168m width. The resistance of five bed materials classified as 12.7, 19.5, 38.1, 50.8 and 63.5mm were tested. Experiments were performed with 3 flume slopes of 0.02, 0.05 and 0.08. Experimental data used for verification of proposed equations (4.30) and (4.31) are summarised in Table 4-14.

Table 4-14 Summary of Bathurst et al., (1981) experimental data

Bed material (mm)	D_{84} long axis (mm)	D_{84} median axis (mm)	D_{84} short axis (mm)	Discharge (m^3/s)	y_measured (m)
12.7	17.0	11.5	7.8	0.0019-0.0490	0.012-0.046
19.5	28.0	19.3	12.3	0.0021-0.0546	0.016-0.054
38.1	59.0	43.0	27.0	0.0018-0.0802	0.023-0.101
50.8	73.0	47.0	34.0	0.0025-0.0495	0.041-0.095
63.5	90.0	58.0	44.0	0.0037-0.0497	0.049-0.108

Application of the proposed equations (4.30) and (4.31) required estimation of the resistance coefficient *F*, friction factor *f*, and the relative submergence. It has been assumed that the short axis of D_{84} represents the height of the bed substrate. The relative submergence for each experiment was therefore calculated as the ratio of the measured depth to the short axis of D_{84}. Application of equation (4.30) required estimation of *F* and *f*. For each experimental run values of *F* (equation (4.10)) and *f* (equation (2.4)) were calculated. For each test, graphs of *F* and *f* as functions of the relative submergence were plotted and were extended, if necessary, to relative submergences equal to one for graphs of *F* and to four for graphs of *f*. These graphs were used to estimate the values of *F* and *f*. These values are listed in Table 4-15.

Table 4-15 Values of resistance coefficient *F* and friction factor *f* estimated from Bathurst et al., (1981) experimental data for use in equation (4.30)

Bed material (mm)	Slope	y/D_{84}	F	f
12.7	0.02	1.65 - 2.46	1.534	0.236
	0.05	2.53 - 5.91	0.734	0.208
	0.08	1.59 - 4.59	1.010	0.231
19.5	0.02	2.29 - 5.22	1.443	0.232
	0.05	1.66 - 4.36	0.890	0.172
	0.08	1.29 - 3.66	1.04	0.137
38.1	0.02	1.10 - 3.74	0.730	0.181
	0.05	0.85 - 2.93	0.673	0.169
	0.08	0.92 - 2.43	0.494	0.216
50.8	0.02	1.48 - 2.79	2.939	0.040
	0.05	1.30 - 2.32	1.978	0.146
	0.08	1.21 - 2.20	1.200	0.162
63.5	0.02	1.29 - 2.46	1.035	0.158
	0.05	1.11 - 2.02	0.937	0.089
	0.08	1.05 - 1.84	0.798	0.071

Measured and predicted (equations (4.30) and (4.31)) velocities together with the perfect fit line and 25 % accuracy limits for experiments with five flume beds are plotted in Figure 4-16.

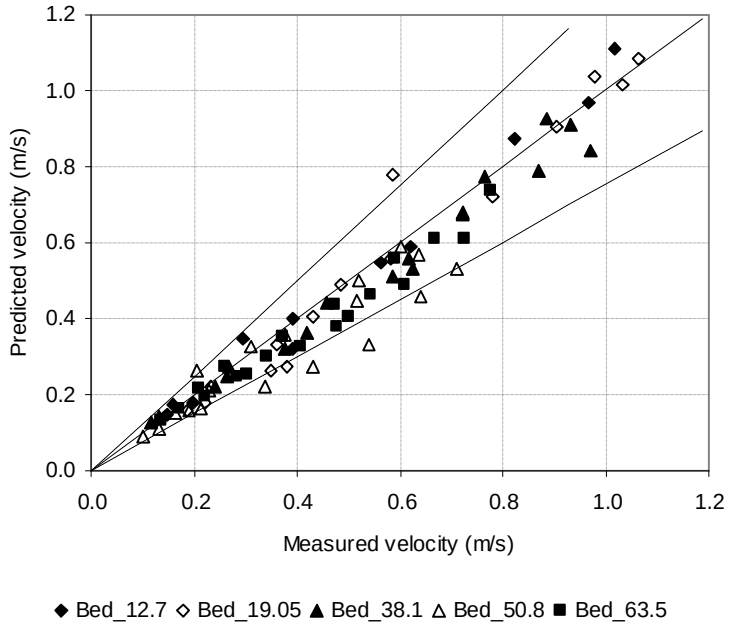

Figure 4-16 Measured and predicted (equations (4.30) and (4.31)) velocities with 25% accuracy limits for Bathurst et al (1981) experiments listed in Table 4-14

Average, maximum and minimum absolute errors in prediction of flow velocity were calculated for each bed material size and slope, and these are listed together with the standard deviation in Table 4-16.

Table 4-16 Average, maximum and minimum prediction (equations (4.30) and (4.31)) errors

Bed material (mm)	Slope	Average error (%)	Maximum error (%)	Minimum error (%)	St. deviation of prediction error (%)
12.7	0.02	2.50	2.73	2.27	0.23
	0.05	9.25	16.85	4.46	4.23
	0.08	7.76	18.06	0.18	6.98
19.5	0.02	19.70	32.57	1.30	11.52
	0.05	5.26	8.37	0.17	2.60
	0.08	10.26	28.62	1.27	10.28
38.1	0.02	8.48	13.83	1.16	4.40
	0.05	8.85	15.39	2.21	4.51
	0.08	6.76	13.40	1.66	3.85
50.8	0.02	7.06	15.33	1.63	4.66
	0.05	29.49	38.73	15.08	8.23
	0.08	14.60	27.40	3.67	8.85
63.5	0.02	14.75	20.13	6.19	4.71
	0.05	14.24	20.52	4.26	5.51
	0.08	5.84	8.50	2.70	1.68

The measured and predicted velocities plotted in Figure 4-16, and predicted errors listed in Table 4-16 show that the proposed approach can be recommended for estimation of flow velocity under intermediate-scale roughness conditions.

Verification of proposed equations (4.30) and (4.31) with Bathurst (1985) and Hicks and Mason (1998) published field data

Further verification of the performance of the proposed equations ((4.30) and (4.31)) was carried out by comparison of measured and predicted flow velocities of Bathurst (1985) and Hicks and Mason's (1998) published field data that satisfied the intermediate-scale criterion. Data used for this verification are listed in Table 4-17.

The prediction approach was first applied to the field data of Bathurst (1985). Measured and predicted (equations (4.30) and (4.31)) flow velocities are plotted in Figure 4-17. Predictions by Bathurst's (2002) equations ((2.18) and (2.19)) are included for comparison in Figure 4-17, as these were derived for flow conditions with $y/D_{84}<11$ representing the intermediate-scale roughness. Predicted (equations (2.18) and (2.19)) values are denoted "Bathurst (2002)" while equations ((4.30) and (4.31)) predictions are denoted "Equation (4.31)".

It can be seen (Figure 4-17) that flow velocity prediction for both approaches is very similar. Average, maximum and minimum absolute prediction errors together with the standard deviation are presented in Table 4-18.

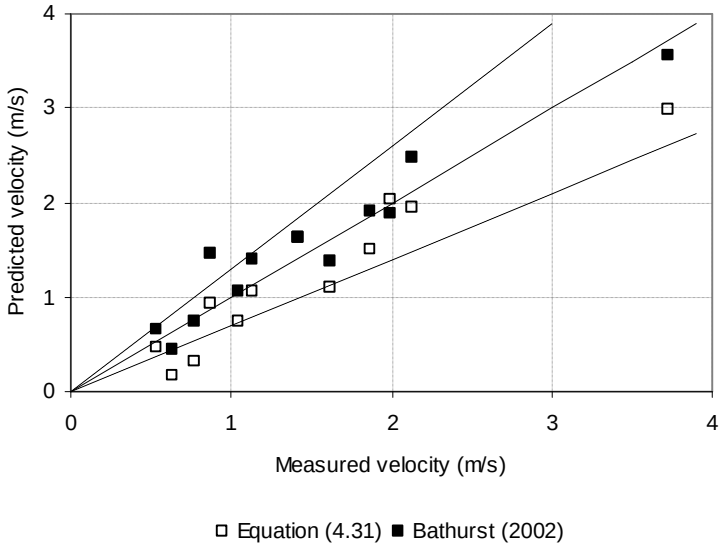

Figure 4-17 Measured and predicted (equations (4.30) and (4.31), and (2.18) and (2.19)) flow velocities with 30% accuracy limits for published field data of Bathurst (1985)

Table 4-17 Published field data used for verification of proposed equations (4.30) and (4.31)

Data source	River (site name)	Mean flow depth (m)	Bed material D_{84} (mm)	Number of measurements
Bathurst (1985)	South Tyne	0.50	240	1
	Ettrick	0.21 - 0.47	193	3
	Tweed	0.72	183	1
	Tromie-2	0.40 – 0.89	387	5
	Findhorn	0.30 and 0.45	140	2
Hicks and Mason (1998)	Waiau Water Race	0.22-0.30	80	3
	Cardrona	0.28 and 0.30	78	3
	Hutt	0.42 – 0.67	212	3
	Clarence	0.38 - 0.77	200	6
	Forks	0.28 and 0.39	104	2
	Waipapa	0.39 and 0.41	91	2
	Flaser	0.31 – 042	208	3
	Rowallanbum	0.62and 0.86	250	2
	Northbrook	0.16 – 0.26	50	4
	Ruakokapatuna	0.24 and 0.42	119	2
	Kapoaiaia	0.26 – 0.54	212	5
	Butchers Creek	0.31 – 0.67	168	5
	Stanley Brook	0.32	106	1

Table 4-18 Average, maximum and minimum absolute predicted errors in application of equations (4.30) and (4.31), and (2.18) and (2.19) to Bathurst (1985) field data

Approach	Average error (%)	Maximum error (%)	Minimum error (%)	St. deviation of prediction error (%)
Equations (2.18) and (2.19)	17.66	69.18	1.60	18.08
Equations (4.30) and (4.31)	23.87	72.41	1.67	21.02

Prediction errors in application of the proposed equations ((4.30) and (4.31)) are slightly higher. Nevertheless, this approach was developed based on the laboratory data only while the development of equations ((2.18) and (2.19)) was based on this field data.

Equations (4.30) and (4.31), and (2.18) and (2.19) were also applied to the Hicks and Mason (1998) field data. Predicted and measured flow velocities together with the perfect fit line and 30% accuracy limits are plotted in Figure 4-18.

Average, maximum and minimum prediction errors and the standard deviations were calculated and are presented in Table 4-19.

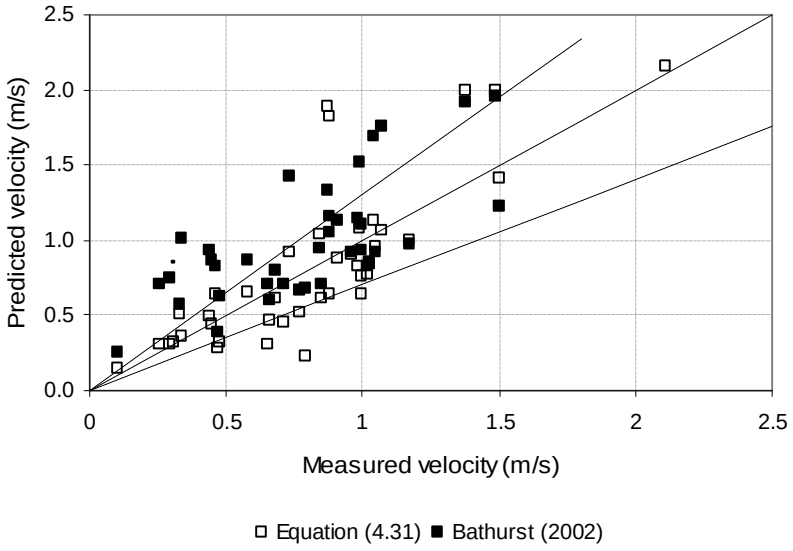

Figure 4-18 Measured and predicted (equations (4.30) and (4.31), and (2.18) and (2.19)) flow velocities with 30% accuracy limits for published Hicks and Mason (1998) field data

Table 4-19 Average, maximum and minimum absolute predicted errors in application of equations (4.30) and (4.31), and (2.18) and (2.19) to Hicks and Mason (1998) field data

Approach	Average error (%)	Maximum error (%)	Minimum error (%)	St. deviation of prediction error (%)
Equations (2.18) and (2.19)	51.48	197.29	0.87	52.88
Equations (4.30) and (4.31)	27.09	116.88	0.20	25.47

As before, when equations (2.18) and (2.19) are applied to the independent field data the resulting prediction is much poorer compared to predictions using the proposed method.

4.5 Conclusions

The different resistance effects in river channels with coarse substrates under small-, intermediate- and large-scale roughness conditions have been described by appropriate equations. Conventional shear resistance type equations are appropriate for small-scale roughness conditions. Equation (4.10) is proposed for estimating velocity under large-scale roughness condition with the resistance coefficient F given as a function of roughness element Reynolds number, Froude number and areal coverage by equation (4.16). These equations were tested against independent laboratory data and Cotter River field data, and proved to give satisfactory performance. For field applications, equation (4.20) is proposed for estimating F. This is similar to equation (4.16) but accounts for bed roughness in terms of the geometric standard deviation of bed material particle sizes rather than the areal coverage of largest clasts. Application to field data showed performance to be at least as good as the best known, but less rationally justifiable as an alternative. Both equations (4.16 and 4.20) can be used for field applications depending on which parameter Λ or σ is estimated for a site under consideration.

Two approaches (Approach 1 and Approach 2) are proposed for estimating velocity under intermediate-scale roughness conditions. Approach 1 is based on an assumption that the total discharge is the sum of the discharges below and above the top of the large roughness elements. Based on this assumption, equation (4.29) for estimating the average velocity was theoretically developed and then applied to experimental data. Application of equation (4.29) to experimental results suggests that the approach performs satisfactorily. Its performance has yet to be tested against field data. An alternative new way (Approach 2) (equation (4.30)) for estimating velocities under intermediate-scale roughness conditions incorporating the influence of both large-and small-scale roughness is proposed. Coefficient a (equation (4.31)) effects partitioning of the influences of the two roughness scales. The proposed equations ((4.30) and (4.31)) were verified against experimental (Bathurst et al, 1981) and field (Bathurst, 1985; Hicks and Mason, 1998) data with promising results.

5 EXPERIMENTAL INVESTIGATION OF HYDRAULIC CONDITIONS WITH LARGE ROUGHNESS ELEMENTS

5.1 Introduction

Flow depth and velocity are hydraulic parameters used to describe aquatic animals' habitats and to predict biotic responses to discharge in a river. Under low flow conditions in a riffle area, a wide range of local flow depths and velocities occur, and the cross-section average depth and average velocity are insufficient to define the aquatic habitats at different flows. Prediction of flow depth and velocity distributions for a given discharge is therefore an important part of environmental studies.

At low flows, rocks and boulders control the local velocity and depth distributions. Flow is rapidly varied, and the occurrence of particular local velocities and depths is caused by the boundary geometry rather than flow resistance phenomena. Under such conditions, hydraulic features such as hydraulic jumps, local backup, contractions and critical controls occur over the whole area (Figure 5-1). Furthermore, all these features change with discharge. Under such conditions an average flow depth and velocity have limited value for ecological interpretation. As the discharge increases, the multiple local controls become submerged and the flow tends towards a resistance controlled condition, with consequent changes in the distributions of local flow depth and velocity.

Prediction of velocity distributions under multiple local control conditions is very difficult. Although the phenomena are easily understandable through elementary rapidly spatially varied flow theory using concepts of Specific Energy, Momentum Function and the occurrence of critical flow, the complexity of the situation (such as shown in Figure 5-1, for example) makes direct application of this theory practically impossible.

An alternative to deterministic prediction is statistical description, and statistical models (Chapter 2) have been proposed for quantifying velocity and depth distributions. These are generally based on field data and do not account explicitly for multiple local control conditions.

Figure 5-1 shows a wide range of flow depths and velocities, typical of multiple local controlled conditions. An understanding of the effect of various controlling factors is required for prediction of velocity and depth distributions under multiple local controlled conditions, whether a deterministic or a statistical approach is followed. For this reason, laboratory experiments were conducted in the hydraulics laboratory of the School of Civil and Environmental Engineering, University of the Witwatersrand. The results of this experimental work are presented in this chapter.

Figure 5-1 Example of multiple local controlled conditions created in the laboratory flume

5.2 Laboratory Investigations of Local Velocity Distributions: Flume C Experiments

5.2.1 Experimental Conditions

A series of experiments were carried out to test the influence of the transverse spacing between roughness elements and the control condition (multiple local control or resistance control) on the statistical distribution of local velocities. The experiments were conducted in a 0.5m wide channel formed within a 2.0m wide, 15.0m long, tilting laboratory flume under controlled and idealized conditions. The flume slope was set to 0.0005 for all experiments. Water was supplied to the flume through a closed circulation system, and a control valve situated in the supply pipe at the head of the experimental flume was used to control the discharge. The discharge was measured with a V-notch, installed downstream of the flume, and by an electronic flow meter with sensors in the water supply pipe. The discharge was $0.0161 m^3/s$ for all experiments. The downstream flow depth was controlled by an adjustable tailgate at the end of the flume.

Experiments were carried out to investigate velocity distributions under local controlled conditions created by two hemispheres (D = 0.112m) representing natural roughness elements. The hemispheres were place in line along the cross section at Chainage 5.5m from the flume entrance, with three different spacing's. Three different tailgate settings were used to induce multiple local controlled or resistance controlled conditions for the different arrangements. The experimental conditions are listed in Table 5-1.

A two-dimensional *Nortek Doppler Velocimeter* (NDV) was used to measure velocity. Velocities were measured in the longitudinal (x) and transverse (y) directions. A total of 1000 samples of a 9mm sampling volume at mid-flow depth were recorded at each measuring point for 40 seconds at a frequency of 25 Hz. Time-averaged velocities obtained by the NDV were determined using the CollectV Data Acquisition Program.

For all the experiments, mid-flow depth velocities were measured on a grid extending from Chainage 5.00m (0.50 m upstream of the hemispheres) to Chainage 7.00m (1.50 m downstream of the hemispheres). Measurements were taken over 20 cross sections at 0.05 m transverse intervals. The cross sections were located with varying spacing, to ensure adequate description of longitudinal variations. From Chainage 5.00m the cross sections were spaced at 0.10m up to Chainage 5.50m, then at 0.05m up to Chainage 5.80m, at 0.10m up to Chainage 6.20m, and at 0.20m up to Chainage 7.00m. It must be recognized that a statistical representation of a velocity distribution in situations such as this will depend on the sample area. The experiments were conducted only to enable comparison of the effects of the different arrangements and are not attempts to define usable distributions.

Table 5-1 Experimental conditions

Test	Discharge (m^3/s)	Slope	Spacing (m)	Tailgate position (m)	Control Condition
1	0.0161	0.0005	0.14	0.1005	MLC
2	0.0161	0.0005	0.24	0.1005	MLC
3	0.0161	0.0005	0.38	0.1005	MLC
4	0.0161	0.0005	0.24	0.1012	RC
5	0.0161	0.0005	0.38	0.1012	RC
6	0.0161	0.0005	0.24	0.1030	RC
7	0.0161	0.0005	0.38	0.1030	RC

Where: MLC: Multiple Local Control, RC: Resistance Control

Flow depths were also measured at the velocity measurement locations but are not presented here because the water surface disturbances in the supercritical flow regions were of the same order of magnitude as the flow depth. The error margins on the measurements are therefore too great for statistical interpretation in the same way as for the velocity measurements.

5.2.2 Results

For better understanding of how local velocities change with spacing between obstacles and with hydraulic conditions (multiple local control or resistance control), a statistical method was used to analyze the measured data. A frequency

distribution approach was applied to all the experimental tests to count numbers of occurrences of each measured value in each data set over the same area. A bar chart graphic format was used for showing the results. The measured velocities are presented in Appendix E, in Tables E-1 to E-7 for each of the 7 conditions tested.

To be able to compare velocity frequency distributions for different experimental runs, the graphs should be plotted in the same velocity scale. The measured velocities (Appendix E) were therefore analyzed to establish the maximum that was measured. Then a decision of how many classes to have and how wide the classes should be was made. As the maximum velocity was measured in Test 2 (0.655 m/s), all results presented here are therefore plotted with 7 classes within the class width of 0.1m/s.

For Test 1, a locally controlled condition was created by setting the tailgate position appropriately (Figure 5-2). The distribution of local velocities is shown by the histogram in Figure 5-3.

Figure 5-2 Tests 1, two hemispheres with spacing of 0.14 m

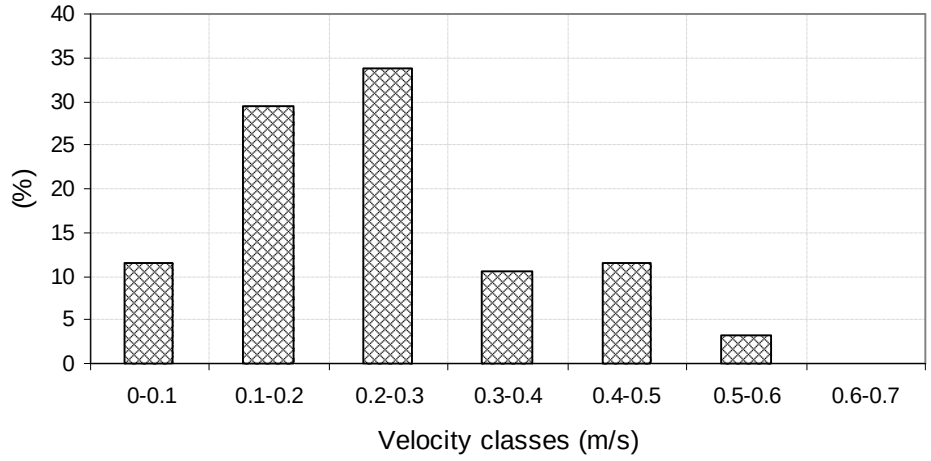

Figure 5-3 Velocity distribution under local controlled condition created by two hemispheres with spacing of 0.14 m

The histogram is unimodal and skewed to the right (Figure 5-3). The mode is within the 0.2 to 0.3m/s velocity class. It can be seen that the highest velocity class is void, presumably because the narrow gap restricted the development of high velocities.

For Test 2, the spacing between the hemispheres was increased to 0.24m (Figure 5-4) and local controlled conditions were maintained. The velocity distribution histogram is shown in Figure 5-5.

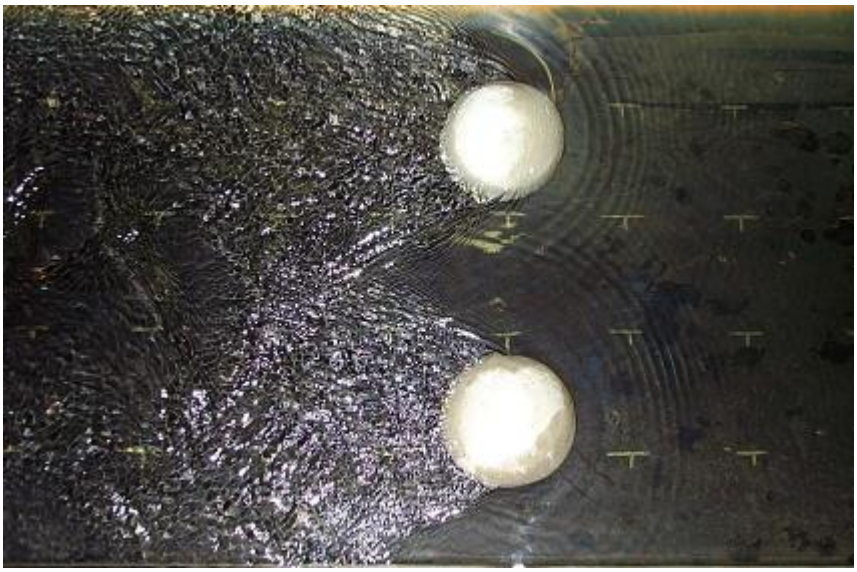

Figure 5-4 Test 2, two hemispheres with spacing of 0.24 m

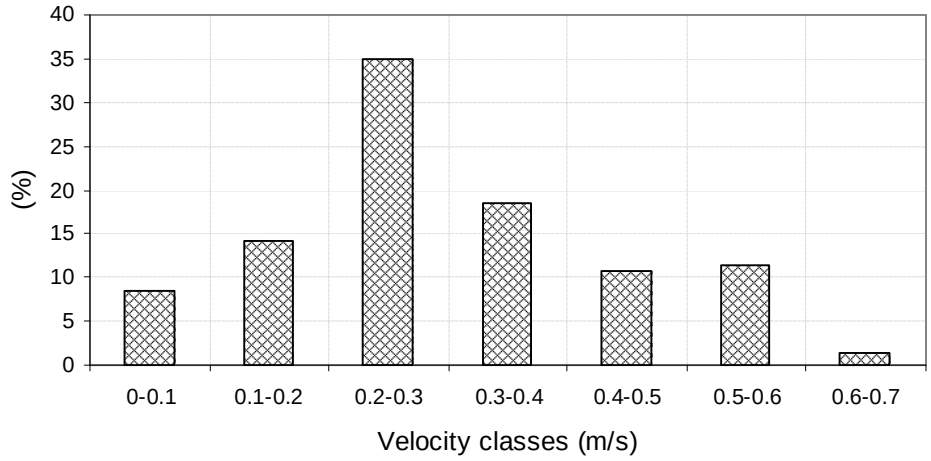

Figure 5-5 Velocity distribution under local controlled condition created by two hemispheres with spacing of 0.24 m

From the histogram can be seen that with an increased spacing of 0.24m, a wider range of velocities occurred.

For Test 3 the two hemispheres were positioned with spacing of 0.38m (Figure 5-6), again with local control. A histogram of the measured velocities is in Figure 5-7. The histogram is unimodel, but skewed to the left.

Figure 5-6 Test 3, hemispheres with spacing of 0.38 m

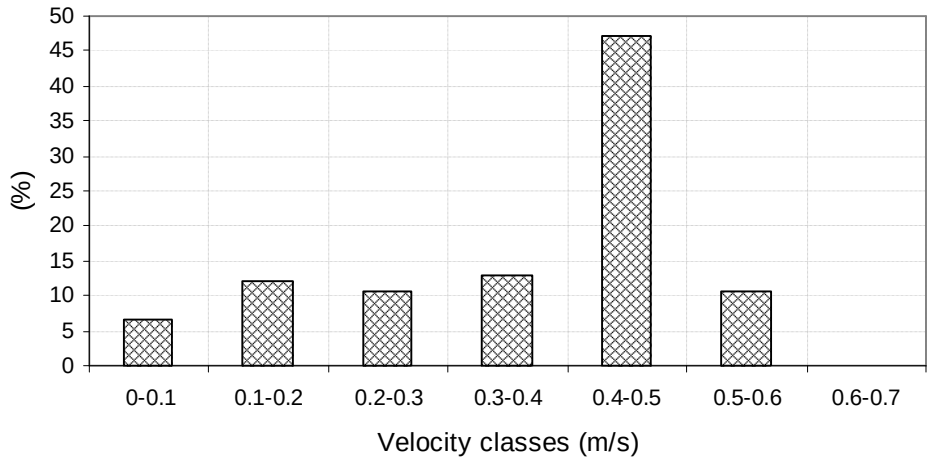

Figure 5-7 Velocity distribution under local controlled condition created by two hemispheres with spacing of 0.38 m

From Figure 5-7 it can be seen that the highest velocity class is void, as for the narrower gap (Figure 5-5), and the strong mode characterizes the uniformity.

For Test 4, the hemispheres were positioned as for Test 2, but the tailgate was raised by 0.007m in order to submerge the local control influences. The resulting velocity histogram is shown in Figure 5-8. The mode is within the same 0.2 to 0.3 velocity class as for Test 2. With this condition another higher velocity class (0.5-0.6m/s) is void, and the mode is within the 0.1-0.2m/s velocity class, indicating greater uniformity than under locally controlled conditions.

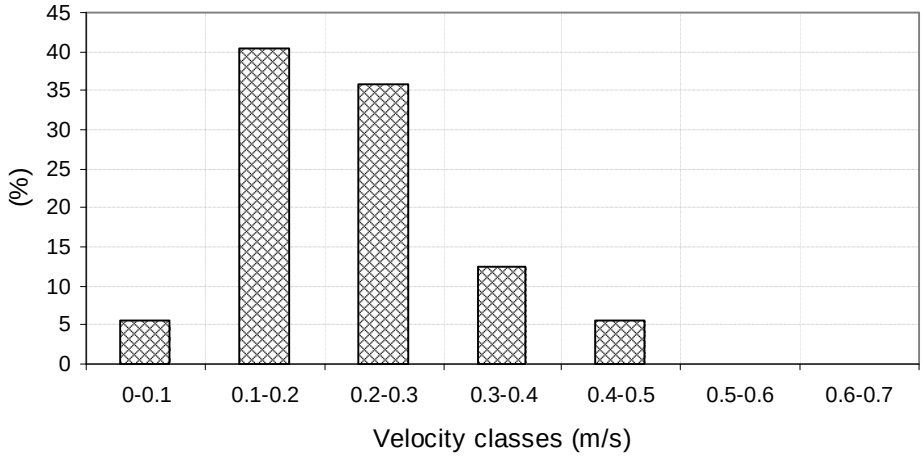

Figure 5-8 Velocity distribution created by two hemispheres with spacing of 0.24 m under submerged local controlled condition

For Test 5, the hemispheres were positioned as in Test 3, and the position of the tailgate was as in Test 4, again to submerge the local control effects. The histogram of velocity distribution is presented in Figure 5-9. This histogram (Figure 5-9) is very different from that for Test 3 (Figure 5-3). No velocities occur in the 0.5-0.6 class, while the other five classes have similar occurrences, showing a more consistent frequency distribution.

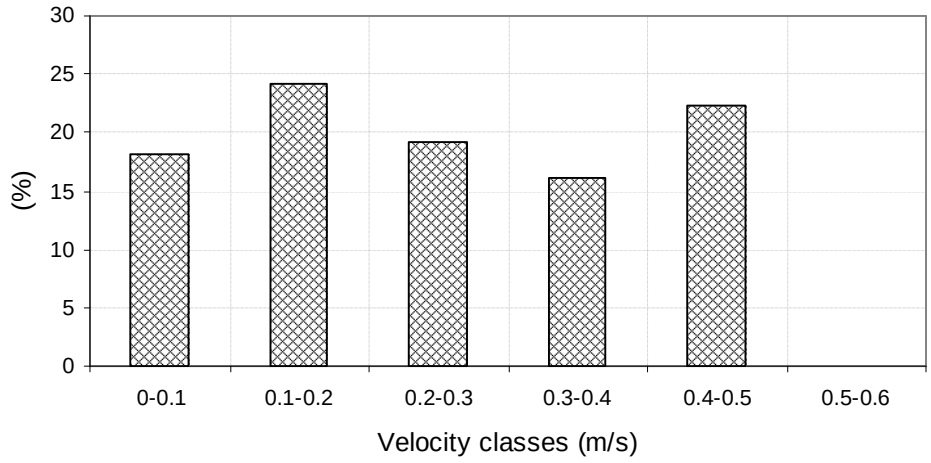

Figure 5-9 Velocity distribution created by two hemispheres with spacing of 0.38 m under submerged local controlled condition

Test 6 was run to investigate increased submergence by raising the height of the tailgate to 0.018m. The velocity distribution histogram is shown in Figure 5-10. About 80% of the measured velocities are within 0.1-0.2m/s class. There are no measured velocities higher than 0.4m/s. The strong mode characterizes the uniformity.

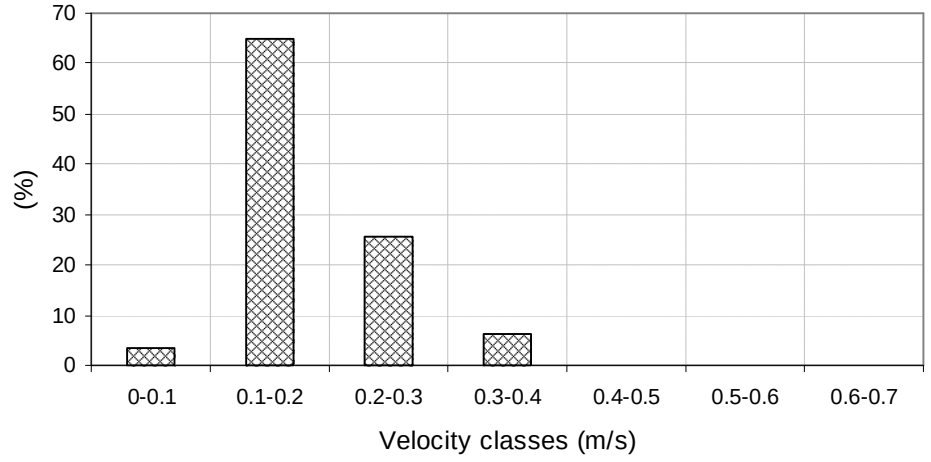

Figure 5-10 Velocity distribution under resistance controlled condition created by two hemispheres with spacing of 0.24 m

Test 7 was conducted for spacing between hemispheres of 0.38m, and the tailgate height as in Test 6. The velocity distribution histogram is plotted in Figure 5-11. All the measured velocities are within the range of 0 to 0.4m/s, with only four classes.

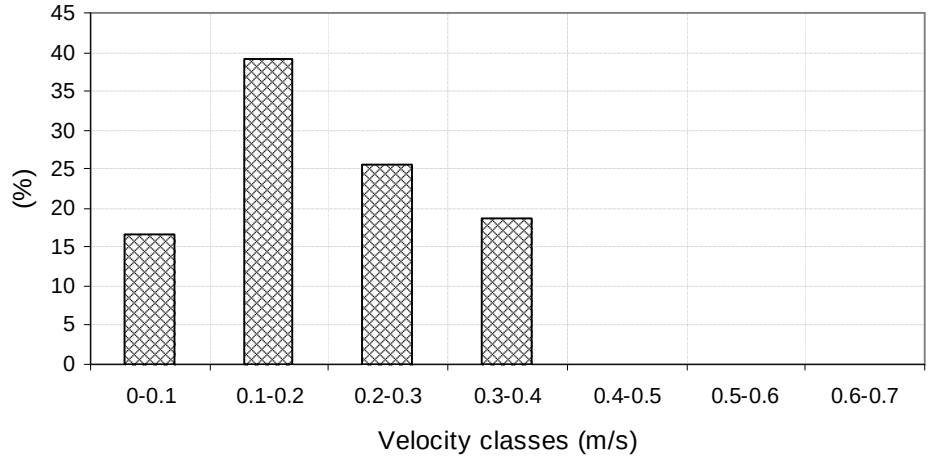

Figure 5-11 Velocity distribution under resistance controlled condition created by two hemispheres with spacing of 0.38 m

5.2.3 Discussion

The influence of the different spacing's of 0.14, 0.24 and 0.38m in Tests 1, 2 and 3 respectively on the velocity distribution under local controlled conditions is shown in the comparison of velocity distribution histograms in Figure 5-12. This shows that with the same tailgate setting, the velocity range is similar for the different spacing's, but the distributions are rather different. The highest range of velocities occurred with the intermediate spacing of 0.24m (Test 2); the highest velocity class was void for a spacing of 0.14m (Test1) and also for the widest spacing (Test 3). It is therefore concluded that spacing between the large roughness elements is one of the parameters that influences the velocity distribution, with large spacing resulting in high local velocities under multiple local control conditions.

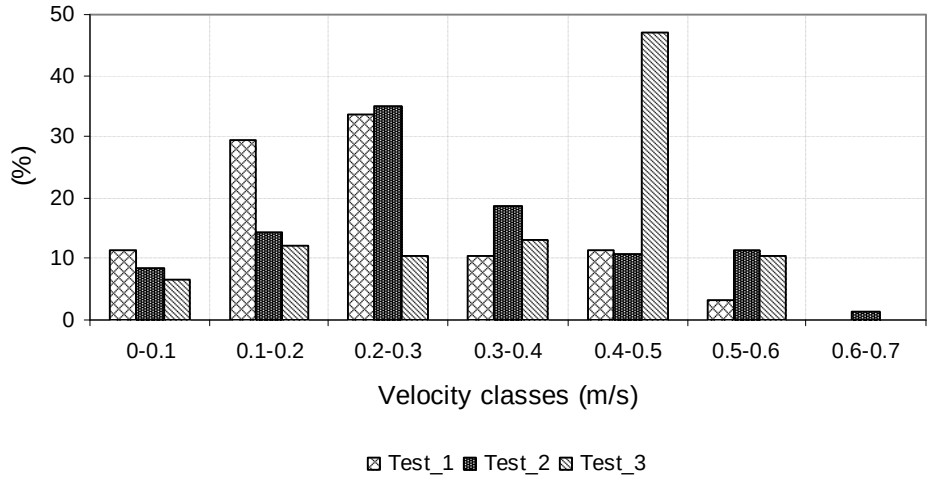

Figure 5-12 Effect of element spacing on velocity distribution under multiple local control condition

The influence of downstream conditions on the velocity distributions for tests 2, 4 and 6 with spacing of 0.24m and tests 3, 5 and 7 with spacing of 0.38m are shown in Figures 5-13 and 5-14 respectively. Spatially explicit velocity distributions for spacing's 0.24m (Tests 2 and 6) and 0.38m (Tests 3 and 7) are presented in Figures 5-15 and 5-16 respectively. It is apparent that locally controlled conditions (Tests 2 and 3) produce a wider range of local velocities than occur under resistance controlled conditions (Tests 6 and 7). Submergence of local controls (Tests 2, 4 and 6, and 3, 5 and 7) therefore decreases the hydraulic diversity and multiple local controlled conditions can be expected to provide a wider variety of physical habitats than resistance controlled conditions. This difference emphasizes the importance of being able to predict velocity distributions in environmental studies in which aquatic animals' habitats need to be specified.

These results suggest that the lack of generality of statistical descriptions of velocity distributions severely limits their useful application in practice.

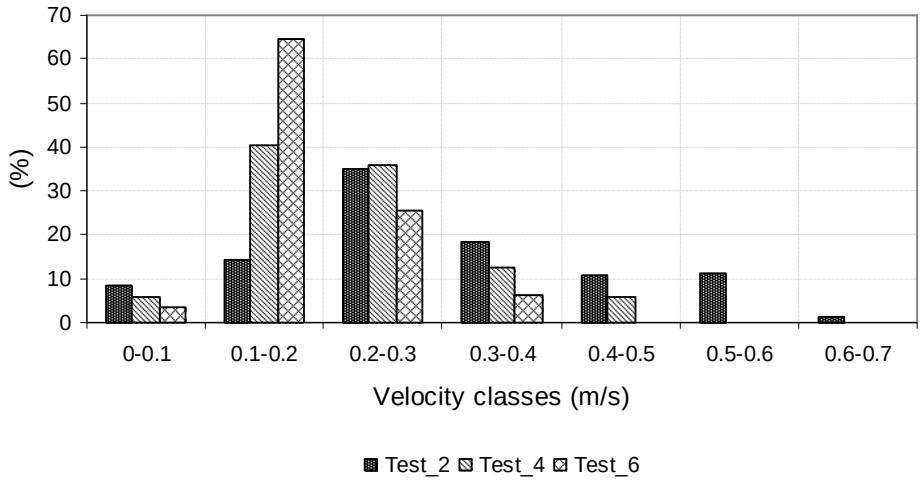

Figure 5-13 Effect of submergence condition on velocity distribution for roughness element with spacing of 0.24 m

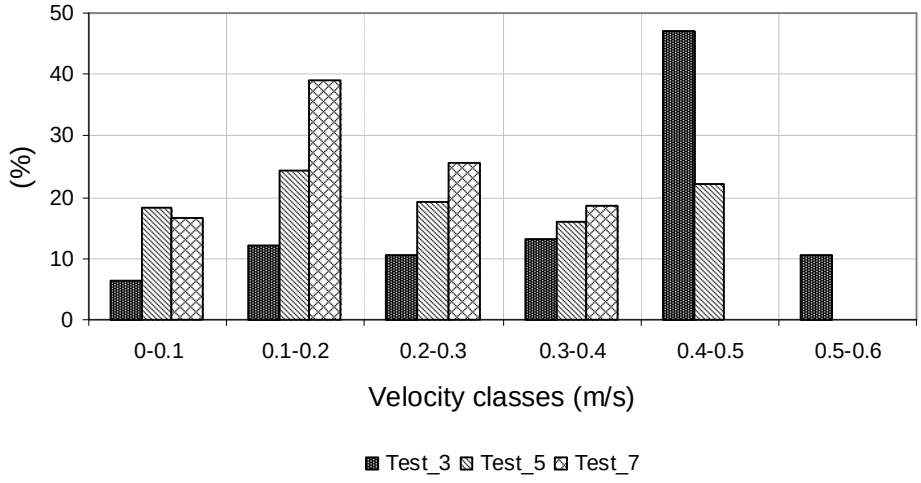

Figure 5-14 Effect of submergence condition on velocity distribution for roughness element with spacing of 0.38 m

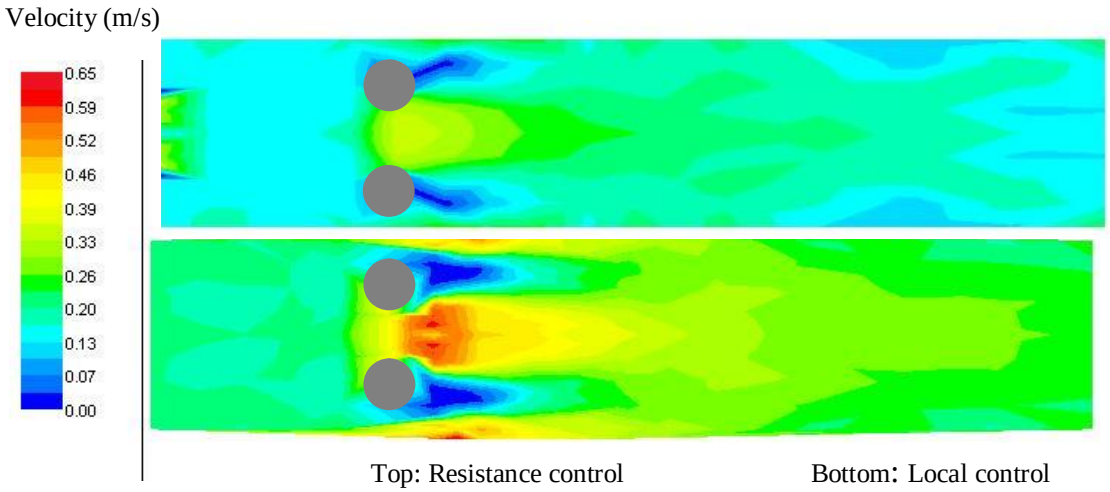

Figure 5-15 Explicit velocity distributions for spacing of 0.24m for Test 2 (bottom graph) and Test 6 (top graph)

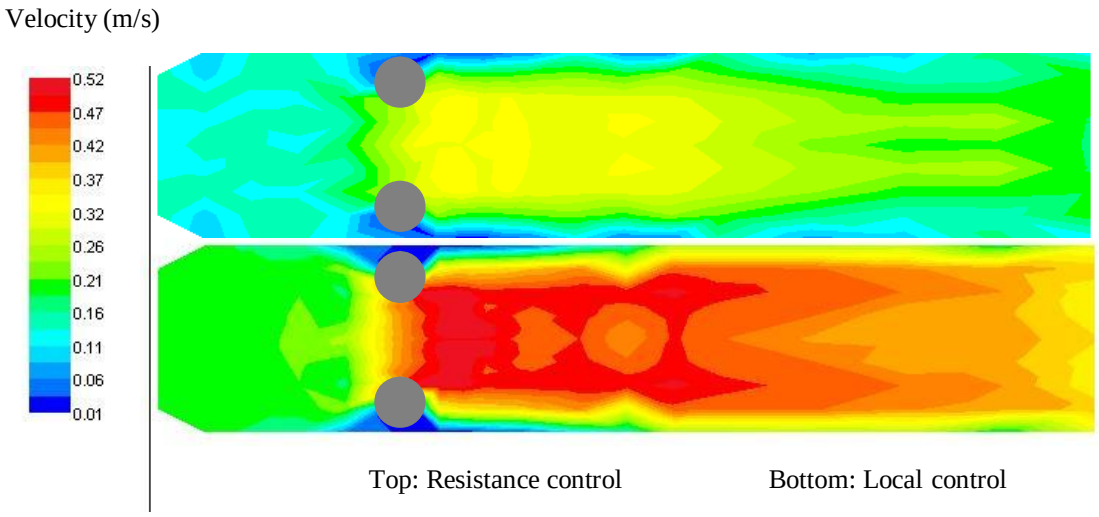

Figure 5-16 Explicit velocity distributions for spacing of 0.38m for Test 3 (bottom graph) and Test 7 (top graph)

5.3 Laboratory Investigations of Local Velocity Distributions: Flume B Experiments

The Flume C experiment results have been presented in the form of local velocity histograms. These give representations of the relative occurrences of different

velocities within specified classes in a reach of channel, without conveying any idea of where the velocities occur in relation to the roughness elements. Aquatic animals often use relatively localized areas of a stream for particular functions, and experience a wide range of hydraulic conditions even around single rocks. It is useful to be able locate suitable habitat areas in a spatially explicit way, and to understand the influence of channel characteristics on hydraulic conditions at particular specified locations. This set of experiments was conducted to gain understanding of the influence on the velocity distributions around a single roughness feature of other features in the channel.

5.3.1 Experimental Conditions

These experiments were conducted in a 0.38m wide, 15.0m long, glass-sided tilting laboratory flume set at a slope of 0.001136. A tailgate fixed downstream of the flume was used to establish uniform flow for a given discharge. Water was supplied to the flume through a closed circulation system, and two valves situated in the supply pipe at the head of the flume were used to control the discharge. The discharge was measured with a V-notch installed downstream of the flume, and by an electronic flow meter with sensors in the supply pipe. The discharge was $0.005 m^3/s$ for all experiments, resulting in resistance controlled conditions.

Two shapes of roughness element, cylindrical and hemispherical, were tested. Test 1 was first carried out in the flume with no roughness elements to determine the uniform flow depth and associated cross-sectional velocity distribution to establish a basis for assessing the effects of the large roughness elements. Tests 2 to 6 were performed using concrete hemispheres with D = 0.114m placed on the flume bed at different chainages (measured from the beginning of the sloping part of the flume), while in Test 7 the roughness element was simulated by a cylinder with D = 50mm. Experimental conditions of all tests are listed in Table 5-2.

Velocities were measured in the longitudinal (x direction) and transverse (y direction) channel directions, using the same NDV apparatus as used in the Flume C experiments. A total of 500 samples in a 9mm sampling volume were recorded at each measuring point for 20 seconds at a frequency of 25 Hz. Time-averaged

velocities obtained by the NDV were assessed using the CollectV Data Acquisition Program. All measured data are included in Appendix F.

Velocities were measured on a grid extending from Chainage 3.5m in each case to an appropriate downstream location. Measurements were taken over a number of cross sections at 0.02m transverse intervals. The cross sections were located at different positions for each experiment to capture the distinct characteristics of each roughness pattern. Velocities were measured over half the channel width in each case.

Table 5-2 Experimental conditions

Test	Element Type	D (mm)	Number of Elements	Chainage (m)	Slope	Discharge (m^3/s)
1	Empty	N/A	N/A	N/A	0.001136	0.005
2	Hemisphere	114	1	4.5	0.001136	0.005
3	Hemisphere	114	2	4.5 and 5.5	0.001136	0.005
4	Hemisphere	114	3	4.5, 5.5 and 6.5	0.001136	0.005
5	Hemisphere	114	4	4.5, 5.5, 6.5 and 7.5	0.001136	0.005
6	Hemisphere	114	2	4.5 and 8.5	0.001136	0.005
7	Cylinder	50	1	4.5	0.001136	0.005

5.3.2 Results

The measured velocities are presented in Appendix F, in Tables F-1 to F- 7 for each of the 7 conditions tested. Note that the velocity profiles presented here are plotted over the full channel width, assuming symmetrical repetition of the measurements over half the width.

The first experiment (Test 1) was conducted to establish uniform conditions and therefore was run without any roughness elements. The measured uniform depth was 0.035m. The transverse velocity distribution is shown in Figure 5-17.

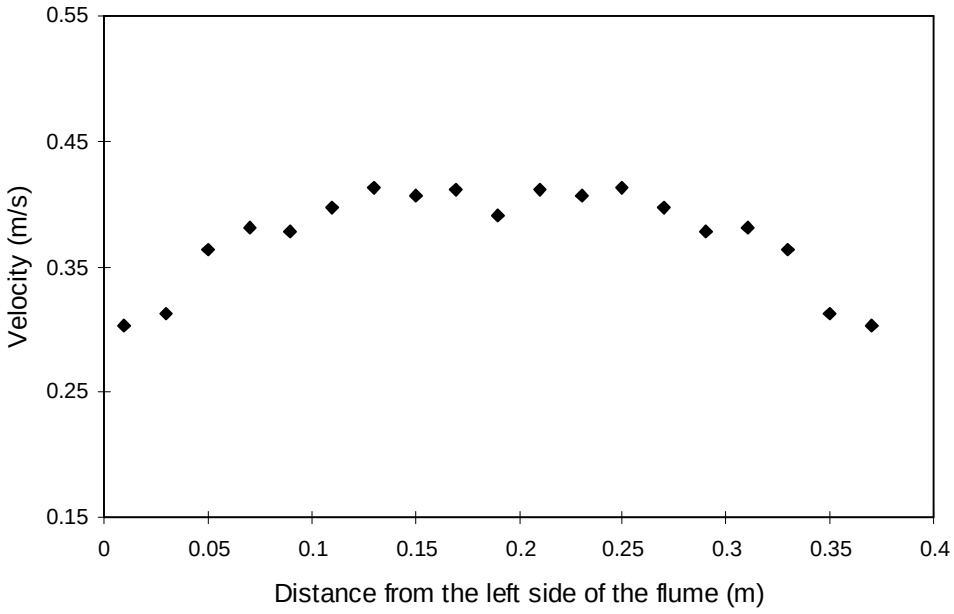

Figure 5-17 Transverse velocity distribution under uniform conditions (Test 1)

For Test 2, a single hemisphere was placed at chainage 4.50m. Velocities were measured at 19 cross-sections along the flume. Transverse velocity distributions at Chainages 3.50, 4.00, 4.40, 5.50 and 6.60m together with that for the empty flume are shown in Figure 5-18. A photograph of the experimental set up of Test 2 is included as Figure F-1 in Appendix F. A plan-view of the spatial distribution of longitudinal velocity is illustrated in Figure 5-19. Variations of longitudinal velocity together with the uniform velocity are shown on Figures F- 7 to F- 10 in Appendix F.

Influence of one hemisphere on the velocity distribution (Test 2) is shown in the comparison with uniform velocity distribution (Test 1) in Figure 5-20. It can be seen that a single hemisphere has changed the velocity distribution creating wider velocity variety.

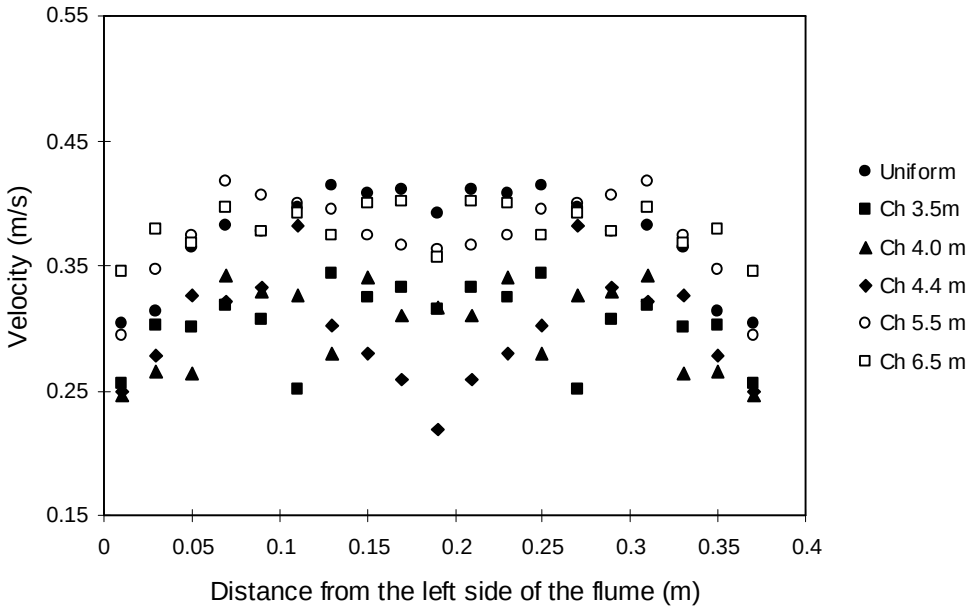

Figure 5-18 Measured transverse velocity distributions for Test 2

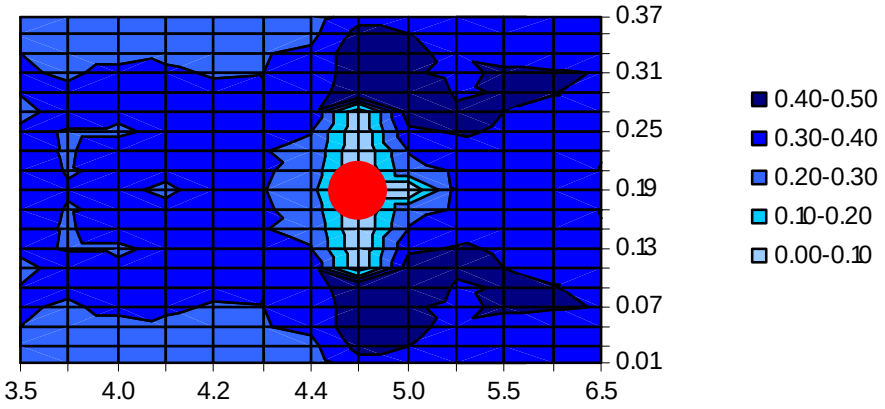

Figure 5-19 Plan-view of spatial distribution of longitudinal velocity for Test 2

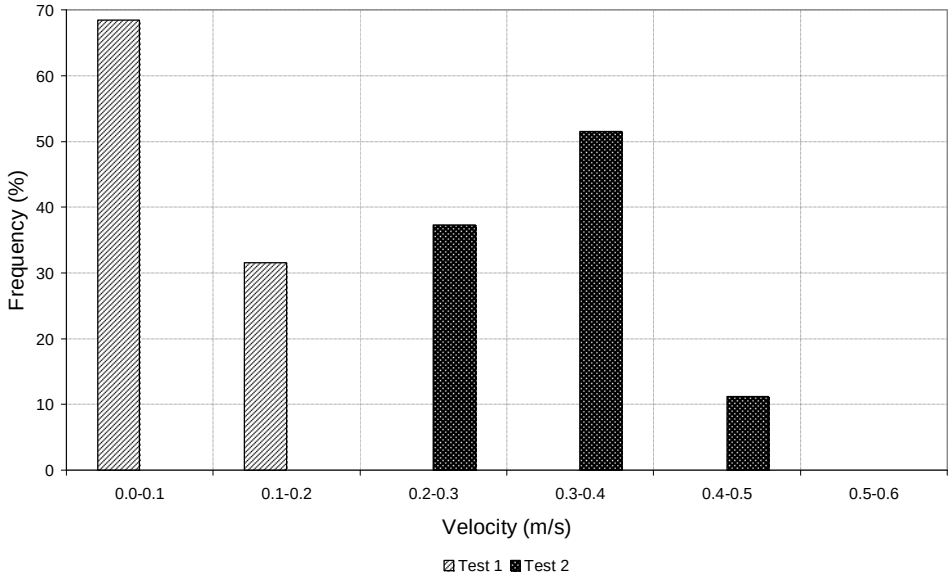

Figure 5-20 Influence of one hemisphere placed at chainage 4.50m on the velocity distributions

For Test 3, two hemispheres were positioned on the bottom of the flume at Chainages 4.50 and 5.50m. Velocity measurements were taken at 24 cross-sections. Transverse velocity distributions at Chainages 3.50, 4.40, 4.70, 5.00, 5.60, 6.10 and 7.00m are shown in Figure 5-21. A photograph of the Test 3 experiment is given as Figure F-2 in Appendix F. The spatial distribution of longitudinal velocity is presented as Figure 5-22. Graphs of the longitudinal distributions of velocity, together with the uniform velocity are included in Appendix F as Figures F-17 to F-26.

The influence of two hemispheres on the velocity distribution (Test 3) is shown in the comparison with uniform velocity distribution (Test 1) in Figure 5-23. It can be seen that two hemispheres have divested the velocity distribution.

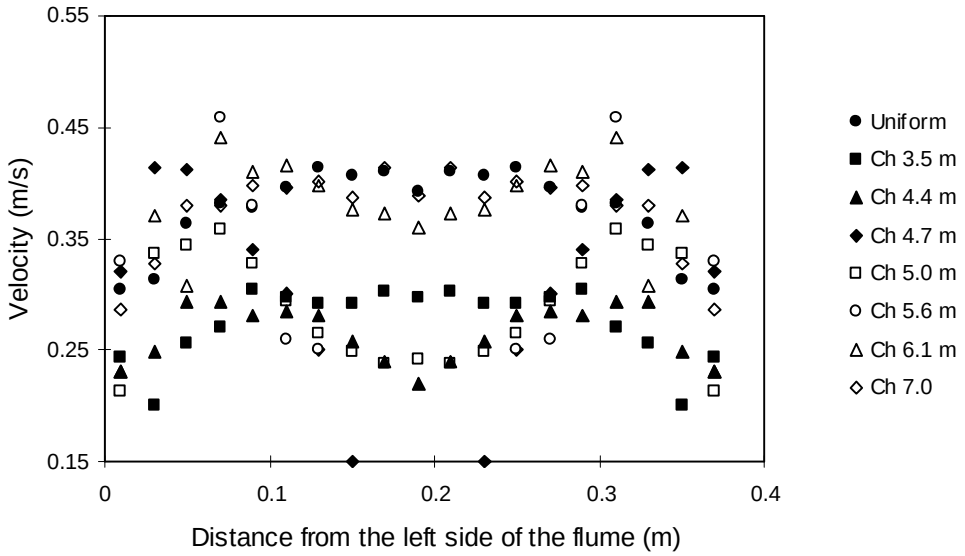

Figure 5-21 Measured transverse velocity distributions for Test 3

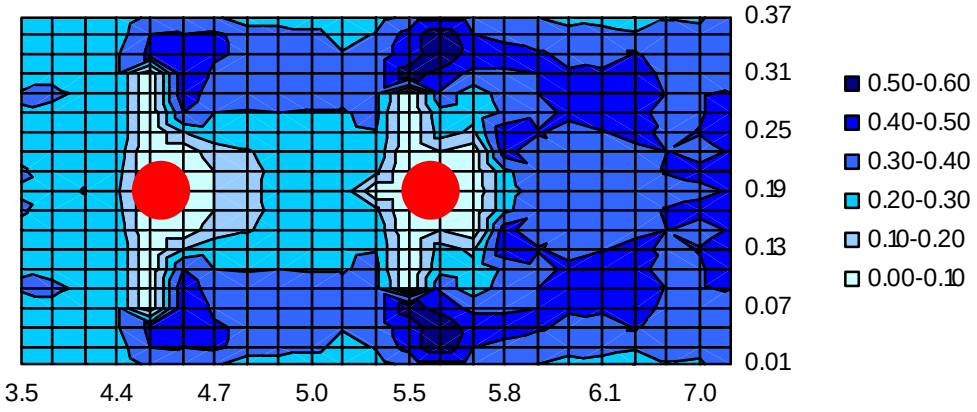

Figure 5-22 Plan-view of spatial distribution of longitudinal velocity for Test 3

One more hemisphere was placed at Chainage 6.50m for Test 4, and velocities were measured at 24 cross-sections. Cross-sectional measured velocities are shown in Figure 5-24. A view of the spatial distribution of longitudinal velocity is presented in Figure 5-25. A photograph of the Test 4 experiment is present in Fig. F-3 (Appendix F). Figure 5-26 presents comparison of the velocity

distributions for the uniform condition (Test 1) and the velocity distribution created by three hemispheres placed along the flume bed. It can be seen that three hemispheres create a wide range of velocity.

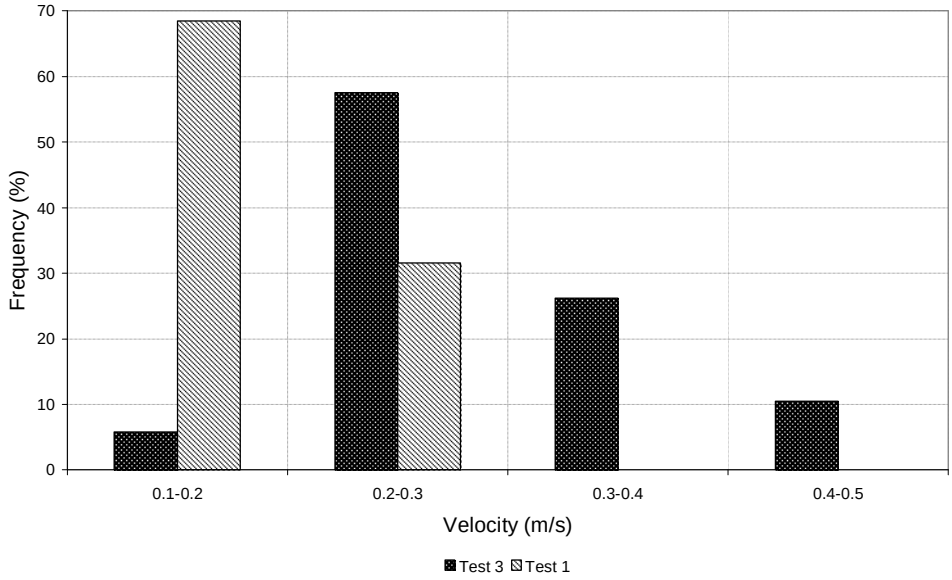

Figure 5-23 Influence of two hemisphere (Test 3) on the velocity distributions in the comparison with uniform velocity distribution (Test 1)

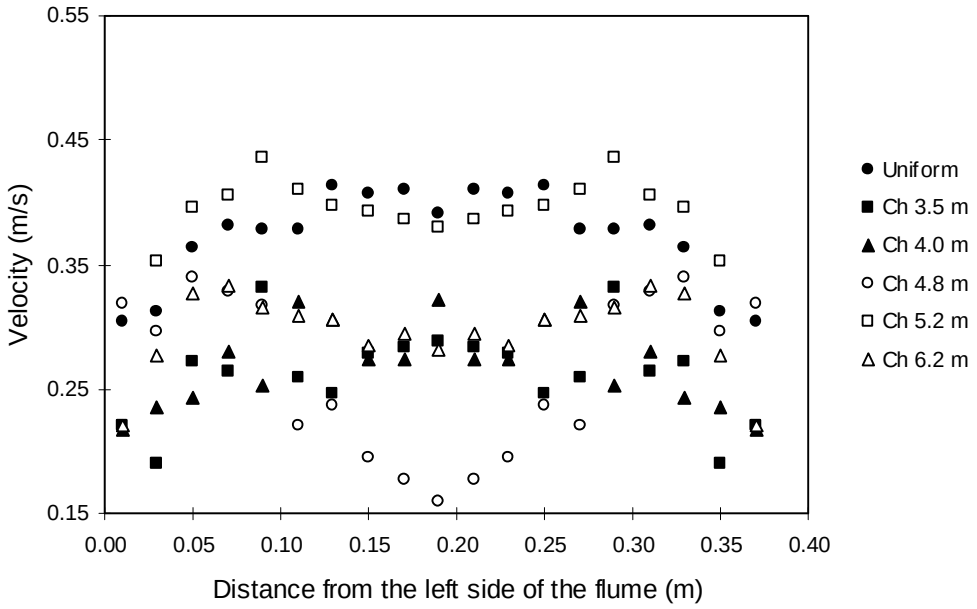

Figure 5-24 Measured transverse velocity distributions for Test 4

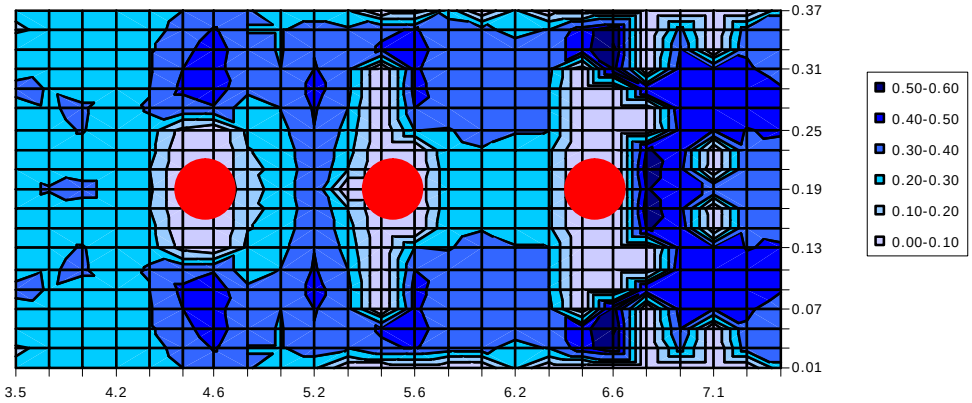

Figure 5-25 Plan-view of spatial distribution of longitudinal velocity for Test 4

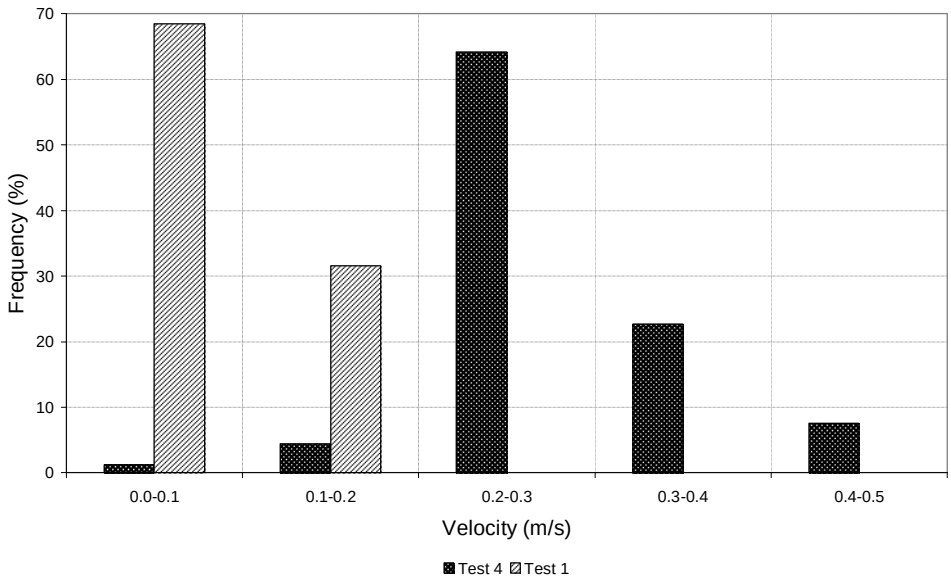

Figure 5-26 Influence of three hemisphere (Test 4) on the velocity distributions in the comparison with uniform velocity distribution (Test 1)

Test 5 was conducted with four hemispheres positioned at Chainages 4.50, 5.50, 6.50 and 7.50m. Velocities were measured at 28 cross-sections; the results are shown in Figure 5-27. A photograph of the experimental setup is showed in Figure F-4 in Appendix F. A view of the longitudinal velocity distribution is presented in Figure 5-28. Velocity distribution histograms for Test 5 and Test 1

are plotted in Figure 5-29. It is clear that the diversity of the velocity distributions for Test 5 is greater than for the uniform flow (Test 1) but less than for Test 4.

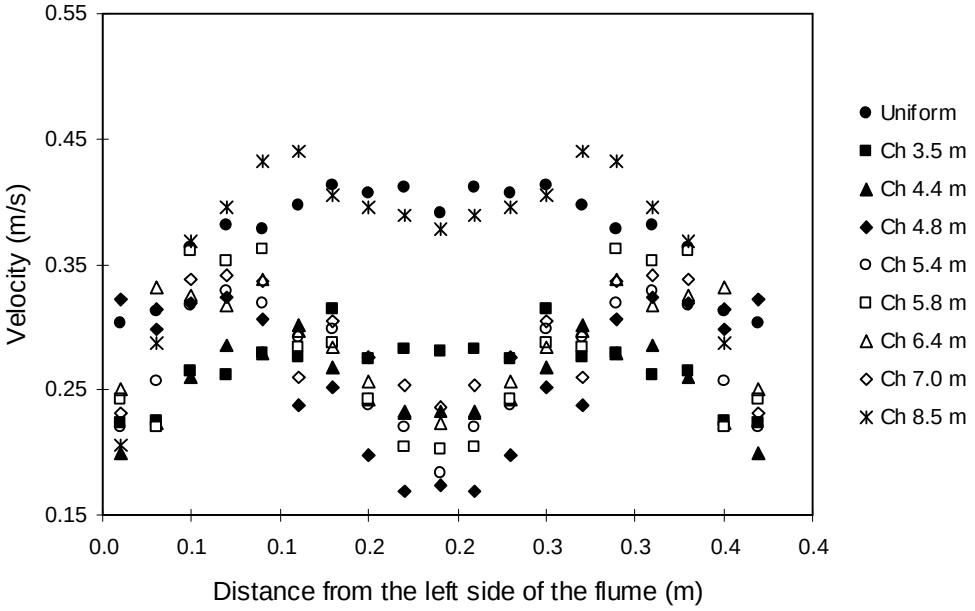

Figure 5-27 Measured transverse velocity distribution for Test 5

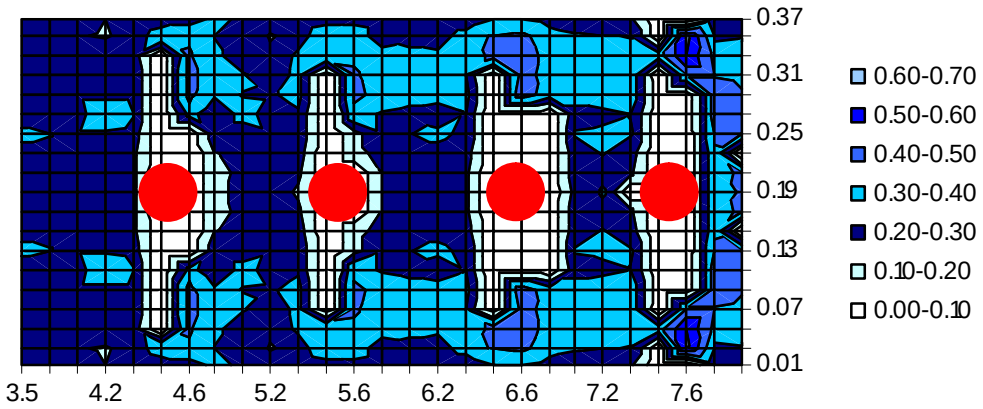

Figure 5-28 Plan-view of spatial distribution of longitudinal velocity for Test 5

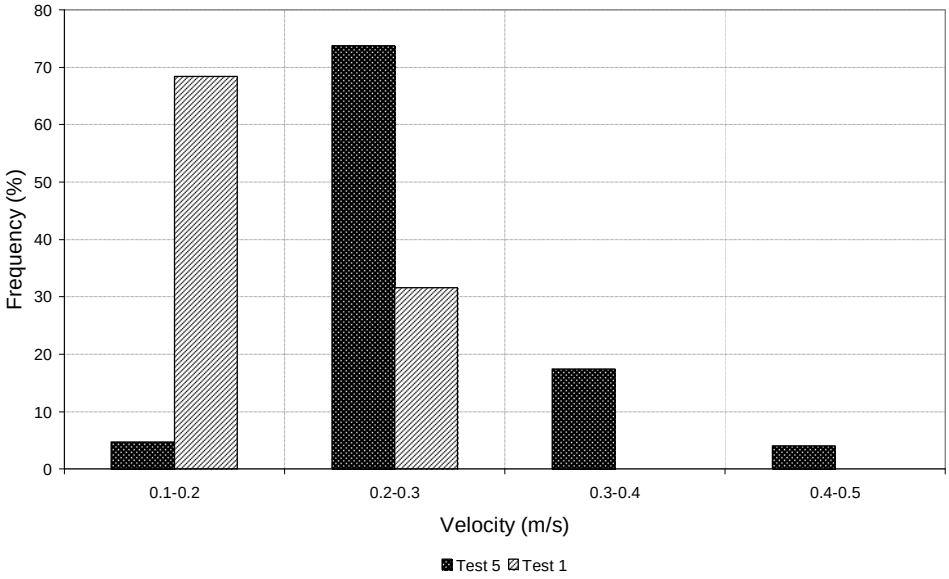

Figure 5-29 Influence of four hemisphere (Test 5) on the velocity distributions in the comparison with uniform velocity distribution (Test 1)

The influence of two hemispheres on velocity and depth distributions was investigated in Test 6. Hemispheres were installed at Chainages 4.50 and 8.50m, and velocities measured at 14 cross-sections. The results are shown in Figure 5-30. Graphs of longitudinal velocities are shown in Figures F-27 to F-36, in Appendix F. The experimental setup is shown in Figure F-5 of Appendix F. A plot of the velocity distribution is given in Figure 5-31. Velocity distributions in the form of a histogram for Tests 1 and 6 are plotted in Figure 5-32.

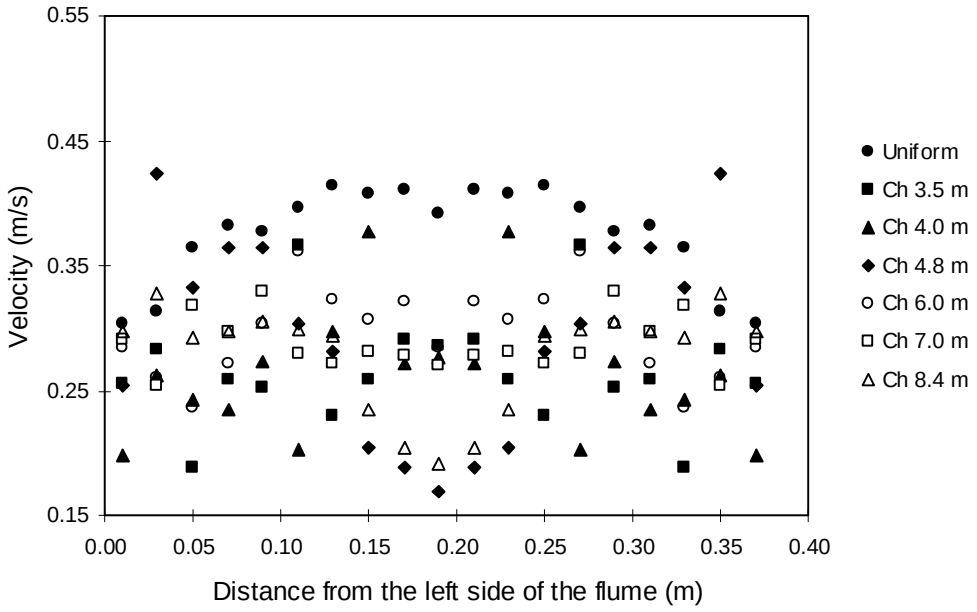

Figure 5-30 Measured transverse velocity distributions for Test 6

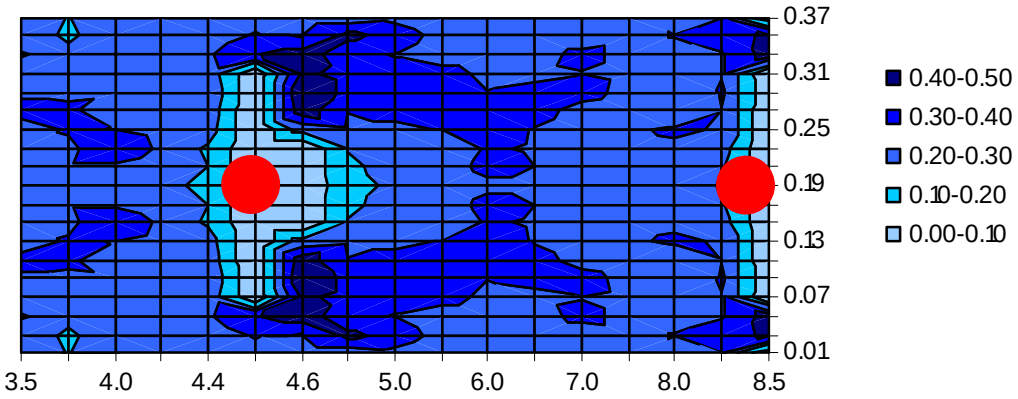

Figure 5-31 Plan-view of spatial distribution of longitudinal velocity for Test 6

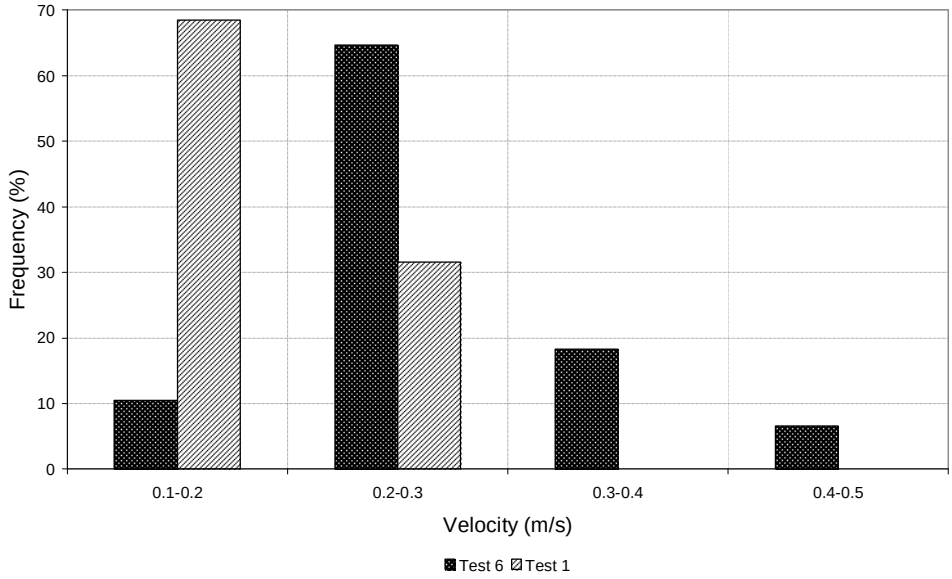

Figure 5-32 Influence of two hemisphere (Test 6) on the velocity distributions in the comparison with uniform velocity distribution (Test 1)

The last experiment (Test 7) was carried out to examine the effect of roughness element shape on velocity distributions. In rivers many large rocks protrude through the water surface, and are better represented by cylinders than hemispherical shapes. The influence of a single cylinder on the velocity distributions was tested here. The cylinder was installed at Chainage 4.50m. The test is similar to Test 2 where the hemisphere was placed at the same chainage. Velocities were recorded at 16 cross-sections, and the results are plotted in Figure 5-33. A photograph of the experiment is shown in Figure F-6 (Appendix F). A view of the velocity distribution is presented in Figure 5-34. The influence of one cylinder on the velocity distribution (Test 7) in comparison with the uniform velocity distribution (Test 1) is presented in Figure 5-35.

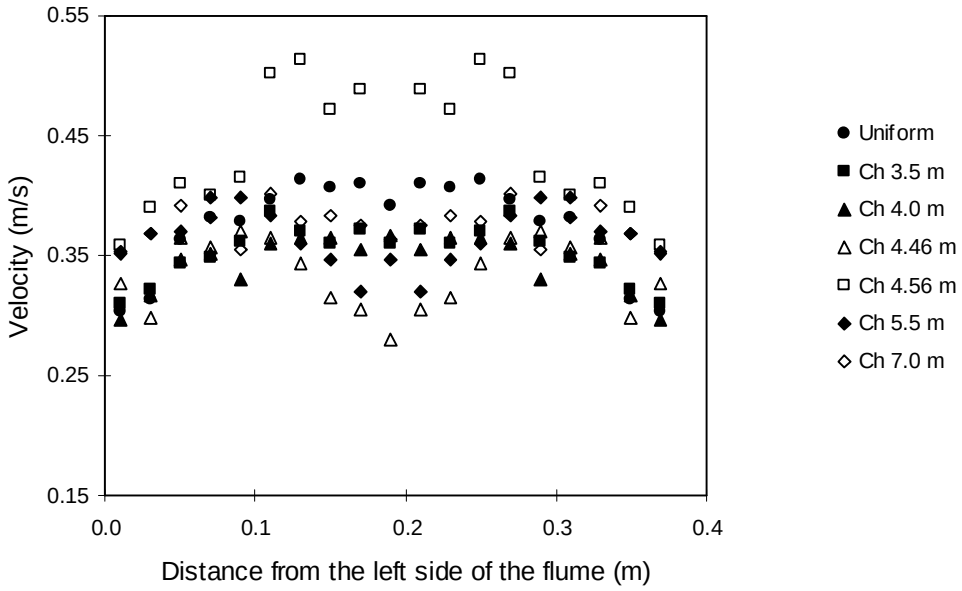

Figure 5-33 Measured transverse velocity distributions for Test 7

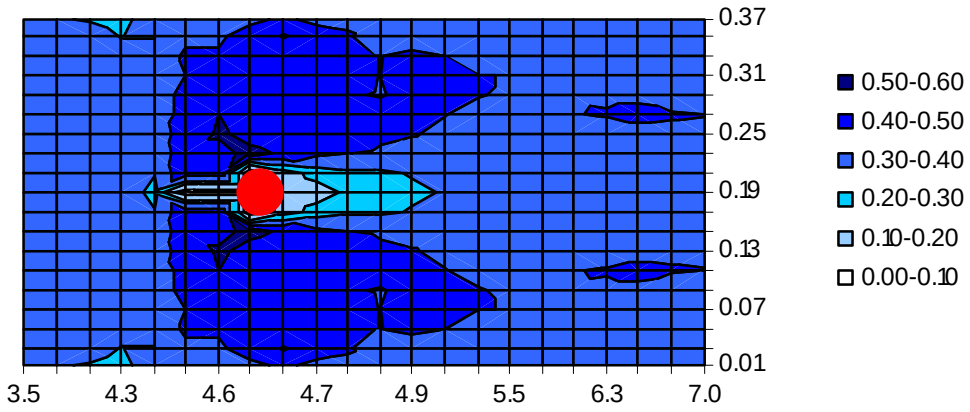

Figure 5-34 Plan-view of spatial distribution of longitudinal velocity for Test 7

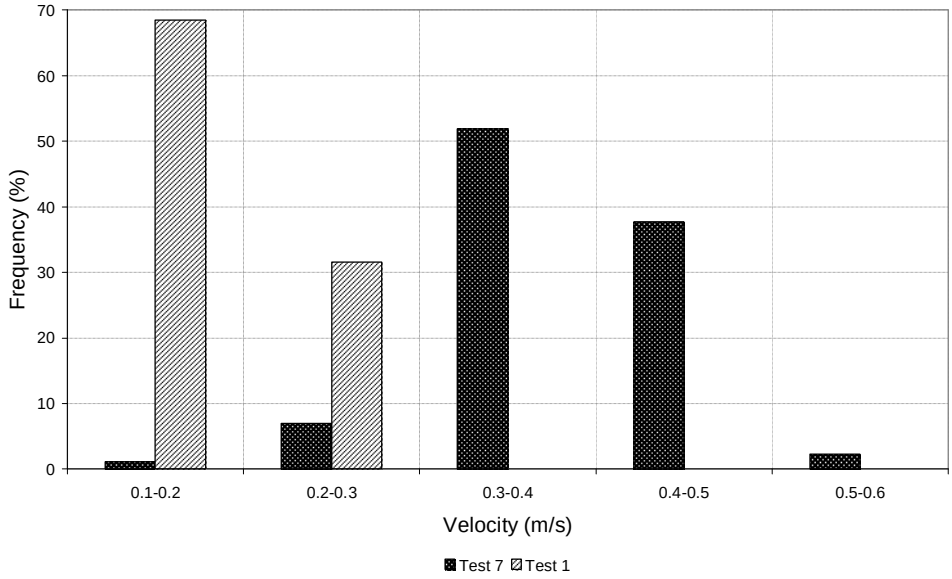

Figure 5-35 Influence of one cylinder (Test 7) on the velocity distributions in the comparison with uniform velocity distribution (Test 1)

5.3.3 Discussion

The experimental results for Test 2 (Figure 5-18) show that a single obstacle affects the velocities for a considerable distance upstream and downstream. The velocities upstream are all reduced by the presence of the obstacle, and even at the first measurement position (about 9 times the obstacle diameter (D) upstream) the maximum velocity is only about 81% of that for the unobstructed flow. At the most downstream section (about 18D downstream), the distribution has recovered almost completely, although the near wall velocities are slightly elevated.

The addition of a second hemisphere 1.0m (9D) downstream of the first (Test 3, Figure 5-21) has a further significant effect on the velocity distribution. The maximum velocity 9D upstream is now only about 70% of that for the unobstructed flow. The profile has recovered completely by 9D downstream of the second hemisphere.

With a third hemisphere 1.0m (9D) further downstream (Test 4, Figure 5-24), the upstream velocity distribution is even further affected. The velocity in the centre

of the channel is reduced to 64% of the unobstructed value, but the profile has become distorted with the maximum value off centre and equal to about 87% of the unobstructed value at this location.

A fourth hemisphere 1.0m (9D) downstream of the third (Test 5, Figure 5-27) has no further effect on the velocity distribution upstream of the first element.

Test 6 (Figure 5-32) had only two hemispheres in line, but spaced very far apart. The influence of the second one on velocities upstream of the first one appears to be much the same as when there are more hemispheres in line over a similar distance. Comparison of Test 3 and Test 6 (Figure 5-37), shows that the effect of the hemisphere spacing on the velocity distributions is not very significant, suggesting that the number of obstacles is an important parameter.

These results suggest that obstacles in the lee zones of upstream obstacles have a significant effect on flow velocities upstream of the first one in line, but that recovery of the transverse profile below the last one in line is not greatly affected by obstacles upstream of the last one.

Comparison of Test 2 (for a single hemispherical obstacle) and Test 7 (for a single cylindrical obstacle), shows the effect of the cylinder on the velocity distributions to be slightly less than that of the hemisphere, suggesting that obstacle shape could be an important consideration.

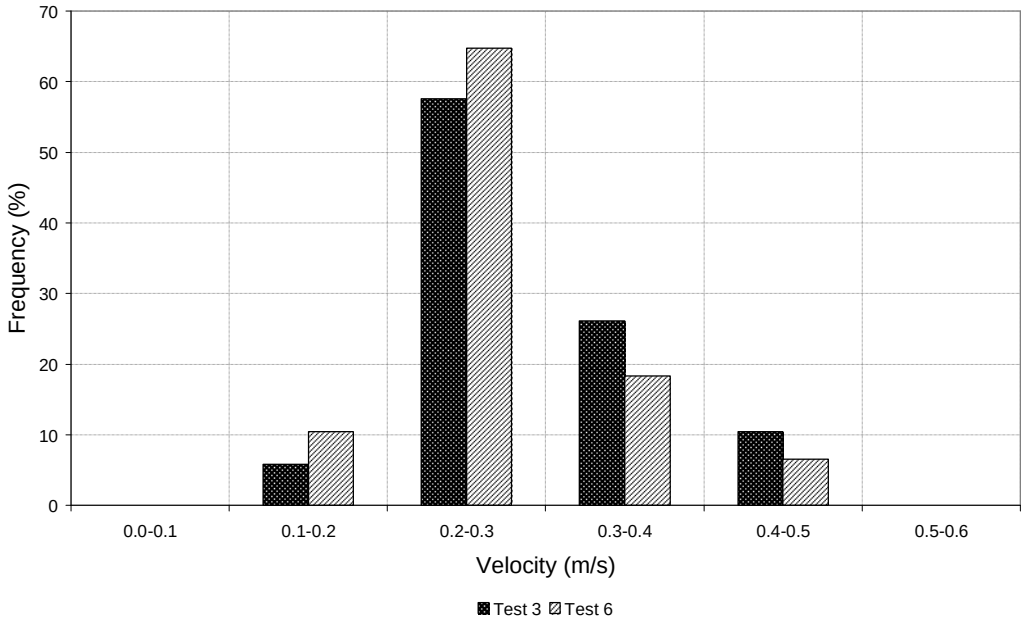

Figure 5-36 Influence of spacing of hemispheres on the velocity distributions

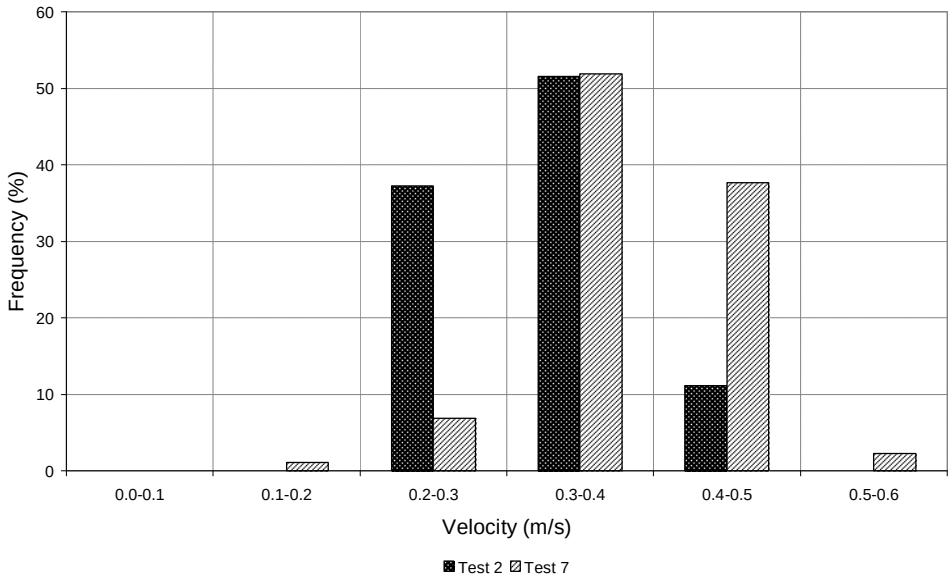

Figure 5-37 Influence of shape of the roughness element in the velocity distributions

5.4 Conclusion

The Flume C experimental results show that local controlled conditions provide greater hydraulic diversity in a channel than resistance controlled conditions. The distributions are also dependent on the spacings between roughness elements. The change in velocity distributions with flow condition makes their prediction very difficult.

The Flume B experimental results show that the distribution of velocity around an obstacle is influenced strongly by other obstacles in its proximity, even if these are within its lee zone. The shape of an obstacle also has an effect on the surrounding velocity distribution.

Use of statistical descriptions of velocity distributions must take cognizance of their sensitivity to channel bed geometry and flow conditions. Computational modelling provides a potentially more reliable approach, and is pursued in Chapter 6.

6 PREDICTION METHODS FOR VELOCITY DISTRIBUTIONS WITH LARGE-SCALE ROUGHNESS

6.1 Multiple Local and Resistance Controlled Conditions

The laboratory investigations of velocity distributions under local and resistance controlled conditions presented in Chapter 5 showed that the velocity frequency distributions induced by the different control conditions are different in nature. The differences are illustrated by the results for the case of two hemispheres spaced 0.24m apart in the Flume C experimental series (Tests 2 and 6) and 0.38m apart (Tests 3 and 7), which are reproduced in Figures 6-1 and 6-2 respectively. The range of velocity classes is wider under locally controlled conditions (Tests 2 and 3) than under resistance controlled conditions (Tests 6 and 7); the diversity of hydraulic conditions is therefore decreased by submergence of local control features. Both conditions commonly occur at the same location in coarse substrate rivers, with local control occurring at very low discharges and submergence taking place as discharge increases. This means that the frequency distributions of velocity at a particular site can be expected to change as discharge varies. Prediction methods of the velocity frequency distributions should clearly be able to distinguish between these control conditions, associate their occurrences with discharge values, and provide the appropriate histograms. Standard regional distribution functions developed from measured data at particular study sites are unable to do this – they do not generally distinguish between the conditions or allow for realistic ranges of discharge.

Computational modelling provides an alternative to data-based statistical distributions for predicting velocity frequency characteristics. There are now a number of commercial and public domain two-dimensional (2D) and three-dimensional (3D) hydraulic models available that may be used for these purposes. They have the advantage of generality in not being based on site-specific data, but rather on rigorous theory; they should therefore be expected to be able to account for changes in control phenomena with discharge. They are also able to predict both velocity and depth simultaneously.

They have the disadvantages of cost (at least for the commercial packages), requiring a high level of user expertise, and requiring detailed site-specific topographical information, which is expensive to obtain.

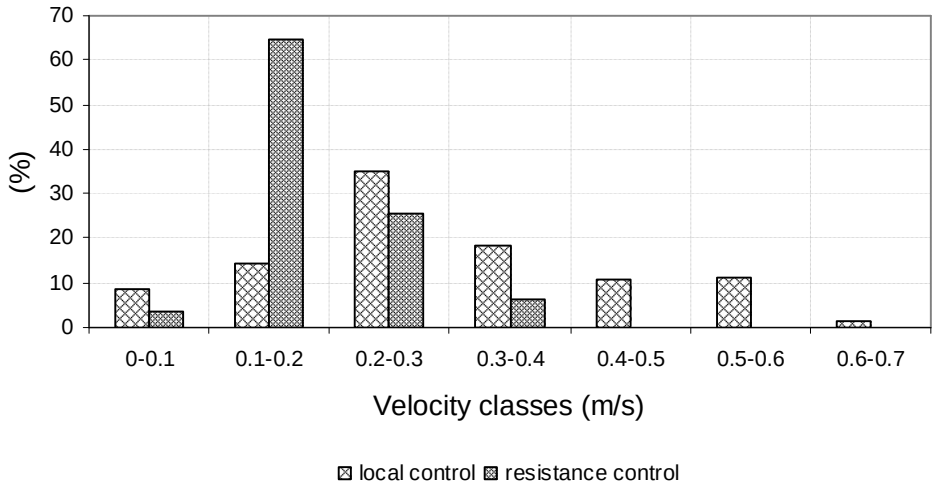

Figure 6-1 Velocity distribution histograms for local control (Test 2) and resistance control (Test 6) (Flume C experiments)

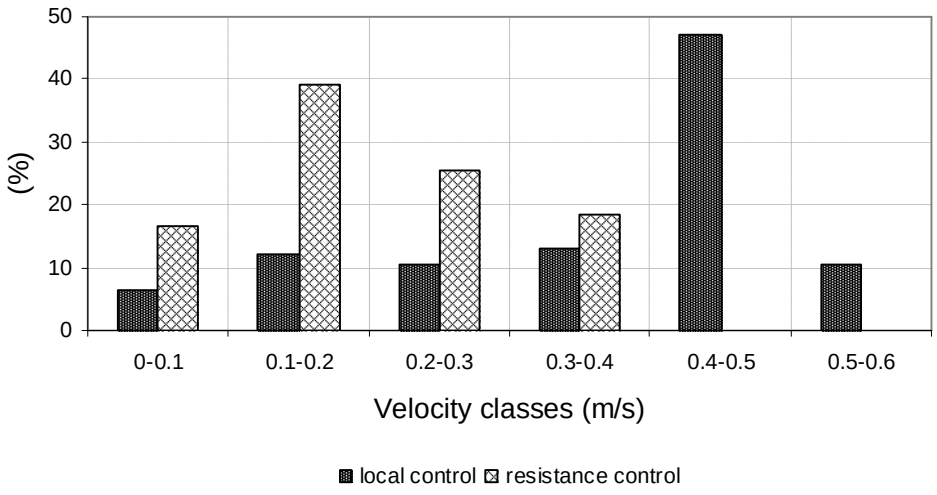

Figure 6-2 Velocity distribution histograms for local control (Tests 3) and resistance control (Test 7) (Flume C experiments)

A public domain 2D model, River2D has been tested for suitability in predicting velocity distributions for environmental flow analysis purposes. In the following

sections the model is described briefly, tested for its ability to simulate locally controlled flow conditions, and tested for accuracy against some of the laboratory results presented in Chapter 3.

6.2 River2D modelling

Implementation of River2D for eco-hydraulic modelling in South Africa is being investigated as part of Water Research Commission project K5/1508 (Hirschowitz et al., 2007). That project will report on the model's applicability for different levels of Ecological Reserve determination, and present a set of guidelines for its use in South Africa.

River2D is a two-dimensional, depth average hydrodynamic and fish habitat model developed specifically for use in natural streams and rivers. It is a Finite Element model, based on the basic physical principles of conservation of mass and momentum, and on a set of constitutive laws which relate the driving and resisting forces to fluid properties and motions. It features subcritical-supercritical and wet-dry area solution capabilities.

River2D is one of a suite of four programmes which also include R2D_Bed, R2D_Mesh and R2D_Ice. The general modelling procedure applies the following steps:

- Develop a bed topography using R2D_Bed (and R2D_Ice where applicable).
- Develop a mesh (a computational discretization) using R2D_Mesh
- Apply River2D to solve for water depths and velocities.

6.2.1 Trans-critical flow simulation

The River2D suite has been used to simulate some hypothetical rapidly varied flow conditions to test its ability to describe the trans-critical flow conditions associated with multiple local controlled conditions. The simulations have been performed for different sizes of roughness elements (D from 0.10m to 0.40m).

The number of obstacles was varied from 2 to 10. The predicted distributions of Froude number are shown in Figures 6-3 to 6-7.

The simulations presented in Figure 6-3 show that the spacing between two obstacles influences the flow pattern. Here, two hemispherical roughness elements are located on the same cross section in a 1.8m wide channel with their centres 0.36m and 1.6m apart, similar to the situations presented in the adjacent photographs. In both cases the situation is clearly locally controlled, and the simulations show realistic transitions between subcritical and supercritical flow. They also show expected differences in flow pattern associated with the different spacing's.

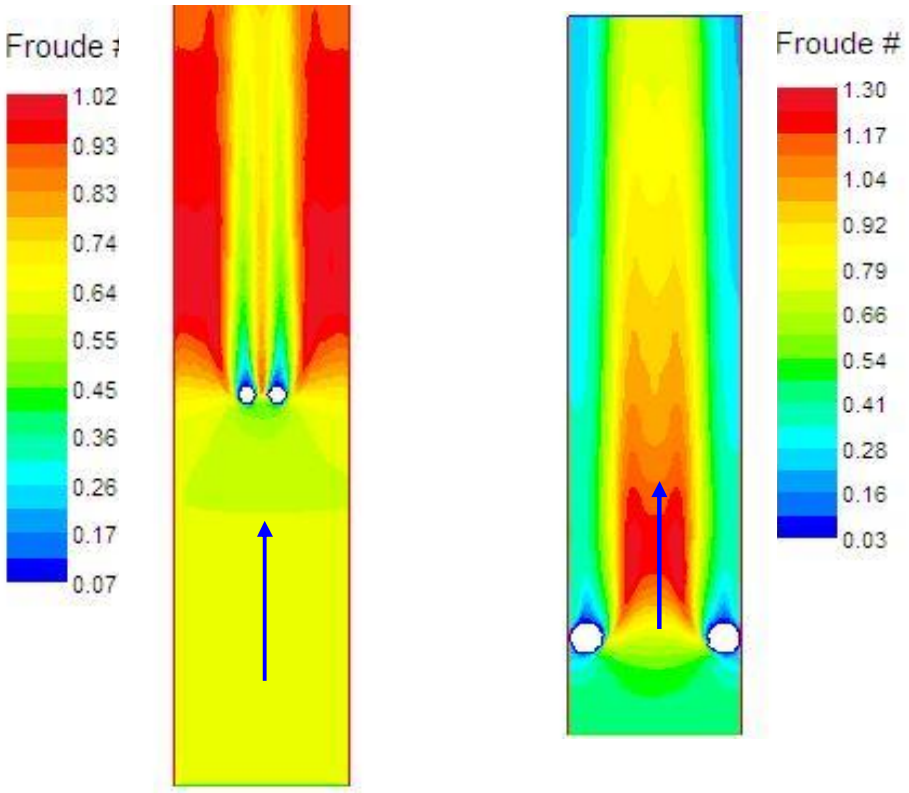

Figure 6-3 River2D modelling, (left) D=0.10 m, centre to centre spacing = 0.36m

(right) D=0.20 m, centre to centre spacing = 1.6m

The effect of differences in size of roughness elements is shown in Figure 6-4, where simulations with different sizes as well as spacing and channel width are presented. The Froude number varies over a wider range in the right hand diagram where the roughness element size is bigger (D = 0.35m) compared with the left hand one (D = 0.25m). In Figure 6-5 the combined influence of longitudinal spacing and size of obstacles is shown (D = 0.35m in the left hand and D = 0.40m in the right hand one). The influence of the number of obstacles and their arrangement on the flow pattern is shown in Figures 6-6 and 6-7.

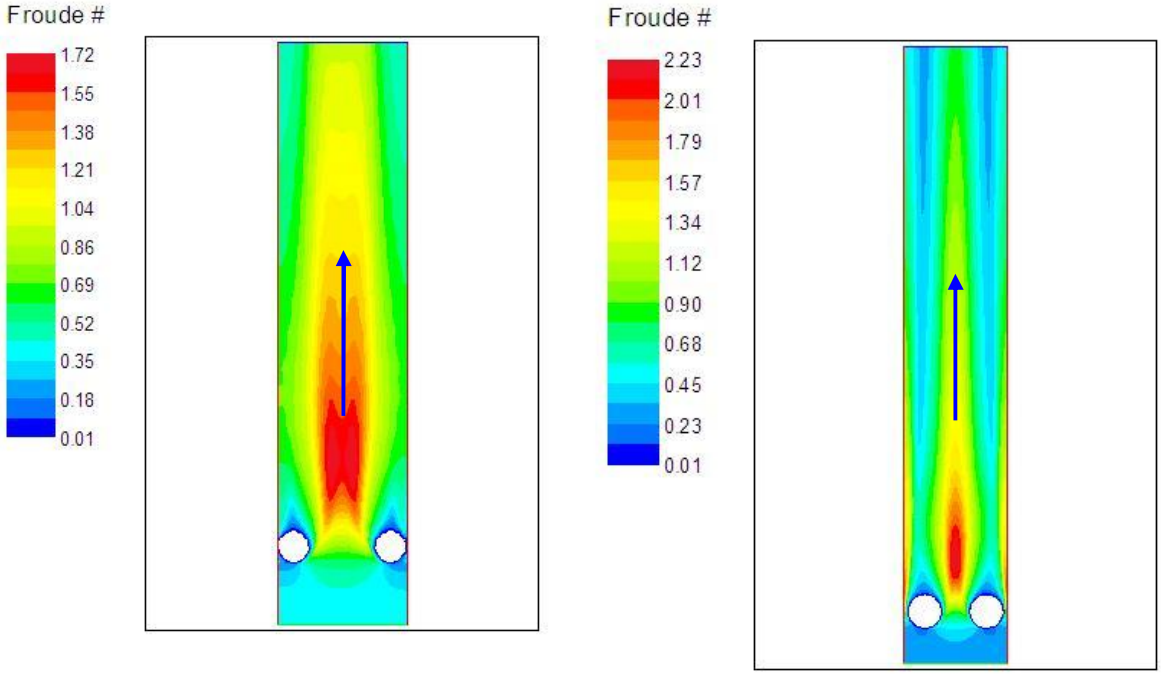

Figure 6-4 River2D modelling, (left) D=0.25m, centre to centre spacing = 1.5m, (right) D=0.35m, centre to centre spacing =1.2m

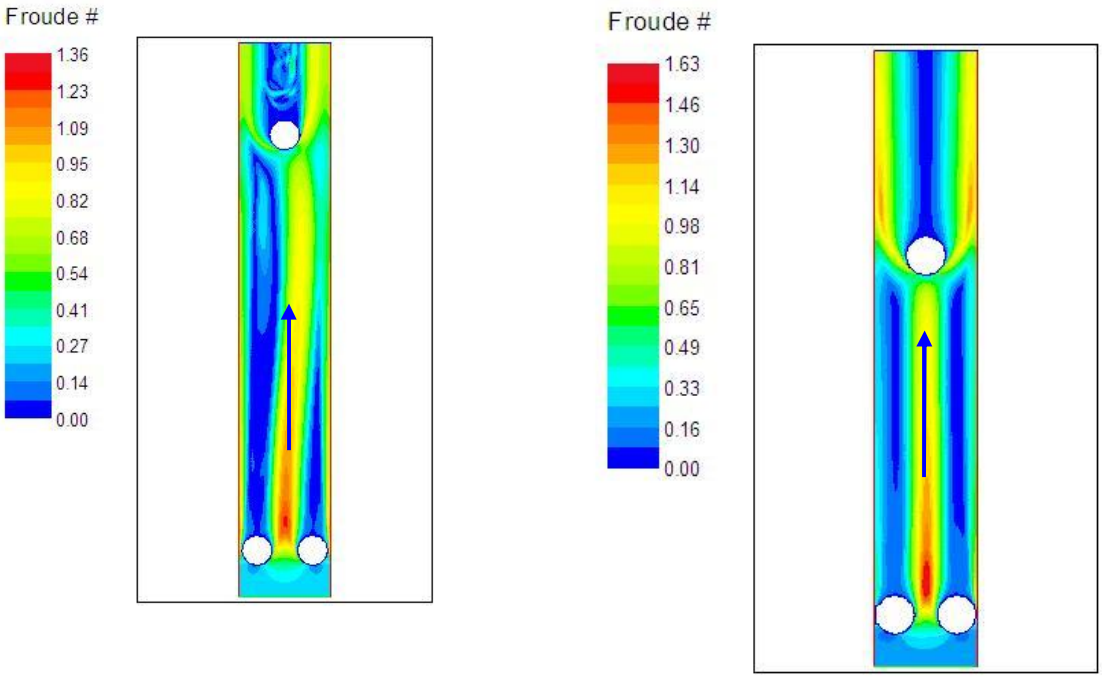

Figure 6-5 River2D, (left) D=0.35m, c/c transverse=1.20m, longitudinal=9m (right) D=0.40m, c/c transverse=1.20m, longitudinal=7m

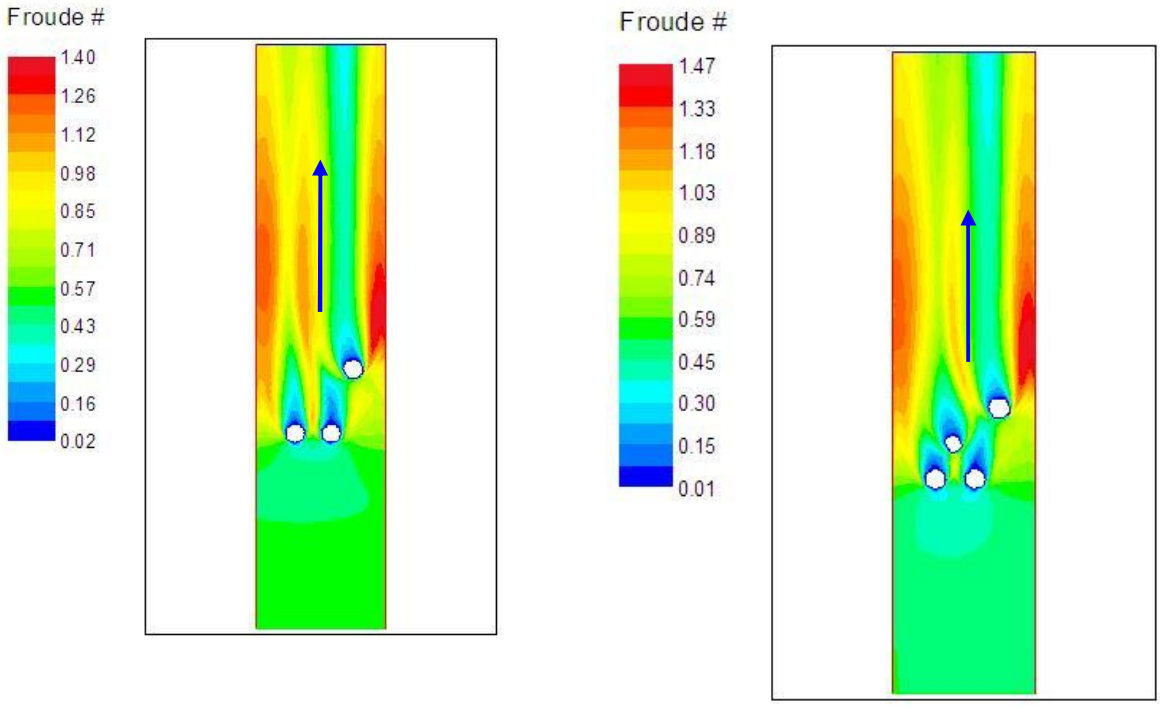

Figure 6-6 River2D modelling, D=0.15m at the left and the right plots

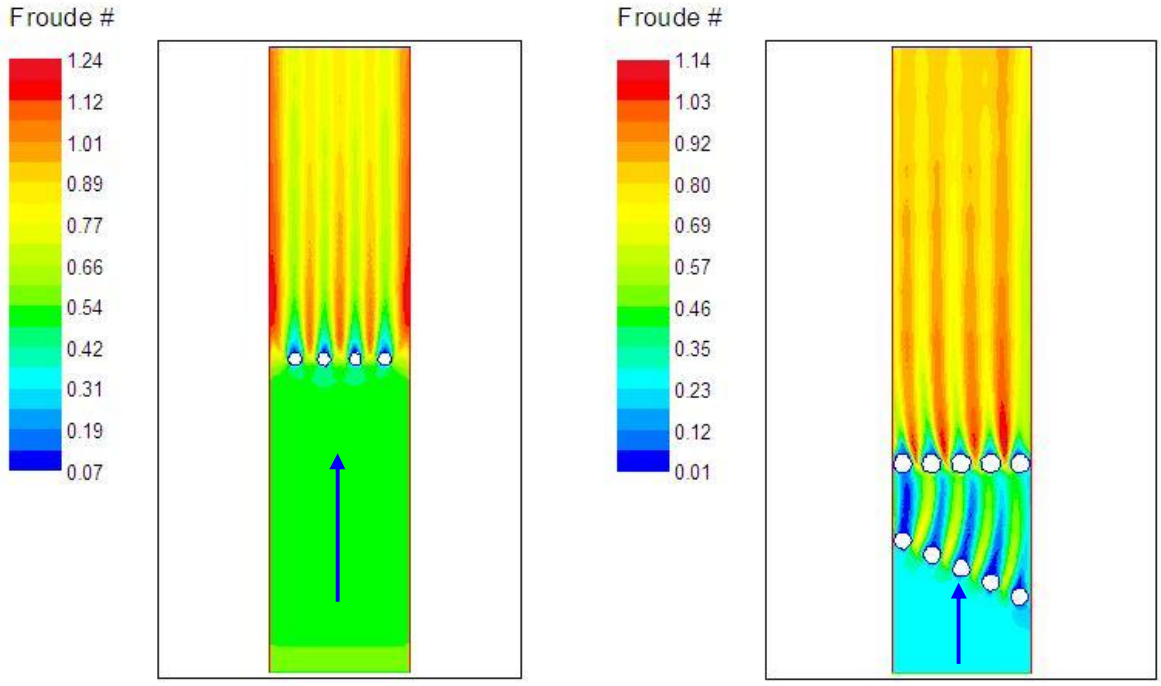

Figure 6-7 River2D modelling, D=0.15m

These hypothetical applications show that it is possible to describe a complex bed geometry comprising large roughness elements using River2D_Bed. The model is able to simulate realistically the complex flow patterns associated with locally controlled conditions, and particularly transitions between subcritical and supercritical flow.

6.2.2 Prediction of velocity frequency distributions

The previous section established that River2D is able to simulate complex flow patterns associated with locally controlled flow. In this section its accuracy in predicting velocity distributions around large roughness elements under resistance controlled conditions is tested. The laboratory measurements described in Section 3.3 provide the test data. Here, the local velocities around one of the hemispheres in the experiment for Series 2.2, Pattern 6 (Figure C-6, Appendix C) were measured. The channel was 12.00m long and 2.00m wide, set on a slope of 0.0005. Hemispheres with 0.072 m diameter were arranged in staggered pattern with 0.20m centre to centre spacings.

To model this situation, a mesh of 0.05m size was set up over the whole bed, and refined to 0.02m over each hemisphere for more accurate representation of the bed topography.

Modelling was performed for the two experimental discharges, Q = 3.0l/s and Q = 21.0l/s, for which velocity distributions around the one hemisphere were measured. Details of the experiments related to velocity measurements are given in Chapter 3, sections 3.3.1 and 3.3.2 for Q = 21.0l/s and Q = 3.0l/s respectively.

The local velocities predicted by River2D were extracted in Excel format, and were analysed using the same velocity classes as the measured data.

Modelled (River2D) and measured velocity distributions in histogram format for Q = 3.0l/s with velocity classes of 0.01m/s and 0.02m/s, and for Q = 21.0l/s with velocity classes of 0.01 and 0.02m/s are plotted in Figures 6-8, 6-9, 6-10 and 6-11 respectively.

The predicted velocity frequency distributions agree well with the measured ones with both specified velocity classes for Q = 3.0l/s. The dominant velocity is slightly underestimated and the highest velocity classes are slightly over-represented, but the shape of the distribution is well reproduced. In contrast, the predicted frequency distributions for Q = 21.0l/s are rather poor. For the finer resolution histogram, the dominant velocity is in the wrong class, and in the coarser resolution histogram the dominant class is over-represented. The distributions are also skewed the wrong way, with the higher classes being emphasized rather than the lower ones.

The difference in performance for the two cases is a result of the different flow conditions and the appropriateness of the type of model for each of these. In 2D modelling a vertical distribution of velocity at each calculation point is assumed, which is realistic in some situations, but not others. The flow condition for Q = 3.0l/s is a large-scale roughness one. Under such conditions the vertical velocity

profiles are not unduly distorted by the roughness elements, and the assumption made in 2D modelling is reasonable. (In fact, for this experiment only a single velocity – at mid flow depth – was measured, and was regarded as representative of the depth-averaged value). The flow condition for 21l/s is one of intermediate-scale roughness. The vertical velocity profiles are highly variable from position to position, and a single assumed profile must be a very poor representation at many locations. This situation requires 3D modelling for accurate representation of local velocities. However, it must be acknowledged that for environmental flow analysis purposes, velocities and their distributions are usually required at coarser scales under these conditions. In other words, while the flow is highly nonuniform at the bed roughness scale, it is relatively uniform at the flow depth scale. Velocity variations of concern at this scale would be determined by channel characteristics at the cross-section scale, rather than the roughness element scale. The choice of 1D, 2D or 3D model is ultimately dictated by the question being asked and the scale of features inducing non-uniformity as well as the resources available to carry out the study.

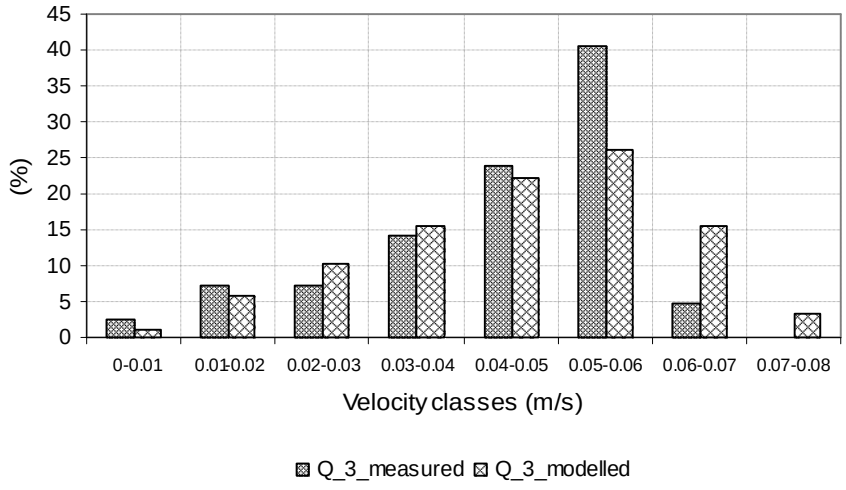

Figure 6-8 Measured and modelled velocity distributions with 0.01 m/s classes for Q=3l/s

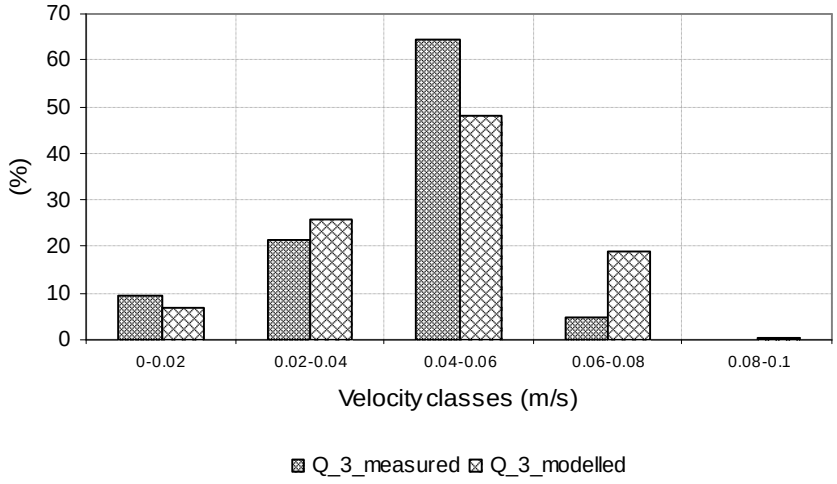

Figure 6-9 Measured and modelled velocity distributions with 0.02 m/s classes for Q=3l/s

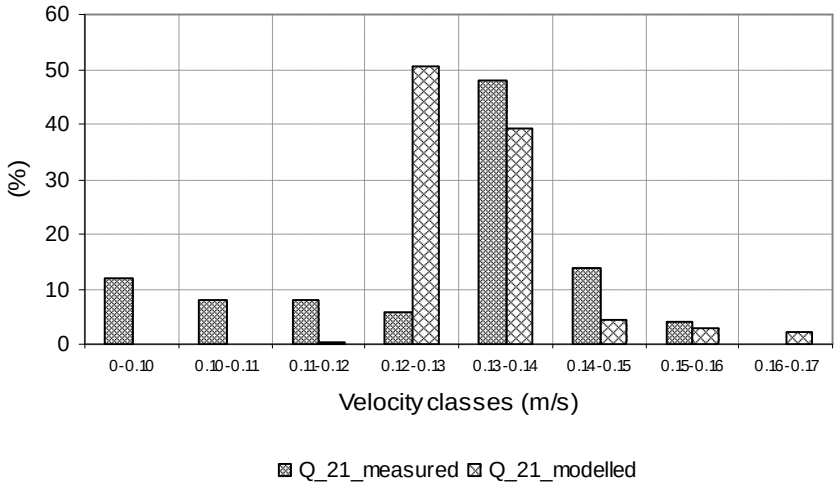

Figure 6-10 Measured and modelled velocity distributions with 0.01 m/s classes for Q=21l/s

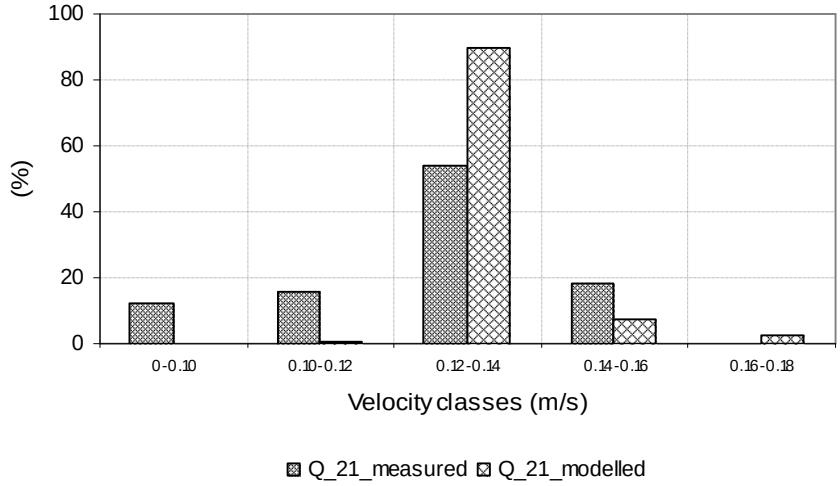

Figure 6-11 Measured and modelled velocity distributions with 0.02 m/s classes for Q=21l/s

6.3 Conclusions

Statistical models for describing velocity frequency distributions in rivers that are based on measured field data generally do not distinguish between multiple local control and resistance control flow conditions. They are therefore not generally applicable, and cannot account for velocity distribution changes associated with varying discharge.

Complex bed geometry can be modelled by R2D_Bed.

The River2D model can describe multiple local control conditions realistically, and trans-critical flows in particular.

River2D can predict velocity frequency distributions reliably under large-scale roughness conditions where the vertical velocity profiles are not unduly distorted by the roughness elements (Figures 6-8 and 6-9). Application of the River2D model for prediction of the velocity frequency distributions under intermediate-scale roughness showed a very poor representation. It can be explained by variation of the vertical velocity profiles, under such condition 3D modelling for accurate representation of local velocities is required.

7 VEGETATION FLOW RESISTANCE

7.1 Background

Reeds are a vegetation type widely present in South African rivers and wetlands, and they contribute significantly to flow resistance. The ability to quantify reed resistance is therefore essential for engineering applications and environmental management of these systems. The influence of reeds and similar emergent vegetation types on overall flow resistance depends on their foliage characteristics and distribution patterns. There are three situations pertaining to the occurrence of vegetation in rivers and wetlands, viz. flow through emergent vegetation, flow in channels with emergent vegetation boundaries, and flow in channels with discrete vegetation patches.

The basic flow resistance of reeds is determined by the morphology of the individual reed stems and characteristics of the whole reedbed. Plant characteristics such as stem diameter, stem height and the distribution of leaves and branches influence the drag imposed on the flow, and all vary seasonally. A practical 6-step iterative procedure is developed for routine conveyance estimation.

Vegetation in strips along the channel banks increases overall resistance by imposing greater local resistance and retarding flow in adjacent clear water zones. Under such conditions discharges can be calculated separately for the vegetated and clear zones of a cross section, and added together to obtain the total discharge.

The third type of instream vegetation that influences overall flow resistance is discrete patches, where the flow resistance is strongly influenced by the overall areal coverage, and varies significantly with the overall distribution pattern of the patches, their size and shape, and the degree of longitudinal and transverse fragmentation.

The resistance phenomenon under such conditions is very complex, and conveyance cannot be described by a single equation or simple procedure. River2D software was tested for prediction of overall flow resistance with discrete patches.

7.2 Estimation of Flow Resistance through Emergent Vegetation

7.2.1 Introduction

The effect of reeds on flow resistance is a complex phenomenon, and is determined by the morphology of the individual reed stems and characteristics of the whole reedbed. As part of a study of reedbed dynamics, associated hydraulics and sedimentation and their mutual interaction, James et al (2001) developed a rigorous simulation model (REEDFLO) for flow through reeds that accounts for the fundamental processes influencing flow resistance.

REEDFLO provides a realistic description of the resistance phenomenon and can account for the influential parameters with a high level of detail. It is, however, too complex and cumbersome for practical application, and provides a level of resolution beyond what is usually necessary. The computational model of vegetation-influenced flow has been applied hypothetically to identify the variables most significant in determining resistance to flow through emergent reed-type vegetation, and to develop a simple procedure for estimating conveyance. A rational form of stage-discharge relationship is adopted and a formulation for the resistance coefficient in terms of the significant variables (stem spacing, stem diameter and stem drag coefficient) is derived through application of the computational model. Experimental results (James et al, 2001) are used to relate the stem drag coefficient to stem Reynolds number and foliage state. The stage-discharge and resistance coefficient equations and the drag coefficient relationship are applied through a simple 6-step iterative procedure for routine conveyance estimation (Jordanova et al, 2006). The procedure is verified by comparison of predicted and measured discharges for flow through natural vegetation.

7.2.2 The REEDFLO model (Jordanova et al 2006)

REEDFLO is based on force balance principles. The classic drag force equation is used to describe stem drag, with local approach velocity determined through the defect model of Petryk (1969). Both submerged and emergent conditions can be accounted for, using eddy-viscosity and mixing length functions to describe flow through and above the stem zone. The model includes some empirical content, requiring calibration with experimental data. For a specified discharge, REEDFLO predicts the flow depth, the vertical distribution of velocity, the bed shear stress, the total stem drag, the effective drag coefficient based on average velocity, and the effective channel resistance in term of Manning's *n* or Darcy-Weisbach friction factor *f*. The development for emergent conditions is described below.

The model uses numerical techniques to obtain solutions to the finite-difference equations describing the balance of applied and resisting forces acting on flow elements (Li and Shen, 1973; Petryk and Bosmajian, 1975; Christensen, 1976; Lindner, 1982; Kosorin, 1983)

$$F_A = F_B + F_V \qquad 7.1$$

where F_A : the applied force per unit plan area,

F_B : the resistance force per unit plan area contributed by the bed, and

F_V : the resistance force per unit plan area contributed by the vegetation.

The applied force per unit plan area is given by

$$F_A = g\, y S_f (1 - n_x n_y \frac{p\, D^2}{4}) \qquad 7.2$$

where γ : the unit weight of water,

y : the flow depth,

S_f : the energy slope,

n_x : the numbers of stems in the longitudinal direction

n_y : the numbers of stems in the lateral direction, and

D : the stem diameter.

The resistance force contributed by the bed per unit plan area is related to bed shear stress by

$$F_B = t_B(1 - n_x n_y \frac{p D^2}{4}) \qquad 7.3$$

in which τ_B is the bed shear stress.

The resistance force contributed by the vegetation per unit plan area (F_v) is determined by the empirical drag force relationship for vertical cylinders

$$F_V = \frac{1}{2} C_{De} r y D n_x n_y u_{a^\infty}^2 \qquad 7.4$$

where u_{a^∞} : the asymptotic approach velocity (the velocity attained within a large stand of stems),

ρ : the water density, and

C_{De} : the effective drag coefficient that accounts for the influence of adjacent obstructions and surface wave effects in a multi-stem arrangement, as proposed by Richter (1973), i.e.

$$C_{De} = \left(1 + 1.9 C_D \left(\frac{D}{a_y}\right)\right) C_D \qquad 7.5$$

where a_y : the distance between reed stems in the lateral direction, and

C_D : the drag coefficient for isolated cylindrical elements, which is a function of the cylinder Reynolds number.

7.2.3 Development of a practical resistance equation (Jordanova et al, 2006)

REEDFLO is too computationally intensive for practical direct application and predicts flow characteristics through emergent reeds at a higher level of resolution

than is generally necessary or justified, considering the uncertainties associated with vegetation characteristics and drag coefficient values. The model has therefore been applied hypothetically to develop a simple resistance relationship for flow through emergent vegetation stems, using the following steps (described in the sections that follow) (Jordanova et al, 2006):

- Identification of factors that determine flow resistance,
- Determination of the form of the flow resistance equation,
- Estimation of drag coefficient values, and
- Development of a resistance coefficient relationship.

Identification of factors that determine flow resistance

The development of a general resistance equation for different conditions requires identification of the factors that significantly influence flow resistance. The impact of vegetation depends on many complex interacting factors, including parameters related to vegetation - stem diameter, spacing and drag coefficient, and channel properties represented by slope and substrate. Flow conditions were therefore simulated for a wide range of input variable values, which were varied systematically to explore their effects on flow resistance, and to enable identification of the most important ones. The variables investigated and the ranges of their variations are listed in Table 7-1. Simulations were performed for discharges of 0.01 and 0.05 $m^3/s/m$.

Table 7-1 Variables and their range used in REEDFLO simulations

Variable	Range	Variables value				
		Base	+10 % -10 %	+25 % -25 %	+50 % -50 %	+75 % -75 %
Stem diameter, D (mm)	5.0-20.0	5.0	5.5 4.5	6.3 3.8	7.5 2.5	8.8 1.3
Stem spacing, s (m)	0.05-0.45	0.05	0.0550 0.0450	0.0625 0.0375	0.0750 0.0250	0.0875 0.0125
Bed slope, S	0.0005-0.005	0.001	0.0011 0.0009	0.0013 0.0008	0.0015 0.0005	0.0018 0.0003
Bed roughness, k_s (m)	0.0125-0.003	0.0125	0.0138 0.1130	0.0156 0.0094	0.0188 0.0063	0.0219 0.0031
Drag coefficient, C_D	1.0-2.2	1.15	1.2650 1.0350	1.4375 0.8625	1.7250 0.5750	2.0125 0.2875

In the first series of simulations, the base values of the variables were increased by up to 75 %. The responses of flow depth for a discharge of q=0.05 m^3/s/m (Figure 7-1) show that changes in different variables affect flow resistance (and hence flow depth) differently. Change in stem diameter (D) and spacing (s) has significant influence on flow resistance, change in slope (S) and drag coefficient (C_D) has moderate influence, while the influence of bed roughness (k_s) change is small.

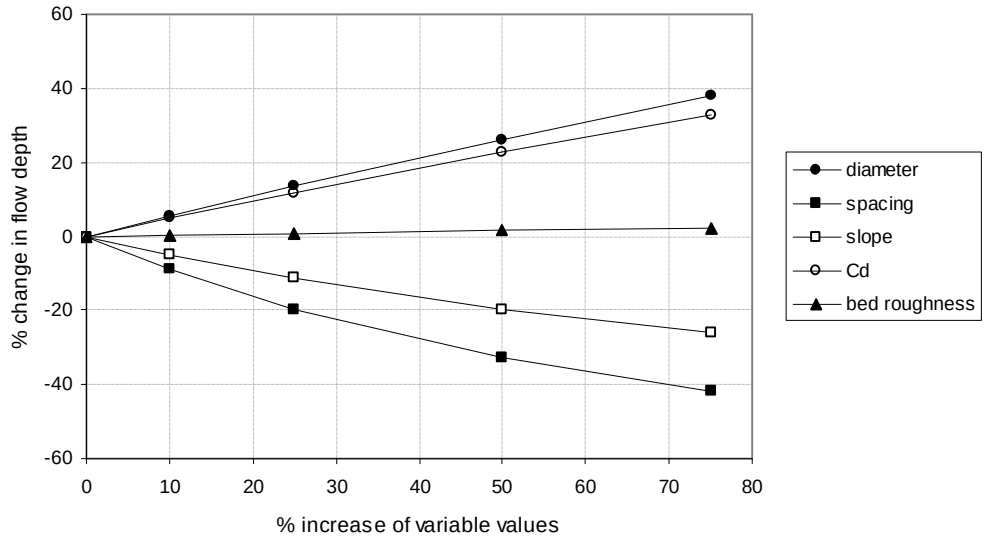

Figure 7-1 Effect of increasing variable values on change of flow depth for q=0.05 m^3/s/m

In the second series of investigations, the values of the variables were decreased by up to 75 % (Table 7-1). The responses of flow depth for a discharge of q=0.05 m^3/s/m are shown in Figure 7-2. The curves for stem spacing (Figure 7-2) and slope show significant influence: flow depth increases by 285 % for a decrease in stem spacing of 75 % and by 100% for a decrease in bed slope of 75 %. As shown in Figure 7-1 the effect of bed roughness change on flow depth is very small. Stem spacing and diameter are therefore important in determining flow resistance, and further investigation of their influence was carried out. Figure 7-3 shows the influence on flow depth of three realistic diameter values (D=5.0 mm, D=10.0 mm and D=20.0 mm) at a slope of 0.0005, a discharge of 0.05 m^3 /s/m, and stem spacing's in the range 0.05 to 0.18 m. The influence of diameter on flow depth can be seen to decrease slightly with increased stem spacing, suggesting that the influence can not be accounted for in terms of relative spacing (s/D) only, but also depends on absolute values of stem spacing and stem diameter. For example (Figure 7-3), for a spacing of 0.1 m and diameter of 20.0 mm (relative spacing of 5) the flow depth is about 1.3 m, while for the same

relative spacing with a stem spacing and stem diameter of 0.05 m and 10.0 mm, respectively, the depth is 1.75 m.

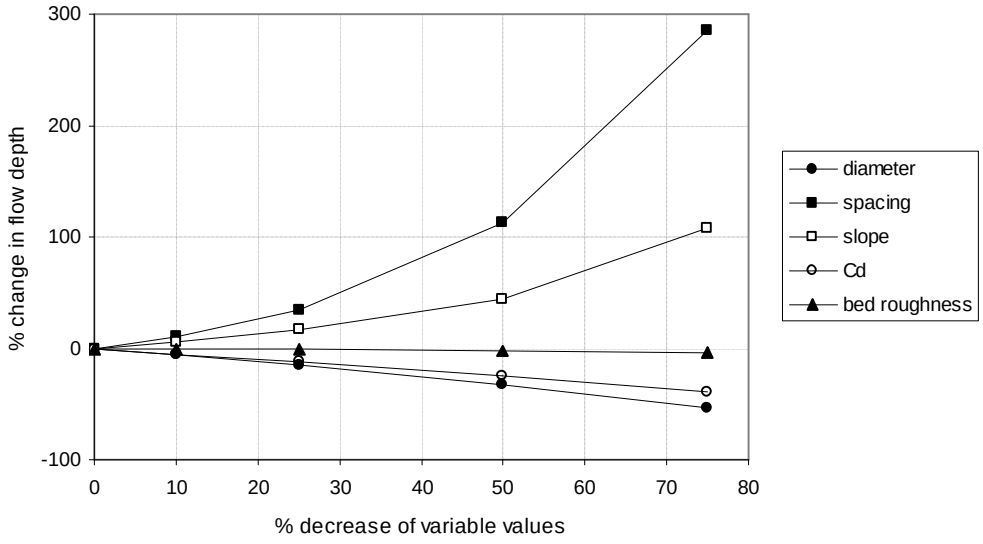

Figure 7-2 Effect of decreasing values on change in flow depth for q=0.05 $m^3/s/m$

The results of simulations performed enable us to investigate how different parameters affect the flow resistance. It has been found that bed roughness, as was expected, has a small or even negligible effect on flow resistance. Vegetation parameters - stem diameter, stem spacing and drag coefficient have a significant effect on flow resistance. This is understandable, because resistance in reedbeds is dominated by stem drag, which depends strongly on the morphology and density of stems (James et al, 2001). Bed slope also strongly influences flow resistance indicating that it would be a parameter in defining the retardance to flow (Kouwen and Unny, 1973; Wu et al, 1999).

On the basis of this analysis, the vegetation parameters of stem diameter, stem spacing and drag coefficient, and the bed slope have been identified as the most important parameters determining flow resistance.

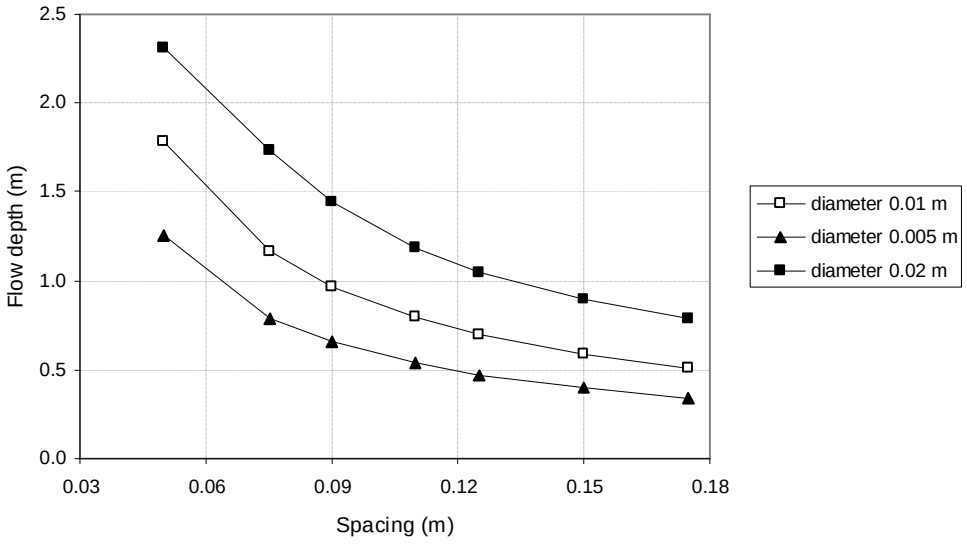

Figure 7-3 Effect of stem spacing on flow depth for stem diameters of 0.005, 0.01 and 0.02 m for slope of 0.0005 and q=0.05 $m^3/s/m$

Determination of form of the flow resistance equation

Although widely used, Manning's equation is poorly suited to vegetated channels (James et al, 2001; Turner et al, 1978; Turner and Chanmeesri, 1984; James et al, 2004) and a more general form of resistance equation, such as proposed by Turner and Chanmeesri (1984) and Smith et al (1990) is considered here. The discharge-depth equation offered by Turner and Chanmeesri (1984) is given by

$$q = G^{-1} y^m S^{0.5} \qquad 7.6$$

where q : the discharge per unit width,

G : a coefficient of roughness which is independent of slope, and

S : the channel slope.

The roughness coefficient (G) and exponent (m) need to be determined experimentally.

Smith et al (1990) recommended a similar equation,

$$q = a S_f^{\ b} y^c \qquad 7.7$$

in which *a*, *b* and *c* are experimentally fitted parameters. However, the suggested parameters were determined from experiments for a particular crop type, geometry and flow conditions, and this limits their application.

James et al (2001, 2004) showed that from the balance of forces driving and resisting the water movement, where the resistance to flow is caused exclusively by stem drag rather than boundary shear, the velocity is independent of flow depth. The proposed equation is

$$V = \frac{1}{F}\sqrt{S} \tag{7.8}$$

in which F is a resistance coefficient dependent on stem diameter (D), stem density (N) and drag coefficient (C_D) given by

$$\frac{1}{F} = \sqrt{\frac{2g}{C_D N D}\left(1 - \frac{NpD^2}{4}\right)} \tag{7.9}$$

Equation (7.8) suggests that the exponent of S in equation (7.7) should be 0.5, and flow depth is present for continuity reasons only, and its exponent should be 1.0. The discharge-depth equation is accordingly given by

$$q = yV \tag{7.10}$$

Equation (7.9) was developed theoretically for cylindrical rods and simple hydraulic conditions without accounting for the influence of adjacent obstructions and surface wave effects in a multi-stem arrangement.

The computationally intensive REEDFLO model determines the velocity at a longitudinal position within a multi-stem arrangement by deducting from the velocity in the absence of vegetation, V_0, the sum of the velocity defects arising from all upstream stems and adjacent obstructions. The velocity per unit flow width in a multi-stem arrangement is given by (James et al, 2001; Li and Shen, 1973)

$$V = V_0 - \frac{1}{W}\int_{-s_w/2}^{s_w/2} u_d \, dz \qquad 7.11$$

where V : the average velocity,

W : the flow width,

s_w : the spread of the wake,

u_d : the flow velocity defect, and

z : the lateral distance relative to the obstruction.

Application of REEDFLO allows development of an empirical resistance coefficient (F) that accounts for surface wave and blockage effects within a large reed stand. The most suitable way of expressing the functional relationship in terms of dimensionless parameters was found to be

$$F = fn\left(\frac{s}{D}, \frac{D}{y}, C_D\right) \qquad 7.12$$

Estimation of drag coefficient values

The range of drag coefficient (C_D) values for reeds has been determined from results of laboratory experiments with real reed and morphologically similar bulrush stems (James et al, 2001). Two reed stems (reed 1 and 2 in Table 7-2) and a bulrush stem were harvested from stands of ***Phragmites australis*** and ***Typha capensis*** in the Braamfontein Spruit, in Johannesburg. The characteristics of the freshly cut stems are listed in Table 7-2.

Table 7-2 Drag coefficient values for reed and bulrush stems

Stem Type	Foliage	Foliage Area, (m^2)	Stem diameter, (mm)	Re	C_D
Reed 1	Full foliage	0.0292	10.8	638-4838	1.35-3.46
Reed 2	Full foliage	0.0340	8.40	457-4347	1.75-6.79
Reed 2	6 leaves	0.0318	8.40	246-4347	1.55-16.2
Reed 2	3 leaves	0.0158	8.40	246-4731	1.27-16.2
Reed 2	Stem only	0	8.40	255-4686	1.25-4.34
Bulrush	Full foliage	0.0339	11.57	501-5981	2.22-5.34

Drag force experiments were performed in a 24 m long, 0.915 m wide, horizontal flume. Vegetation stems were held normal to the flow in a rectangular aluminium frame mounted on a pivot that allowed the applied force to be measured by maintaining moment equilibrium. Flow velocities were measured at the stem level with the stem removed.

The drag force (F_D) on a stem is related to flow and stem characteristics by

$$F_D = C_D A_{pr} \frac{1}{2} r V^2 \qquad 7.13$$

where A_{pr} : the stem area projected in the flow direction, and

V : the local flow velocity.

The drag coefficient (C_D) depends on the stem size and shape and the Reynolds number (Re) expressed in terms of stem diameter (D)

$$\mathrm{Re} = \frac{VD}{u} \qquad 7.14$$

Experimentally determined values of C_D with corresponding Reynolds numbers for all three stems are plotted together with the standard curve presented by Albertson et al (1960) in Figure 7-4. The stem of reed 2 was progressively stripped of leaves and branches to determine the relative contributions of the main

stem and the foliage to drag. It was tested first with all its leaves and branches, then with 6 leaves, 3 leaves, and finally with only the bare stem. The foliage areas of the stems were measured by tracing the outlines on to squared paper (Table 7-2). Values of C_D are plotted against Reynolds number (*Re*) in Figure 7-5 for the reed stem with no leaves, and in Figure 7-6 for the reed with 6 and 3 leaves. All the experimentally determined C_D values are plotted together in Figure 7-7, which includes curves for the upper and lower limits and a best-fit curve through all the values.

The relationship between drag coefficient, C_D, and stem Reynolds number (*Re*) can be represented by

$$C_D = \alpha \, Re^b \qquad 7.15$$

Best-fit values of coefficients *a* and β for all the experimental conditions are listed in Table 7-3.

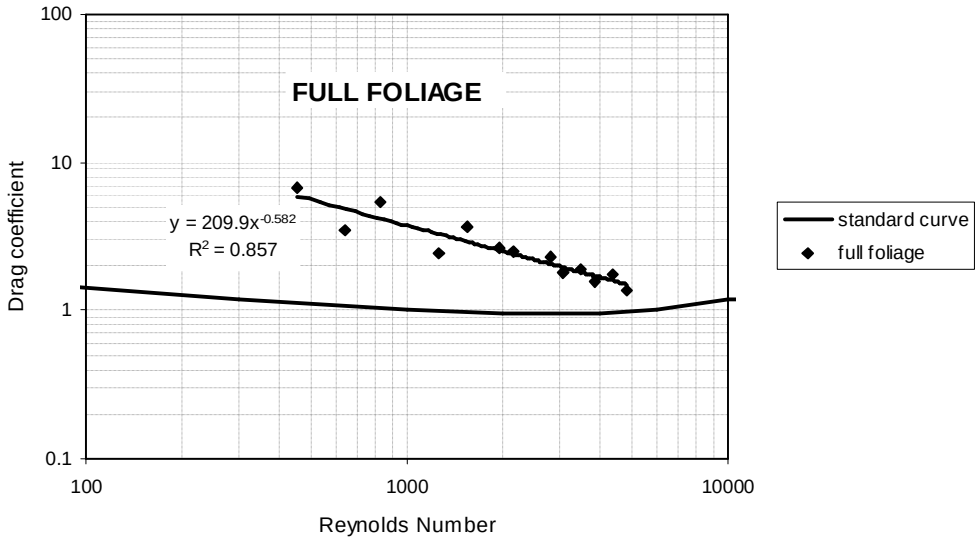

Figure 7-4 Drag coefficient for natural reed and bulrush stems

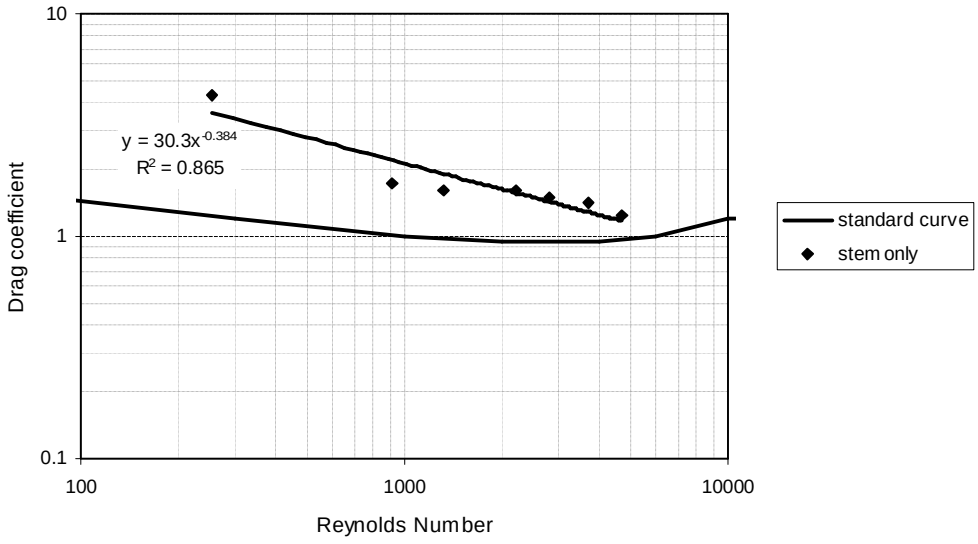

Figure 7-5 Drag coefficient for reed stem with no leaves

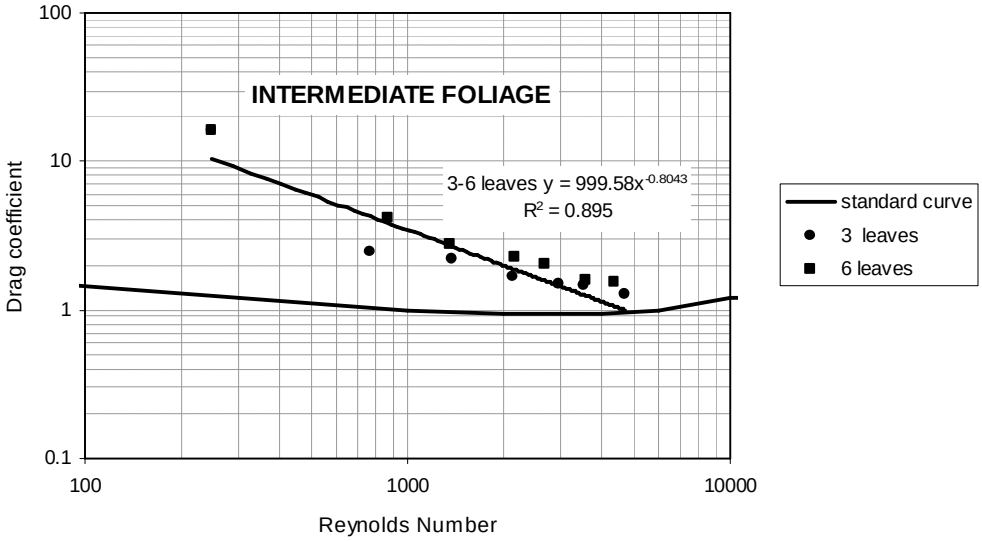

Figure 7-6 Variation of drag coefficient with varying degree of leaf foliage

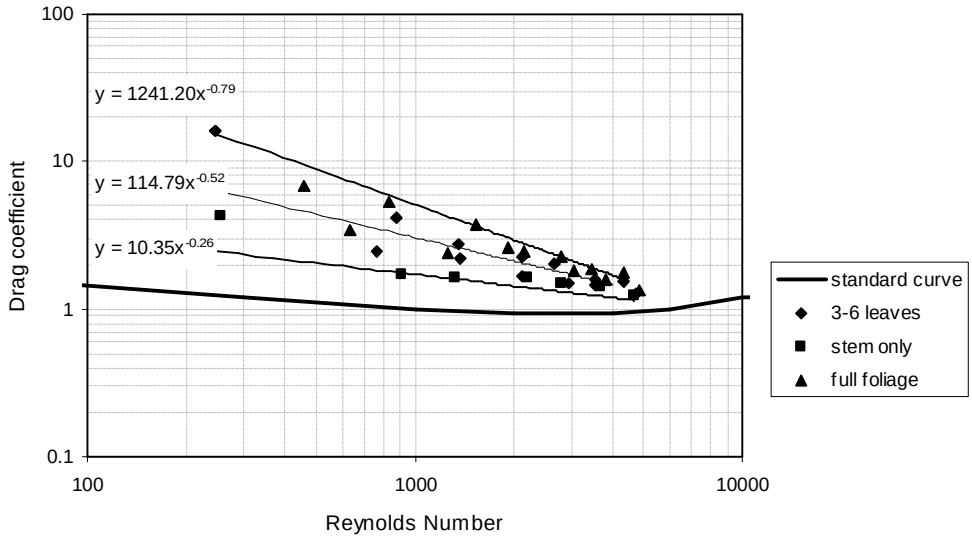

Figure 7-7 Variation of drag coefficient with degree of foliage

Table 7-3 Values of α and β coefficients for estimation of the drag coefficient as a function of the stem Reynolds number

Description	α	β
Stem only	30.3	-0.38
3 – 6 leaves	999.58	-0.80
Full Foliage	209.9	-0.58
Upper limit	1241.2	-0.79
Lower limit	10.35	-0.28
Average	114.79	-0.62

Development of resistance relationship

The functional relationship for *F* (Eq. 7.12) has been quantified by multiple regression analysis of the results of 270 REEDFLO simulations for a wide range of all the input variables. Realistic ranges of values of stem spacing, stem diameter and bed slope were selected according to field data from the Sabie, Letaba and Sand Rivers within the Kruger National Park, South Africa (Kotschy, 2003; Carter, 1995; van Coller et al, 1997). This established appropriate ranges of relevant parameter values for practical application of the proposed equation. The ranges of input variables used in the simulation runs are given in Table 7-4.

Table 7-4 Range of variables for which the resistance equation (7.16) is applicable

Variable	Range
Discharge, q ($m^3s^{-1}m^{-1}$)	0.005-0.5
Bed slope, S	0.0005-0.002
Stem diameter, D (mm)	5.0-20.0
Stem spacing, s (m)	0.05-0.1

The following relationship has been derived for the conditions listed in Table 7-4.

$$F = 1.885\left(\frac{s}{D}\right)^{-0.65}\left(\frac{D}{y}\right)^{0.07} C_D^{\,0.48} \qquad 7.16$$

with r^2 equal to 0.95. The predictions of equation (7.16) are compared with values derived from the REEDFLO simulations in Figure 7-8. Equation (7.6) reproduces the REEDFLO values with an absolute error of 11.5 %, a standard deviation of 8.4 % and a maximum error of 33.3 %.

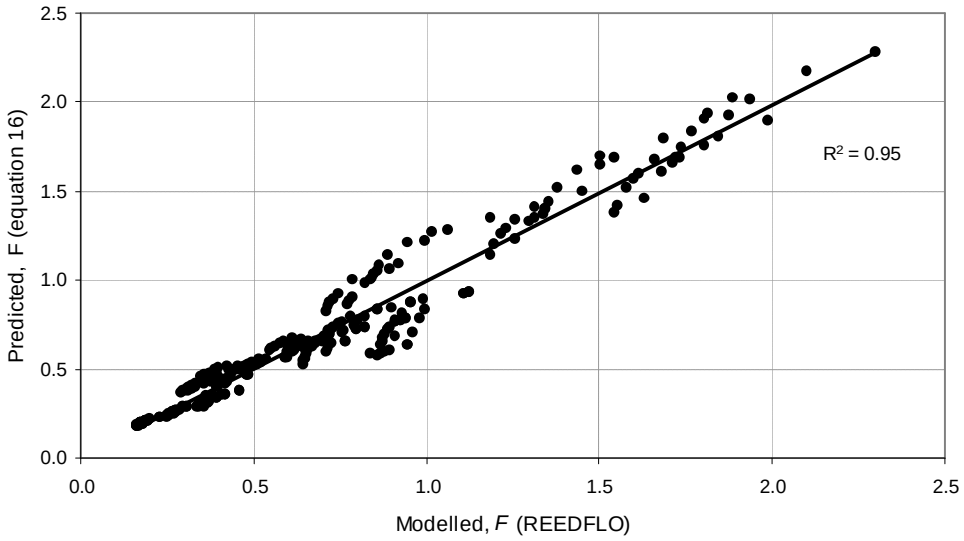

Figure 7-8 Predicted (equation (7.16)) and modelled (REEDFLO) resistance coefficient *F* (James et al, 2001)

7.2.4 Proposed procedure for practical application (Jordanova et al 2006)

A simple procedure using equations (7.8), (7.10), (7.14), (7.15) and (7.16) is proposed for practical stage-discharge determination for waterways with emergent vegetation.

Application of the procedure consists of 6 steps:

- From field data, obtain representative values for stem diameter (D), stem spacing (s), bed slope (S) and the average height of stems from the bed to the first leaf.
- For a specified flow depth assume a flow velocity (V) and calculate the Reynolds number in terms of the stem diameter (D) (equation (7.14).
- Depending on the flow depth of interest in relation to the height of the first leaf, estimate the drag coefficient (C_D) from Figure 7-7 or by using Eq. 7.15 and Table 7-3, according to the degree of foliage.
- From equation (7.16) calculate the resistance coefficient, F, and from equation (7.8) calculate the velocity, V.
- Compare the calculated velocity with the initially assumed one, and if there is a difference, repeat steps 2, 3 and 4 until the assumed and calculated velocities are the same.
- From equation (7.10) calculate the discharge (q) for the nominated flow depth.

7.2.5 Procedure verification

Assessment of the proposed procedure (Section 7.2) for practical application requires field or experimental data on flow resistance with real reeds or similar plants. Published data on flow resistance with real vegetation is very limited, and often does not include information about hydraulic conditions. Suitable experimental data for flow through crops of wheat, reeds and bulrushes are, however, available from the work of Turner and Chanmeesri (1984), Hall and

Freeman (1994), Meijer and van Velzen (1999) and James et al (2004). For each data set the discharge was calculated for each experimental flow depth and compared with the measured value.

Turner and Chanmeesri (1984)

Laboratory experiments with crops of wheat were carried out in a long concrete channel on a fixed slope, and in a smaller flume with a variable slope. The tests were conducted for different sowing patterns, stem densities, stages of growth, and slopes. The experimental data used to verify the proposed procedure (Section 7.2) were extracted from their observations, and are presented in Table 7-5.

Table 7-5 Data from experiments of Turner and Chanmeesri (1984)

Test	Discharge, Q (m^3/s)	Flow depth, *y* (m)	Stem diameter, *D* (mm)	Spacing, *s* (m)	Slope, S
B	0.0007	0.0161	2.72	0.03	0.002
	0.0011	0.0247	2.72	0.03	0.002
	0.0015	0.0328	2.72	0.03	0.002
	0.0020	0.0445	2.72	0.03	0.002
	0.0025	0.0555	2.72	0.03	0.002
	0.0031	0.0665	2.72	0.03	0.002
	0.0036	0.0750	2.72	0.03	0.002
	0.0040	0.0860	2.72	0.03	0.002
H	0.0010	0.0140	2.89	0.05	0.0028
	0.0015	0.0220	2.89	0.05	0.0028
	0.0018	0.0260	2.89	0.05	0.0028
	0.0026	0.0360	2.89	0.05	0.0028
	0.0032	0.0415	2.89	0.05	0.0028
	0.0036	0.0495	2.89	0.05	0.0028
	0.0040	0.0535	2.89	0.05	0.0028
	0.0046	0.0585	2.89	0.05	0.0028
	0.0049	0.0670	2.89	0.05	0.0028

Hall and Freeman (1994)

Hall and Freeman (1994) carried out laboratory experiments on flow through bulrushes (*Scirpus validus*) at different growth stages. A weir installed downstream of the channel was used to control backwater. The first sets of experiments were conducted for “low” and “high” tailwater conditions, the stem diameter was 7.0 mm and the density of the stems was 403 per square metre. The second set of experiments was run for “high” tailwater conditions only, when the

stem diameter was 7.6 mm and the stem density was 807 per square metre. The experimental stage-discharge data used for verification are listed in Table 7-6.

Table 7-6 Data from experiments of Hall and Freeman (1994)

Test	Discharge, Q (m^3/s)	Flow depth, y (m)	Stem diameter, D (mm)	Spacing, s (m)	Slope, S
June 1992 Tests (low tailwater)	0.009	0.103	7.0	0.05	0.0088
	0.026	0.215	7.0	0.05	0.0105
	0.044	0.268	7.0	0.05	0.0145
	0.057	0.306	7.0	0.05	0.0145
June 1992 Tests (high tailwater)	0.009	0.313	7.0	0.05	0.0010
	0.026	0.339	7.0	0.05	0.0035
	0.044	0.403	7.0	0.05	0.0040
	0.057	0.432	7.0	0.05	0.0050
November 1992 Tests	0.010	0.347	7.6	0.035	0.0028
	0.026	0.374	7.6	0.035	0.0085
	0.044	0.417	7.6	0.035	0.0120
	0.064	0.448	7.6	0.035	0.0198

Meijer and van Velzen (1999)

In addition to their studies with artificial vegetation represented by steel rods, Meijer and van Velzen (1999) also carried out some tests with natural reeds in a 3.0 m wide, 100 m long laboratory flume. The data for these were used for verification and are given in Table 7-7.

Table 7-7 Data from experiments of Meijer and van Velzen (1999)

Test	Discharge, Q (m^3/s)	Flow depth, y (m)	Stem diameter, D (mm)	Spacing, s (m)	Slope, S
Emergent reeds	0.36	1.22	5.7	0.063	0.0013
	0.53	1.27	5.7	0.063	0.0026

James et al (2004)

The hydraulic and resistance characteristics of flow through reeded channels were investigated using harvested reed (***Phragmites australis)*** in a 0.38 m wide, 0.66 m high and 10.4 m long flume. Two test series were undertaken to differentiate between the leaf and stem resistance of reeds, the first with foliated and the

second with defoliated reeds set vertically in a regular rhomboidal pattern. Experimental data are listed in Table 7-8.

Table 7-8 Data from experiments of James et al (2004)

Test	Discharge, Q (m^3/s)	Flow depth, y (m)	Stem diameter, D (mm)	Spacing, s (m)	Slope, S
Full foliage	0.0014	0.047	9.5	0.071	0.0015
	0.0029	0.134	9.5	0.071	0.0015
	0.0049	0.331	9.5	0.071	0.0015
	0.0064	0.482	9.5	0.071	0.0015
Stem only	0.0030	0.078	9.5	0.071	0.0015
	0.0067	0.165	9.5	0.071	0.0015
	0.0096	0.239	9.5	0.071	0.0015
	0.0152	0.353	9.5	0.071	0.0015

The proposed procedure (Section 7.2) was applied to the four sets of experimental data. A summary of comparisons between predicted and measured discharges in terms of maximum, minimum and average absolute errors, and their standard deviations is given in Table 7-9. The average absolute error in the predicted discharge for all 39 tests is 12.9%. An application of the proposed procedure was performed on the same sets of experimental data using the resistance coefficient (equation (7.9)), and the average absolute error in the predicted discharge is 18.1%. The difference in performance of the proposed procedure with the resistance coefficients (equations (7.9) and (7.16)) in terms of the average absolute error shows equation (7.16) to be superior. The performance of equation (7.9) deteriorates significantly as the amount of foliage increases.

Available data required for verification of prediction of the proposed procedure is limited, and for the data used, not all information on hydraulic and vegetation conditions was available. At this stage it is therefore difficult to evaluate why the method performed better or worse for different conditions. However, considering the limited data on which the method is based, particularly for C_D, the proposed procedure performs reasonably well. It provides a workable method that can be improved as new data become available.

Table 7-9 Summary of comparison between predicted and measured discharges

Source	Test	No. of tests	Discharge computation			
			Min absolute error (%)	Max absolute error (%)	Average absolute error (%)	Standard deviation (%)
Turner and Chanmeesri (1984)	B	8	3.7	12.6	7.4	2.5
	H	9	0.3	9.5	3.7	8.8
Hall and Freeman (1994)	Low tailwater	4	3.7	23.3	13.5	6.9
	High tailwater	4	0.9	30.5	17.2	12.6
	November 1992	4	9.2	20.3	13.2	4.3
Meijer and van Velzen (1999)	Emergent reeds	2	3.1	9.2	6.1	3.1
James et al (2004)	Full foliage	4	1.5	17.0	11.6	6.1
	Stem only	4	28.2	31.7	30.5	1.4

7.2.6 Conclusions

A computational model of vegetation-influenced flow has been applied to identify the characteristics that most significantly influence resistance to flow through emergent reed-type vegetation, and to develop a simple, direct approach for resistance calculations.

The most important variables influencing emergent vegetation resistance are the vegetation stem diameter, the stem spacing, the stem drag coefficient and the channel slope. Bed roughness has little influence in drag dominated flows.

The proposed stage-discharge relationship (equation (7.8)) is rational in origin, but includes an empirical resistance coefficient. A formulation for this coefficient is presented (equation (7.16)) that accounts rationally for the underlying variables and processes (through the REEDFLO model), and reduces the empirical content to the stem drag coefficient only.

The stem drag coefficient depends on the stem Reynolds number and the stem foliage, as presented in Figure 7-7, based on available real vegetation stem drag data.

Resistance to flow through emergent vegetation can be estimated through a simple iterative procedure (Section 7.2) employing equations (7.8) and (7.16) and the drag coefficient diagram (Figure 7-7). Predictions show satisfactory agreement with measured stage-discharge data for emergent vegetation.

Field data, required for Step 1, should be collected with an understanding of the influence of each parameter on overall resistance. Reed stem attribute data have to be subjectively sampled to cover the range of densities, stem diameters and leaf distributions. Seasonal changes in stem characteristics need to be understood and taken into account where necessary for effective prediction of the interaction between reeds and flow.

The proposed procedure has been tested only against the limited available laboratory data, and has not yet been verified against field data. Nevertheless, it provides a simple conveyance estimation method for flow through emergent vegetation with reliability consistent with current knowledge, which can be refined as suitable field data become available.

7.3 Conveyance Estimation for Channels with Emergent Vegetation Boundaries

7.3.1 Introduction

Emergent vegetation is a common feature along river banks. It can influence flow resistance significantly even if it occupies only a relatively small part of the channel (James et al, 2001), and should be accounted for in estimation of the channel conveyance. Vegetation increases overall resistance by imposing greater local resistance where it occurs, and by retarding flow in adjacent clear water zones.

The well-structured distribution of roughness presented by vegetation occurring in strips along the channel banks suggests channel subdivision as a suitable strategy for practical conveyance calculation. Discharges can be calculated separately for the vegetated and clear zones of a cross section, and added together to obtain the

total discharge. The effects of flow interaction between the zones can be quantified for this purpose through recognition of an apparent shear stress at the zonal interface, tending to resist flow in the clear channel and propel it within the vegetation.

The flow contribution of the vegetated zones for channels with bank vegetation is usually small, and may often be ignored. Where it is significant, the discharge may be estimated using the procedure presented in Section 7.2, although this method will underpredict the discharge slightly because of the propelling influence of the adjacent clear channel flow.

The conveyance estimation method for the clear channel zone between the bank vegetation zones has been proposed by James and Makoa (2006). A discussion of this method is presented below.

7.3.2 Clear channel zone discharge

A clear channel between vegetation strips can be considered as one of composite roughness, with different roughnesses on the sides and the bed. If resistance coefficients for the different surfaces are known, then an equivalent coefficient for the whole clear channel can be determined by well-known composite roughness formulae (Chow, 1959; French, 1985). For the following formulations the channel cross section is divided into a number of subsections (N), each with a wetted perimeter (P_i) (which does not include the interfaces with adjacent subsections), and with a known subsection value of the resistance coefficient (n_i).

Various equations, based on different assumptions, have been proposed for estimation of the equivalent, overall, value of Manning's n.

Horton (1933):

$$n_e = \left(\frac{\sum_{i=1}^{N} \left(P_i \, n_i^{3/2} \right)}{P} \right)^{2/3} \qquad 7.17$$

where n_e : the equivalent value and

P : the total wetted perimeter.

Pavlovski (1931):

$$n_e = \left(\frac{\sum_{i=1}^{N} \left(P_i \, n_i^{2} \right)}{P} \right)^{1/2} \qquad 7.18$$

Lotter (1933):

$$n_e = \frac{P \, R^{5/3}}{\sum_{i=1}^{N} \frac{P_i \, R_i^{5/3}}{n_i}} \qquad 7.19$$

where R_i : the hydraulic radius of the i^{th} subsection, and

R : the total hydraulic radius.

Colebatch (1941):

$$n_e = \left(\frac{\sum_{i=1}^{N} \left(A_i \, n_i^{3/2} \right)}{A} \right)^{2/3} \qquad 7.20$$

where A_i : the area of the i^{th} subsection, and

A : the total area.

These equations have been tested (James and Makoa, 2006) for the situation of vegetation-type side boundaries using laboratory data obtained by James et al (2001). A brief review of the laboratory experimental set up is presented below.

7.3.3 Laboratory experiments (James et al, 2001)

The influence of vegetation strips (including those wholly within the channel as well as along the banks) on channel conveyance was investigated experimentally by James et al (2001). Experiments were carried out in a 12.26 m long, 1.0 m wide, rectangular channel lined with cement plaster and set on a slope of 0.00107. Vegetation stems were represented by 5 mm diameter steel rods set in a regular, staggered grid pattern with centre spacings of 25 mm in both the longitudinal and transverse directions. 7 distribution patterns were tested. All the patterns contain the same total number of stems with the same local density and the same overall coverage of 50% of the channel area (James et al, 2001).

For the basic channel with no stems, experiments were performed for a range of discharges between 5 l/s and 35 l/s. For the vegetated channels, experiments were performed for discharges from 5 l/s up to 22.5 l/s. Stage-discharge measurements were taken for all the distribution patterns, and for the basic channel. Longitudinal flow velocities were also measured with a miniature propeller current meter over one cross section in the clear channels to enable the clear channel discharges to be determined by integration. Velocities were measured at 0.2, 0.4 and 0.8 of the flow depth from the bed to enable a depth-averaged velocity (V) to be determined. Water temperatures were also measured to enable accurate specification of viscosity values. (All details of experimental procedure and measurements are presented by James et al, 2001).

7.3.4 Composite roughness concept approach (James and Makoa, 2006)

Application of the equivalent resistance coefficient formulae presented above (equations (7.17) to (7.20)) requires resistance coefficient values for the plaster

bed and side boundaries of the basic channel and for the stem-water interfaces. Manning's n for the solid boundaries (n_b) was calculated from the stage-discharge measurements in the basic channel. Values of the Darcy-Weisbach friction factor for both solid boundaries (f_b) and stem-water interfaces (f_s) were also determined from the integrated clear channel discharges and associated flow depths by an inverse application of the side-wall correction procedure proposed by Brownlie (1981). The corresponding values of Manning's n were then calculated from the f values using the hydraulic radius values for the bed and interface determined by the side-wall correction calculations.

To test the composite roughness concept, the actual values of n_e were determined directly from Manning's equation for the clear channels using discharges determined by integration of the measured velocity distributions. The n_e values were also predicted using the composite roughness formulas, equations (7.17) to (7.20). The n_e values predicted using equations (7.17) to (7.20) show the same trend with width to depth ratio as the measured data, suggesting that the variation is explained by the composite roughness effect.

The application of the equations (7.17) to (7.20) showed that the method of Lotter (1933) clearly exaggerates the relative influence of the bed roughness over the entire range of conditions while the methods of Horton (1933) and Pavlovski (1931) perform the best, with Horton's being superior in the more realistic higher range of width to depth ratios.

Total clear channel discharges have been predicted for all the experimental conditions using n_e from equations (7.17) to (7.20). The absolute prediction errors are listed in Table 7-10.

Table 7-10 Absolute errors (%) for prediction of experimental clear channel discharge

Method	Absolute errors (%)		
	maximum	minimum	average
Pavlovski (1931)	14.28	2.09	7.32
Horton (1933)	19.60	1.96	8.68
Colebatch's (1941)	27.52	10.33	15.12
Lotter (1933)	215.1	70.71	122.20

The method of Lotter (1933) is clearly unsatisfactory (as was also found by Flintham and Carling (1991)). Colebatch's (1941) formula consistently overpredicts discharge, with higher average errors than the remaining two methods. Both the methods of Pavlovski (1931) and Horton (1933) give satisfactory results, and there is little to choose between them. These two methods have the added advantage that only the channel perimeter (and not the flow area) needs to be subdivided, obviating the necessity of attempting to define shear-free surfaces.

All details of vegetated zone and total discharge calculations for the laboratory experiments are presented by James et al (2001) and James and Makoa (2006).

7.3.5 Conclusions

Conveyance in channels with emergent bank vegetation can be estimated by a zonal approach, whereby the total discharge is calculated as the sum of discharges in the vegetated and clear channel zones, calculated separately.

Laboratory applications show that clear channel discharges can be reliably estimated using conventional resistance equations, such as Manning's. The variation of Manning's n with width to depth ratio can be attributed to the varying proportional contributions of composite roughness components, and can be

reliably accounted for by the Horton (1933) (equation (7.17)) and Pavlovski (1931) (equation (7.18)) formulae.

7.4 Modelling of Flow Resistance for Discrete Reed Patches

7.4.1 Introduction

Vegetation is one of the river features that has significant contribution to overall flow resistance, and its prediction is therefore essential in hydraulic modelling. A prediction method for estimating the average velocity and hydraulic resistance within vegetation is presented in Section 7.2. Conveyance estimation for channels with continuous emergent vegetation strips is discussed in Section 7.3. Besides the longitudinal strips, vegetation within a channel often forms discrete, longitudinally discontinuous patches. The influence of discrete reed patches on overall flow resistance has been investigated (James et al, 2001) and it was found that the resistance is strongly influenced by the overall areal coverage, and varies significantly with the overall distribution pattern of the patches, the size and shape of the patches, and the degree of longitudinal and transverse fragmentation. The resistance phenomenon under such conditions is very complex, and conveyance cannot be described by a single equation or simple procedure. Computational modelling in two or three dimensions provides a realistic alternative approach.

In this section an attempt to model the flow resistance with discrete patches using River2D software is presented.

7.4.2 River2D software

River2D is a two-dimensional hydraulic and habitat simulation model, capable of predicting values of hydraulic parameters such as depth and velocity in a spatially explicit way. The programme is designed for both steady and unsteady flow analyses, and the numerical solutions are obtained using finite element methods.

River2D consists of four modules that run separately:

- R2D_bed - bed topography module,
- R2D_ice – ice cover module,

- R2D_mesh - finite element mesh module, and
- River2D - flow and habitat analysis module.

River2D software and documentation are available free of charge for download from website http://www.river2d.ualberta.ca/.

Implementation of River2D for modelling in South Africa is a part of a present Water Research Commission project K5/1508. The project will present research related to the best use of River2D as a hydraulic analysis tool. Discussions of modelling considerations, inputs and parameters, the sensitivity of two-dimensional hydraulic model to these inputs and parameters, and a set of guidelines for the use of River2D for eco-hydraulic modelling in South Africa will be included in the final report.

7.4.3 Laboratory experiments (James et al, 2001)

Discrete vegetation patch experiments were performed in the same facility used for the longitudinal strip experiments. The discrete patches were simulated by the same frames (Section 7.3.3). The frames were arranged in 15 different discrete patch distribution patterns, and numbering of the distribution patterns used here is the same as in James et al (2001) in their Figure 8-24.

Experiments were conducted for different areal coverages. The maximum total channel area covered by the patches was 50%, while the minimum was 12.5%. Percentages of total area covered by patches for each pattern are listed in Table 7-11.

Table 7-11 Percentages of total area covered by patches

Pattern	Aria covered (%)
8	25.00
9	37.50
10	37.50
11	50.00
12	28.125
13	28.125
14	28.125
15	50.00
16	50.00
17	12.50
18	12.50
19	25.00
20	37.50
21	25.00
22	12.50

Flow depths were measured at different discharges for different patterns, and the flow resistance in terms of Manning's n for each measurement was calculated. Manning's n values calculated for measured depths at a discharge of 10 l/s are plotted against proportion of total area covered (AC) by patches for all patterns in Figure 7-9. It is evident that resistance increases with increasing total area covered, but it is also clear that for the same area covered it varies over a very wide range for different patch arrangement patterns.

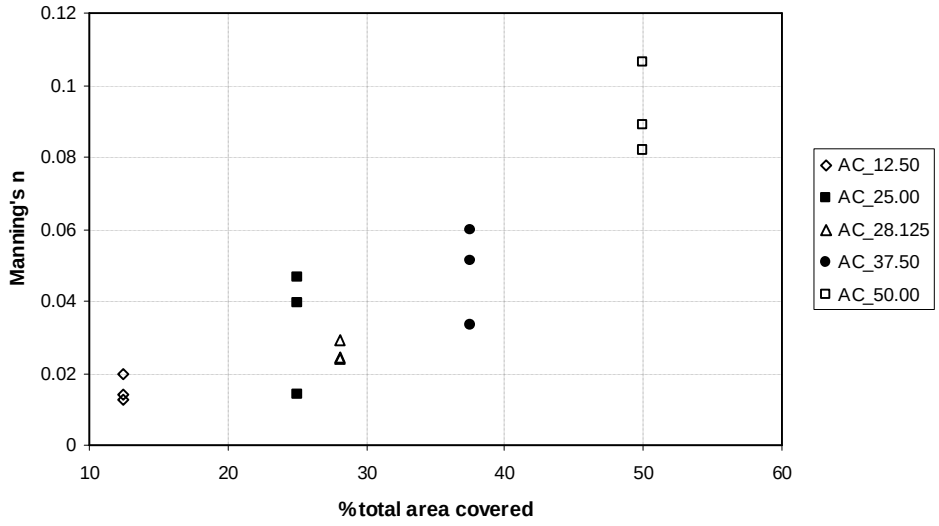

Figure 7-9 Manning's *n* variation with proportion of total area covered by patches, Q=10 l/s

The experiments to investigate resistance due to longitudinal vegetation strips (James et al, 2001) were carried out with a total areal coverage of 50 %. The overall resistance (Manning's *n*) values for a discharge of 10 l/s are included in Figure 7-10 for comparison with other patch distribution patterns with the same areal coverage.

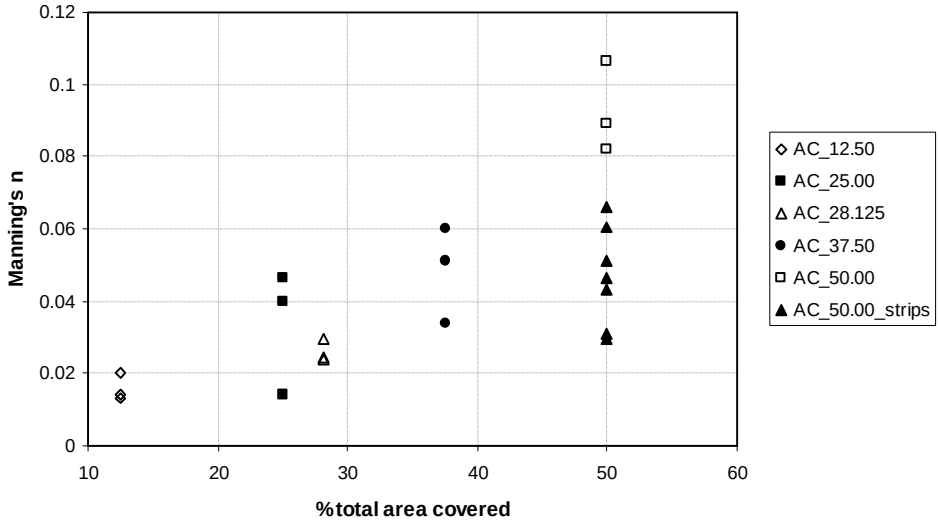

Figure 7-10 Flow resistance in term of Manning's *n* against area covered by vegetation including longitudinal strips, Q=10 l/s

From Figure 7-10 it can be seen that Manning's *n* for an areal coverage of 50 % varies from 0.03 to 0.106, showing that overall resistance depends significantly on the degree of fragmentation of patches and the length of stem-clear water interface. As vegetation patches are often irregular in shape and distribution, conveyance prediction for such channels is not simple and requires computational modelling for adequate description.

Application of River2D model to reproduce experimental results of some of the 15 discrete patch patterns is discussed in the next section.

7.4.4 Modelling channels with discrete patches using River2D

Introduction

As mentioned above, a current Water Research Commission project (K5/1508) related to eco-hydraulic modelling includes investigation of the applicability of the River2D model to provide prediction of effects of vegetation on overall resistance. The two ways of modelling flow through vegetation by the model – by treating it either as large-scale roughness or as a porous material – have been

investigated. It has been concluded that River2D can be used to predict the resistance of vegetated channel with reasonable accuracy.

The following sections describe the application of River2D to discrete patch patterns 11, 15, 16, 20 and 22.

Modelling setup

The layouts of modelled Patterns 11, 15, 16, 20 and 22 are shown in Figures 7-11, 7-12, 7-13, 7-14 and 7-15 respectively. In each case the vegetated channel has a length of 12.00 m, a width of 1.00 m, and a slope of 0.00107.

A mesh of 0.25 m size was set up over the whole bed, and was refined to 0.05 m over the clear channel, spaces between the discrete patches. Modelling was carried out for a discharge of 10 l/s only, and this value was set as a boundary condition of inflow.

Vegetation patches were modelled as:

- **large-scale roughness with a high value of the bed roughness** k_s in the vegetation zones referred to as bed_1, and
- zones of porous material, treated as groundwater flow by River2D, and referred to as bed_2.

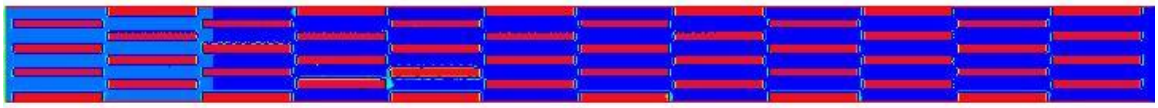

Figure 7-11 Layout of Pattern 11. Vegetation in Red

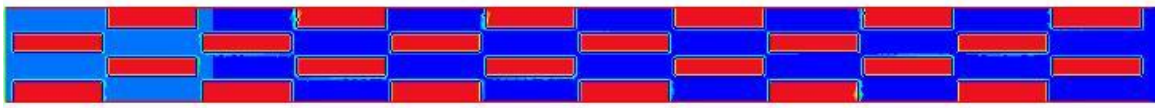

Figure 7-12 Layout of Pattern 15. Vegetation in Red

Figure 7-13 Layout of Pattern 16. Vegetation in Red

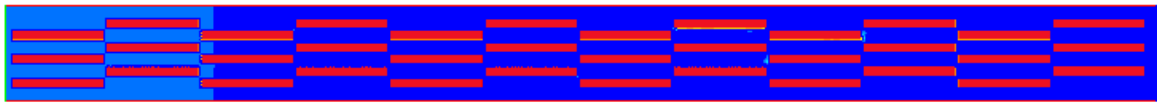

Figure 7-14 Layout of Pattern 20. Vegetation in Red

Figure 7-15 Layout of Pattern 22. Vegetation in Red

Large-scale roughness approach

Vegetation patches were modelled as areas with large-scale roughness, requiring specification of a corresponding value of roughness size k_s. Laboratory experiments on flow resistance within vegetation (James et al, 2001) indicate values of the Chézy resistance coefficient (used in River2D) as low as 2.7 $m^{1/2}/s$. The vegetation used in the laboratory experiments was very dense (with a stem spacing of 25 mm), resulting in this very high resistance. The calculated value of flow resistance exceeds the limit that can be specified in the River2D. Therefore the highest permissible value of the bed roughness k_s was used, and it was expected that the modelled flow resistance might be lower than that measured. Measured and modelled flow depths and corresponding resistance in term of Manning's *n* for considered patterns are presented in Figure 7-16 and Figure 7-17 respectively. Modelled data for this condition are labelled "bed_1".

Groundwater approach

River2D includes groundwater flow equations that can be used to model vegetation patches as a porous material. The programme automatically switches

from the surface flow equations to groundwater flow equations when no water occurs over a part of the modelled area. The vegetation patch levels were therefore increased to above the water level so that the groundwater flow equations would be implemented in the discrete patch regions. Modelled flow depths and flow resistances in terms of Manning's *n* for each pattern, labelled "bed_2", are presented in Figure 7-16 and Figure 7-17 respectively.

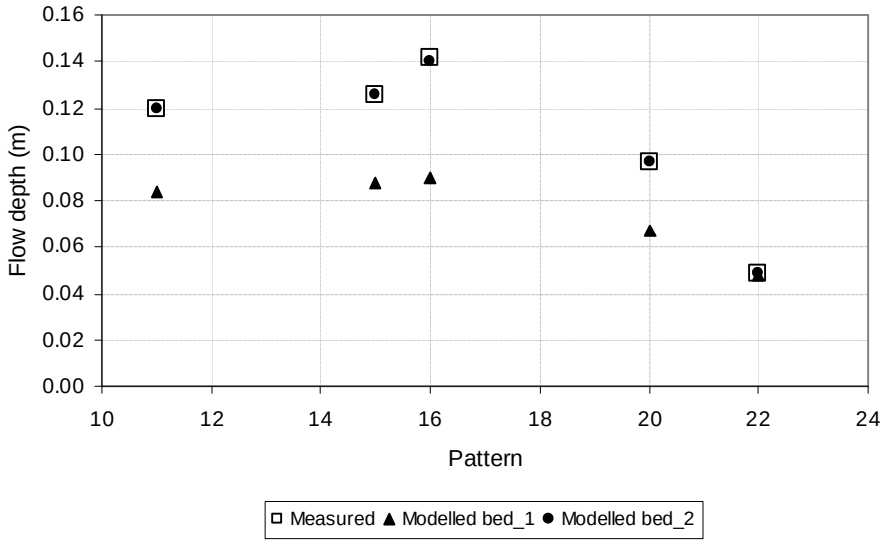

Figure 7-16 Measured and modelled River2D flow depths

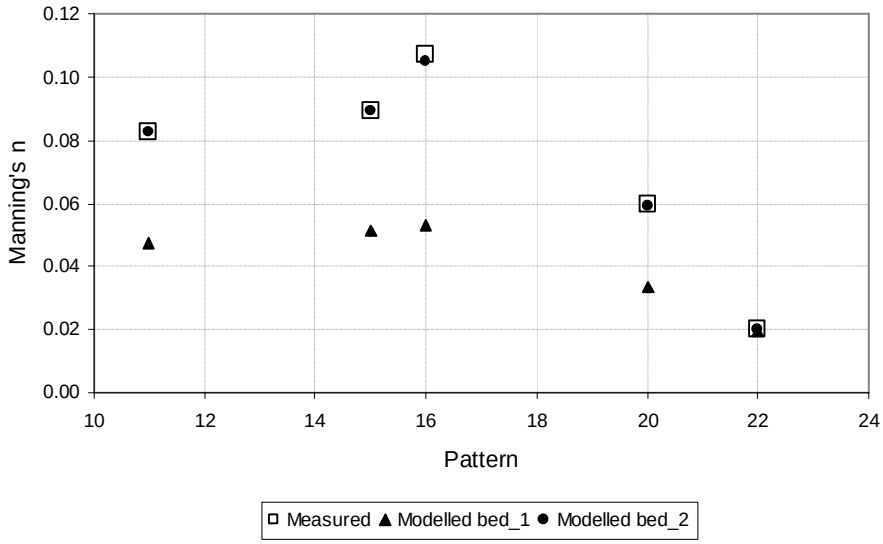

Figure 7-17 Flow resistance in term of Manning's n for measured and modelled River2D data

Results and discussion

The results of River2D modelling for discrete vegetation patch distribution patterns in terms of flow depth and Manning's *n* resistance coefficient are shown in Figure 7-16 and Figure 7-17 respectively. Modelling vegetation as a porous material reproduced the measured flow depth and the resistance well for all the patterns considered. Modelling vegetation as a surface with large-scale roughness produced flow depths and resistance values lower than were measured; this was expected as the true roughness exceeded the input limit of River2D. The difference between measured and modelled values also varies between the different patch patterns. The highest modelled error is for pattern 16, while the modelled flow depth for pattern 22 with areal coverage of 12.50 % is about the same as was measured. It also can be seen that the modelled error for pattern 16 is higher than for patterns 11 and 15, even though they all have the same areal coverage of 50 %. This difference can be explained by lateral momentum transfers caused by the vegetation patches. Pattern 16 has the largest patches, and hence the largest in-vegetation flow areas that would not be affected by momentum transfer and where the resistance is closest to the uninfluenced

vegetation value; it is therefore the pattern most affected by the input limitation on resistance coefficient.

7.4.5 Conclusions

The River2D model has been tested for prediction of flow resistance in channels with discrete patches. Experimental data of James et al (2001) were reproduced, and modelled and measured resistance values were compared. Discrete vegetation patches were represented as regions of large-scale roughness with high values of bed roughness size k_s ("bed_1" model) and as regions of porous material ("bed_2" model). Modelled results showed that the "bed_2" representation reproduced the experimental data very well, while the "bed_1" model underestimated the measured flow resistance. The difference in performance of two models can be explained by the very dense vegetation used in the laboratory experiments, which had a very high flow resistance that exceeded the limitation of the programme. On the other hand, the "bed_2" model has an un-realistic flow through the vegetation patches, while the "bed_1" model provides a better cross-sectional velocity distribution. In general, River2D can be used to predict the flow resistance of vegetation patches with reasonable accuracy.

8 RIVER2D APPLICATION TO FIELD DATA

8.1 Introduction

The model River2D is recommended in this report for predicting velocity and flow depth distributions under low flow conditions. Its performance has been demonstrated in Chapters 6 and 7 by comparison of its predictions with laboratory data. In this chapter, its application to two field situations where appropriate data are available is presented. Two sites, Spur Hole and Vanities Crossing, on the Cotter River in Australia and one site, Site A, of the Driehoeks River in South Africa were used for this application. The sites are very different in terms of dominant river-bed substratum (Figures 8-2, 8-3 and 8-26). The Spur Hole site is dominated by cobble and gravel substrate. Bedrock and cobble represent the Vanities Crossing site, while Site A is characterized by a gravel bed with vegetation patches.

8.2 Cotter River Modelling

8.2.1 Introduction

The Cotter River in Australia has been studied intensively by the Riverine Landscapes Research Laboratory at the University of Canberra. This river presents features and hydraulic characteristics similar to those of many South African rivers, and is suitable for assessing the capabilities of River2D. The data used for this application were made available by Professor Martin Thoms (pers. comm.).

The Cotter River catchment is situated in the Brindabella Range within the Australian Capital Territory (ACT), Australia, and occupies an area of 48,300 hectares (Figure 8-1). The river flows in a northerly direction before joining the Murrumbidgee River approximately 72 km downstream at Cotter Reserve. The area consists of steep slopes and rock outcrops, with granite, limestone, siltstone and shales present. Most of the catchment (88%) lies within the Namadgi National Park with land-use dominated by native forest. Plantation forestry of predominantly pine trees occupies the lower catchment. Because the

majority of the catchment is managed for nature conservation and protection of water supply, the Cotter River flows through a largely unmodified area. It is an upland boulder, cobble and gravel-bed river with a highly heterogeneous bed topography including bedrock outcrops.

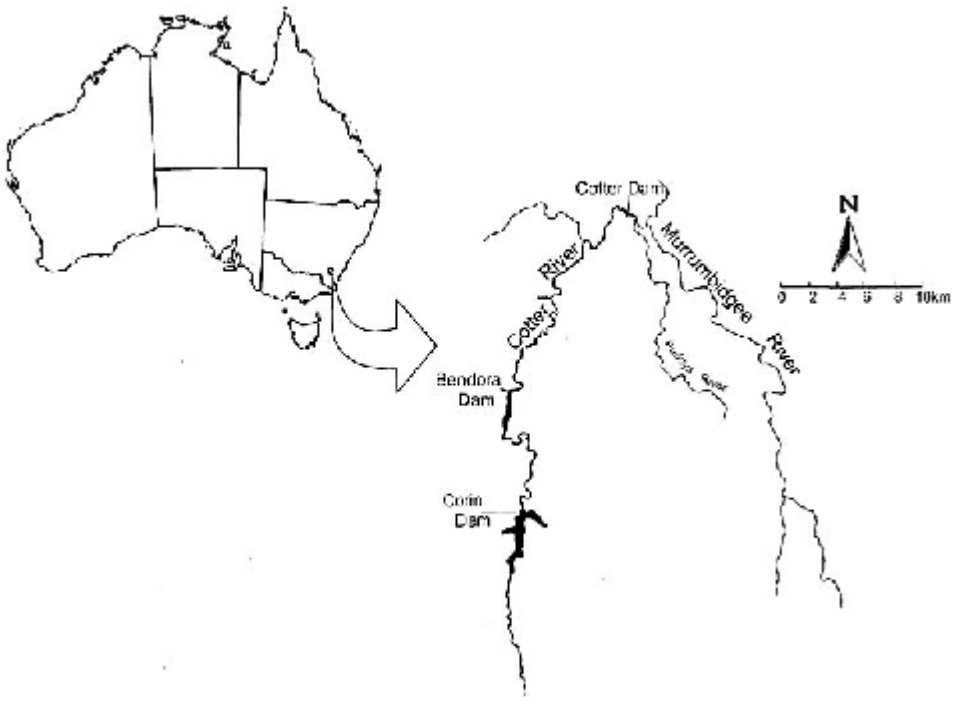

Figure 8-1 Location of the Cotter River Catchment and study area (Dyer and Thoms, 2006)

8.2.2 Selection of sites

Two sites were selected, i.e. one at Spur Hole and one a short distance downstream from Vanities Crossing. The selected sites are shown in Figure 8-2 and Figure 8-3 respectively.

Standard techniques (Elliott et al., 1996) were used to collect data on site topography, substrate and hydraulics. Survey markers were used to identify the locations of the cross-sections, transect-profiles were surveyed and substrate sizes present were visually assessed (Appendix G). The two sites were visited under three different flows between April and June 2002 in order to collect field data across the range of discharges of prime interest to this study.

Figure 8-2 Cotter River, Spur Hole Site

Figure 8-3 Cotter River, Vanities Crossing Site

8.2.3 Cross-section data

At Spur Hole, cross-sections 2, 3, 4 and 5 were surveyed relative to each other and therefore bed heights are also relative to each other. Cross-section 1 is a 'stand alone' cross-section some distance downstream from the other four, and bed heights are not relative to other cross-sections. An arbitrary datum of 100 m was given to the right bank marker at cross-sections 1 and 5. At Vanities Crossing, all cross-sections are in close proximity and were surveyed relative to each other. Therefore bed heights are also relative to each other. An arbitrary datum of 100 m was given to the left bank marker at cross-section 5.

The bed profiles for each cross-section with the water surface levels during each of the three surveys are illustrated in Appendix G, Figures G-1 and G-2 for Spur Hole site and in Figures G-3 and G-4 for Vanities Crossing. Cross-sectional surveyed and substrate data are also presented in Appendix G.

8.2.4 Flow data

The two sites were visited under three different flow conditions between April and June 2002 in order to collect field data across the range of discharges of prime interest to this study. During each of the three site visits, water surface elevations were recorded. Cross-sectional water velocities and water depths were measured at 0.5m intervals across all transects during the low and medium flow calibration data collection, and at a limited number of cross-sections (i.e. those that could be accessed safely) during the high flow data collection.

Table 8-1 summarises the dates when the field data were collected and the flows (in m^3/s and Ml/d) that were present during each of the surveys.

Table 8-1 Flow data

Field data collection	Spur Hole		Vanities Crossing	
	m^3/s	Ml/d	m^3/s	Ml/d
Low flow (24/4/02)	0.3427	29.6	0.3305	28.6
Medium flow (20/6/02)	1.2686	109.6	1.308	113.1
High flow (30/5/02)	2.2498	194.4	2.1118	182.5

8.2.5 River2D modelling

River2D modelling of two sites, (Spur Hole and Vanities Crossing, both on the Cotter River) with two discharges (low and medium) (Table 8-1) were performed by the following steps:

- Processing of survey data,
- Specification of bed roughness (k_s),
- Mesh generation,
- Boundary condition specification,
- Analysis, and
- Evaluation of results.

Modelling approach

All survey data, at five cross-sections for each site, were linked in a "xyz" co-ordinate system. During the field work substrate sizes were assigned at each surveyed point. The value of the bed roughness (k_s) for the surveyed points was estimated using the Conveyance Estimation System of Wallingford Software (2004). Resistance coefficients in term of Manning's *n* that they suggest (for a flow depth of 1m) have been converted to equivalent values of roughness *ks* (Hirschowitz et al, in preparation) and these were used in the model. Values of roughness k_s for different bed materials are show in Table 8-2.

Topography and bed roughness data of the considered sites were saved in a text file using the format required by River2D. A mesh of 0.5m size was set up over the whole bed. The upstream boundary condition was specified as a discharge, while a water surface elevation was set up as the downstream boundary condition.

Table 8-2 Natural bed material resistance according to Wallingford Software (2004)

Bed Material	Manning's n ($s^{-1/3}m^{-1}$)			Equivalent k_s (m)		
	Typical	Minimum	Maximum	Typical	Minimum	Maximum
Bedrock	0.025	0.023	0.028	0.072	0.046	0.125
Cobbles	0.035	0.031	0.039	0.311	0.194	0.452
Coarse gravel	0.027	0.025	0.03	0.105	0.072	0.169
Gravel	0.025	0.020	0.028	0.072	0.020	0.125
Fine gravel	0.022	0.017	0.025	0.036	0.007	0.072
Sand	0.020	0.017	0.025	0.020	0.007	0.072
Silt	0.018	0.015	0.022	0.010	0.002	0.036
Clay	0.020	0.018	0.023	0.020	0.010	0.046
Peat	0.020	0.018	0.023	0.020	0.010	0.046
Earth	0.020	0.018	0.023	0.020	0.010	0.046

Spur Hole Site modelling and results

River2D steady flow modelling was performed with two discharges ($0.343m^3/s$ and $1.27m^3/s$). Before running the model, it is necessary to specify boundary locations and conditions. Locations for the upstream and downstream boundaries of the model should be cross-sections. For steady models, the upstream boundary condition is usually specified as a flow rate, and the downstream boundary condition is specified as a set water surface elevation.

The following locations and conditions for the upstream and downstream boundaries were specified:

- Location of the upstream boundary - 1st upstream cross-section,
- Location of the downstream boundary - the last downstream cross-section,
- Condition of the upstream boundary – $Q=0.343m^3/s$ and $Q=1.27m^3/s$ for runs 1 and 2 respectively, and
- Condition of the downstream boundary - the last downstream cross-section water surface elevations related to Q=0.343m3/s and Q=1.27m3/s for runs 1 and 2 respectively.

A plan view of the velocity distribution for $Q= 0.343m^3/s$ is shown in Figure 8-4 as an example of River2D output results.

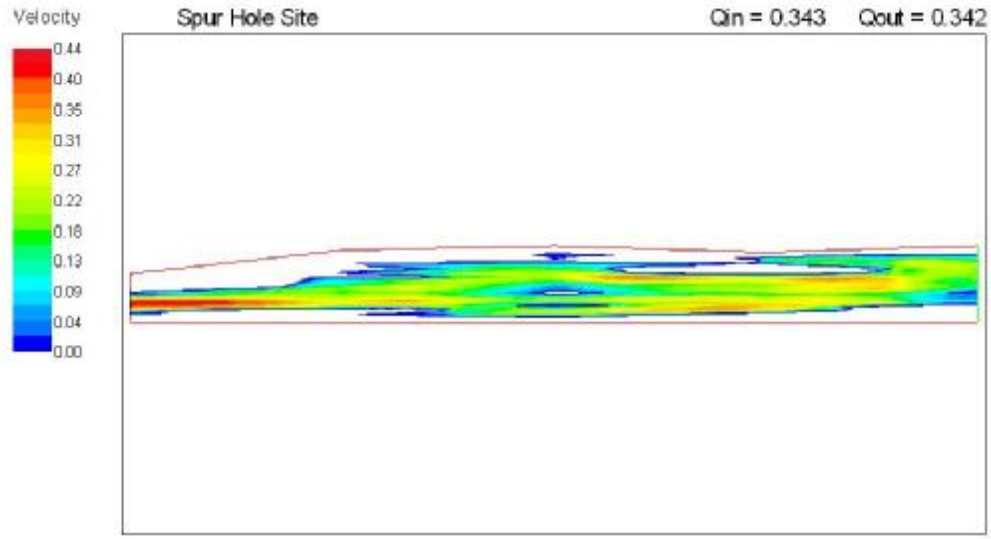

Figure 8-4 Spur Hole Site, overview of velocity distribution for Q=0.343 m^3/s

More meaningful interpretations of the predictions are possible from comparison of modelled and measured frequency distributions of velocity and depth in the form of a histogram. Figures 8-5 and 8-6 present the histograms for sections 2, 3 and 4 for the discharge Q = 0.343m^3/s. Figures 8-7 and 8-8 are for the discharge Q = 1.27m^3/s.

Generally, the modelled frequencies of velocity and depth reproduce the measured values well. It also can be seen that River2D performs better in terms of depth distribution than velocity distribution. The model did not predict occurrence of velocities higher than 0.4m/s and 0.6m/s for Q=0.343 and 1.27m^3/s respectively (Figures 8-6 and 8-8).

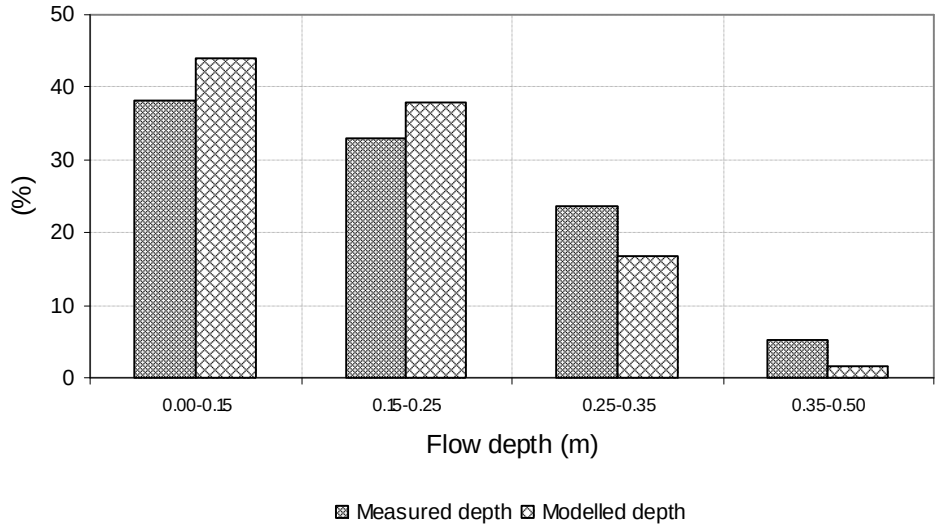

Figure 8-5 Spur Hole Site, modelled and measured frequency-depth distributions through cross-sections 2, 3 and 4, for Q = 0.343m^3/s

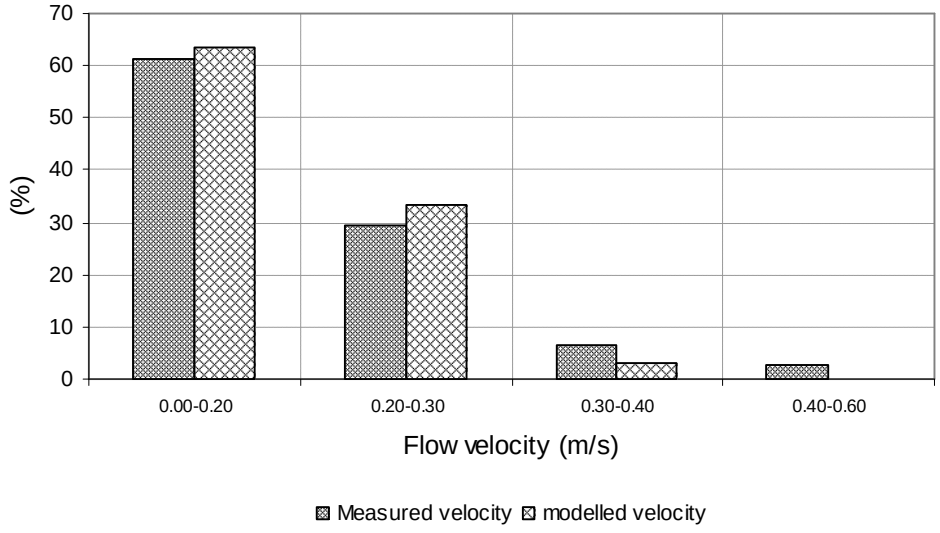

Figure 8-6 Spur Hole Site, modelled and measured frequency-velocity distributions through cross-sections 2, 3 and 4 for, Q = 0.343m^3/s

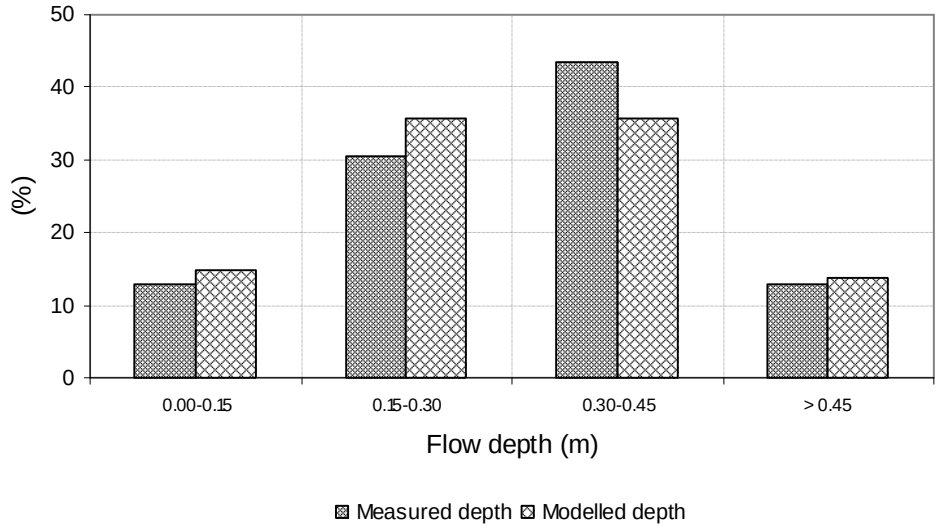

Figure 8-7 Spur Hole Site, modelled and measured frequency-depth distributions through cross-sections 2, 3 and 4, for Q = 1.27m^3/s

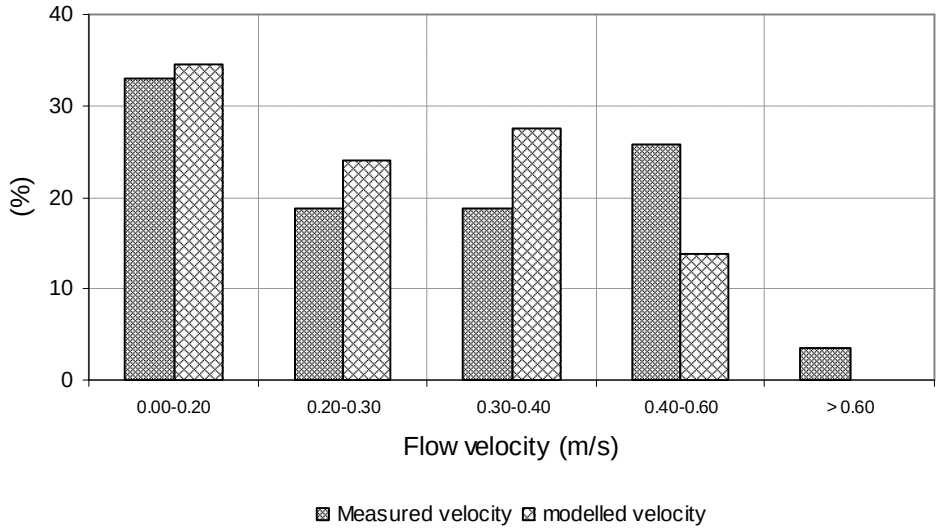

Figure 8-8 Spur Hole Site, modelled and measured frequency-velocity distributions through cross-sections 2, 3 and 4, for Q = 1.27m^3/s

For South African rivers, Kleynhans (1999) has recommended characterization of hydraulic habitats for fish according to the following four velocity-depth classes:

- Slow-Deep (SD): depth > 0.5m, and velocity < 0.3m/s (including deep pools and backwaters),

- Slow-Shallow (SS): depth < 0.5m, and velocity < 0.3m/s (including shallow pools and backwaters),
- Fast-Deep (FD): depth > 0.3m, and velocity > 0.3m/s (including deep runs, rapids and riffles), and
- Fast-Shallow (FS): depth < 0.3m, and velocity > 0.3m/s (including shallow runs, rapids and riffles).

These depth-velocity classes, together with features that provide cover for fish, are usually used in Reserve determination studies. For further evaluation of River2D performance, modelled and measured velocity and depth were therefore classified into these classes. A comparison was performed for Q = 0.343m^3/s and 1.27m^3/s for cross-sections 2, 3 and 4 combined. These results are plotted as depth/velocity class frequency distributions in Figures 8-9 and 8-10 respectively. The combined results for cross sections 2, 3 and 4 will be referred to as "cross sectional scale" results.

From Figures 8-9 and 8-10 it can be concluded that River2D reproduces the measured class distributions reasonably well, with better performance for a discharge of 1.27m^3/s.

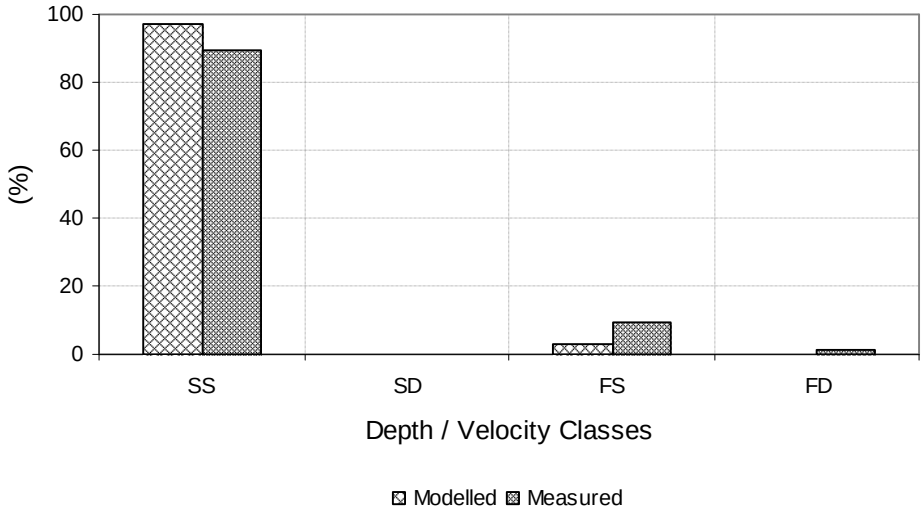

Figure 8-9 Spur Hole Site, modelled and measured frequency-depth/velocity class distributions, for Q = 0.343m^3/s

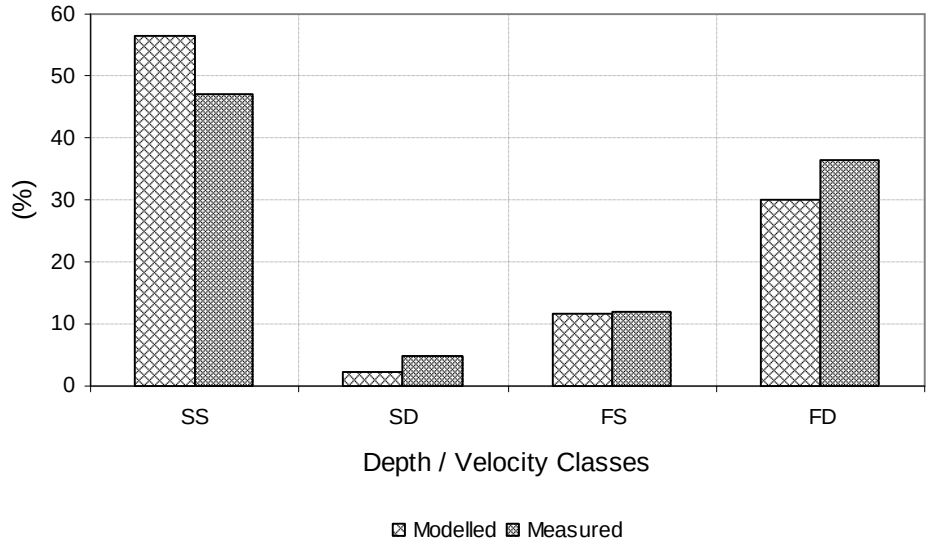

Figure 8-10 Spur Hole Site, modelled and measured frequency-depth/velocity class distributions for Q = 1.27m^3/s

As aquatic scientists interest is usually related to the whole area of a site rather than just at the surveyed cross-sections, modelled velocities and depths were extracted in a longitudinal and transverse grid of 0.5m (the same as used in the field for depth and velocity measurements) to show depth-velocity class distributions over the whole modelled river bed (from cross-section 1 to cross-section 5) of the site. Modelled depth/velocity class frequency distributions for the two discharges, (Q = 0.343m^3/s and 1.27m^3/s) are shown in Figure 8-11. In further discussions these results will be referred to as "areal scale" results.

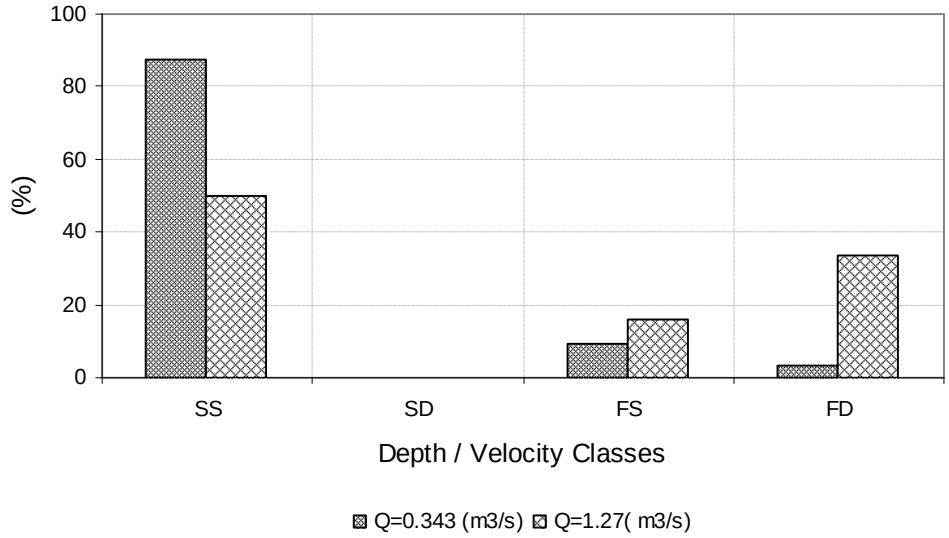

Figure 8-11 Spur Hole Site, modelled frequency-depth/velocity class distributions over the whole river bed for Q = 0.343m^3/s and 1.27m^3/s

From Figure 8-11 it can be seen that the modelled frequency depth/velocity class distributions obtained at the areal scale are different from those related to the cross sectional scale (Figures 8-9 and 8-10). For a discharge of 0.343m^3/s two classes, slow-shallow (SS) and fast-shallow (FS) are represented in the cross sectional scale results (Figure 8-9) while with the areal scale results includes the fast-deep (FD) class as well, with 3.3% frequency. Comparison of the results for a discharge of 1.27m^3/s, Figures 8-10 and 8-11, shows that the frequencies of slow-shallow (SS), fast-shallow (FS) and fast-deep (FD) classes are similar for both the cross-sectional and the areal scales, while the frequency of slow-deep (SD) class being 2.3% in the cross-sectional scale (Figure 8-10) decreased to 0.2% (too small to be seen in Figure 8-11) in the areal scale. The differences between the two analyses are small, and it can therefore be noted that modelled results can be extracted at any resolution and scale depending on the questions we have to answer.

Vanities Crossing Site modelling and results

The same approach was applied to modelled and measured data for the Vanities Crossing Site. All results at a cross sectional scale with discharges of 0.331m^3/s

and 1.308m^3/s are presented in Figures 8-12, 8-13 and 8-16, and Figures 8-14, 8-15 and 8-17 respectively.

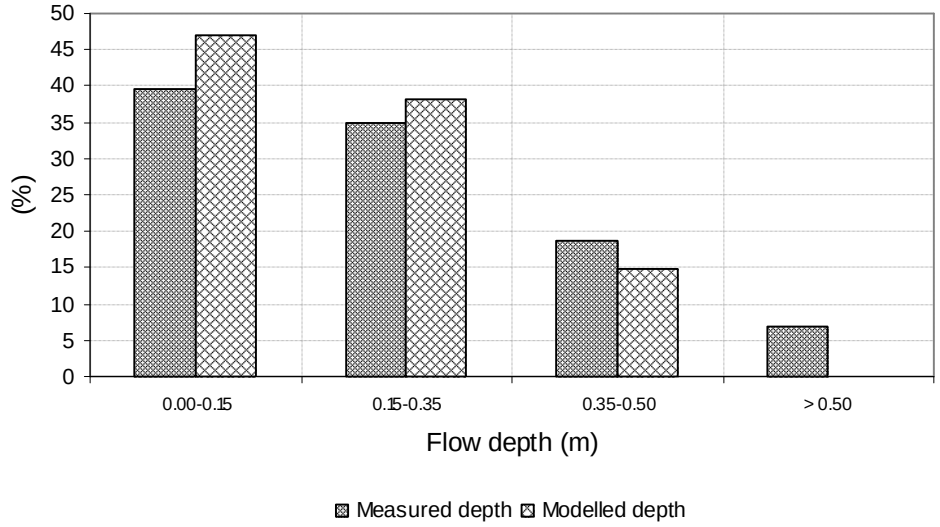

Figure 8-12 Vanities Crossing Site, modelled and measured frequency-depth distributions for Q = 0.331m^3/s

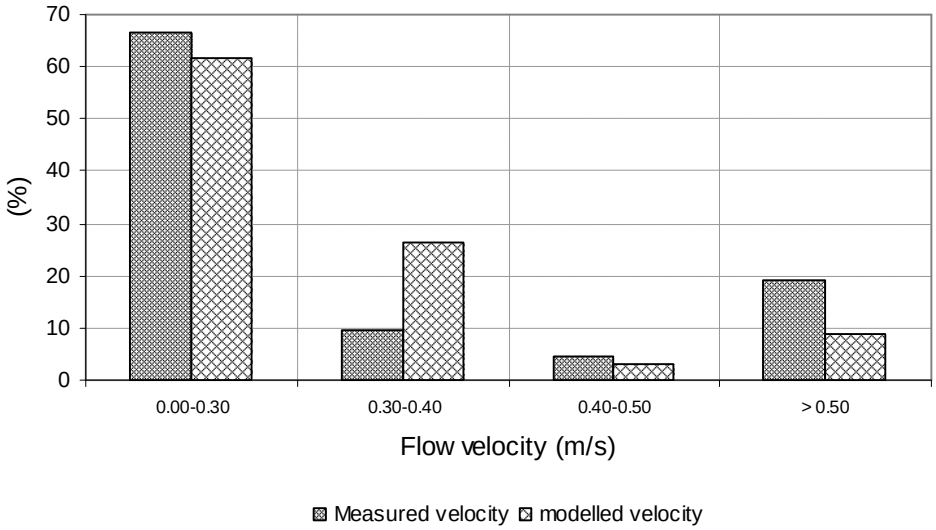

Figure 8-13 Vanities Crossing Site, modelled and measured frequency-velocity distributions for Q = 0.331m^3/s

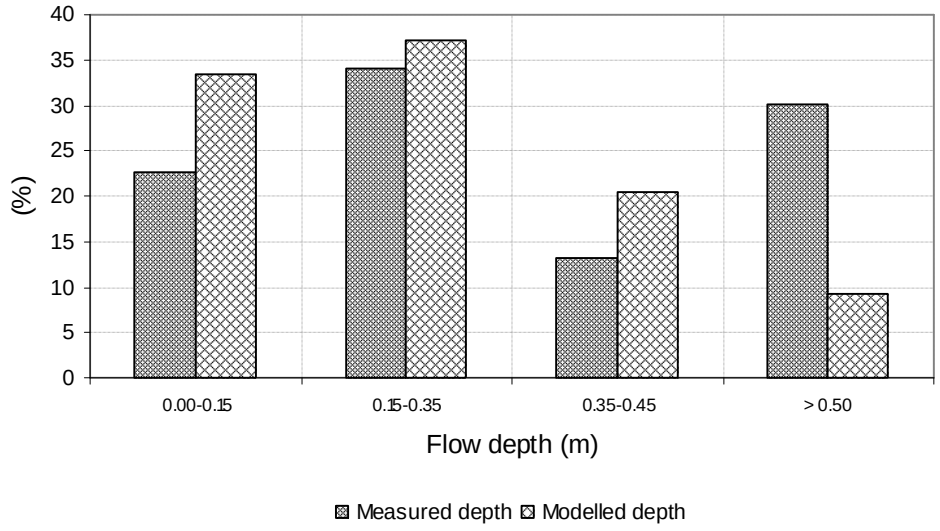

Figure 8-14 Vanities Crossing Site, modelled and measured frequency-depth distributions for Q = 1.308m^3/s

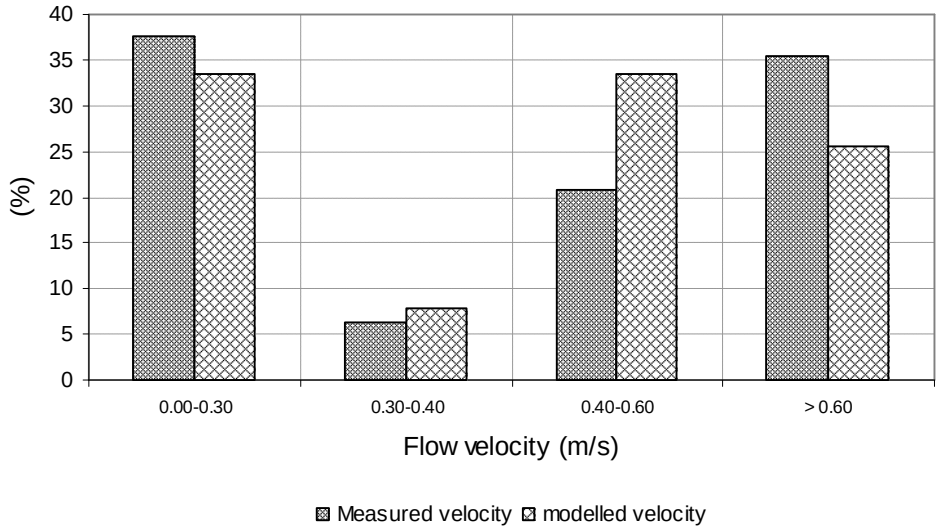

Figure 8-15 Vanities Crossing Site, modelled and measured frequency-velocity distributions for Q = 1.308m^3/s

From the modelled depth and velocity frequency distributions it can be seen that: Modelled results of the depth frequency distribution with discharges of 0.331m^3/s and 1.308m^3/s (Figures 8-12 and 8-14) reproduced the measured data well. For a discharge of 0.331m^3/s the modelled result is better for a depth less than 0.5m,

while the class of flow depth ">0.5" is not reproduced. For a discharge of 1.308m^3/s all depth classes appeared, showing that model performance is better for the higher discharge than for the lower one.

Modelled results of the velocity frequency distribution for the two discharges show good agreement with the measured data (Figures 8-13 and 8-15). All four classes appear in the modelled distributions. The velocity class scale is very coarse, (smaller or bigger than 0.3 m/s) therefore it can be seen (Figures 8-13 and 8-15) that modelled and measured frequency velocity distributions at this scale show reasonable correlation.

Measured and modelled depths and velocities were combined into depth/velocity classes for discharges of 0.331m^3/s and 1.308m^3/s, and are plotted in frequency distribution form in Figures.8-16 and 8-17 respectively.

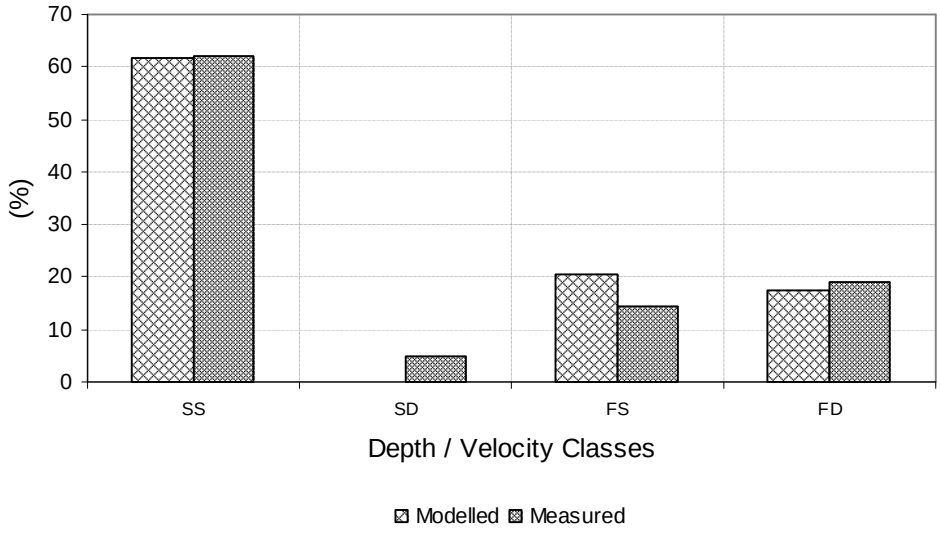

Figure 8-16 Vanities Crossing Site, modelled and measured frequency-depth/velocity class distributions for Q = 0.331m^3/s

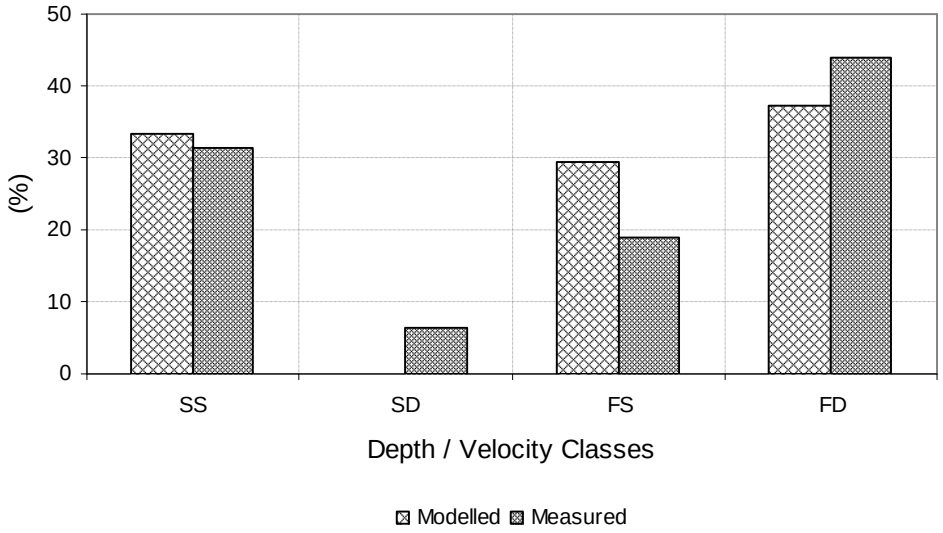

Figure 8-17 Vanities Crossing Site, modelled and measured frequency-depth/velocity class distributions for Q = 1.308m^3/s

The modelled depth/velocity class frequency distributions show good agreement with the measured ones for slow-shallow (SS), fast-shallow (FS) and fast-deep (FD) classes (Figures 8-16 and 8-17). However, the slow-deep class is not represented in the modelling results.

Modelled results of depth/velocity class frequency distributions at the areal scale for discharges of 0.331m^3/s and 1.308m^3/s are shown in Figure 8-18.

Comparing the cross sectional scale modelling results (Figures 8-16 and 8-17) with the areal scale one (Figure 8-18) shows that modelled depth/velocity class frequency distributions are similar for both scales. It also can be noted that a small frequency of 0.5% for the slow-deep (SD) class is represented for a discharge of 0.331m^3/s.

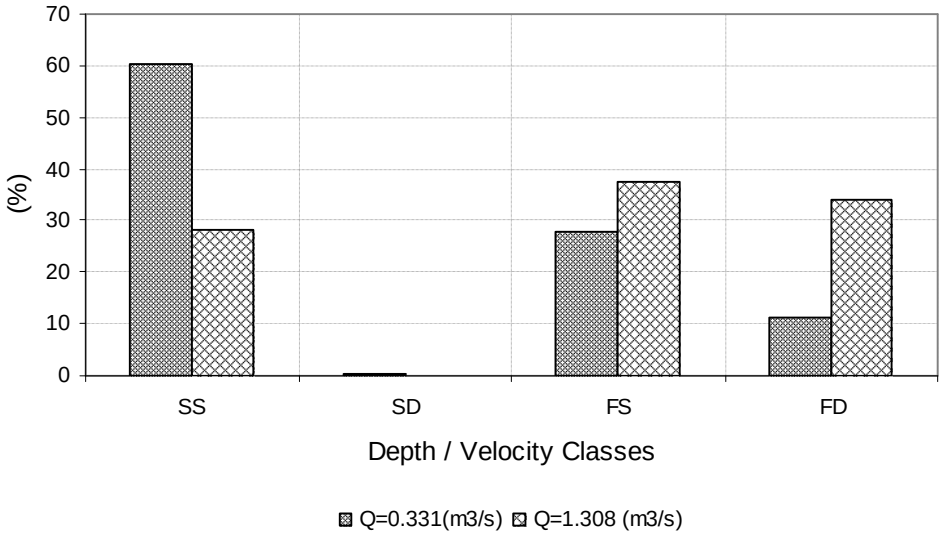

Figure 8-18 Vanities Crossing Site, modelled frequency depth/velocity class distribution in areal scale for Q=0.331 and 1.308m^3/s

One cross-section approach

In the previous sections, the River2D modelling was performed using 5 surveyed cross-sections for each site. In South Africa, time allocated for field work depends on the level at which a Reserve determination is to be done. For rapid and intermediate levels, the time for a river survey is restricted, and insufficient to survey as many cross-sections as are needed for confident hydraulic modelling. Often, one cross-section with a longitudinal slope is used in hydraulic modelling. In this section, an experiment to evaluate the use of only one cross-section in River2D modelling is discussed. This modelling will be referred to as the "one cross-section" approach.

Cross-section 3 of the Spur Hole site was chosen to be tested for the one cross-section approach. Survey data of cross-section 3, together with two additional (the same as cross-section 3) cross-sections, one 25 m down stream and the other 35 m up stream, were linked in a "xyz" co-ordinate system. The values of the bed roughness (k_s) for all surveyed points were kept the same as in the cross-section scale modelling. The modelled bed topography and bed roughness data were saved in a text file. A mesh of 0.3m size was used. The upstream boundary

condition was specified as a discharge. The water surface elevation at cross-section 3 was extended 25m downstream using the water slope for a given discharge, and this water surface elevation was set as the downstream boundary condition.

Modelling was performed with two discharges, Q = 0.343m^3/s and 1.27m^3/s. Modelled flow depths and velocities were extracted for cross-section 3 and compared with the measured values. Modelled and measured cross-sectional flow depths for a discharge of 0.343m^3/s are shown in Figure 8-19. It can be seen that model reproduced the measured depths reasonably well.

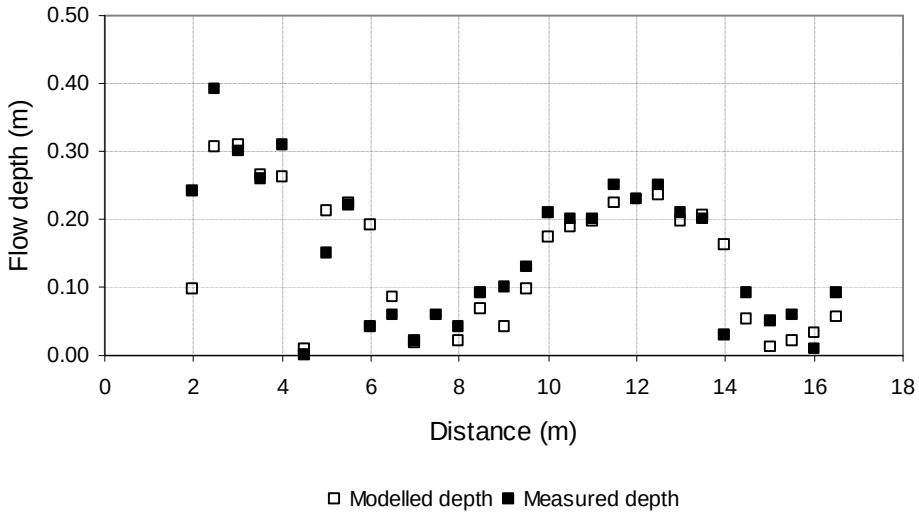

Figure 8-19 Spur Hole Site, modelled and measured cross-sectional flow depth distribution for cross section 3 with Q = 0.343m^3/s

Modelled and measured flow velocities for a discharge of 0.343m^3/s are shown in Figure 8-20. The modelled velocities are very different to the measured velocities. This difference can be explained by limited river bed topography information, resulting from the use of data for one cross-section only. The photograph of the Spur Hole Site (Figure 8-2) shows clearly a lot of substrate features upstream and downstream of the cross-section that would influence flow velocity.

Modelled and measured results of depth/velocity class frequency distributions for a discharge of 0.343m^3/s are shown in Figure 8-21. Only the slow-shallow (SS) depth/velocity class was predicted to occur.

Modelling was also performed for a discharge of 1.27m^3/s, and the results are shown in Figures 8-22, 8-23 and 8-24. The results showed better agreement between modelled and measured flow depths than for flow velocities.

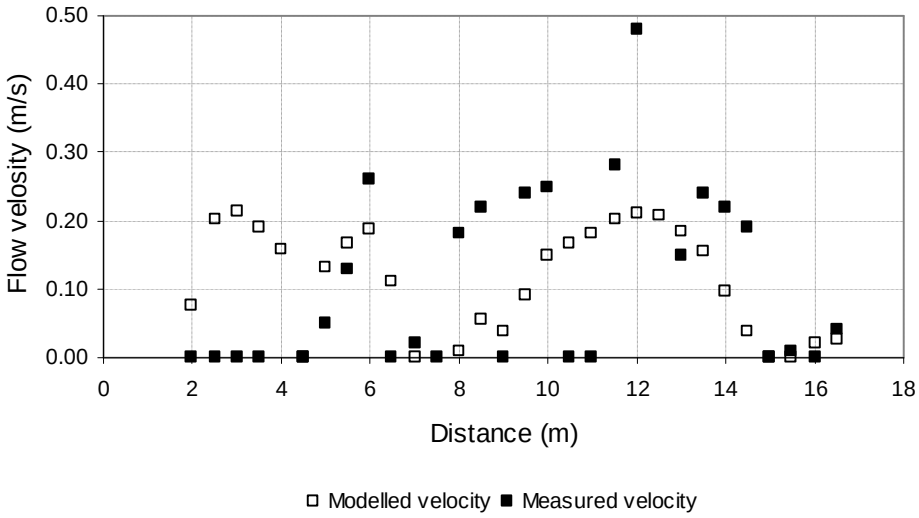

Figure 8-20 Spur Hole Site, modelled and measured cross-sectional velocity distribution for cross-section 3 for Q = 0.343m^3/s

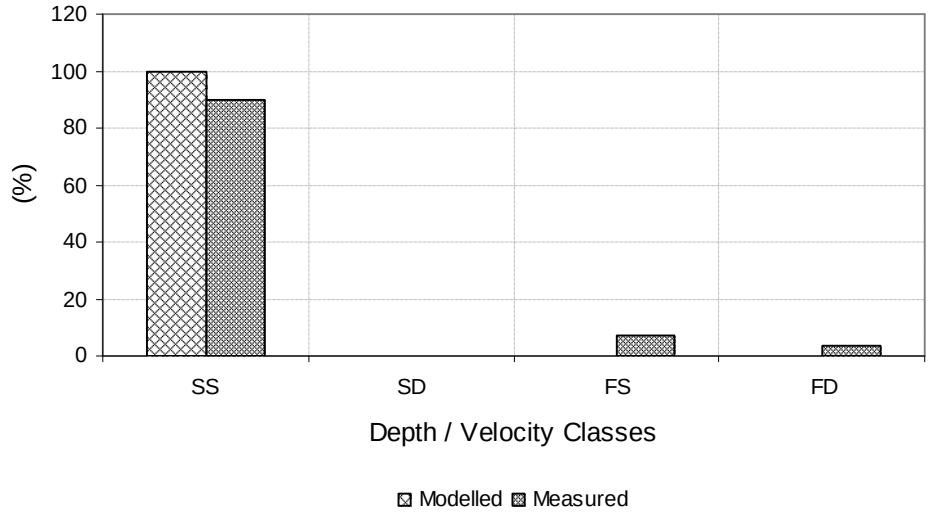

Figure 8-21 Spur Hole Site, modelled and measured depth/velocity classes for cross-section 3 for Q = 0.343m^3/s

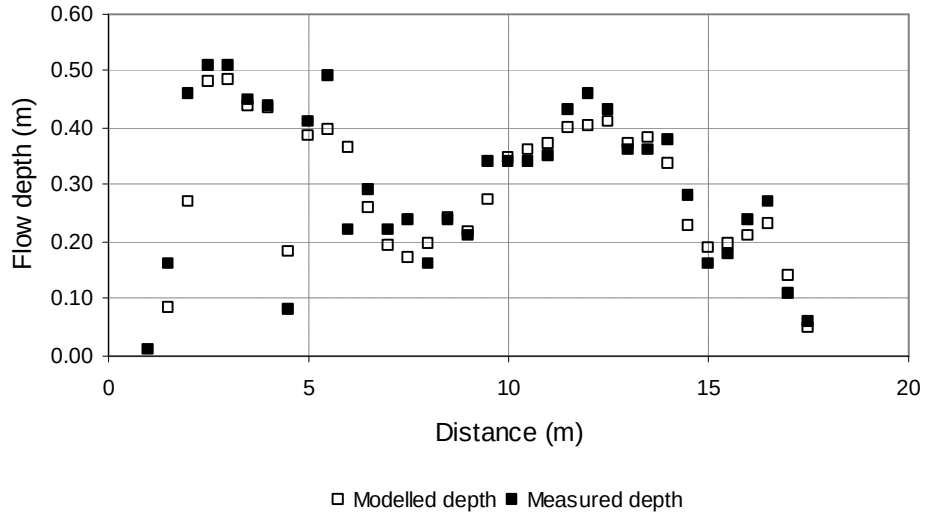

Figure 8-22 Spur Hope Site, modelled and measured cross sectional depth distribution for cross-section 3 for Q = 1.27m^3/s

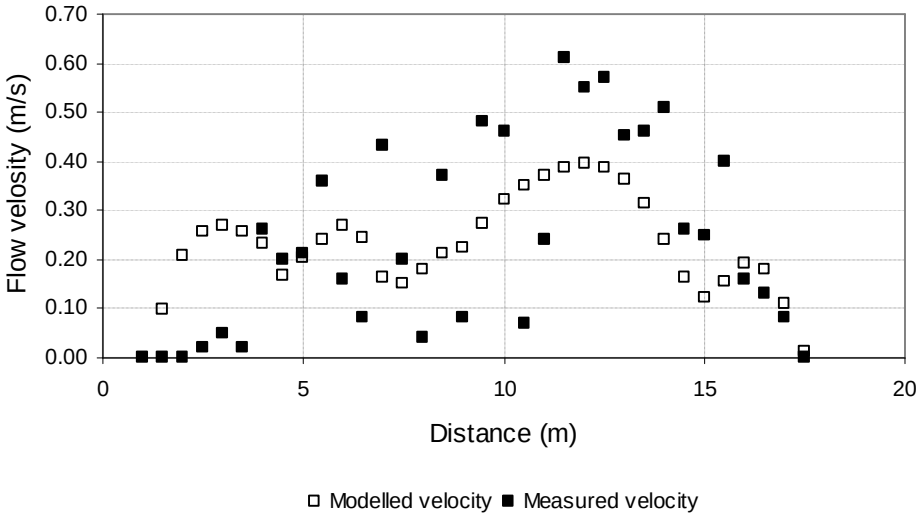

Figure 8-23 Spur Hole Site, modelled and measured cross sectional velocity distribution for cross-section 3 for Q = 1.27m^3/s

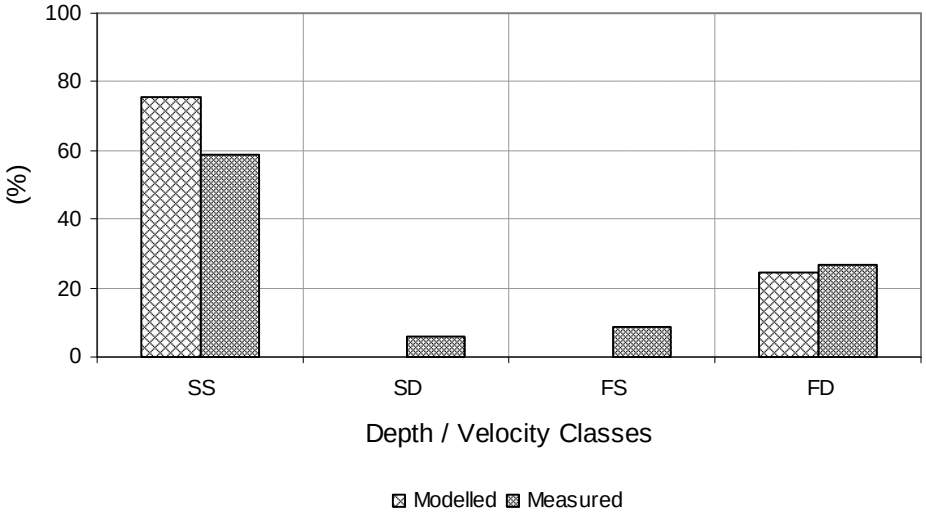

Figure 8-24 Spur Hole Site, modelled and measured depth/velocity class frequency distributions for cross-section 3 for Q = 1.27m^3/s

From the above it can be seen that the one cross-section approach can be used if appropriate field data are collected. It is important to note that the survey of a river site for River2D modelling must be performed by somebody who has hydraulic and River2D knowledge and expertise, somebody who understands low

flow hydraulics phenomena, and who can identify river bed features (such as vegetation patches, big isolated boulders or rocks) that will influence depth and velocity distributions. Such features must be incorporated in the riverbed topography description, and upstream and downstream controls must be correctly identified and included in River2D modelling.

8.3 Driehoeks River Modelling

8.3.1 Introduction

The Driehoeks River is being studied in Water Research Commission Project K5/1403: Multi-scale Habitat Use and Movement of Freshwater Fish Species in a Large River System: Implications for Dam Placement, Operation and Design. The river has also been selected as a case study in WRC project K5/1508: Eco-Hydraulic Modelling in River Systems. A map of the catchment of the Olifants and Doring Rivers, showing the location of the Driehoeks River is presented in Figure 8-25.

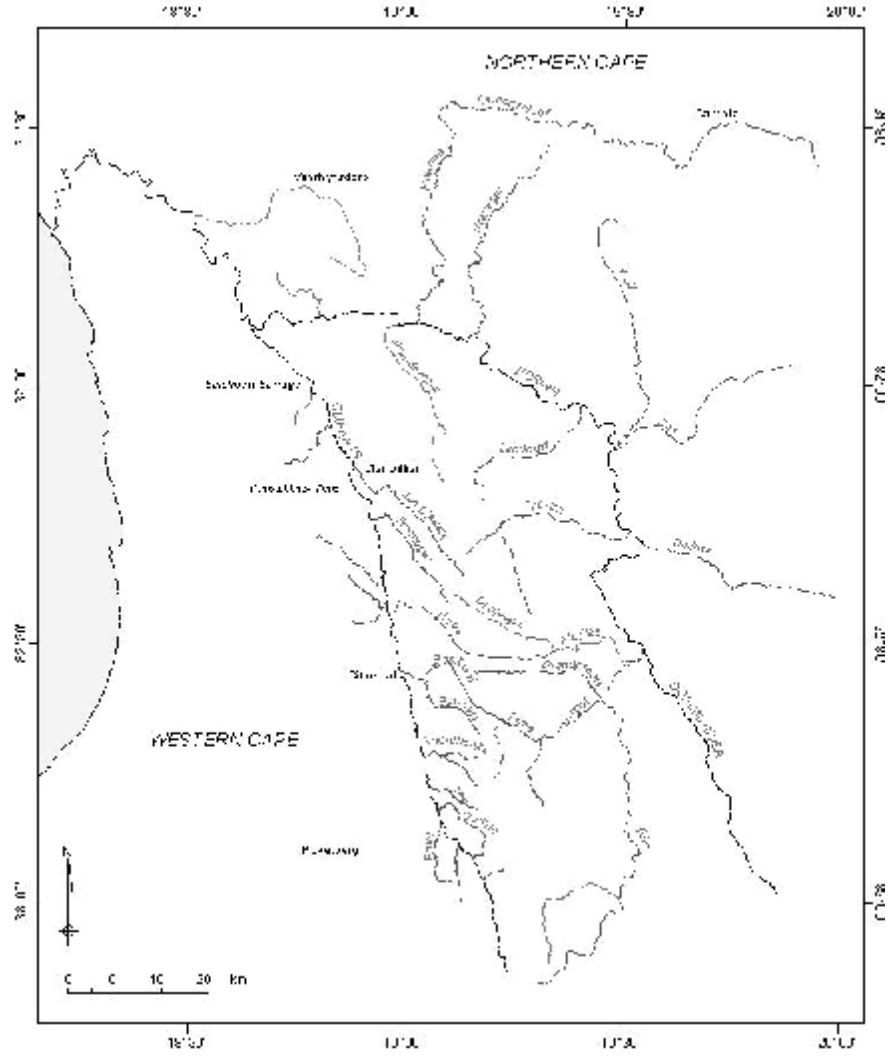

Figure 8-25 The Olifants and Doring Rivers catchment and location of the Driehoeks River

8.3.2 Field data

A site selection and data collection field trip was undertaken together with a member of the research team of Project K5/1405 from 30 June to 11 July 2005. Five sites were selected, named Sites 1, 2, A, B and D, surveys of bed topography and sediment type were carried out, and comprehensive hydraulic data (845 measurements of flow depth and flow velocity) were collected. These data form part of the set compiled for Project K5/1508 and will be included in that project's report. Two further field trips were carried out and comprehensive velocity and

depth data were obtained. In this report, only Site A has been used to verify River2D performance. The complexity of this site can be seen in Figure 8-26.

Figure 8-26 Driehoeks River Site A

8.3.3 River2D modelling

River2D modelling was performed with Q = 0.13m^3/s. The topography of the river bed was modelled from the survey data. A mesh of 0.5m size was set up over the whole bed. The bed roughness was represented by k_s = 0.1 m, while all vegetation patches were modelled with a higher k_s value of 0.6 m. Modelled flow depths and velocities are presented in Figures 8-27 and 8-28 respectively. Measured and modelled velocities in histogram form are presented in Figure 8-29. It can be seen (Figure 8-29) that modelled and measured frequency-velocity distributions are very similar, confirming that River2D can be used for rivers under low flow conditions.

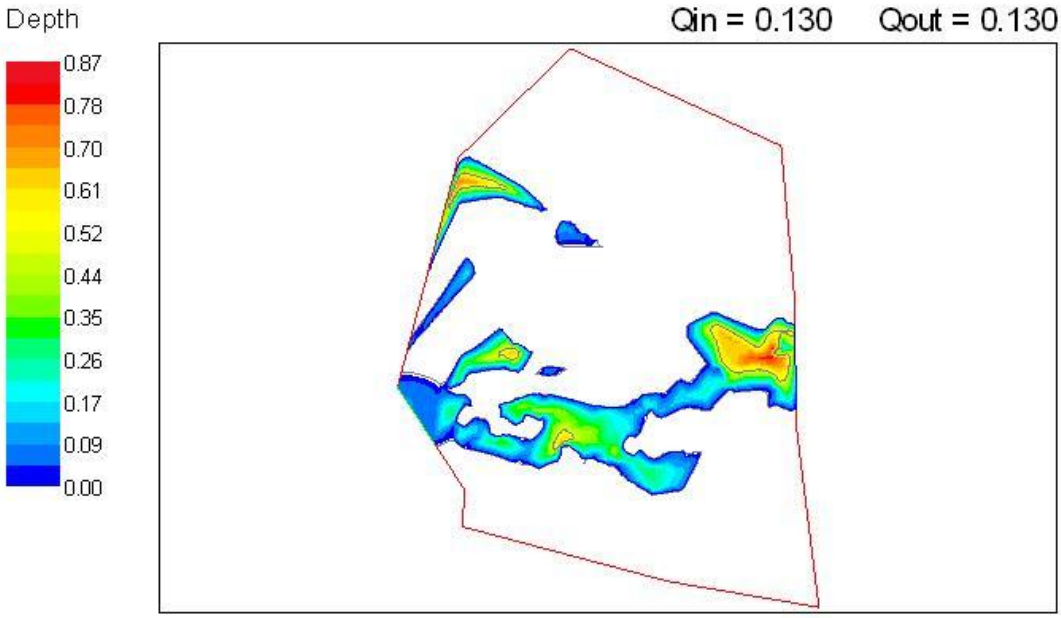

Figure 8-27 River2D predicted flow depths at Driehoeks River Site A with Q = 0.13m^3/s

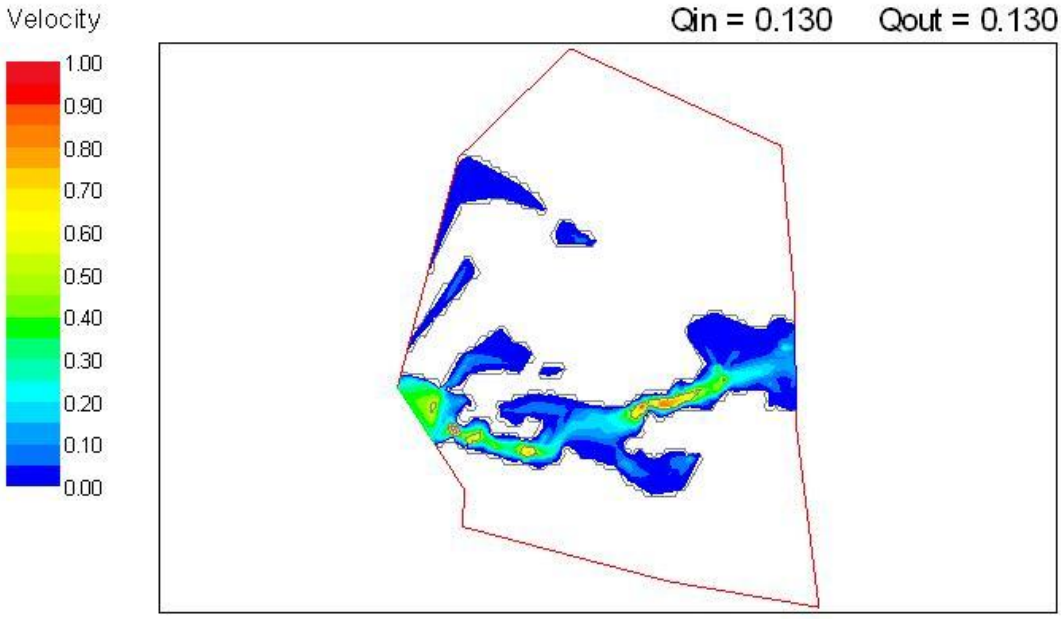

Figure 8-28 River2D predicted flow velocities at Driehoeks River Site A with Q = 0.13m^3/s

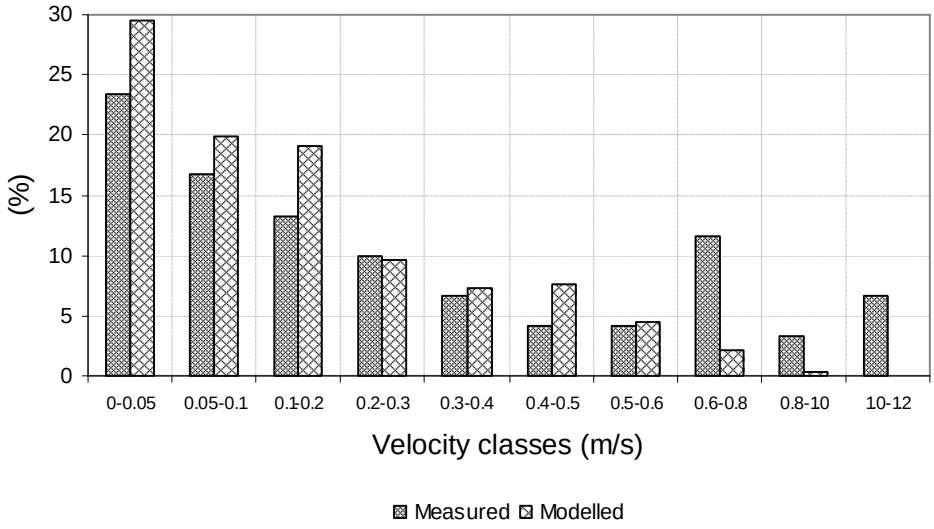

Figure 8-29 Measured and modelled velocity frequency distribution for Driehoeks River Site A for Q = 0.13m^3/s

More detailed modelling of the Driehoeks River sites is part of WRC Project K5/1508 and will be included in that project report (Hirschowitz et al, 2007).

8.4 Conclusions

River2D modelling was performed for two sites, Spur Hole and Vanities Crossing, of the Cotter River in Australia and one site, Site A, of the Driehoeks River in South Africa. The sites are very different in term of dominant river-bed substratum containing a wide range of river-bed features such as big rocks and vegetated patches. Modelled results of all sites showed good agreement with measured data.

River2D output results can be present in different types of plots and can be extracted at different resolutions in Excel format. Modelling success depends on careful, interpretive surveys of river sites, which must be done by a hydraulics expert with knowledge and experience in River2D modelling. Correct identification of the river bed features (such as vegetation patches, big isolated boulders or rocks) that influence depth and velocity distributions, and the relevant

upstream and downstream controls, require intuitive understanding of low flow hydraulics phenomena.

9 CONCLUSIONS AND RECOMMENDATIONS

9.1 Summary

Implementation of the National Water Act in South Africa requires an ecological Reserve to be determined for all significant resources. The ecological Reserve determination involves an estimation of the amount of water required to maintain the system in a particular ecological condition. It was shown in the second chapter of this thesis that considerable efforts have been devoted over the last decade to developing methodologies and methods for Reserve determination in South Africa. Each methodology regarding the Reserve determination requires hydraulic analyses, primarily for low flow conditions. Available equations have been reviewed (Chapter 2), and it has been concluded that they are mostly not well-suited for application in South Africa. The primary purpose of this thesis has been to develop appropriate methods for describing the hydraulic characteristics of South African rivers under conditions of low discharge required for environmental applications. There are four areas in which this thesis has made a contribution for the development of low flow hydraulics: (1) New methods for resistance controlled conditions have been developed. (2) A method for predicting velocity distributions with large-scale roughness has been proposed. (3) Vegetation flow resistance has been investigated and three approaches for prediction of flow resistance related to the occurrence of vegetation in rivers have been proposed. (4) Application of the two-dimensional River2D model for practical use in South African conditions was tested, and it is recommended for environmental studies. These contributions are outlined in the following sections.

9.2 Prediction Methods for Resistance Controlled Conditions

Conventionally, flow resistance in rivers is described using equations (such as those of Chézy, Darcy-Weisbach and Manning) that implicitly assume the dominant resistance phenomenon to be boundary shear stress. Such equations are inherently unsatisfactory for low flow conditions, where the size of roughness elements is comparable to the flow depth and resistance is dominated by form drag. The major contribution of this thesis is the development of new methods for

predicting flow resistance under conditions of large- and intermediate-scale roughness.

The new method for large-scale roughness (when the flow depth is less than the height of the roughness elements) includes a new form of resistance equation (equation (4.10)) and an expression for the corresponding resistance coefficient (equation (4.16)).

Two methods for predicting flow resistance under conditions of intermediate-scale roughness (when the flow depth is between one and four times the height of the roughness elements), combining both roughness element drag and boundary friction effects, have been developed.

The first method is based on the assumption that under intermediate-scale roughness the total discharge can be considered to be the sum of the discharges below and above the tops of the large roughness elements.

The second method combines the influences of roughness element drag and boundary friction. It is based on the following hypothesis:

- If the flow is deep and the relative submergence is greater than four, then boundary friction dominates, and the velocity can be calculated by equation (2.4).
- If the relative submergence is less than or equal to one, flow resistance is dominated by the drag of roughness elements, and the proposed large-scale equation (4.10) should then be used.
- With increasing relative submergence from one to four, the dominant resisting effect changes from element drag to friction, and both drag and friction effects therefore contribute to flow resistance but with varying relative importance.
- Equation (4.30) has been developed for flow resistance under intermediate-scale roughness.

The new methods present an advance on current practice by explicitly accounting for the distinctly different resistance phenomena encountered under small- and large-scale roughness conditions. Their rational basis gives them greater

generality and reduces reliance on case-specific calibration of resistance coefficients using inappropriate equation forms.

9.3 Prediction Methods for Velocity Distributions with Large-Scale Roughness

The spatial distributions of local flow depth and velocity in a river reach are important determinants of habitat suitability. Experimental investigation (Chapter 5) has demonstrated that the distributions are highly dependent on discharge and whether the flow is controlled by general distributed resistance or multiple local occurrences of critical flow, with greater diversity produced by the multiple local control condition. Statistical approaches exist for predicting depth and velocity distributions, but their development and application does not distinguish between the resistance controlled and the multiple local control conditions. The use of statistical descriptions based on field data must therefore be used with caution and cognizance must be taken of their sensitivity to channel bed geometry and flow conditions. The statistical representation of distributions is also sensitive to the scale and resolution of both the collection and presentation of data. During this investigation, the River2D model has been tested for suitability in predicting velocity distributions for resistance controlled conditions and the trans-critical flow associated with multiple local controlled conditions (Chapter 6). It has been shown that River2D can describe multiple local control conditions realistically, and trans-critical flows in particular, and its therefore provides a potentially more reliable approach.

9.4 Prediction Methods for Vegetated Channels

Conventional resistance equations are not applicable for vegetated channels. Alternative practical conveyance prediction methods are proposed for three situations pertaining to the occurrence of vegetation in rivers and wetlands. The methods represent three different levels of complexity, viz. flow through extensive emergent vegetation, flow in channels with emergent vegetation boundaries, and flow in channels with discrete vegetation patches (Chapter 7).

Flow through extensive and effectively uniform emergent vegetation is the simplest situation, and requires the simplest solution – application of a single resistance equation. A practical equation is proposed for emergent, reed-type vegetation. This equation has a different form from the conventional resistance equations, reflecting the dominant role of stem drag rather than boundary shear stress. Equations and a graph for estimating the required drag coefficient have also been developed. A simple procedure using the equations is proposed for practical stage-discharge determination for waterways with emergent vegetation. The practical procedure has already been published (Jordanova et al, 2006).

Flow in channels with emergent vegetated banks represents the next level of complexity. The effect on flow resistance of transverse fragmentation of vegetation into longitudinal strips was demonstrated and elucidated by James et al (2001). This situation cannot be described realistically by a single equation, and a zonal approach where conveyances in the vegetated and unvegetated zones are calculated separately using appropriate equations proposed by James and Makoa (2006), can be used. The effect of the interaction between the zones on the clear channel flow is accounted by well-established composite roughness equations, requiring specification of a resistance coefficient for the interface. Laboratory application shows that clear channel discharges can be reliably estimated using conventional resistance equations, such as Manning's. The variation of Manning's n with width to depth ratio can be attributed to the varying proportional contributions of composite roughness components, and can be reliably accounted for by the Horton (1933) and Pavlovski (1931) formulae. It should be noted that this approach was not developed as part of this thesis.

The third level of complexity occurs when vegetation is fragmented longitudinally as well as transversely. The distribution pattern of vegetation patches, as well as the overall areal coverage, has a significant influence on flow resistance. This situation cannot be described by hand-calculation based methods, and recourse must be made to computational modelling. The two-dimensional model River2D was tested against the extensive laboratory data on flow in channels with

fragmented vegetation patches. It is concluded that flow in a river with vegetation patches can be satisfactorily modelled by River2D.

9.5 Application of River2D Model for Rivers under Low Flow Conditions

The River2D model has been applied to the Cotter River (Australia) and the Driehoeks River (South Africa) (Chapter 8). The rivers are very different in terms of dominant river-bed substratum, containing a wide range of riverbed features such as big rocks and vegetation patches. The applications showed that complex bed geometry can be modelled by R2D_Bed, providing good agreement with measured data. It has also been shown that River2D can predict velocity frequency distributions reliably under large-scale roughness conditions.

In South Africa, time allocated for field work depends on the level at which a Reserve determination is to be done. For rapid and intermediate levels, the time for a river survey is restricted, and insufficient to survey as many cross-sections as are needed for confident hydraulic modelling. Often, one cross–section with a longitudinal slope is used in hydraulic modelling. The River2D model has been applied to evaluate the use of one cross-section of field data only. Modelling results showed that for limited data River2D can be used if required field data are collected.

9.6 Recommendations for further research

This thesis has produced complete and usable methods for predicting low flow conditions in rivers. As with all existing methods that rely wholly or partly on empiricism, their generality and reliability could be enhanced by extending the data base underlying the empirical content. Most of the relationships presented in this thesis are based on laboratory data, and further field confirmation would be valuable.

Flow in rivers with large roughness elements has been inadequately studied in the field, except for steep mountain streams which present rather different hydraulic phenomena to those in the riffle situations that are important in South African

applications. Field-based investigations would be valuable to test and refine the approaches presented for predicting resistance under intermediate- and large-scale conditions. In particular, it would be useful to be able to recommend a percentile bed material size to define the roughness size, and to assess the contribution of the relatively small material between the largest elements to overall resistance. Surprisingly, even relationships for resistance in terms of bed characteristics under small-scale roughness conditions are limited and unreliable; a reassessment of currently used equations and a detailed laboratory and field study of appropriate coefficients would be valuable.

Under low flow conditions the flow is controlled by general distributed resistance or multiple local occurrences of critical flow. Further investigation is required to enable the resistance controlled and the multiple local control conditions to be distinguished.

The method for predicting vegetation resistance depends on knowledge of the stem drag coefficient. It would be useful to carry out extensive measurements to relate the coefficient directly to vegetation morphological characteristics. Further field data for quantifying the resistance coefficient of vegetated bank boundaries directly, or developing a method for its estimation would be valuable.

Most guidelines for estimating resistance coefficients do so in terms of equations (such as those of Chézy, Darcy-Weisbach and Manning) that implicitly assume boundary shear to be the dominant resisting influence. In many situations, particularly with low flows, the resistance is dominated by form drag, and the equation form presented for vegetation and the large-scale roughness condition is more appropriate. Reinterpretation of existing guidelines in terms of this form would reduce the uncertainty of resistance coefficient estimation significantly.

REFERENCES

Aberle, J and Smart, GM (2003) The influence of roughness structure on flow resistance on steep slopes, Journal of Hydraulic Research, Vol. 41, No. 3, pp. 259-269.

Albertson, ML, Barton, J R and Simons, DB (1960) Fluid Mechanics for Engineers. Prentice-Hall. Englewood Cliffs, N. J.

Armitage, PD, Gunn, RJM, Furse, MT, Wright, JF and Moss, D (1987) The use of prediction to assess macroinvertebrate response to river regulation, Hydrobiologia, No. 144, pp 25-32.

ASCE Task Force on Friction Factors in Open Channels (1963) Friction factors in open channels, Journal of the Hydraulics Division, ASCE, Vol. 89, No. HY2, pp 97-143.

Baiamonte, G and Ferro, V (1997) The influence of roughness geometry and Shields parameter on flow resistance in gravel bed channels, Journal of Earth Surface Processes and Landforms, No.22, pp759-772.

Bain, MB and Stevenson, NJ (1999) Aquatic habitat assessment: common methods, American Fisheries Society, Bethesda, Maryland.

Barbour, MT, Gerritsen, J, Griffith, GE, Frydenborg, R, McCarron, E, Whith, JS and Bastian, ML (1996) A framework for biological criteria for Florida streams using benthic macroinvertebrates, Journal of the North American Benthological Society, Vol. 15, No. 2, pp 185-211.

Bathurst, JC (1978) Flow resistance of large-scale roughness, Journal of Hydraulic Division, ASCE, Vol.104, No. HY12, pp 1587-1603.

References

Bathurst, JC (1982) Theoretical aspects of flow resistance, in Gravel-bed tivers, Hey RD.

Bathurst, JC (1985) Flow resistance estimation in mountain rivers, Journal of Hydraulic Engineering, Vol. 111, No. 4, pp. 625-643.

Bathurst, JC (2002) At-a-site variation and minimum flow resistance for mountain rivers, Journal of Hydrology, No. 269, pp 11-26.

Bathurst, JC, Li, R and Simons, DB (1981) Resistance equation for large-scale roughness, Journal of the Hydraulic Division, ASCE, Vol. 107, No. HY12, pp. 1593-1613.

Bathurst, JC, Li, RM and Simons DB (1981) Resistance equation for large-scale roughness, Journal of Hydraulic Engineering, ASCE, 107 (12), pp 1593-1613.

Bayazit, M (1976) Free surface flow in a channel of large relative roughness, Journal of Hydraulic Research, No. 14, pp 115-126.

Birkhead AL (2002) The procedure for generating hydraulic information for the Intermediate and Comprehensive Ecological Reserves (Quantity). Appendix in Resource Directed. Measures for Protection of Water Resources: River Ecosystems - Revision of the quantity component (Louw MD and Hughes DA, eds). Prepared for the Department of Water Affairs and Forestry, South Africa.

Bisson, PA, Nielsen, JL, Palmason, RA and Grove, LE (1982) A system of naming habitat types in small streams with example of habitat utilization by salmonids during low Streamflow, in Acquisition and Utilization of Aquatic Habitat Inventory Information (Ed. N.B. Armantrout), pp 62-73, American Fishery Society, Western Division, Bethesda, MD, USA.

References

Bouckaert, FW and Davis, J (1998) Microflow regimes and the distributio of macroinvertebrates around stream boulders, Freshwater Biology, No. 40, pp 77-86.

Bovee, KD (1982) A guide to stream habitat analysis using the Instream Flow Incremental Methodology, US Fish Wildlife Service, Instream Flow Info. Pap. 12, FWS/OBS-82/26, Washington, DC.

Bray, DI (1979), Estimating average velocity in gravel-bed rivers, Journal of Hydraulic Division, Vol 105, No HY9, September, pp 1103-1122.

Bray, DI and Davar, KS (1987) Resistance to flow in gravel-bed rivers, Canadian Society of Civil Engineering, Vol. 14, pp 77-86.

Brown, CA, Pemberton, CW, Greyling, A and King, JM (2005) DRIFT user Manual: Biophysical module for predicting overall river condition on small to medium sized river with relatively-predictable flow regimes, WRC Report 1404/1/05.

Brownlie, WR (1981) Re-examination of Nikuradse roughness data. J. Hydr. Div., ASCE, Vol. 107, No. HY1, pp115-119.

Carter, AJ (1995) A Markovian approach to investigating landscape change in the Kruger National Park rivers. PhD thesis, University of the Witwatersrand, Johannesburg.

Chadwick, A., Morfett, J. and Borthwick, M (2004) Hydraulics in civil and environmental engineering, London and New York, Spon Press.

Chow, VT (1959) Open-Channel Hydraulics. McGraw-Hill, New York.

References

Christensen, BA (1976) Hydraulics of sheet flows in wetlands. Proceedings of the 3rd Annual Symposium of the Waterways, Harbors and Coastal Division of ASCE, Colorado State University, Fort Collins, Colorado, pp 746-759.

Colebatch, GT (1941) Model tests on the Liwanee Canal roughness coefficients. J. Inst. Civ. Engrs (Australia), Vol. 13, pp 27-32.

Collings, M (1972) A methodology for determining instream flow requirements for fish, Proceeding of Instream Flow Methodology Workshop, Washington Department of Ecology, Olympia (as cited by Wesche and Rechard, 1980).

Connell, R, Beffa, C and Painter, D (1998) Comparison of observations by flood plain residents with results from a two-dimensional flood plain model: Waihao River, New Zealand, Journal of Hydrology (NZ), No. 37, pp 55-79.

Cortes, RMV, Ferreira, MT, Oliveira, SV and Oliveira, D (2002) Macroinvertebrate community structure in a regulated river segment with different flow conditions, River Research and Applications, No. 18, pp 367-382.

Davies, BR, O'Keeffe, JH and Snaddon, CD (1993) A synthesis of the ecological functioning, conservation and management of South African ecosystems, Water Research Commission Report No. TT 62/93.

Davis, JA and Barmuta, LA (1989) An ecologically useful classification of mean and near-bed flows in stream and rivers, Freshwater Biology, No. 21, pp 271-282.

Dawson, F H and Charlton, F G (1988) Bibliography on the hydraulic resistance or roughness of vegetated watercourses, Freshwater Biological Association, Occasional Publication No. 25.

DEAT (1989) Environmental Conservation Act (No.73 of 1989), Department of Environment Affairs and Tourism, South Africa.

References

DEAT (1994) The Integrated Environmental Management Process, Department of Environment Affairs and Tourism, South Africa.

Department of Agriculture (1983) Conservation of Agricultural Resources Act (No, 43 of 1983), Department of Agriculture, South Africa.

Dickens, CWS and Graham, PM (2002) The South African Scoring System (SASS) version 5 Rapid Bioassessment Method for Rivers, African Journal of Science, No. 27, pp 1-10.

Dingman, SL (1989) Probability distribution of velocity in natural channel cross sections. Water Resources Research, Vol. 25, No. 3, pp 509-518.

Diplas, P and Sutherland, A (1988) Sampling techniques for gravel sized sediments, Journal of Hydraulic Engineering, Vol. 114, No. 5, pp. 484-501.

Dittrich, A and Koll, K (1997) Velocity field and resistance of flow over rough surfaces with large and small relative submergence, Journal of Sediment Research, Vol.12, No.3, pp 21-33.

DWAF (1996a) South African Water Quality Guidelines, Volume 1, Domestic Use, Department of Water Affairs and Forestry, Pretoria, South Africa.

DWAF (1996b) South African Water Quality Guidelines, Volume 7, Aquatic Ecosystem, Department of Water Affairs and Forestry, Pretoria, South Africa.

DWAF (1996c) Water quality management in a changing regulatory environment in South Africa: Water Law Principles Nov 1996, Department of Water Affairs and Forestry, Pretoria, South Africa.

DWAF (1997) White Paper on a National Water Policy for South Africa, Department of Water Affairs and Forestry, Pretoria, South Africa.

References

DWAF (1999) Resource directed measured for protection of water resources. Volume 2: Integrated Manual. Version 1.0. Department of Water Affairs and Forestry, Pretoria.

DWAF (1998) National Water Act (No.36 of 1998), Department of Water Affairs and Forestry, South Africa.

Dyer, F and Thoms, MC (2006) Managing river flows for hydraulic diversity. River Research and Applications, No. 22, pp 257-267.

Elliott, CRN, Johnson, IW, Sekulin, AE, Dunbar, MJ and Acreman, MC (1996) Guide to the use of the Physical Habitat Simulation System, NRA Release Version. Report undertaken by the Institute of Hydrology for the National Rivers Authority.

Englund, G and Malmqvist, B (1996) Effect of flow regulation, habitat area and isolation on the macroinvertebrate fauna of rapids in north Swedish rivers, Regulated Rivers: Research and Management, No. 12, pp 433-445.

Ferro, V (1999) Friction factor for gravel bed channel with high boulder concentration, Proceedings of ASCE, Journal of Hydraulic Engineering, Vol. 125, No. 7, pp 771-778.

Ferro, V (2003) Flow resistance in gravel-bed channels with large-scale roughness, Journal of Earth Surface Processes and Landforms, No. 28, pp 1325-1339.

Ferro, V and Giordano, G (1991) Experimental study of flow resistance in gravel bed rivers, Proceedings of ASCE, Journal of Hydraulic Engineering, Vol.117, No. 10, pp 1239-1246.

Finlayson, BL, Gippel, CJ and Brizga, SO (1994) Effects of reservoirs on

downstream aquatic habitat, Water, August, pp 15-20.

Flammer, GH, Tullis, JP and Mason, ES (1970) Free surface velocity gradient flow past hemisphere, Journal of Hydraulic Engineering, ASCE, Vol. 96, No. 7, pp 1485-1502.

Flintham, TP and Carling, PA (1991) Manning's n of composite roughness in channels of simple cross section. Channel Flow Resistance: Centennial of Manning's Formula, (Yen, B C (ed.)). Water Resources Publications, Littleton, Colo., pp 328-340.

Flipp, JB and Diplas, P (1993) Surface sampling in gravel streams, Journal of Hydraulic Engineering, Vol. 119, No. 4, pp. 473-490.

French, RH (1985) Open-Channel Hydraulics. McGraw-Hill, New York.

Gordon, NC, McMahon, TA and Finlayson, BL (1992) Stream hydrology – An Introduction for Ecologist, John Wiley and Sons, England.

Gore, JA, Layzer, JB and Russell, IA (1992) Non-traditional applications of instream flow techniques for conserving habitat of biota in the Sabie River of South Africa. IN; Boon, PJ, Calow, P and Petts, GE. River Conservation and Management. John Wiley and Sons Ltd.

Gore, JA, Nestler, JM and Layzer, JB (1989) Instream flow predictions and management for biota affected by peaking-power hydroelectric operations, Regulated Rivers: Research and Management, No. 3 pp 35-48.

Government Gazette (1998) National Environmental Management Act 107, Cate Town, South Africa, www.info.gov.za/gazette/acts.

References

Graf, WH and Yulistiyanto,B (1998) Experiments on flow around a cylinder; the velocity and vorticity fields, Journal of Hydraulic Research, Vol.36, No.4, pp 637-653.

Griffiths, GA (1981) Flow resistance in coarse gravel bed rivers, Journal of Hydraulic Division, Vol. 107, No. HY 7, pp 899-918.

Hall, BR and Freeman, GE (1994) Study of hydraulic roughness in wetland vegetation takes new look at Manning's n. The Wetlands Research Program Bulletin, 4, No. 1, pp 1-4.

Henderson, F M (1966) Open Channel Flow, Macmillan.

Hervouet, J_M and van Haren, L (1996) Recent advances in numerical methods for fluid flows, In Floodplain Processes, Anderson MG, Hoey TB, Bates PD (eds), Wiley: Chichester, pp 183-214.

Hey, RD (1979) Flow resistance in gravel-bed rivers, Journal of the Hydraulic Division, ASCE, Vol. 105, No. HY4, pp. 365-379.

Hey, RD and Thorne, CR (1983) Accuracy of surface samples for gravel bed material, Journal of Hydraulic Engineering, Vol. 109, No. 6, pp. 842-851.

Hicks, DM and Mason, PD (1998) Rougness Characteristics of New Zealand Rivers, National Institute of Water and Atmospheric Research Ltd, Christchurch, New Zealand.

Hirschowitz, PM, Birkhead, AL and James, CS (2007) Hydraulic modelling for ecological studies for South African rivers, WRC Report No. 1508.

Horton, RE (1933) Separate roughness coefficients for channel bottom and sides, Engineering News Record, III, No. 22, pp 652-653.

References

Hughes, DA and Hannart, P (2003) A desktop model used to provide an initial estimate of the ecological instream flow requirements of rivers in South Africa, Journal of Hydrology, Vol. 270, No. 3-4, pp 167-181.

Hughes, DA and Münster, (2000) Hydrological information and techniques to support the determination of the water quantity component of the ecological reserve for rivers. WRC Report No. 867/3/2000, Pretoria.

Hughes, DA and Munster, F (2000) Hydrological information and techniques to support the determination of the water quantity component of the ecological reserve for rivers, Water Research Commission Report No. TT 137/00.

Ingram, RG and Chu, VH (1987) Flow around islands in Rupert Bay: an investigation of the bottom friction effect, Journal of Geophys. Research, Vol.92 (C13), pp 14521-14533.

Inoue, M and Nunokawa, M (2002) Effects of longitudinal variations in stream habitat structure on fish abundance: an analysis based on subunit-scale habitat classification, Freshwater Biology, No. 47, pp 1594-11607.

James, CS and Makoa, MJ (2006) Conveyance estimation for channels with emergent vegetation boundaries, Proceedings of the Institution of Civil Engineers, Water Management, in press.

James, CS, Birkhead, AL, Jordanova, AA and O'Sullivan, JJ (2004) Flow resistance of emergent vegetation, Journal of Hydraulic Research, Vol. 42, No. 4, pp 390-398.

James, CS, Birkhead, AL, Jordanova, AA, Kotschy, KA, Nicolson, CR and Makoa, M J (2001) Interaction of reeds, hydraulics and river morphology, Water Research Commission Report No. 856/1/01, 371 pp.

References

Jarrett, RD, (1984) Hydrauliks of high gradient streams. ASCE, Journal of Hudraulic Engineering, Vol. 110, No. 11, pp 1519-1539.

Jonker, V, Rooseboom, A, and Görgens, AHM (2001) Environmentally significant morphological and hydraulic characteristics of cobble and boulder bed rivers in the Western Cape, WRC Report No. 979/1/01, Water Research Commission, South Africa.

Jordanova, A A, James, C S and Birkhead, A L (2006) Practical resistance estimation for flow through emergent vegetation, Journal of Water Management of ICE Proceeding, Vol.159, issue WM3, pp 173-181.

Jordanova, AA and James CS (2004) Hydraulic characterization of riverin habitat for Reserve determination, South African Society of Aquatic Scientists, Midrand, South Africa, 5 – 7 July 2004.

Jordanova, AA, Birkhead, AL, James, CS and Kleynhans, CJ (2004) Hydraulics for determination of the ecological Reserve for rivers, WRC Report No. 1174/1/04, South Africa.

Kellerhals, AM (1967) Stable channels with gravel-paved beds, Journal of Waterways Harbors Division, ASCE, 93 (WW1), pp63-84.

Kemp, J, Harper, DM and Crosa, GA (1999) Use of functional habitats to link ecology with morphology and hydrology in river rehabilitation, Aquatic Conservation: Marine and Freshwater Ecosystems, No.9, pp 159-178.

King J M and Louw, D (1998) Instream flow assessments for regulated rivers in South Africa using the Building Block Methodology. Aquatic Ecosystem Health and Management, No.1, pp 109-124.

References

King J M and Louw, D (1998) Instream flow assessments for regulated rivers in South Africa using the Building Block Methodology. Aquatic Ecosystem Health and Management, No.1, pp 109-124.

King JM (1996) Quantifying amount of water required for maintenance of aquatic ecosystems. Water law review. Discussion document for policy development. Report for the Department of Water Affairs and Forestry. August 1996. Freshwater Research Unit, University of Cape Town.

King, JM and Tharme, RE (1994) Assessment of the Instream Flow Incremental Methodology and initial development of alternative instream flow methodologies for South Africa, WRC Report No.295/1, Pretoria.

King JM, Tharme RE and de Villiers MS, eds (2000) Manual for the Building Block Methodology, 339 pp. WRC Report no. TT131/00, Water Research Commission, Pretoria, South Africa.

Kleynhans, CJ (1996) A qualitative procedure for the assessment of the habitat integrity status of the Luvuvhu river (Limpopo system, South Africa), Journal of Aquatic Ecosystem Health, No. 5, pp 41-54

Kleynhans, CJ (1999) The development of a fish index to assess the biological integrity of South African rivers, Water SA, No. 25, pp 265-278

Koll, K (2002) Feststofftransport und Geschwindigkeitsverteilung in Raugerinnen, Diss. Univ. Karlsruhe.

Kosorin, K (1983) Turbulent shear stress and velocity distribution in vegetated zone of open channel, Proceeding, 20th IAHR Congress, Moscow, pp 572-579.

References

Kotschy, K (2003) Clonal growth and colonization of sediment by reeds (Phragmites mauritianus) in the Letaba River, Kruger National Park. MSc dissertation, University of the Witwatersrand, Johannesburg.

Kouwen, N and Unny, TE (1973) Flexible roughness in open channels, Journal of the Hydraulics Division, ASCE, Vol. 99, No. HY5, pp 713-728.

Lamouroux, N (1998) Depth Probability Distributions in Stream Reaches, Journal of Hydraulic Engineering, February, pp 224-227.

Lamouroux, N, Souchon, Y and Herouin, E (1995) Predicting velocity frequency distributions in stream reaches, Water Resources Research, Vol. 31, No. 9, pp 2367-2375.

Lawrence, DSL (1997) Macroscale surface roughness and frictional resistance in overland flow, Journal of Earth Surface Processes and Landforms, Vol.22, pp 365-382.

Lawrence, DSL (2000) Hydraulic resistance in overland flow during partial and marginal surface inundation: Experimental observations and modelling, Water Resources Research, Vol.36, No.8, pp 2381-2393.

Leopold,LB, Bagnold, RA, Wolman, MG and Brush, LM (1960) Flow resistance in Sinuous of irregular channels, Physiographic and Hydraulic Studies of Rivers, U.S. Geological Survey Professional Paper 282-D.

Li, R-M. and Shen, H W (1973) Effect of tall vegetations on flow and sediment, Journal of the Hydraulics Division, ASCE, Vol. 99, No. HY5, pp 793-814.

Lindner, K (1982) Der Strömungswiderstand von Pflanzenbeständen. Leichtweiss-Institut für Wasserbau der TU Braunschweig, Heft 75.

Livingston, AC and Rabeni, CF (1991) Food-habitat relations that determine the

success of young-of-year smallmouth bass in Ozark streams, Proceedings of the First International Symposium on Smallmouth Bass (Ed. DC Jackson), Mississippi Agricultural and Forest Experimental Station, Mississippi State University.

Lloyd, PM and Stansby, PK (1997) Shallow-water flow around model conical islands of small side slope. I: Surface piercing, Journal of Hydraulic Engineering, Vol.123, No.12, pp 1057-1067.

Lotter, GK (193) Considerations on hydraulic design of channels with different roughness of walls, Transactions All-Union Scientific Research Institute of Hydraulic Engineering, Leningrad, Vol. 9, pp 238-241 (in Russian).

Meijer, DG and Van Velzen, EH (1999) Prototype-scale flume experiments on hydraulic roughness of submerged vegetation, Proceeding of the 28th International IAHR Conference, Graz.

Milhous RT, Updike MA, Schneider DM (1989) Physical Habitat Simulation System Reference Manual. US Fish and Wildlife Service Biological Report 89(16).

Mirajgaoker, AG and Charlu, KLN (1963) Natural roughness effects in rigid open channels, Journal of Hydraulic Division, Transactions of the ASCE, Vol. 89, No. HY5, paper No. 3630.

Morgan, RP, Jacobsen, RE, Weisberg, SB, McDowell, LA, and Wilson, HT (1991) Effect of flow alteration on benthic macroinvertebrate communities below Brighton Hydroelectric dam, Freshwater Ecology, No. 6, pp 419-429.

Morris, HM (1954) Flow in rough conduits, ASCE, Transactions, Paper No. 2745.

References

Mosley, MP (1983) Flow requirements for recreation and wildlife in New Zealand rivers-A review, Journal of Hydrology (NZ), No. 22, pp 152-174 (as cited by Gordon, 1992).

Murray, K (1999) National Aquatic Ecosystem Biomonitoring Programme: National Implementation Assessment, NAEBP Report Series No. 8, Institute for Water Quality Studies, Department of Water Affairs and Forestry, Pretoria, South Africa.

Naot, D, Nezu, I and Nakagawa, H (1996) Hydrodynamic behavior of partly vegetated open channels, Journal of Hydraulic Engineering, Vol.122, No.11, pp 625-633.

Nestler, JM, Milhous, RT and Layzer, JB (1989) Instream habitat modelling techniques, in Alternatives in Regulated River Management (Eds JA Gore and GE Petts), pp 295-315,CRC Press, Boca Raton, Florida (as cited by Gordon, 1992).

Newson, MD and Newson, CL (2000) Geomorphology, ecology and river channel habitat: mesoscale approaches to basin-scale challenges, Progress in Physical Geography, N0.24, pp 195-217.

Nicholas, AP (2003) Investigation of spatially distributed braided river flows using a two-dimensional hydraulic model, Earth Surface Processes and Landforms, No. 28, pp 655-674.

Nikora, VI, Goring, DG and Biggs, BJF (1998) On gravel-bed roughness characterization, Water Resources Research, Vol. 34, No. 3, pp. 517-527.

Nikora, V, Goring, D, McEwan, I and Griffiths, G (2001) Spatially Averaged Open-Channel Flow over Rough Bed, Journal of Hydraulic Engineering, Vol.127, No.2, pp 123-133.

References

Nuding, A (1991) Flieβwiderstadsverhalten in Gerinnen mit Ufergebüsch: Entwicklung eines Flieβgesetzes für Flieβgewässer mit und ohne Gehölzufer, unter besonderer Berücksichtigung von Ufergebüsch, PhD Thesis submitted to: Wasserbau-Mitteilung der Technische Hochschule Darmstadt, Darmstadt, Germany.

Nuding, A (1994) Hydraulic resistance of river banks covered with trees and brushwood. 2nd International Conference on River Flood Hydraulics, 22-25 March, York, England, pp 427-437, John Wiley and Sons.

O'Keeffe, J and Dickens, C (2000) Aquatic Invertebrates, In: Environmental flow assessment for rivers: Manual for the Building Block Methodology, King, JM, Tharme, RE and de Villiers, MS, (Eds), Water Research Commission report No.TT 131/00, Pretosia, South Africa.

O'Keeffe JH and Hughes, DA (2004) Flow-Stressor Response approach to environmental flow requirement assessment. In: Hughes, DA (Ed) SPATSIM, an integrating framework for ecological Reserve determination and implementation, Water Research Commission Report No. 1160/1/04.

O'Loughlin, E and MacDonald, E (1964) La Houille Blanche, No.7, pp 773-782.

Oswood, ME and Barber, WE (1982) Assessment of fish habitat in streams: Goals, constraints, and a new technique, Fishers, No. 7, pp 8-11.

Palmer, MA, Swan, CM, Nelson, K, Silver, P and Alvestad, R (2000) Streambed landscapes: evidence that stream invertebrates respond to the type and spatial arrangement of patches, Landscape Ecology, No.15, pp 563.576.

Pavlovski, N N (1931) On a design formula for uniform flow movement in channels with non-homogeneous walls, Transactions All-Union Scientific

Research Institute of Hydraulic Engineering, Leningrad, Vol. 3, pp 157-164 (in Russian).

Petryk, S (1969) Drag on cylinders in open channel flow, PhD thesis, Colorado State University, Fort Collins, Colorado.

Petryk, S and Bosmajian, G (1975) Analysis of flow through vegetation, Journal of the Hydraulics Division, ASCE, Vol. 101, No. HY7, pp 871-884.

Petts, GE, Armitage, P and Castella E (1993) Physical Habitat changes and macroinvertebrate response to river regulation: the River Rede, UK, Regulated Rivers: Research and Management, No. 8, pp 167-178.

Poff, NL and Ward, JV (1990) Physical habitat template of lotic systems: Recovery in the context of historical pattern of spatiotemporal heterogeneity, Environmental Management, No. 14, pp 629-646.

Probst, W, Rabeni, CF, Covington, CG and Marteney, RE (1984) Resource partitioning between stream-dwelling rock bass (Ambloplites rupestris) and smallmouth bass (Micropterus dolomieu), Transactions of the American Fisheries Society, No. 113, pp 283-294.

Richter, A (1973) Stömungskräfte auf starre Kreiszylinder zwischen parallelen Wänden, Diss., Universität Karlsruhe.

Richter, BR, Baumgartner, JV, Wigington, R and Braun, DP (1997) How much water does a river need? Freshwater Biology, No.37, pp 231-249.

Rickenmann, D (1994) An alternative equation for the mean velocity in gravel-bed rivers and mountain torrents, Proceeding of ASCE Conf. Hyd. Engng'94, Buffalo, NY 1, pp. 672-676.

References

Rickenmann, D (1996) Fliessgeschwindigkeit in Wildbaechen und gebirgsflussen, Wasser, Energie, Luft 88 (11/12), 298-304 (in German).

Roberson, JA and Wright, SJ (1973) Analysis of flow in channels with gravel beds, ASCE, Vol. 27 (II), pp 63-72.

Rosenberg, DM and Resh, VH (1993) Freshwater Biomonitoring and Benthic Macroinvertebrates. Chapman and Hall, New York, United States of America.

Rouse, H (1965) Journal of Hydraulic Division, Proceedings of ASCE, Vol. 91, No. HY4, pp 1-25.

Rowlston, B, Jordanova, AA and Birkhead, AL (2000) Hydraulics In: Environmental flow assessment for rivers: Manual for the Building Block Methodology, King, JM, Tharme, RE and de Villiers, MS, (Eds), Water Research Commission report No.TT 131/00,Pretosia, South Africa.

Rowntree, K M and Wadeson, R A (1998) A Hierarchical Geomorphological Model for the Classification of Selected South African Rivers, Water Research Commission Report.

Schlosser IJ (1995) Dispersal, boundary processes, and trophic-level interactions in streams adjacent to beaver ponds, Ecology, No. 76, pp 908-925.

Shamloo, H, Rajaratnam, N and Katopodis, C (2001) Hydraulics of simple habitat structures, Journal of Hydraulic Research, Vol.39, No.4, pp 351-366.

Smart, GM (2001) A new roughness estimation technique for granular-bed flow resistance, Proceeding of XXIX IAHR Hyd. Eng. Congress, Beijing.

Smart, GM, Duncan, MJ and Walsh, JM (2002) Relatively rough flow resistance equations, Journal of Hydraulic Engineering, Vol.128, No.6, pp 568-578.

Smith, RJ, Hancock, NH and Ruffini, JL (1990) Flood flow through tall vegetation, Agricultural Water Management, Vol. 18, pp 317-332.

Stalnaker, CB and Arnette JL (1976) Methodologies for the determination of stream resource flow requirements: an assessment, prepared for US Fish & Wildlife Service by Utah State University, Logan, Utah (as cited by Gordon, 1992).

Starosolszky, Ö (1983) The role of reeds in the shaping of currents, Proceedings, 20th congress, International Association for Hydraulic Research, Moscow, pp 498-509.

Statzner, B, Gore, JA and Resh, VH (1988) Hydraulic stream ecology: observed patterns and potential applications, Journal of the North American Benthological Society, No. 7, pp 307-360.

Stewardson, MJ. and TA. McMahon (2002) A stochastic model of hydraulic variations within stream channels, Water Resources Research Vol. 38, No.1.

Stewart, MD, Bates, PD, Anderson, MG, Price, DA and Burt, TP (1999) Modelling floods in hydrologically complex lowland river reaches, Joirnal of Hydrology, No. 223, pp 85-106.

Tennant, DL (1976) Instream flow regimes for fish, wildlife, recreation and related environmental resources, Fisheries, Vol. 1, No. 4, pp 6-10.

Tharme, RE (1996) Review of international methodologies for the quantification of the instream flow requirements of rivers, Water law review, Final report for policy development, Commissioned by the Department of Water Affairs and Forestry, Pretoria, Freshwater Research Unit, University of Cape Town, Cape Town, 116 pp.

References

Tharme, RE (2002) A global perspective on environmental flow assessment: Emerging trends in the development and application of environmental flow methodologies for rivers, CD Proceeding of the 4th International Ecohydraulics Symposium, Cape Town, South Africa.

Tharme, RE and King, JM (1998) Development of the Building Block Methodology for instream flow assessment and supporting research on the effects of different magnitude flows on riverine ecosystems, WRC Report No. 576/1, Pretoria, South Africa.

Thoms, MC and Reid, M (2007) Defining hydraulic habitat: Is what you see what you get - the near bed flow conditions of surface flow types, CD proceeding of the 6th International Symposium on Ecohydraulics, Christchurch Convention Centre, New Zealand.

Thorne, CR, ASCE and Zevenbergen LW, (1985) Estimating Mean velocity in Mountain rivers, Journal of Hydraulic Eng. Vol. 111, No. 4, pp 612-624.

Todd, BL and Rabeni, CF (1989) Movement and habitat use by stream-dwelling smallmouth bass, Transactions of the American Fisheries Society, No. 118, pp 229-242.

Turner, AK and Chanmeesri, N (1984) Shallow flow of water through non-submerged vegetation, Agricultural Water Management, Vol. 8, pp 375-385.

Turner, AK, Langford, KJ, Myo Win and Clift, TR (1978) Discharge-depth equation for shallow flow, Proc. ASCE, Vol. 104 No.IR1, pp 95-110.

US Geological Survey (1989) Guide for selecting Manning's roughness coefficients for natural channels and flood plains, Water-Supply Paper 2339.

References

Uys, M, (2001) River rehabilitation experience in Australia and Hawaii, SA Water Bulletin, Vol.27, No.3, pp18-20.

Van Coller, A L, Rogers, K H and Heritage, G L (1997) Linking riparian vegetation types and fluvial geomorphology along the Sabie River within the Kruger National Park, South Africa, African Journal of Ecology, Vol. 35, pp 194-212.

Vanoni, V and Brooks, N (1957) Laboratory Study of the Roughness and Suspended Load of Alluvial Streams, Sedimentation Laboratory Report No. E68, California Institute of Technology, Pasadena, California, USA.

Wadeson, R A (1996) The Development of the Hydraulic Biotope Concept Within a Hierarchical Geomorphological Model, PhD thesis, Rhodes University, Grahamstown, South Africa.

Wallingford Software (2004) Conveyance Estimation System Version 1.0.1.1 DEFRA/ Environmental Agency (2004) Reducing Uncertainty in River Flood Conveyance: Conveyance Manual Project W5A-057/PR/1

Ward, J and Stanford, J (1979) The Ecology of Regulated Streams, Plenum Press: New York.

Wesche, TA and Rechard, PA (1980) A summary of instream flow methods for fisheries and related research needs, Eisenhower Consortium Bulletin, US Govt Printing Office, Washington, DC.

Wiberg, PL and Smith, JD (1991) Velocity distribution and bed roughness in high-gradient streams, Water Resources Research, Vol.27, No.5, pp 825-838.

References

Wohl, EE and Ikeda, H (1998) The effect of roughness configuration on velocity profiles in an artificial channel, Earth surface processes and landforms, Vol. 23 pp 159-169.

Wohl, EE, Anthony, DJ, Madsen, SW and Thomson, DM (1996) A comparison of surface sampling methods for coarse fluvial sediments, Water Resources Research, Vol. 32, No. 10, pp. 3219-3226.

Wolman, MG (1954) A method of sampling coarse river-bed material, Eos Trans. AGU, No. 35, pp. 951-956.

Wu, F-C, Shen, H W and Chou, Y-J (1999) Variation of roughness coefficients for unsubmerged and submerged vegetation, Journal of Hydraulic Engineering, Vol. 125, No. 9, pp 934-942.

Yen, BC (2002) Open channel flow resistance, Journal of Hydraulic Engineering, Vol. 128, No. 1, pp 20-39.

Young, WJ (1992) Clarification of the criteria used to identify near-bed flow regimes, Freshwater Biology, No. 28, pp 383-391.

Young, WJ (1993) Field techniques for the classification near-bed flow regimes, Freshwater Biology, No. 29, pp 377-383.

Young, WJ (1996) Laboratory investigations of near-bed hydraulics in a reconstructed cobble-bed stream section, Proceeding of the 2nd Symposium on Habitat Hydraulics, Volume A, pp 203-213.

Zgheib, PW (1994) Profiles and energy of transitional tumbling flow around a large bed element, Journal of Hydraulic Research, Vol.31, No.4, pp 479-49.

APPENDIX A

LISTING OF SERIES 1 EXPERIMENTAL DATA

Table A-1 Flume B experimental data

Flume B
Series 1 Experiments

Hemisphere	radius (m)	height (m)
	0.047	0.029

Test	Q (cumecs)	y_measured (m)	Covered area (%)	y/h	Slope
1.1.1	0.0152	0.178	82	6.1	0.0011
1.1.2	0.0094	0.133	82	4.6	0.0011
1.1.3	0.0053	0.105	82	3.6	0.0011
1.1.4	0.0039	0.092	82	3.2	0.0011
1.1.5	0.0018	0.070	82	2.4	0.0011
1.1.6	0.0006	0.050	82	1.7	0.0011
1.1.7	0.0004	0.042	82	1.4	0.0011
1.2.1	0.0055	0.083	82	2.9	0.0021
1.2.2	0.0022	0.061	82	2.1	0.0021
1.2.3	0.0004	0.038	82	1.3	0.0021
1.2.4	0.0109	0.117	82	4.0	0.0021
1.2.5	0.0152	0.137	82	4.7	0.0021
1.3.1	0.0014	0.066	47	2.3	0.0011
1.3.2	0.0033	0.094	47	3.2	0.0011
1.3.3	0.0089	0.147	47	5.1	0.0011
1.3.4	0.0148	0.187	47	6.4	0.0011
1.3.5	0.0042	0.104	47	3.6	0.0011
1.4.1	0.0009	0.054	30	1.8	0.0011
1.4.2	0.0043	0.103	30	3.6	0.0011
1.4.3	0.0096	0.153	30	5.3	0.0011
1.4.4	0.0159	0.199	30	6.8	0.0011
1.5.1	0.0139	0.180	22	6.2	0.0011
1.5.2	0.0091	0.142	22	4.9	0.0011
1.5.3	0.0040	0.094	22	3.2	0.0011
1.5.4	0.0004	0.037	22	1.3	0.0011

Figure A-1 Series 1, Tests 1 and 2

Figure A-2 Series 1, Test 3

Figure A-3 Series 1, Test 4

Figure A-4 Series 1, Test 5

APPENDIX B

LISTING OF SERIES 2.1 EXPERIMENTAL DATA

Table B-1 Flume C, Series 2.1 experiments

Flume C
Series 2.1 Experiments

Bed Slope	0.001	
	radius	height
Big Hemisphere (BH)	0.058	0.062
Small Hemisphere (SH)	0.027	0.0286

Patterns	Q (cumecs)	y_measured (m)	No BH/m	No SH/m	y/h (BH)	y/h (SH)
Pattern 1 (BH)	0.0027	0.025	28	0	0.40	0
	0.0042	0.036	28	0	0.58	0
	0.0069	0.048	28	0	0.77	0
	0.0095	0.055	28	0	0.89	0
	0.0119	0.064	28	0	1.03	0
	0.0174	0.074	28	0	1.19	0
Pattern 2 (BH+SH)	0.0012	0.020	28	26	0.32	0.70
	0.0018	0.026	28	26	0.42	0.91
	0.0026	0.031	28	26	0.50	1.08
	0.0043	0.042	28	26	0.68	1.47
	0.0093	0.062	28	26	1.00	2.17
	0.0125	0.069	28	26	1.11	2.41
Pattern 3 (BH+SH)	0.0029	0.028	28	20	0.45	0.98
	0.0045	0.035	28	20	0.56	1.22
	0.0066	0.045	28	20	0.73	1.57
	0.0098	0.061	28	20	0.98	2.13
	0.0145	0.073	28	20	1.18	2.55
	0.0214	0.080	28	20	1.29	2.80
Pattern 4 (BH+SH)	0.0020	0.020	28	18	0.32	0.70
	0.0035	0.030	28	18	0.48	1.05
	0.0076	0.045	28	18	0.73	1.57
	0.0102	0.055	28	18	0.89	1.92
	0.0149	0.070	28	18	1.13	2.45
	0.0257	0.085	28	18	1.37	2.97
Pattern 5 (BH+SH)	0.0018	0.020	28	24	0.32	0.70
	0.0028	0.026	28	24	0.42	0.91
	0.0075	0.047	28	24	0.76	1.64
	0.0145	0.069	28	24	1.11	2.41
	0.0200	0.075	28	24	1.21	2.62
	0.0214	0.081	28	24	1.31	2.83
	0.0247	0.082	28	24	1.32	2.87
Pattern 6 (BH)	0.0032	0.025	28	0	0.40	0
	0.0075	0.043	28	0	0.69	0
	0.0138	0.065	28	0	1.05	0
	0.0220	0.080	28	0	1.29	0
	0.0273	0.085	28	0	1.37	0
Pattern 7 (SH)	0.0070	0.029	0	28	0	1.01
	0.0100	0.035	0	28	0	1.22
	0.0129	0.039	0	28	0	1.36
	0.0171	0.043	0	28	0	1.50

	0.0217	0.050	0	28	0	1.75
	0.0276	0.055	0	28	0	1.92
Pattern 8 (SH)	0.0053	0.025	0	26	0	0.87
	0.0088	0.032	0	26	0	1.12
	0.0145	0.040	0	26	0	1.40
	0.0238	0.052	0	26	0	1.82
	0.0283	0.056	0	26	0	1.96

Figure B-1 Pattern 1

Figure B-2 Pattern 2

Figure B-3 Pattern 3

Figure B-4 Pattern 4

Figure B-5 Pattern 5

Figure B-6 Pattern 6

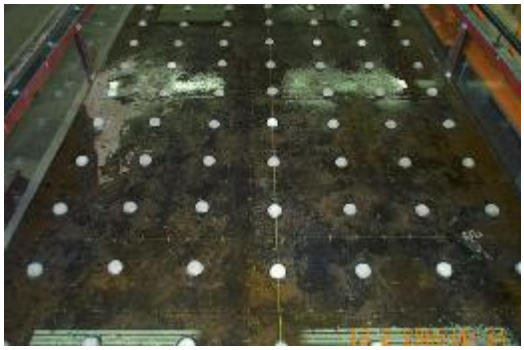

Figure B-7 Pattern 7

Figure B-8 Pattern 8

APPENDIX C

LISTING OF SERIES 2.2 EXPERIMENTAL DATA

Table C-1 Flume C Series 2.2 experiments

Flume C Experiments
Series 2.2 Experiments

Bed Slope	H1_radius	H1_height	H2_radius	H2_height	H3_radius	H3_height
0.0005	0.054	0.054	0.036	0.036	0.023	0.023

Spacing (m)	Q (cumecs)	y_measured (m)	No H1/m	No H2/m	No H3/m	y/h (H1)	y/h (H2)	y/h (H3)
Pattern 1	0.0006	0.0319	116	0	0	0.59	0	0
H1	0.0012	0.0495	116	0	0	0.92	0	0
spacing 0.125m	0.0016	0.0552	116	0	0	1.02	0	0
	0.0029	0.0643	116	0	0	1.19	0	0
	0.0119	0.1012	116	0	0	1.87	0	0
	0.0311	0.1452	116	0	0	2.69	0	0
	0.0417	0.1698	116	0	0	3.14	0	0
	0.0557	0.1894	116	0	0	3.51	0	0
Pattern 2	0.0011	0.024	47.5	0	0	0.45	0	0
H1	0.0016	0.035	47.5	0	0	0.64	0	0
spacing 0.200m	0.0019	0.039	47.5	0	0	0.72	0	0
	0.0033	0.055	47.5	0	0	1.01	0	0
	0.0042	0.058	47.5	0	0	1.07	0	0
	0.0071	0.066	47.5	0	0	1.22	0	0
	0.0187	0.093	47.5	0	0	1.72	0	0
	0.0206	0.099	47.5	0	0	1.83	0	0
	0.0344	0.126	47.5	0	0	2.33	0	0
	0.0475	0.148	47.5	0	0	2.73	0	0
	0.0547	0.164	47.5	0	0	3.04	0	0
Pattern 3	0.0552	0.129	26	0	0	2.39	0	0
H1	0.0468	0.122	26	0	0	2.25	0	0
spacing 0.300m	0.0246	0.091	26	0	0	1.68	0	0
	0.0160	0.071	26	0	0	1.31	0	0
	0.0137	0.067	26	0	0	1.24	0	0
	0.0082	0.059	26	0	0	1.08	0	0
	0.0050	0.044	26	0	0	0.81	0	0
	0.0034	0.034	26	0	0	0.62	0	0
	0.0020	0.023	26	0	0	0.42	0	0
Pattern 4	0.0552	0.121	14	0	0	2.24	0	0
H1	0.0333	0.092	14	0	0	1.71	0	0
spacing 0.400m	0.0140	0.060	14	0	0	1.10	0	0
	0.0072	0.046	14	0	0	0.86	0	0
	0.0027	0.023	14	0	0	0.43	0	0
Pattern 5	0.0552	0.107	0	14	0	0	2.98	0
H2	0.0322	0.080	0	14	0	0	2.21	0
spacing 0.400m	0.0066	0.036	0	14	0	0	1.00	0
	0.0032	0.023	0	14	0	0	0.65	0
Pattern 6	0.06	0.13	0	47.5	0	0	3.52	0
H2	0.0360	0.100	0	47.5	0	0	2.78	0
spacing 0.200m	0.01	0.05	0	47.5	0	0	1.52	0
	0.0028	0.034	0	47.5	0	0	0.95	0
Pattern 7	0.0552	0.149	0	116	0	0	4.14	0
H2	0.0360	0.125	0	116	0	0	3.48	0
spacing 0.125m	0.0088	0.066	0	116	0	0	1.84	0
	0.0041	0.050	0	116	0	0	1.38	0

Pattern 8	0.0547	0.164	47.5	47.5	0	3.04	4.57	0
H1 and H2	0.0358	0.132	47.5	47.5	0	2.45	3.68	0
spacing 0.200m	0.0187	0.102	47.5	47.5	0	1.89	2.83	0
	0.0080	0.074	47.5	47.5	0	1.37	2.05	0
	0.0043	0.060	47.5	47.5	0	1.10	1.65	0
	0.0029	0.054	47.5	47.5	0	0.99	1.49	0
	0.0022	0.046	47.5	47.5	0	0.85	1.28	0
	0.0015	0.038	47.5	47.5	0	0.70	1.05	0
	0.0007	0.020	47.5	47.5	0	0.37	0.56	0
Pattern 9	0.0008	0.020	47.5	0	47.5	0.37	0	0.88
H1 and H3	0.0019	0.039	47.5	0	47.5	0.72	0	1.69
spacing 0.200m	0.0048	0.062	47.5	0	47.5	1.14	0	2.69
	0.0112	0.081	47.5	0	47.5	1.50	0	3.52
	0.0302	0.124	47.5	0	47.5	2.30	0	5.39
	0.0434	0.145	47.5	0	47.5	2.69	0	6.30
Pattern 10	0.0552	0.137	26	19.5	0	2.54	3.81	0
H1 and H2	0.0283	0.098	26	19.5	0	1.81	2.72	0
spacing 0.300m	0.0179	0.081	26	19.5	0	1.50	2.25	0
	0.0114	0.066	26	19.5	0	1.23	1.84	0
	0.0089	0.059	26	19.5	0	1.09	1.63	0
	0.0051	0.049	26	19.5	0	0.91	1.37	0
	0.0033	0.040	26	19.5	0	0.74	1.11	0
	0.0014	0.024	26	19.5	0	0.44	0.66	0
Pattern 11	0.0552	0.131	26	0	19.5	2.43	0	5.70
H1 and H3	0.0193	0.076	26	0	19.5	1.41	0	3.32
spacing 0.300m	0.0121	0.066	26	0	19.5	1.22	0	2.87
	0.0052	0.047	26	0	19.5	0.87	0	2.03
	0.0028	0.033	26	0	19.5	0.61	0	1.42
	0.0020	0.026	26	0	19.5	0.47	0	1.11
Pattern 12	0.0037	0.031	13.5	9	0	0.57	0.86	0
H1 and H2	0.0063	0.047	13.5	9	0	0.88	1.31	0
spacing 0.400 (1)	0.0333	0.100	13.5	9	0	1.85	2.78	0
	0.0552	0.129	13.5	9	0	2.38	3.57	0
Pattern 13	0.0552	0.131	13.5	9	0	2.43	3.64	0
H1 and H2	0.0316	0.100	13.5	9	0	1.84	2.76	0
spacing 0.400 (2)	0.0070	0.053	13.5	9	0	0.98	1.46	0
	0.0045	0.040	13.5	9	0	0.75	1.12	0
	0.0025	0.027	13.5	9	0	0.51	0.76	0
Pattern 14	0.0557	0.136	0	47.5	47.5	0	3.78	5.92
H3	0.0348	0.104	0	47.5	47.5	0	2.90	4.53
spacing 0.200m	0.0073	0.052	0	47.5	47.5	0	1.44	2.26
	0.0036	0.036	0	47.5	47.5	0	1.01	1.58
Pattern 15	0.0004	0.043	162	0	0	0.78	0	0
H1	0.0018	0.059	162	0	0	1.07	0	0
spacing 0.110m	0.0015	0.058	162	0	0	1.06	0	0
	0.0011	0.054	162	0	0	0.99	0	0
	0.0033	0.068	162	0	0	1.23	0	0
	0.0103	0.098	162	0	0	1.78	0	0
	0.0250	0.127	162	0	0	2.30	0	0
	0.0012	0.055	162	0	0	1.00	0	0
Pattern 16	0.0016	0.057	136	0	0	1.04	0	0
H1	0.0012	0.052	136	0	0	0.95	0	0
spacing 0.110/0.125m	0.0006	0.04	136	0	0	0.74	0	0

	0.0099	0.09	136	0	0	1.64	0	0
	0.0214	0.117	136	0	0	2.13	0	0
	0.0014	0.055	136	0	0	1.00	0	0
Pattern 17	0.0009	0.041	90	0	0	0.74	0	0
H1	0.0006	0.031	90	0	0	0.56	0	0
spacing 0.110/0.167m	0.0018	0.055	90	0	0	0.99	0	0
	0.0078	0.082	90	0	0	1.48	0	0

Figure C-1 Pattern 1 - H 1 spacing 0.125 m

Figure C-2 Pattern 2 - H 1 spacing 0.200 m

Figure C-3 Pattern 3 - H 1 spacing 0.300 m

Figure C-4 Pattern 4 - H 1 spacing 0.400 m

Figure C-5 Pattern 5 - H 2 spacing 0.400 m

Figure C-6 Pattern 6 - H 2 spacing 0.200 m

Figure C-7 Pattern 7 - H 2 spacing 0.125

Figure C-8 Pattern 8 - H 1 and H 2 spacing 0.200 m

Figure C-9 Pattern 9 - H 1 and H 3 spacing 0.200 m

Figure C-10 Pattern 10 - H 1 and H 2 spacing 0.300 m

Figure C-11 Pattern 11 - H1 and H 3 spacing 0.300 m

Figure C-12 Pattern 12 - H1 and H 2 spacing 0.400 m

Figure C-13 Pattern 13 - H 2 and H3 spacing 0.400 m

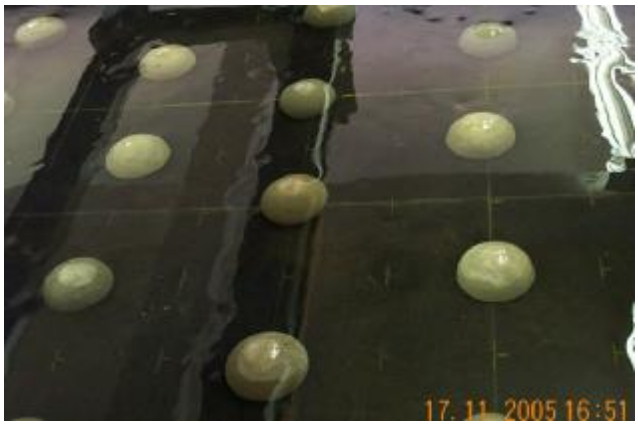

Figure C-14 Pattern 14 - H 3 spacing 0.200m

Figure C-15 Pattern 15 - H1 spacing 0.110m

Figure C-16 Pattern 16 - H1 spacing cross-sectional 0.110m, longitudinal 0.125m

Figure C-17 Pattern 17 - H1 spacing cross-sectional 0.110m, longitudinal 0.167m

APPENDIX D

LISTING OF MEASURED VELOCITIES AROUND ONE HEMISPHERE FOR Q=3 l/s and Q=21 l/s

Table D-1 Measured velocities around a hemisphere (Q=3.0 l/s)

Measured point	x (m)	y (m)	vel (cm/s)	vel (m/s)
1.1	0.01	0.01	2.81	0.028
2.1	0.01	0.03	3.28	0.033
3.1	0.01	0.05	4.73	0.047
4.1	0.01	0.07	3.59	0.036
5.1	0.01	0.09	4.98	0.050
1.2	0.03	0.01	2.96	0.030
2.2	0.03	0.03	3.17	0.032
3.2	0.03	0.05	3.82	0.038
4.2	0.03	0.07	5.09	0.051
5.2	0.03	0.09	4.04	0.040
1.3	0.05	0.01	0.71	0.007
2.3	0.05	0.03	4.33	0.043
3.3	0.05	0.05	4.47	0.045
4.3	0.05	0.07	5.48	0.055
5.3	0.05	0.09	2.64	0.026
1.4	0.07	0.01	4.72	0.047
2.4	0.07	0.03	4.49	0.045
3.4	0.07	0.05	3.76	0.038
4.4	0.07	0.07	6.24	0.062
2.5	0.09	0.03	5.17	0.052
3.5	0.09	0.05	5.48	0.055
2.6	0.11	0.03	5.52	0.055
3.6	0.11	0.05	5.25	0.053
1.7	0.13	0.01	5.68	0.057
2.7	0.13	0.03	5.25	0.053
3.7	0.13	0.05	5.37	0.054
4.7	0.13	0.07	6.39	0.064
1.8	0.15	0.01	1.59	0.016
2.8	0.15	0.03	5.44	0.054
3.8	0.15	0.05	5.92	0.059
4.8	0.15	0.07	5.68	0.057
5.8	0.15	0.09	1.22	0.012
1.9	0.17	0.01	5.66	0.057
2.9	0.17	0.03	5.29	0.053
3.9	0.17	0.05	5.65	0.056
4.9	0.17	0.07	4.76	0.048
5.9	0.17	0.09	1.95	0.020
1.10	0.19	0.01	4.97	0.050
2.10	0.19	0.03	5.19	0.052
3.10	0.19	0.05	4.58	0.046
4.10	0.19	0.07	5.32	0.053
5.10	0.19	0.09	3.44	0.034

Table D-2 Measured velocities at longitudinal section 1

Vertical position (m)	Velocity (x) (m/s)	Velocity (y) (m/s)	Total velocity (m/s)	Average (x) (m/s)	Average total (m/s)
Measured point 1.1					
0	0	0	0		
0.01	0.0552	-0.0083	0.0558		
0.02	0.0567	-0.0064	0.0571		
0.03	0.0826	-0.0020	0.0826		
0.04	0.1326	0.0031	0.1326		
0.05	0.1533	0.0046	0.1534		
0.06	0.1589	0.0053	0.1590		
0.07	0.1645	0.0077	0.1647		
0.083	0.1701		0.1704		
				0.1120	0.1122
Measured point 1.2					
0	0	0	0		
0.01	0.0194	-0.0031	0.0196		
0.02	0.0177	-0.0022	0.0178		
0.03	0.0993	-0.0021	0.0993		
0.04	0.1261	0.0021	0.1261		
0.05	0.1458	0.0037	0.1458		
0.06	0.1521	0.0068	0.1523		
0.07	0.1676	0.0082	0.1678		
0.083	0.1831		0.1833		
				0.1043	0.1044
Measured point 1.3					
0	0	0	0		
0.01	0.0744	0.0058	0.0746		
0.02	0.0790	-0.0014	0.0790		
0.03	0.1075	0.0022	0.1075		
0.04	0.1258	0.0008	0.1258		
0.05	0.1465	0.0032	0.1465		
0.06	0.1576	0.0072	0.1578		
0.07	0.1596	0.0052	0.1597		
0.083	0.1616		0.1616		
				0.1183	0.1183
Measured point 1.4					
0	0	0	0		
0.01	0.0912	0.0019	0.0912		
0.02	0.1054	-0.0035	0.1055		
0.03	0.1150	-0.0013	0.1150		
0.04	0.1375	0.0019	0.1375		
0.05	0.1510	0.0046	0.1511		
0.06	0.1557	0.0054	0.1558		
0.07	0.1650	0.0072	0.1652		
0.083	0.1743		0.1745		
				0.1275	0.1276
Measured point 1.5					
0	0	0	0		
0.01	0.1059	0.0079	0.1062		

Vertical position (m)	Velocity (x) (m/s)	Velocity (y) (m/s)	Total velocity (m/s)	Average (x) (m/s)	Average total (m/s)
0.02	0.1106	0.0021	0.1106		
0.03	0.1244	0.0026	0.1244		
0.04	0.1380	0.0048	0.1381		
0.05	0.1492	0.0075	0.1494		
0.06	0.1674	0.0045	0.1675		
0.07	0.1600	0.0051	0.1601		
0.083	0.1600		0.1527		
				0.1313	0.1311
Measured point 1.6					
0	0	0	0		
0.01	0.0990	0.0900	0.1338		
0.02	0.1149	0.0034	0.1150		
0.03	0.1257	0.0050	0.1258		
0.04	0.1418	0.0047	0.1419		
0.05	0.1519	0.0083	0.1521		
0.06	0.1631	0.0061	0.1632		
0.07	0.1666	0.0085	0.1668		
0.083	0.1701		0.1704		
				0.1326	0.1385
Measured point 1.7					
0	0	0	0		
0.01	0.1031	0.0094	0.1035		
0.02	0.1175	0.0021	0.1175		
0.03	0.1377	0.0022	0.1377		
0.04	0.1415	0.0069	0.1417		
0.05	0.1509	0.0066	0.1510		
0.06	0.1652	0.0046	0.1653		
0.07	0.1673	0.0073	0.1675		
0.083	0.1694		0.1697		
				0.1356	0.1357
Measured point 1.8					
0	0	0	0		
0.01	0.1168	0.0060	0.1170		
0.02	0.1198	0.0088	0.1201		
0.03	0.1316	0.0068	0.1318		
0.04	0.1452	0.0047	0.1453		
0.05	0.1475	0.0075	0.1477		
0.06	0.1624	0.0090	0.1626		
0.07	0.1686	0.0083	0.1688		
0.083	0.1748		0.1750		
				0.1370	0.1372
Measured point 1.9					
0	0	0	0		
0.01	0.10375	0.0003	0.1038		
0.02	0.118	0.0013	0.1180		
0.03	0.131	0.0069	0.1312		
0.04	0.1447	0.0058	0.1448		
0.05	0.1539	0.0053	0.1540		
0.06	0.1552	0.0081	0.1554		

Vertical position (m)	Velocity (x) (m/s)	Velocity (y) (m/s)	Total velocity (m/s)	Average (x) (m/s)	Average total (m/s)
0.07	0.1651	0.0096	0.1654		
0.083	0.1750		0.1753		
				0.1344	0.1345
Measured point 1.10					
0	0	0	0		
0.01	0.0907	0.0056	0.0909		
0.02	0.1162	0.0053	0.1163		
0.03	0.1288	0.0048	0.1289		
0.04	0.135	0.0073	0.1352		
0.05	0.1466	0.0089	0.1469		
0.06	0.1565	0.0091	0.1568		
0.07	0.1635	0.0095	0.1638		
0.083	0.1705		0.1708		
				0.1293	0.1295

Table D-3 Measured velocities at longitudinal section 2

Vertical position (m)	Velocity (x) (m/s)	Velocity (y) (m/s)	Total velocity (m/s)	Average (x) (m/s)	Average total (m/s)
Measured point 2.1					
0	0	0	0		
0.01	0.0962	-0.0109	0.0968		
0.02	0.1063	-0.0125	0.1070		
0.03	0.1297	-0.0065	0.1299		
0.04	0.1484	-0.0042	0.1485		
0.05	0.1576	-0.0012	0.1576		
0.06	0.1607	0.0019	0.1607		
0.07	0.1623	0.0044	0.1624		
0.083	0.1639		0.1640		
				0.1324	0.1326
Measured point 2.2					
0	0	0	0		
0.01	0.0821	-0.0022	0.0821		
0.02	0.1126	-0.0075	0.1128		
0.03	0.1323	-0.0056	0.1324		
0.04	0.1397	-0.0041	0.1398		
0.05	0.1518	0.0011	0.1518		
0.06	0.1555	0.0034	0.1555		
0.07	0.1629	0.0025	0.1629		
0.083	0.1703		0.1703		
				0.1293	0.1293
Measured point 2.3					
0	0	0	0		
0.01	0.1034	-0.0107	0.1040		
0.02	0.1128	-0.0079	0.1131		
0.03	0.1299	-0.005	0.1300		
0.04	0.1437	-0.0027	0.1437		

Vertical position (m)	Velocity (x) (m/s)	Velocity (y) (m/s)	Total velocity (m/s)	Average (x) (m/s)	Average total (m/s)
0.05	0.1502	0.0015	0.1502		
0.06	0.1601	0.0034	0.1601		
0.07	0.1668	0.0039	0.1668		
0.083	0.1735		0.1736		
				0.1337	0.1338
Measured point 2.4					
0	0	0	0		
0.01	0.0932	-0.004	0.0933		
0.02	0.1162	-0.0098	0.1166		
0.03	0.1387	-0.0047	0.1388		
0.04	0.1489	-0.0042	0.1490		
0.05	0.1549	-0.0001	0.1549		
0.06	0.1624	0.0026	0.1624		
0.07	0.1703	0.0077	0.1705		
0.083	0.1782		0.1785		
				0.1359	0.1360
Measured point 2.5					
0	0	0	0		
0.01	0.1249	-0.0036	0.1250		
0.02	0.1223	-0.0058	0.1224		
0.03	0.1384	-0.0014	0.1384		
0.04	0.1543	-0.0023	0.1543		
0.05	0.162	0.0001	0.1620		
0.06	0.1665	0.0051	0.1666		
0.07	0.1687	0.0033	0.1687		
0.083	0.1709		0.1709		
				0.1430	0.1431
Measured point 2.6					
0	0	0	0		
0.01	0.1217	-0.0006	0.1217		
0.02	0.1335	0.0005	0.1335		
0.03	0.1417	-0.0023	0.1417		
0.04	0.1573	-0.0003	0.1573		
0.05	0.161	0.0054	0.1611		
0.06	0.1644	0.0048	0.1645		
0.07	0.1715	0.0061	0.1716		
0.083	0.1786		0.1787		
				0.1447	0.1447
Measured point 2.7					
0	0	0	0		
0.01	0.1125	0.0076	0.1128		
0.02	0.1311	0.0043	0.1312		
0.03	0.1498	0.0035	0.1498		
0.04	0.1552	0.0023	0.1552		
0.05	0.1626	0.0065	0.1627		
0.06	0.1698	0.0057	0.1699		
0.07	0.1683	0.0087	0.1685		
0.083	0.1668		0.1672		
				0.1438	0.1440

Vertical position (m)	Velocity (x) (m/s)	Velocity (y) (m/s)	Total velocity (m/s)	Average (x) (m/s)	Average total (m/s)
Measured point 2.8					
0	0	0	0		
0.01	0.1049	0.0069	0.1051		
0.02	0.1309	0.008	0.1311		
0.03	0.1454	0.0076	0.1456		
0.04	0.1525	0.0051	0.1526		
0.05	0.1619	0.0071	0.1621		
0.06	0.1643	0.0104	0.1646		
0.07	0.1689	0.01	0.1692		
0.083	0.1735		0.1738		
				0.1414	0.1416
Measured point 2.9					
0	0	0	0		
0.01	0.1068	0.0113	0.1074		
0.02	0.1131	0.011	0.1136		
0.03	0.1378	0.0095	0.1381		
0.04	0.1524	0.0068	0.1526		
0.05	0.1555	0.0102	0.1558		
0.06	0.1609	0.0101	0.1612		
0.07	0.1687	0.0085	0.1689		
0.083	0.1765		0.1766		
				0.1377	0.1380
Measured point 2.10					
0	0	0	0		
0.01	0.1035	0.0083	0.1038		
0.02	0.1226	0.0125	0.1232		
0.03	0.1323	0.0098	0.1327		
0.04	0.1467	0.0075	0.1469		
0.05	0.1545	0.0101	0.1548		
0.06	0.1567	0.0105	0.1571		
0.07	0.1651	0.0116	0.1655		
0.083	0.1735		0.1740		
				0.1353	0.1357

Table D-4 Measured velocities at longitudinal section 3

Vertical position (m)	Velocity (x) (m/s)	Velocity (y) (m/s)	Total velocity (m/s)	Average (x) (m/s)	Average total (m/s)
Measured point 3.1					
0	0	0	0		
0.01	0.0873	-0.0057	0.0875		
0.02	0.1187	-0.0062	0.1189		
0.03	0.1411	-0.0058	0.1412		
0.04	0.1487	-0.0032	0.1487		
0.05	0.155	-0.0005	0.1550		

Vertical position (m)	Velocity (x) (m/s)	Velocity (y) (m/s)	Total velocity (m/s)	Average (x) (m/s)	Average total (m/s)
0.06	0.1643	0.0011	0.1643		
0.07	0.1684	0.004	0.1684		
0.083	0.1725		0.1726		
				0.1351	0.1352
Measured point 3.2					
0	0	0	0		
0.01	0.0896	-0.0044	0.0897		
0.02	0.118	-0.0075	0.1182		
0.03	0.1404	-0.0043	0.1405		
0.04	0.1511	-0.0033	0.1511		
0.05	0.1561	0.0001	0.1561		
0.06	0.1627	0.003	0.1627		
0.07	0.1658	0.0021	0.1658		
0.083	0.1689		0.1689		
				0.1350	0.1351
Measured point 3.3					
0	0	0	0		
0.01	0.0824	-0.0037	0.0825		
0.02	0.1181	-0.009	0.1184		
0.03	0.1396	-0.0076	0.1398		
0.04	0.1488	-0.0058	0.1489		
0.05	0.1529	-0.0009	0.1529		
0.06	0.1583	0.0011	0.1583		
0.07	0.164	0.0027	0.1640		
0.083	0.1697		0.1697		
				0.1323	0.1324
Measured point 3.4					
0	0	0	0		
0.01	0.1079	-0.0153	0.1090		
0.02	0.1119	-0.0113	0.1125		
0.03	0.1424	-0.0076	0.1426		
0.04	0.1535	-0.0066	0.1536		
0.05	0.1558	-0.0003	0.1558		
0.06	0.1659	0.0022	0.1659		
0.07	0.17	0.0011	0.1700		
0.083	0.1741		0.1741		
				0.1392	0.1395
Measured point 3.5					
0	0	0	0		
0.01	0.1207	-0.013	0.1214		
0.02	0.1368	-0.0122	0.1373		
0.03	0.1488	-0.0094	0.1491		
0.04	0.1579	-0.0047	0.1580		
0.05	0.1629	-0.0016	0.1629		
0.06	0.1671	0.0005	0.1671		
0.07	0.1731	0.0069	0.1732		
0.083	0.1791		0.1794		
				0.1469	0.1471
Measured point 3.6					

Vertical position (m)	Velocity (x) (m/s)	Velocity (y) (m/s)	Total velocity (m/s)	Average (x) (m/s)	Average total (m/s)
0	0	0	0		
0.01	0.1346	-0.0006	0.1346		
0.02	0.1455	-0.0023	0.1455		
0.03	0.1593	-0.0046	0.1594		
0.04	0.165	-0.0009	0.1650		
0.05	0.1661	0.0014	0.1661		
0.06	0.1684	0.0049	0.1685		
0.07	0.1755	0.0061	0.1756		
0.083	0.1826		0.1827		
				0.1534	0.1535
Measured point 3.7					
0	0	0	0		
0.01	0.125	0.0153	0.1259		
0.02	0.1387	0.0073	0.1389		
0.03	0.1573	0.0041	0.1574		
0.04	0.1588	0.0023	0.1588		
0.05	0.1651	0.0078	0.1653		
0.06	0.169	0.0078	0.1692		
0.07	0.1737	0.01	0.1740		
0.083	0.1784		0.1788		
				0.1498	0.1501
Measured point 3.8					
0	0	0	0		
0.01	0.116	0.0231	0.1183		
0.02	0.1426	0.015	0.1434		
0.03	0.1513	0.0131	0.1519		
0.04	0.1574	0.0091	0.1577		
0.05	0.1641	0.0096	0.1644		
0.06	0.1695	0.0074	0.1697		
0.07	0.1751	0.0109	0.1754		
0.083	0.1807		0.1812		
				0.1477	0.1484
Measured point 3.9					
0	0	0	0		
0.01	0.1093	0.0196	0.1110		
0.02	0.1184	0.0172	0.1196		
0.03	0.1493	0.0144	0.1500		
0.04	0.1522	0.0098	0.1525		
0.05	0.1581	0.0115	0.1585		
0.06	0.1681	0.0114	0.1685		
0.07	0.1687	0.0095	0.1690		
0.083	0.1693		0.1694		
				0.1412	0.1419
Measured point 3.10					
0	0	0	0		
0.01	0.1067	0.018	0.1082		
0.02	0.1193	0.0154	0.1203		
0.03	0.1378	0.0156	0.1387		
0.04	0.15	0.0116	0.1504		

Vertical position (m)	Velocity (x) (m/s)	Velocity (y) (m/s)	Total velocity (m/s)	Average (x) (m/s)	Average total (m/s)
0.05	0.1537	0.011	0.1541		
0.06	0.1611	0.0121	0.1616		
0.07	0.1689	0.0105	0.1692		
0.083	0.1767		0.1769		
				0.1377	0.1384

Table D-5 Measured velocities at longitudinal section 4

Vertical position (m)	Velocity (x) (m/s)	Velocity (y) (m/s)	Total velocity (m/s)	Average (x) (m/s)	Average total (m/s)
Measured point 4.1					
0	0	0	0		
0.01	0.0843	0.0048	0.0844		
0.02	0.1169	-0.0001	0.1169		
0.03	0.139	-0.0013	0.1390		
0.04	0.1558	0.0008	0.1558		
0.05	0.1533	0.0042	0.1534		
0.06	0.1613	0.0017	0.1613		
0.07	0.1655	0.0042	0.1656		
0.083	0.1697		0.1698		
				0.1336	0.1336
Measured point 4.2					
0	0	0	0		
0.01	0.0836	0.0031	0.0837		
0.02	0.1121	-0.0059	0.1123		
0.03	0.134	-0.0002	0.1340		
0.04	0.148	-0.0024	0.1480		
0.05	0.1543	0.0012	0.1543		
0.06	0.1571	0.002	0.1571		
0.07	0.1638	0.0023	0.1638		
0.083	0.1705		0.1705		
				0.1312	0.1312
Measured point 4.3					
0	0	0	0		
0.01	0.1069	-0.012	0.1076		
0.02	0.1096	-0.0079	0.1099		
0.03	0.1359	-0.0074	0.1361		
0.04	0.1443	-0.0031	0.1443		
0.05	0.156	0.0004	0.1560		
0.06	0.1571	0.0024	0.1571		
0.07	0.1654	0.0024	0.1654		
0.083	0.1737		0.1737		
				0.1355	0.1357
Measured point 4.4					
0	0	0	0		
0.01	0	-0.0015	0.0015		
0.02	0.0358	-0.0044	0.0361		

Vertical position (m)	Velocity (x) (m/s)	Velocity (y) (m/s)	Total velocity (m/s)	Average (x) (m/s)	Average total (m/s)
0.03	0.0818	-0.0021	0.0818		
0.04	0.1429	-0.006	0.1430		
0.05	0.1525	-0.0025	0.1525		
0.06	0.1671	-0.0009	0.1671		
0.07	0.1669	0.003	0.1669		
0.083	0.1667		0.1668		
				0.1026	0.1029
Measured point 4.5					
0	0	0	0		
0.01	0	0	0.0000		
0.02	0	-0.0009	0.0009		
0.03	0.028	0.0026	0.0281		
0.04	0.1282	-0.0015	0.1282		
0.05	0.1631	-0.0024	0.1631		
0.06	0.166	0.0017	0.1660		
0.07	0.1688	0.0035	0.1688		
0.083	0.1716		0.1717		
				0.0917	0.0918
Measured point 4.6					
0	0	0	0		
0.01	0	0	0.0000		
0.02	0	0.0001	0.0001		
0.03	0.0319	-0.0076	0.0328		
0.04	0.1411	-0.0032	0.1411		
0.05	0.1684	0.0004	0.1684		
0.06	0.1676	0.0038	0.1676		
0.07	0.1751	0.0057	0.1752		
0.083	0.1826		0.1827		
				0.0959	0.0961
Measured point 4.7					
0	0	0	0		
0.01	0	0.0003	0.0003		
0.02	0.0257	-0.0073	0.0267		
0.03	0.0909	-0.0142	0.0920		
0.04	0.1554	0.0014	0.1554		
0.05	0.1685	0.0062	0.1686		
0.06	0.1707	0.0074	0.1709		
0.07	0.1735	0.0093	0.1737		
0.083	0.1763		0.1766		
				0.1088	0.1092
Measured point 4.8					
0	0	0	0		
0.01	0.0596	0.024	0.0643		
0.02	0.0934	0.0187	0.0953		
0.03	0.14	0.0131	0.1406		
0.04	0.1613	0.0096	0.1616		
0.05	0.1615	0.0095	0.1618		
0.06	0.1644	0.0088	0.1646		
0.07	0.1712	0.0087	0.1714		

Vertical position (m)	Velocity (x) (m/s)	Velocity (y) (m/s)	Total velocity (m/s)	Average (x) (m/s)	Average total (m/s)
0.083	0.1780		0.1782		
				0.1311	0.1322
Measured point 4.9					
0	0	0	0		
0.01	0.0943	0.0332	0.1000		
0.02	0.1008	0.0246	0.1038		
0.03	0.1314	0.0192	0.1328		
0.04	0.153	0.0117	0.1534		
0.05	0.1597	0.0126	0.1602		
0.06	0.1634	0.0129	0.1639		
0.07	0.1672	0.0135	0.1677		
0.083	0.1710		0.1716		
				0.1340	0.1357
Measured point 4.10					
0	0	0	0		
0.01	0.0973	0.0282	0.1013		
0.02	0.1082	0.0228	0.1106		
0.03	0.1292	0.0175	0.1304		
0.04	0.147	0.0133	0.1476		
0.05	0.1521	0.0123	0.1526		
0.06	0.1623	0.0131	0.1628		
0.07	0.1652	0.0125	0.1657		
0.083	0.1681		0.1685		
				0.1324	0.1338

Table D-6 Measured velocities at longitudinal section 5

Vertical position (m)	Velocity (x) (m/s)	Velocity (y) (m/s)	Total velocity (m/s)	Average (x) (m/s)	Average total (m/s)
Measured point 5.1					
0	0	0	0		
0.01	0.1074	0.0072	0.1076		
0.02	0.1098	0.0076	0.1101		
0.03	0.1312	0.0036	0.1312		
0.04	0.1399	0.0034	0.1399		
0.05	0.151	0.0065	0.1511		
0.06	0.1568	0.0054	0.1569		
0.07	0.1636	0.0059	0.1637		
0.083	0.1704		0.1705		
				0.1332	0.1333
Measured point 5.2					
0	0	0	0		
0.01	0.1002	0.0011	0.1002		
0.02	0.1121	0.0044	0.1122		
0.03	0.1255	0.0041	0.1256		
0.04	0.146	0.002	0.1460		

Vertical position (m)	Velocity (x) (m/s)	Velocity (y) (m/s)	Total velocity (m/s)	Average (x) (m/s)	Average total (m/s)
0.05	0.1535	0.0051	0.1536		
0.06	0.1516	0.0015	0.1516		
0.07	0.166	0.0093	0.1663		
0.083	0.1804		0.1809		
				0.1325	0.1326
Measured point 5.3					
0	0	0	0		
0.01	0.0658	-0.0045	0.0660		
0.02	0.082	-0.0043	0.0821		
0.03	0.0975	0.0074	0.0978		
0.04	0.1326	0.0021	0.1326		
0.05	0.1465	0.005	0.1466		
0.06	0.1529	0.0036	0.1529		
0.07	0.164	0.0059	0.1641		
0.083	0.1751		0.1753		
				0.1169	0.1170
Measured point 5.4					
0	0	0	0		
0.01	0	0.0001	0.0001		
0.02	0.0027	-0.0007	0.0028		
0.03	0.0259	0.0014	0.0259		
0.04	0.0615	0.0017	0.0615		
0.05	0.1416	0.0053	0.1417		
0.06	0.1576	0.0046	0.1577		
0.07	0.1683	0.0051	0.1684		
0.083	0.1790		0.1791		
				0.0819	0.0820
Measured point 5.5					
0	0	0	0		
0.01	0	0	0.0000		
0.02	0	0	0.0000		
0.03	0	0	0.0000		
0.04	0.0089	0.0012	0.0090		
0.05	0.0461	0.0001	0.0461		
0.06	0.1382	0.0079	0.1384		
0.07	0.1695	0.0055	0.1696		
0.083	0.2008		0.2008		
				0.0566	0.0566
Measured point 5.6					
0	0	0	0		
0.01	0	0	0.0000		
0.02	0	0	0.0000		
0.03	0	0	0.0000		
0.04	0.0237	0.0027	0.0239		
0.05	0.0646	0.0098	0.0653		
0.06	0.1358	0.0005	0.1358		
0.07	0.162	0.0056	0.1621		
0.083	0.1882		0.1884		
				0.0589	0.0591

Vertical position (m)	Velocity (x) (m/s)	Velocity (y) (m/s)	Total velocity (m/s)	Average (x) (m/s)	Average total (m/s)
Measured point 5.7					
0	0	0	0		
0.01	0	0	0.0000		
0.02	0	0	0.0000		
0.03	0.0003	0.0003	0.0004		
0.04	0.0783	0.0113	0.0791		
0.05	0.103	-0.0012	0.1030		
0.06	0.1515	0.0034	0.1515		
0.07	0.1749	0.0105	0.1752		
0.083	0.1983		0.1989		
				0.0738	0.0739
Measured point 5.8					
0	0	0	0		
0.01	0.0596	0.024	0.0643		
0.02	0.0934	0.0187	0.0953		
0.03	0.14	0.0131	0.1406		
0.04	0.1613	0.0096	0.1616		
0.05	0.1615	0.0095	0.1618		
0.06	0.1644	0.0088	0.1646		
0.07	0.1712	0.0087	0.1714		
0.083	0.1780		0.1782		
				0.1311	0.1322
Measured point 5.9					
0	0	0	0		
0.01	0.0167	0.0258	0.0307		
0.02	0.0135	0.007	0.0152		
0.03	0.0573	0.0051	0.0575		
0.04	0.1378	0.0087	0.1381		
0.05	0.158	0.0103	0.1583		
0.06	0.1628	0.0096	0.1631		
0.07	0.169	0.0095	0.1693		
0.083	0.1752		0.1755		
				0.1003	0.1030
Measured point 5.10					
0	0	0	0		
0.01	0.0598	0.0303	0.0670		
0.02	0.0477	0.0053	0.0480		
0.03	0.0861	0.0025	0.0861		
0.04	0.1408	0.005	0.1409		
0.05	0.1474	0.008	0.1476		
0.06	0.1588	0.0085	0.1590		
0.07	0.1602	0.0081	0.1604		
0.083	0.1616		0.1618		
				0.1113	0.1126

APPENDIX E

LISTING OF MEASURED VELOCITIES UNDER LOCAL CONTROLLED CONDITIONS

APPENDIX F

LISTING OF MEASURED LOCAL VELOCITY DISTRIBUTIONS

APPENDIX G

COTTER RIVER FIELD DATA